Spring 2016

Modeling of rheological properties for entangled polymer systems

Nilanjana Banerjee

Department: Chemical and Biochemical Engineering

MODELING OF RHEOLOGICAL PROPERTIES FOR ENTANGLED POLYMER SYSTEMS

by

NILANJANA BANERJEE

A DISSERTATION

Presented to the Faculty of the Graduate School of the

MISSOURI UNIVERSITY OF SCIENCE AND TECHNOLOGY

In Partial Fulfillment of the Requirements for the Degree

DOCTOR OF PHILOSOPHY

in

CHEMICAL ENGINEERING

2016

Approved by

Joontaek Park, Advisor

Parthasakha Neogi

Jee-Ching Wang

Dipak Barua

V. A. Samaranayake

PUBLICATION DISSERTATION OPTION

This dissertation consists of the following three articles that have been published/submitted for publication as follows:

Paper I, pages 37-79 have been published in KOREAN JOURNAL OF CHEMICAL ENGINEERING.

Paper II, pages 80-145 have been published in JOURNAL OF RHEOLOGY.

Paper III, pages 146-188 have been submitted for publication in JOURNAL OF RHEOLOGY. Appendices A and B have been added for purposes normal to dissertation writing.

ABSTRACT

The study of entangled polymer rheology both in the field of medicine and polymer processing has their major importance. Mechanical properties of biomolecules are studied in order to better understand cellular behavior. Similarly, industrial processing of polymers needs thorough understanding of rheology so as to improve process techniques. Work in this dissertation has been organized into three major sections. Firstly, numerical/analytical models are reviewed for describing rheological properties and mechanical behaviors of cytoskeleton. The cytoskeleton models are classified into categories according to the length scales of the phenomena of interest. The main principles and characteristics of each model are summarized and discussed by comparison with each other, thus providing a systematic understanding of biopolymer network modeling. Secondly, a new constitutive "toy" Mead-Banerjee-Park (MBP) model is developed for monodisperse entangled polymer systems, by introducing the idea of a configuration dependent friction coefficient (CDFC) and entanglement dynamics (ED) into the MLD "toy" model. The model is tested against experimental data in steady and transient extensional and shear flows. The model simultaneously captures the monotonic thinning of the extensional flow curve of polystyrene (PS) melts and the extension hardening found in PS solutions. Thirdly, the monodisperse MBP model is accordingly modified into polydisperse MBP "toy" constitutive model to predict the nonlinear viscoelastic material properties of model polydisperse systems. The polydisperse MBP toy model accurately predicts the material properties in the forward direction for transient uniaxial extension and transient shear flow.

ACKNOWLEDGEMENTS

The accolade for the success of this research project is not alone mine, rather it goes to a lot of people who have been there behind the scene but have equally played an important role to make this endeavor a success.

First and foremost, I thank God for giving me the strength and guidance to do things in the right way.

My heartfelt gratitude and thanks goes to my advisor Dr. Joontaek Park, without whom, even the smallest of the steps towards the completion of these projects would not have been possible. His help and support has made it possible for me to do whatever I have accomplished. His continuous encouragement has allowed me to overcome my obstacles. His guiding hands have taught me to think and work as a better engineer.

Special thanks to my committee members, Dr. Parthasakha Neogi, Dr. V. A. Samaranayake, Dr. J. C. Wang and Dr. Dipak Barua, without whose support, fulfillment of this dissertation would not have been possible.

A big hug, thanks and lots of love for my parents and my sister Payal, for being my support. For keeping the trust in me and for believing in my capabilities.

Last but not the least, I thank Missouri University of Science and Technology for giving me a forum to enhance my knowledge and learn to become a professional. Thanks to the institute also for giving me innumerable memories to be cherished throughout my life.

TABLE OF CONTENTS

APPENDICES

LIST OF ILLUSTRATIONS

PAPER II

PAPER III

LIST OF TABLES

NOMENCLATURE

Symbol	Description
C_∞	Characteristic ratio of the polymer
G_N^0	Equilibrium plateau modulus of fully entangled chain
$G_N(t)$	Dynamic plateau modulus of partially disentangled chain
$\underline{\underline{I}}_{jj}$	Tension induced orientation tensor
J	Number of C-C sigma bonds in the backbone of polymer monomer
k_{id}	Non-linear spring constant for diluted tube
k_s / k_{si}	Non-linear spring constant
L(t)	Current tube contour length
L_{eq}	Initial equilibrium length
$L_{eq}(t)$	Current equilibrium length
M/M_i	Molecular weight of component
M_c	Critical molecular weight
M_e	Entanglement molecular weight
$M_e(t)$	Entanglement molecular weight of partially disentangled chain
M_n	Number average molecular weight
M_o	Molecular weight of a single monomer of the polymer system
n	Number of Kuhn bonds in an entanglement segment
$\dot{N}(t)$	Rate of change of number of entanglements on a chain
N(t) / $N_{ij}(t)$	Number of entanglements on a partially disentangled chain

N_e / N_{ij}^0	Average equilibrium number of entanglements per chain
$\hat{R}$	Unit end-to-end vector of a tube segment
S_{kuhn}	Net Kuhn bond orientation
$\underline{\underline{S}}_{id}$	Orientation tensor of the diluted tube
$\underline{\underline{S}}_{tube}$	Orientation tensor
S_{tubeij}	Tube segment orientation of the ij^{th} entanglement pair
S_{tube}/S_{tubei}	Single tube segment orientation
S_{xx}, S_{yy}, S_{xy}	Tube segment orientation in x, y and xy direction.
w_i / w_j	Weight fraction of the i^{th} / j^{th} component in MWD
x / x_i	Fractional extension of the chain
x_{id}	Fractional extension of the diluted tube

Greek nomenclature

α / α_i	Ratio between the maximum stretch ratios of relative stretches
$\dot{\alpha}(t)/\dot{\alpha}_i(t)$	Rate of change of the maximum stretch ratios
$\dot{\alpha_{id}}(t)$ / α_{id}	α values for diluted tube
β	Entanglement dynamics efficiency
$\dot{\epsilon}$ and $\dot{\gamma}$	Extension rate and shear rate respectively
$\zeta(t)$	Friction factor
ζ_{eq}	Equilibrium friction factor
η_e and η	Extensional viscosity and shear viscosity respectively
κ	Velocity gradient
$\lambda(t)$	Relative stretch of a fully entangled chain

λ_{max}	Maximum relative stretch of a fully entangled chain
Λ / $\Lambda(t)$	Relative stretch of partially disentangled chain
$\dot{\Lambda}(t)/\dot{\Lambda}_1(t)$	Rate of change of relative stretch
Λ_{id}	Relative stretch of the diluted tube
Λ_{maxid}	Maximum relative stretch of the diluted tube
$\Lambda_{max}(t)$	Maximum relative stretch of the chain as a function of ED
τ_{d0}	Equilibrium reptation / disengagement / orientation time
$\tau_d(t)/\tau_{di}(t)$	Reptation / disengagement / orientation time
τ_{dij}	Reptation / orientation time of ijth entanglement pair
τ_{s0}	Equilibrium longest rouse / stretch relaxation time
$\tau_s(t)/\tau_{si}(t)$	Longest rouse / stretch relaxation time
τ_{si}^{eff}	Effective rouse time for the diluted tube
$\sigma_{xx\text{-}yy}(t)$	Extensional Stress or Normal stress difference in case of shear flow
$\sigma_{xy}(t)$	Shear stress
φ_p	Weight fraction (solution or melt)
$\dot{\Phi}$	Fractional rate of matrix entanglement renewal
ψ_i	Fractional dilution level of the ith component of the MWD

Abbreviations

CCR	Convective constraint release
CDFC	Configuration dependent friction coefficient
CR	Constraint release
DE	Doi and Edwards model

DEMG	Doi – Edwards – Marrucci – Grizzuti model
ED	Entanglement dynamics
LCB	Long chain branched polymer
LVE	Linear viscoelastic envelope
MBP	Mead – Banerjee – Park model
MFI	Melt flow index
MLD	Mead – Larson – Doi model
MW	Molecular weight
MWD	Molecular weight distribution
PI	Polydispersity index and/or Polyisoprene (refer to context)
PS	Polystyrene
RVE	Representative volume element

1. INTRODUCTION

1.1 OVERVIEW

Studies of entangled polymer systems have been underway for a long time both in the field of biological sciences and commercial polymer industries. The macromolecules, like proteins, and more complex structures, like cytoskeletons and external cellular matrix, have been under exploration in order to understand cellular behavior and diseases more thoroughly. Similarly, the rheological behavior of commercial polymer macromolecules, both linear and linear branched chains, is important to understand, as they are exposed to high shear and extension deformation conditions during industrial processing. Better understanding of the mechanical properties of these polymers allows better process design and material handling. The discussion in subsequent sections, is categorized in three major parts. Paper I consists of the classification of the cytoskeleton models according to multiple scales. The discussion in Papers II and III are dedicated to the development of constitutive "toy" models for both monodisperse and polydisperse entangled polymer systems respectively.

The discussion in the section below has been organized as follows. In Section 1.2, the motivation and objectives behind the research topic "modeling and simulation of biopolymer network classification of the cytoskeleton models according to multiple scales" are discussed. A very brief glance at how the classification of models has been organized is also included. Section 2 is dedicated to discussing the constitutive models for monodisperse and polydisperse entangled polymer systems. The Section 2 is further categorized into sub sections as follows. In Sections 2.1 and 2.2, the motivation and the

objectives behind the research respectively are discussed. The constitutive models for the monodisperse and polydisperse systems are a modification of the Doi-Edwards' "tube model." Thus, a brief introduction to the tube theory and basic polymer relaxation mechanism is imperative before moving forward with the model development, which is taken up in Section 2.3. In Sections 3 and 4 the history of the mathematical models that have been developed over time to describe the rheology of entangled monodisperse and polydisperse polymer systems are respectively discussed.

1.2. MODELING AND SIMULATION OF BIOPOLYMER NETWORKS: CLASSIFYING THE CYTOSKELETON MODELS ACCORDING TO MULTIPLE SCALES

Cytoskeleton mechanics and the field of biomechanics have been topics of research for last couple of decades, as they are pathways to explain various cellular behaviors and also answer certain pertinent questions regarding recent diseases like cancer, tumour growth, neural degeneration, etc. The cytoskeleton, which is the structure providing component of the cell, changes its behavior under different mechanical conditions, changing the cellular activity accordingly. The questions here are what happens to the cytoskeleton structure under a certain mechanical perturbation and what are the reasons behind the observed deformations. The understanding of the above questions can be extended to answering what happens to the cellular activity under the deformation of the cytoskeleton (Banerjee & Park, 2015).

1.2.1. Research Motivation. The questions regarding the cytoskeleton mechanical behavior and properties and their answers have been one of the major

motivations behind studying this particular topic. From the onset of the research, it was clear that numerous mathematical models to describe the behavior of the cytoskeleton structure exist. The range of the models was extremely varied from that of viscoelastic to glassy material to that of a Brownian dynamic simulation of a discrete polymer network system. Many attempts have been made to provide a clear demarcation between the various models and their results (Banerjee & Park, 2015), but there is a lack of review articles that bring in all the various models together and put forward a clear picture of how and why the models are different. This was the second major motivation to bring together a review article that could bring all the present mathematical models together, explain their differences and provide a literature structure for future research in this field (Banerjee & Park, 2015).

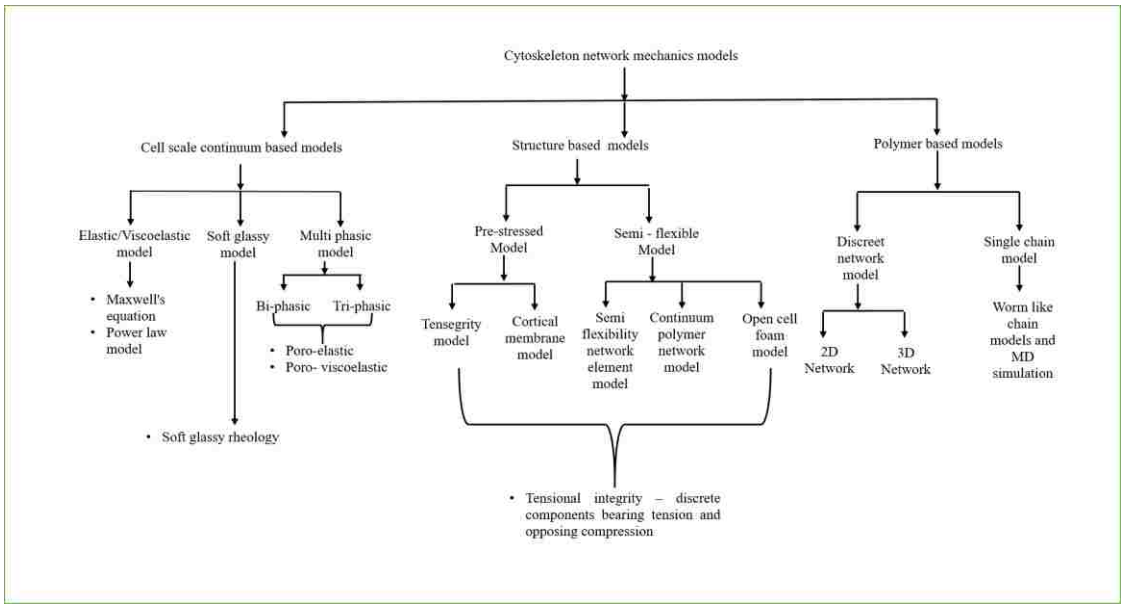

Figure 1.1. Classification of the cytoskeleton mechanics models and their underlying principles. The models are classified based on the length scales of study, varying from cell size (~10mm) to that of molecular level (~1nm).

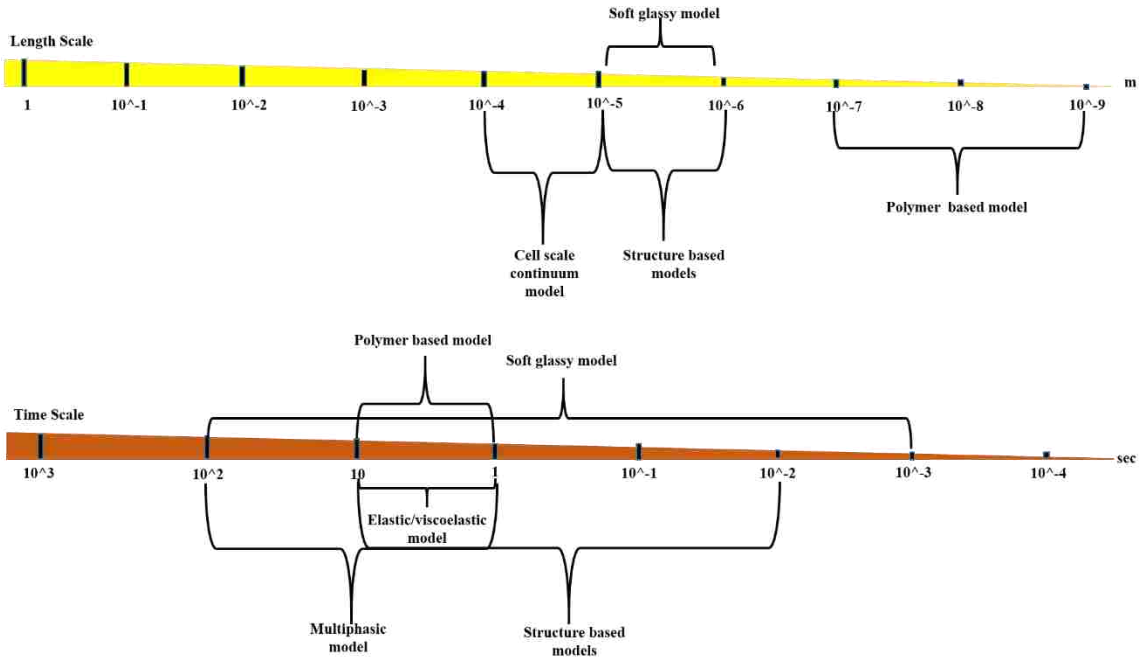

Figure 1.2. Classification of the cytoskeleton mechanics model based on both length and time scales. It can be clearly seen that the chosen time and length scales cause drastic difference in the model consideration for cytoskeleton rheological study.

1.2.2. Research Objectives. The objectives behind the research are as follows (Banerjee & Park, 2015):

1. This research was intended to provide a systematic understanding of cytoskeleton models in terms of length scales, which, in turn, affects the mechanical stress behavior of the cytoskeleton. Figures 1.1. and 1.2. provide a brief description of the classification of the models based on the length and time scales. It can be seen that depending on the chosen length scale or the time scale of the cytoskeleton mechanics model, the rheological behavior being described changes.
2. The final objective was to provide a framework for the future development of the cytoskeleton mechanical models.

3. This research was designed to assimilate all major recently published mathematical models and provide a summary of their underlying principles, main applications, and advantages and disadvantages.

The detailed discussion regarding the classifications, the underlying mechanism, and their pros and cons appears in Paper I, in the later part of the dissertation.

2. CONSTITUTIVE MODELS FOR MONODISPERSE AND POLYDISPERSE ENTANGLED POLYMER SYSTEMS

Nonlinear rheological behavioral studies of both entangled polymer melts and solutions (both monodisperse and polydisperse) under high deformation conditions have been underway for more than half a century. The tube theory developed by Doi and Edwards in 1986 provided a platform that has been modified and re-modified numerous times to date, generating different models, but has been unable to provide a single unified approach to describe the system as a whole (Doi & Edwards, 1986). Simultaneously there have been molecular dynamics simulation, stochastic Brownian dynamics approaches to study the same system of polymer under low and high deformation conditions (Park et al., 2012; Xu et al., 2006).

2.1. RESEARCH MOTIVATION

One of the major motivations behind this particular research has been to provide a generalized "toy" constitutive model that correctly and consistently describes all the physics behind the rheological behavior of the entangled polymer in a fast flow nonlinear regime. The system in this study was restricted to only that of polystyrene (PS) melts and solutions. The conclusions drawn from the same study can easily be transcribed to any other polymer systems (Mead et al., 2015).

Secondly, a strong physical basis was sought in order to describe the nonlinear rheological behavior for both the monodisperse polymer melt and solution systems. Experimental observations demonstrated that under high extension rates, monodisperse polymer melts exhibit an extension thinning behavior. Figure 2.1., which describes the

steady state extension curve for 200K PS melt w.r.t extension rates (Mead et al., 2015)). The physics behind it is not yet understood. There have been quite a few developments in the field to aid in understanding the reason behind it, but the results have been inconclusive. The approach used in the study was to find the underlying physics to describe this behavior.

Thirdly, monodisperse entangled polymer melt and polymer solution behave differently under similar extension conditions (see Figure 2.1., which provides a comparison between the steady state extensional viscosity behavior of 200K PS melt and 20wt% 1.95M PS solution w.r.t extension rate (Mead et al., 2015)). The entangled polymer melt shows extension thinning behavior, and the polymer solution shows extension thickening, under similar high extension conditions. There was also a desire to determine whether the constitutive "toy" model could both capture and explain the reasons behind this observed difference.

Polydisperse systems, on the other hand, are much more complicated than the monodisperse systems as there are multiple molecular weight components involved. As with monodisperse entangled polymers, there have been numerous attempts to describe the physics behind the observed rheological behavior under high deformation conditions, but there is a definite lack of a single unified approach. The aim of this study has been to extend the understanding of monodisperse systems to that of polydisperse systems and to verify the accuracy of the constitutive "toy" model in predicting the polydisperse rheological behavior.

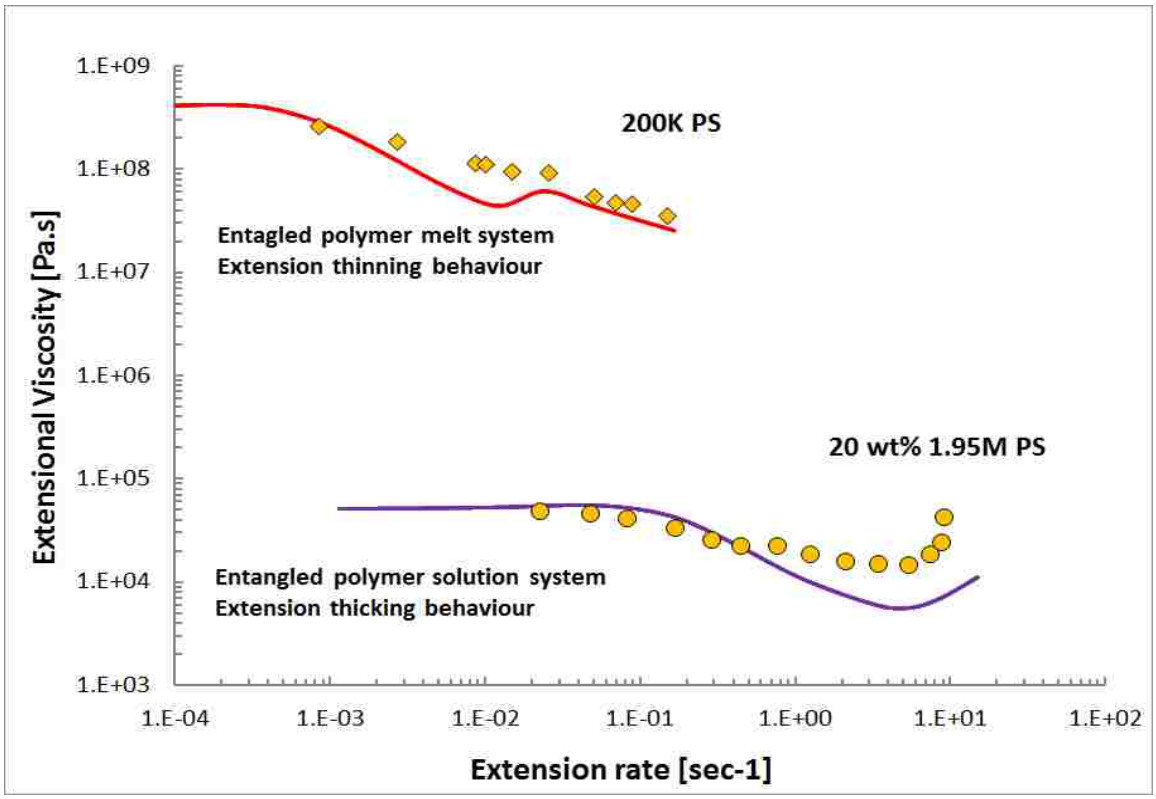

Figure 2.1. The steady state extensional viscosity vs extension rate for 200K PS melt and 20w% 1.95M PS solution respectively (Mead et al., 2015).

2.2. RESEARCH OBJECTIVES

The objectives of this research are as follows (Mead et al., 2015):

1. Develop a constitutive "toy" mathematical model incorporating the concept of a configuration dependent friction coefficient (CDFC) and entanglement dynamics (ED) that can correctly predict the behavior of the melts and solutions under low and high extension and shear flow conditions.

2. Understand why monodisperse entangled melt behaves differently from that of solution under a high extension condition.

3. Understand the effects of each of the underlying physics (CDFC, ED and convective constraint release (CCR)) on the overall behavior of the system under different deformation conditions.

4. Extend the understanding of monodisperse entangled polymer system to that of entangled polydisperse systems. To observe if any different physics is playing a role in describing the polydisperse system and understand the polydispersity in depth.

The details regarding the development of the constitutive "toy" model for both the monodisperse and polydisperse systems, the observed results, and the discussion appear in Papers II and III, respectively, in the later part of the dissertation.

2.3. INTRODUCTION TO DOI AND EDWARDS' TUBE THEORY

In the following sections we are going to discuss the development of Doi and Edwards tube model over the de Gennes' reptation model and the polymer relaxation mechanisms in detail.

2.3.1. Doi and Edwards' Tube Theory. Dense polymer systems, both under melt and solution conditions, are highly entangled. As a result, the motion of a single polymer strand under such conditions is highly constrained as the nearby entanglements pose certain restrictions to its movement, causing lateral motion of the chain to be highly improbable in certain positions. This idea forms the basis of "Tube Theory." Tube theory was initially coined by Doi and Edwards (1978a, 1978b, 1979, 1986), based on Pierre-Gilles de Gennes'

reptation theory (de Gennes, 1971), which became one of the most fundamental approaches used to study the entangled polymer rheological behavior under low and high deformation conditions. The foundation of the theory lies on the work of major pioneers, like Kuhn, who first questioned the length of the macromolecules for linear and branched, and Zimm, and Rouse, who examined the motion of these macromolecules (Kuhn, 1934; Zimm,1956; Rouse, 1953; McLeish, 2002). Doi and Edwards' tube theory garnered popularity, despite its obvious shortcomings, due to the fact that the concept is simple with clear assumptions, and a virtual tube is easier to conceptualize than the other then existing approaches like "mode-coupling" (McLeish, 2002).

The rheological behavior of the polymer system was studied by selecting one single polymer strand from the entire ensemble of entangled polymer strands and studying its movement and process of relaxation. The chain under study is referred to as the "test chain" or "primary/primitive chain" (Rubinstein & Colby, 2003; Larson, 1999).

It is assumed that any deformation observed in the test chain is affine (i.e., the amount of deformation given to the system is proportional to the amount of deformation felt by the test chain) (Rubinstein & Colby, 2003). It is also assumed that the behavior of the test chain is equivalent to that of the entire ensemble. Thus, the understanding gained from studying that one single chain can be extrapolated to the entire ensemble without any loss of information. A test chain can have many points of entanglements with other chains around it, but it is assumed that with a single chain, it is entangled at a single point (Mead et al., 2015). Thus, if there are four entanglements present in a chain, then they are all from four different chains around it (see Figure 2.2., which depicts an entangled polymer system with the primary chain and its entanglements). When a system of entangled polymers is

under deformation, by virtue of thermodynamics, it tries to arrive at an equilibrium condition or a steady state condition. This process of reaching equilibrium is called the relaxation process (Rubinstein & Colby, 2003; Larson, 1999). There are various ways one can quantify the relaxation mechanism in terms of mathematical models, like Doi and Edwards' tube model and its modifications, stochastic modeling, Brownian dynamic simulation, etc. (Doi & Edwards 1978a, 1978b, 1979, 1986; Mead et al., 1998, 2015; Park et al., 2012; Xu et al., 2006). The constitutive "toy" model hereby developed and simulated is a modification of the Doi and Edwards' tube model, and thus, the discussion is restricted to the same (Mead et al., 2015).

As discussed above, the entanglements present in and around the test chain pose a constraint to its lateral movement, and allowing only certain specific conformations and movements. Qualitatively, one may imagine a "virtual tube" along the contour of the chain defined by the sum of all the topological constraints active around the chain.

The tube allows some degree of free movement of the test chain along its contour in the transverse direction (see Figure 2.3.) (McLeish, 2002). The tube has a radius of a, which is in the order of the end-to-end length of the chain of entanglement is molecular weight $M_{e,}$ consisting of N_e monomers. This allows only chains with molecular weights greater than M_e to be strongly affected by the topological constraints around them (McLeish, 2002). As will be discussed later, the number of entanglements on the chain or the entanglement molecular weight of the system is derived from the plateau modulus of the component at a given processing temperature.

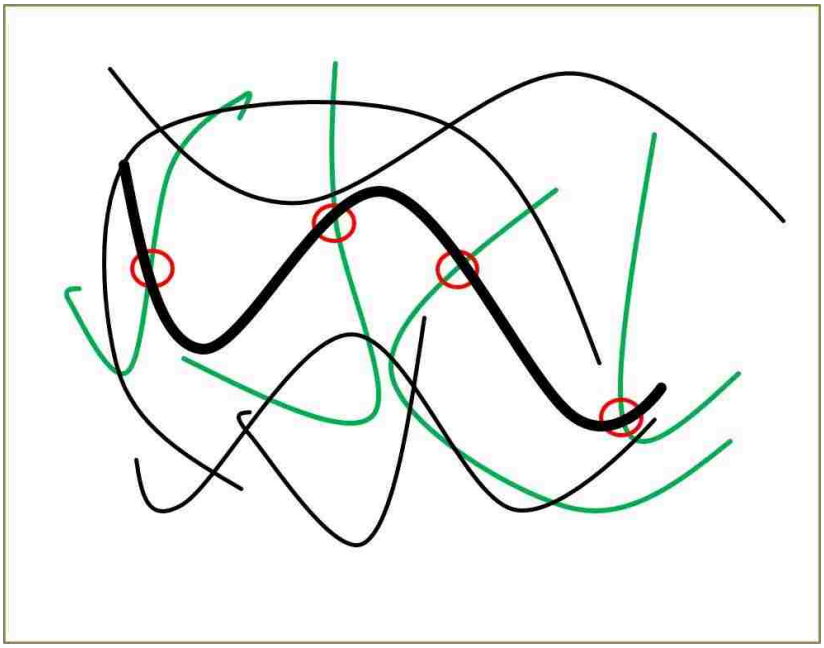

Figure 2.2. An entangled polymer system with the primary chain (bold black) with its entanglements (green) and constraints by other chains around it. The points of entanglements are shown by red circles.

Inside this tube, the test chain will have free transverse motion but will feel the same amount of constraint in the lateral movement at a distance a, as those of without the tube (Barkema et al., 2011; Rubinstein, 1987; Rubinstein & Colby, 2003). The tube diameter a is given by,

$$a = bN_e^{1/2} \quad (1)$$

where b is the Kuhn length (Rubinstein and Colby, 2003).

The primary (or primitive) chain, follows a primitive path along the tube center, defined by the constraining potential (Rubinstein and Colby, 2003).

If the primary chain is assumed to be consist of N Gaussian random walk sub-chains of effective step length (Kuhn length) b, then the defining tube will also have a Gaussian random walk of "curvilinear tube length," "average contour length," or "the average primitive path length" $L_{eq} = \left[{N}/{N_e}\right] a = {Nb^2}/{a}$ (McLeish, 2002; Rubinstein & Colby, 2003). The tube can thus, be considered to consist of $Z = \left[{N}/{N_e}\right]$ segments, each of length a (Rubinstein & Colby, 2003). The term Z also gives the number of entanglements on the chain.

The average primitive path length is the shortest possible length of the chain (shorter than the actual contour length of the chain 'bN' by a factor of ${a}/{b} = \sqrt{N_e}$) at which the chain can still feel the topological constraints (McLeish, 2002; Rubinstein & Colby, 2003).

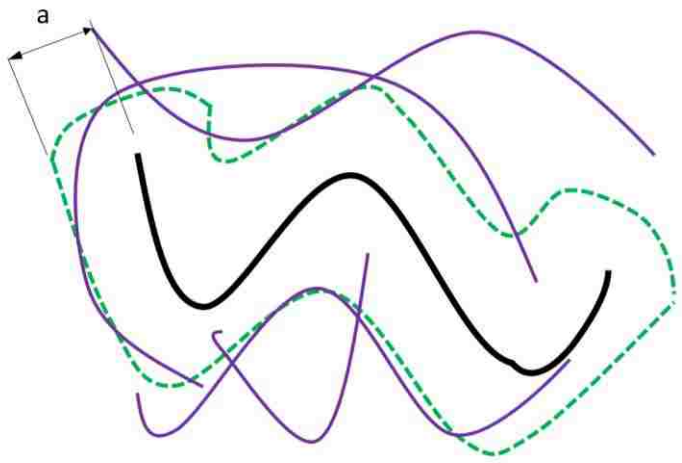

Figure 2.3. A virtual tube (green color) of radius a, created along the contour length of the primitive chain is the sum of the constraints around it. The purple colored lines depict the surrounding strands posing as constraints to the primary chain (black).

It is an important concept as it defines the time scale and nature of the entanglement constraint dynamics (McLeish, 2002). For long chain entangled polymers with N>> Ne, an almost constant modulus, called the plateau modulus (G_N^o) is observed in a stress relaxation experiment. The plateau modulus provides the information regarding the entanglement molecular weight M_e, which, in turn, scales the tube segment being created around the primitive chain.

For entangled polymer melts the plateau modulus is given as follows (Rubinstein & Colby, 2003):

$$G_N^o = \frac{\rho RT}{M_e} \tag{2}$$

Here, R is the universal gas constant, T is the temperature, and ρ is the density (Rubinstein & Colby, 2003).

The tube, which is qualitatively a statistical manifestation, can change by two distinct ways: a) when the chain transversely moves out of the existing tube in order to move a larger distance and b) when the tube fluctuates with the chain length fluctuations (Rubinstein,1987; Rubinstein & Colby, 2003). Figure 2.4 shows that as a chain moves out of the tube, a new tube starts to form, and at the same time, a part of the old tube gets destroyed. This type movement of the chain is called “reptation motion”. The term reptation was first used by de Gennes (1971) due to the snake-like Brownian motion of the chains (McLeish, 2002). The reptative motion of the will decide the longest characteristic time of the chain movement, called “reptation time / disengagement time / orientation time” (τ_d) (Rubinstein, 1987). The reptation time can be defined as “the time the chain takes to

diffuse out of the tube of average length L_{eq}" (Rubinstein & Colby, 2003). The reptation time (τ_d) is given by (Rubinstein & Colby, 2003):

$$\tau_d \approx \frac{L_{eq}^{\ 2}}{D_e} \approx \frac{\zeta b^2 N^3}{kTN_e} \tag{3}$$

Here, $D_e = {kT}/{\zeta N}$ is the curvilinear diffusion coefficient for the chains describing the motion inside the tube, with ζN as the Rouse friction coefficient, and k as the Boltzmann constant (Rubinstein & Colby, 2003).

The chain ends have random Brownian motion, which allows them to take any random path to diffuse in the surrounding melt. Once the chain reptates out of a tube segment, it is allowed to take a random walk, and a new tube segment gets formed along the chosen random path. Similarly, as the chain has a choice of random walk, it can even retract back in the tube, shortening the primitive path (McLeish, 2002). At very small time ($t \ll \tau_e$), the random motion of the chain is not hindered by the topological constraints as the presence of the tube is not yet felt by the chain. At time $t = \tau_e$, the chain starts feeling the presence of the tube (i.e., constraints around it) for the first time. This time τ_e is called the "Rouse time of entanglement strand of length $N_e b$". This is the smallest possible characteristic time for a chain confined in a tube. At any time $t > \tau_e$, the orientation of the chain is always restricted by the tube confinement until it completely moves out of the tube (McLeish, 2002; Rubinstein & Colby, 2003). The Rouse time for the entanglement strand is given by (Rubinstein & Colby, 2003):

$$\tau_e = \frac{\zeta b^2 {N_e}^2}{kT} \tag{4}$$

Thus, the relation between the reptation time and Rouse time of the entanglement strand is given by (Rubinstein & Colby, 2003):

$$\frac{\tau_d}{\tau_e} = \left[\frac{N}{N_e}\right]^3 = Z^3 \tag{5}$$

Vivoy et al. (1991) provides another similar relationship between the reptation and entanglement segment Rouse time, (which is considered as the basis for entanglement calculations in the upcoming sections), as,

$$\tau_d = 3\tau_e Z^3 \tag{6}$$

The Rouse time τ_R of the chain (for Rouse motion), which is the longest relaxation time of the Rouse model, is given by (Rubinstein & Colby, 2003):

$$\tau_R = \tau_e \left[\frac{N}{N_e}\right]^2 = \tau_e Z^2 \tag{7}$$

Here, the Rouse time of a chain is the time taken by a chain to diffuse a distance of the order of its size. The Rouse time in the later sections is also considered as the stretch relaxation time. For a chain trapped inside a tube, the ratio of the reptation time to that of the Rouse time is given as follows (Doi & Edwards, 1986):

$$\frac{\tau_d}{\tau_R} = 3Z \tag{8}$$

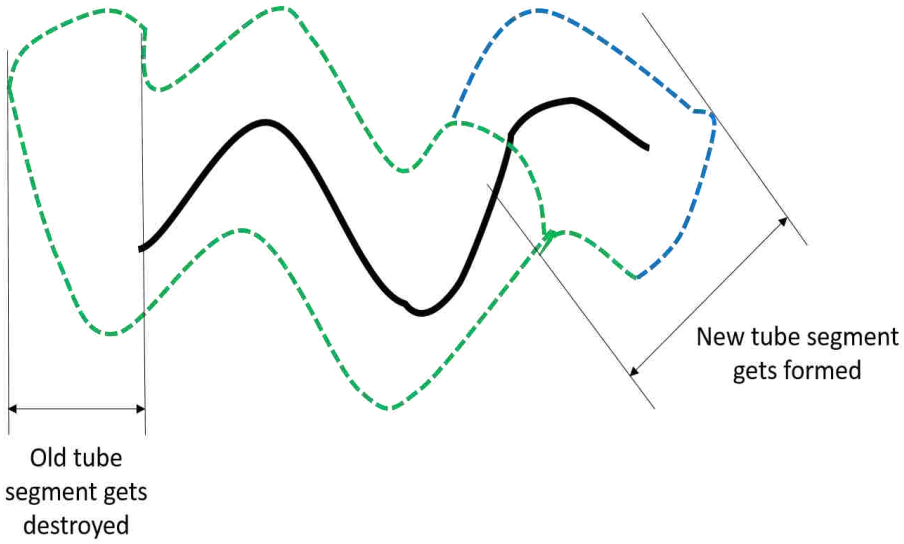

Figure 2.4. Reptative motion of the chain out of a tube causes simultaneous tube creation and destruction along the chain contour length.

In practice, the reptation time τ_d is measured experimentally as the reciprocal of the frequency at which G' = G''. The Rouse time of the chain τ_R is calculated from τ_d using equation 8 (Rubinstein & Colby, 2003; Larson, 1999).

The reptation time τ_d and the Rouse time τ_R, are the two major characteristic times considered for the constitutive "toy" models developed in the later sections. It is also important to note that for a monodisperse system with a single molecular weight component under study, there is one Rouse time and one reptation time that are widely separated numerically (i.e., $\tau_d \gg \tau_R$), as can be seen from Figure 2.5a. However, in the case of a polydisperse system, where there is more than one molecular weight component, there is more than one reptation and Rouse time, and they may overlap. The wider the molecular weight distribution, the greater the overlap, as can be seen from Figure 2.5b

(Mishler & Mead, 2013a). This concept is a crucial factor in modeling a constitutive equation for polydisperse entangled polymer systems and is discussed in detail later in Paper III.

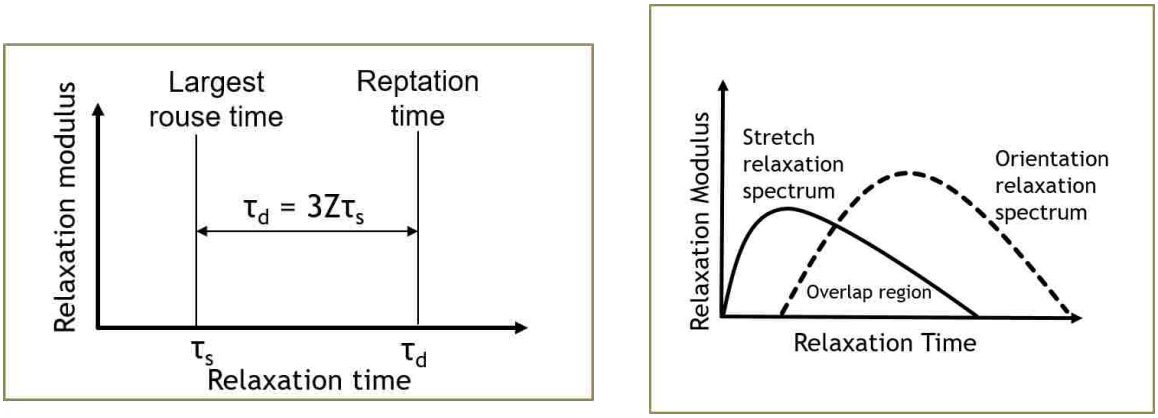

Figure 2.5. Characteristic relaxation times. a) Monodisperse entangled polymer system where the largest Rouse time and the reptation time are widely separated. b) Polydisperse entangled polymer system where the Rouse times (stretch relaxation time) and the reptation times (orientation relaxation time) overlap (redrawn from Mishler and Mead (2013a)).

2.3.2. Polymer Relaxation Mechanism. As discussed earlier, the fundamental objective of the constitutive model is to quantify the steady state or even the transient rheological behavior of the entangled polymer system. The process of reaching a steady condition, or equilibrium condition, after a deformation is called relaxation.

An entangled polymer system reaches its relaxation by a combination of a number of different mechanisms. The few major mechanisms that are included in the original Doi-Edwards' tube model are as follows (Doi & Edwards, 1986):

1. Reptation of the primary chain within the matrix of constrains.
2. Fluctuations of the primary chain length along the primitive path within the matrix of constrains.
3. Constraint release due to the motion of the surrounding chains. This causes two different relaxation scenarios (Mead et al., 1998):
    i. Relaxation by tube shortening
    ii. Relaxation by tube reorientation

Reptation of the primary chain was discussed in the previous section. The movement of an entire chain from an old tube to a new tube (both at the same energy state) completes one single process of relaxation. For high molecular weight monodisperse, linear polymer chains, reptation is the governing relaxation mechanism under low deformation conditions. Initially it was assumed that reptation was the only mechanism to describe the relaxation process. But gradually, due to discrepancies observed between predicted and experimental values, it was realized that other non-reptative processes need to be accounted for (Larson, 1999).

In polydisperse systems (a blend of two or more molecular weight components), there exist combinations of shorter and longer chains. Under any flow conditions, some of the topological constraints get removed due to shorter chains moving faster than longer chains, causing an added relaxation for the longer chain components by a mechanism called "double reptation" (des Cloizeaux, 1988; Tsenoglou, 1991). The idea behind this concept is that an entanglement or a constraint is lost if either the test chain or the matrix chain reptates past the entanglement point (Larson, 1999). Details regarding the double reptation are discussed in Section 4.

Primitive path fluctuation can be most conveniently expressed for branched polymer chains, where one end of the chain is tethered to a polymer branch point. In such cases, the chain cannot move back and forth and thus cannot reptate (Larson, 1999). Such chains relax by a primitive path fluctuation mechanism, also called breathing mode (de Gennes, 1975).

The fluctuations bring the chain ends inside the tube. As a chain end moves inside, the tube segment is vacated, and the stress on the chain relaxes (see Figure 2.6.). The free end of the chain must diffuse to the tether point for a complete relaxation, but such a condition is not entropically favorable (Larson, 1999). Thus, as the chain ends keep on moving towards the tether point, the fluctuations increases, and the time required for relaxation increases exponentially (Doi & Kuzuu, 1980). Hence, a chain that relaxes solely by primitive path fluctuations will have a spectrum of characteristic times.

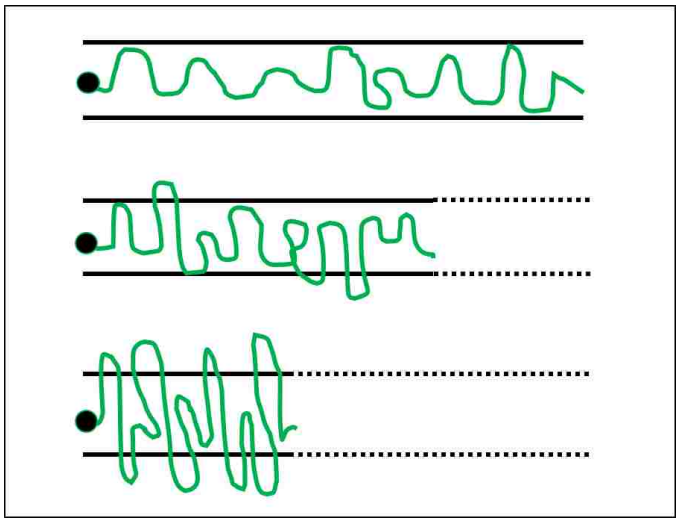

Figure 2.6. Primitive path fluctuation mechanism (redrawn from Rubinstein & Colby, 2003).

The chain segment near the end of the tube will relax fastest with the time required increasing as we move towards the interior of the chain. For the chains that can reptate (both chain ends free), the interior part of the chain will relax by reptation, which will be much faster than by primitive path fluctuations because reptation controls the longest relaxation time scale for the chain (Larson, 1999). However, the chain ends will relax faster by fluctuations than by the process of reptation. For very high molecular weight polymers, these fluctuations are generally very small and confined to a limited portion of the chain, so they can be neglected (Larson, 1999).

Constraint release is a situation in which some of the topological constraints on the test chain get removed automatically due to the flow or deformation. This allows the chain to relax much faster compared to just reptation, as a portion of the chain gets free to relax (Pearson, 1987; Mead et al., 1998; Larson, 1999). When these constraints get removed by the convective flow, it is called convective constraint release (Marrucci, 1996; Marrucci & Ianniruberto, 1996, 1997; Mead et al., 1998), which is discussed in detail in Section 3.

Now, consider a situation where the relaxation is occurring only by constraint release and there is no reptation or Rouse motion of the chain. Here, a very small time scale is considered, $t < \tau_R$, such that only localized Rouse motion and small segment re-orientation of the test chain are allowed. In such a situation, constraint release can manifest itself in two forms, and relaxation will either occur as the tube reorients itself, maintaining the chain length, or as the chain retracts back (tube shortening), keeping the same orientation as before, or it may even be some combination of the two (see Figure 2.7.) (Mead et al., 1998).

It is also important to understand that both these mechanisms relax the same amount of stress when constraint release is the only relaxation mechanism. If reptation, chain end fluctuations, and chain retraction occur along with constraint release, then the above equivalence will not hold (Mead et al., 1998). In a situation where relaxation is occurring by reptation, constraint release, and chain retraction, the orientation of the tube will be a function of both reptation and constraint release. Similarly, stretch in the tube will be defined by chain retraction, chain end fluctuations, and tube shortening. In such cases, the stress relaxed by tube shortening or changes in tube length and tube orientation will be different, and thus the equivalency is lost (Mead et al., 1998).

Constraint release can be completely neglected only in the cases where either the isolated test chain is surrounded by a matrix chain of much higher molecular weight compared to the test chain or if the matrix surrounding the test chain is cross-linked (Larson, 1999).

Many experimental observations (Lodge et al., 1990; Ylitalo et al., 1990; Kremer & Grest, 1990) have validated the presence of reptation in an entangled polymer system by the virtue of the fact that the interior of the chain relaxes much slower than the chain ends. The same experiments also verify that the entire chain relaxation mechanism cannot be explained by reptation alone. There are other relaxation processes occurring along with reptation, like constraint release and primitive path fluctuations (Larson, 1999). Further studies have elucidated that the above mentioned mechanisms are just the most basic of the processes occurring when an entangled polymer system is deforming.

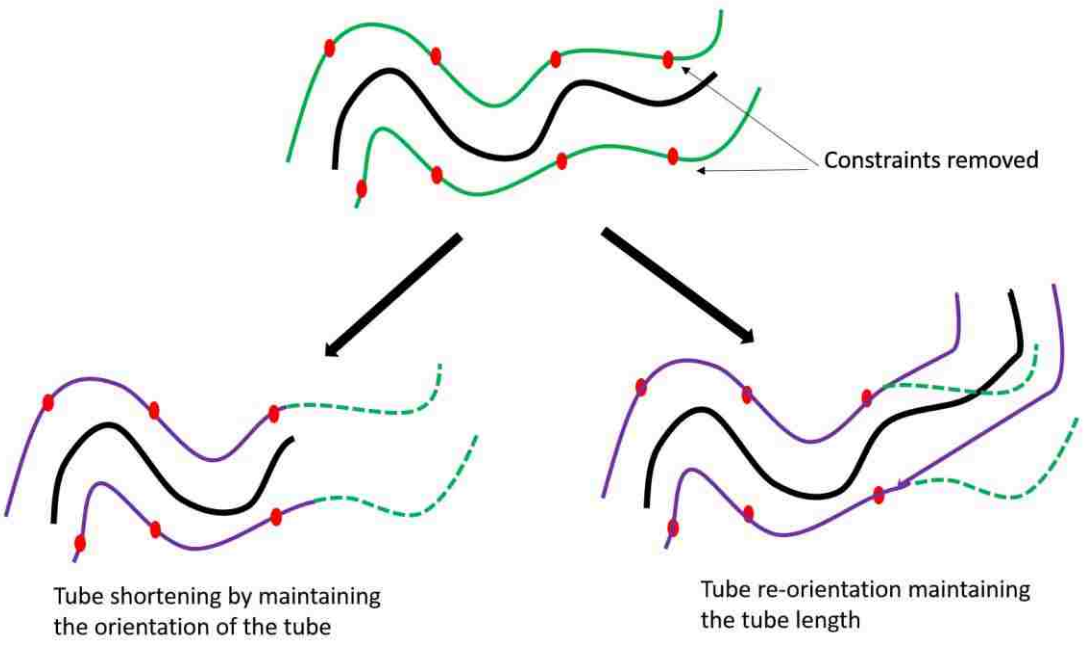

Figure 2.7. Constraint release mechanism. When constraints get removed, the chain can relax by tube shortening, by tube orientation, or by a combination of the two [redrawn from Mead et al., 1998].

There are various other physics like tube stretch or incomplete chain retraction, reduction in friction in the system due to the chain/tube orientation (configuration dependent friction coefficient), fall in number of equilibrium entanglements with deformation (entanglement dynamics), and others which need to be considered while developing the constitutive equations so as to provide accurate qualitative and quantitative descriptions of the rheological behavior (Marrucci & Grizzuti, 1988; Marrucci, 1996; Mead et al., 1998, 2015; Park et al., 2012). These topics are subsequently discussed in the later sections and Papers II and III.

3. HISTORY OF MONODISPERSE SYSTEM CONSTITUTIVE "TOY" MODEL DEVELOPMENT

The constitutive models used to study the rheological behavior of linear entangled monodisperse polymers under low and high flow conditions have evolved over time. As discussed in the previous section, de Gennes proposed the concept of reptation, which was further developed by Doi and Edwards to introduce tube theory. This theory provides the ground work for the subsequent models that have been developed in the last five of decades. Though most of the models are in excellent agreement with the linear rheological behavior of the linear entangled melts and solution, they start to differ in their nonlinear behavior predictions under high flow conditions. Nonlinear flow conditions are still not well understood and have been under investigation since last forty years.

Doi-Edwards (DE) tube model works well for all low flow deformation conditions where the behavior is predominantly linear. It is based on two major relaxation mechanisms of reptation and complete chain retraction within the constrain matrix, under affine deformation (Doi & Edwards, 1978a, 1978b, 1979, 1986). The model is also based on the assumption of a constant number of equilibrium entanglements on the chain under any flow. It also assumes that the constraints are fixed. Though the model very accurately predicts the nonlinear deformation of the linear entangled monodisperse polymer melts under step-shear strains, it fails to both qualitatively and quantitatively predict the nonlinear behavior under other forms of deformations like steady shear and extension (Mead et al., 1998). One major drawback of the theory is the mechanism of "complete chain retraction."

Under fast flow conditions, the chain starts stretching, which means that the length occupied by the tube increases above that of the equilibrium length (Doi & Edwards,

1978a, 1978b, 1979, 1986). Simultaneously, the chain is also allowed to retract back in the tube (i.e. the chain moves back along the contour of the tube). According to Doi-Edwards proposition, the chain retraction time (Rouse relaxation time τ_R) is faster than the strain rates or the reptation time τ_d. Consequently, the chain completely retracts back in the tube after getting stretched and thus maintains a constant equilibrium tube length in any flow (Doi & Edwards, 1978a, 1978b, 1979, 1986; Mead et al., 1998; Larson, 1999). This resulted in the over-prediction of the steady shear thinning behavior for the linear polymer melts and a failure to quantitatively predict the overshoots observed in the transient first normal stress difference curve.

The next improvement in the model, called the Doi-Edward-Marrucci-Grizzuti (DEMG) model, was brought about by Marrucci and Grizzuti in 1988. They modified the chain retraction concept (keeping the assumptions of a constant number of equilibrium entanglements and fixed constraints), and initiated that the retraction process is gradual and incomplete. This implies that there is a finite amount of chain stretching observed above the equilibrium chain length (Marrucci & Grizzuti, 1988; Mead et al., 1998). This concept should have improved the results compared to the DE model, as chain stretching should have increased the predicted shear viscosity. But the entire physics of the model was such that under high shear flow, the tubes got highly oriented in the direction of the flow, causing a loss in the drag. This caused a collapse in the tube stretch effect, lowering the viscosity and reducing the results to same as that of the DE model prediction (see Figure 3.1.) (Larson, 1999; Mead et al., 1998, 2015).

Nevertheless, the tube stretching did improve the overshoot predictions for the first normal stress difference and shear stress. The model also failed to predict the monotonic

extension thinning behavior observed for melts (see Figure 3.2.) (Mead et al., 2015). Both DEMG and DE also predicted that with increase in molecular weight, the melt shear viscosity decreases with increase in high shear rate, under shear thinning regime; which is contrary to the fact that at high shear rates, the shear viscosity is a very weak function of molecular weight (Mead et al., 1998). Thus, even though the physics behind the theory was improved, the DEMG model still could not improve the predictions for steady shear and steady extensional viscosities over that of the DE model. The simplest constitutive equations for the above concept were presented by Pearson et al. (1991).

In 1996 Marrucci, Ianniruberto and Marrucci (1996), introduced another concept called convective constraint release (CCR). Under slow flow, constraint release may not be of much consequence, but under fast flow conditions (at strain rates greater than $1/\tau_d$) by the virtue of the flow itself, some of the topological constraints around the primary chain get removed automatically. In this case, the assumption of fixed tube no longer holds true. This allows the chain to relax much faster compared to relaxing just by reptation. The simplified models developed by Ianniruberto and Marrucci (1996), using the concept of CCR, are based on an assumption that all parts of the molecule experience the same orientation and degree of stretch. One important fact that needs to be elucidated is that not all types of convections can release constraints. If the system is affinely deformed in such a way that all the chains have the same deformation, then both the primary chain and the surrounding matrix chains will deform together. Hence, there will be no constrain release (Ianniruberto & Marrucci, 1996; Marrucci & Ianniruberto, 1997). Thus, the convective constraint release occurs only when the matrix chains around the primary chain are undergoing retraction. As the length of matrix chains reduces, the constraints on the

primary chain get removed. New constraints replace the old ones, but during the process of replacement, the primary chain relaxes (Ianniruberto & Marrucci, 1996; Larson et al., 1998; Mead et al., 1998). To account for the relaxation by constraint release, Ianniruberto and Marrucci (1996) considered time-dependent tube diameter. The reduction in bond orientation order caused by constraint release is accounted for by increasing the tube diameter and thus reducing the length of the primitive path of the tube (Ianniruberto & Marrucci, 1996; Marrucci & Ianniruberto, 1997).

Mead, Larson, and Doi (1998) developed the MLD "toy" model, which is an improvement of the DEMG model, and incorporated the mechanism of CCR into it. The MLD model also allows relaxation of chain ends to occur by fluctuations and improved on the concept that both the chain orientation and degree of stretch are functions of tube coordinates (based on contour variable theory), thus removing the assumptions made by Ianniruberto and Marrucci (1996) in the previous CCR models. The MLD "toy" model like its predecessors, is based the concept of a constant number of equilibrium entanglements, as any entanglement dissolved is immediately replaced by a new one (Mead et al., 1998). Depending on the tube stretch conditions, the CCR effect will manifest itself in either tube orientation or tube shortening.

If the chain is stretched beyond the equilibrium condition ($\lambda > 1$), then it is unable to explore the entire volume of the tube, and constraint release will cause tube shortening. On the other hand, for chains not under tension ($\lambda = 1$), the chain will be slack enough to explore the tube volume and thus allow it to escape the tube, leading to tube reorientation (Mead et al., 1998).

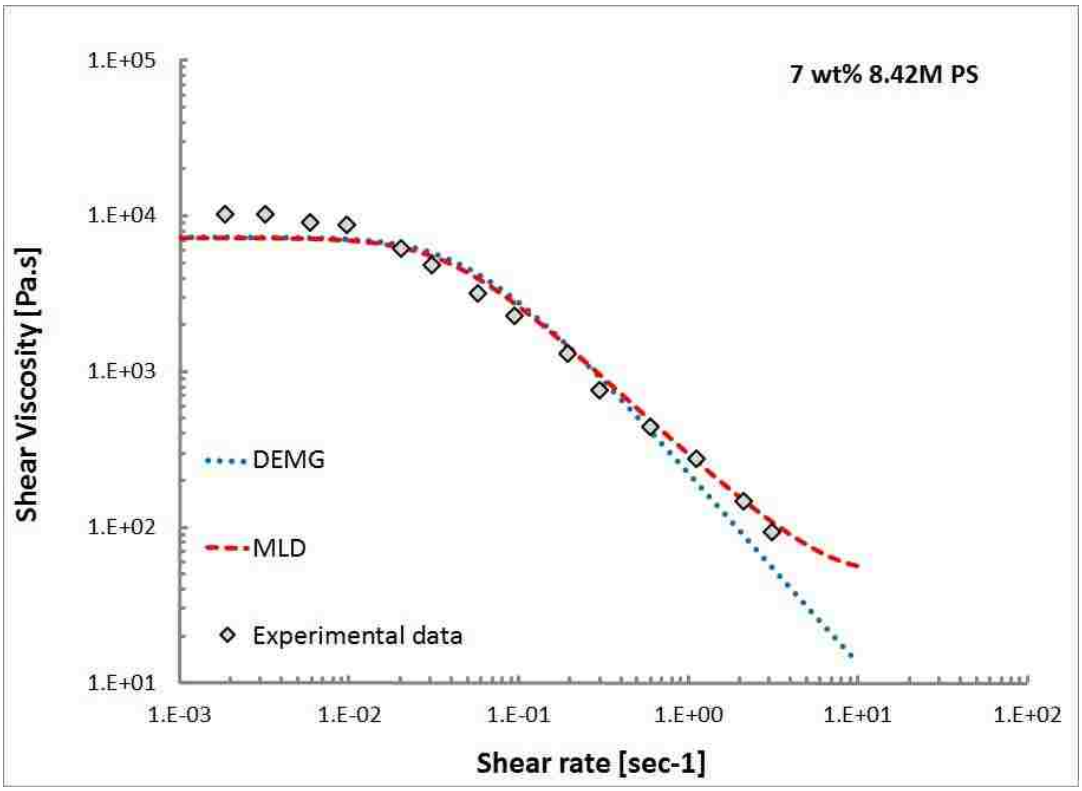

Figure 3.1. Steady shear viscosity vs shear rate curve showing DEMG, MLD, and experimental results for 200KPS monodisperse melt. DEMG over-predicts the shear thinning behavior, where the MLD model has an improved prediction due to the effect of CCR incorporated in it (Mead et al., 2015).

The MLD "toy" model definitely improved the predictions for the steady shear viscosity for linear monodisperse entangled melt, as can be seen from Figure 3.1., confirming that CCR is an important physics to describe the shear system at high deformation condition. The effect of CCR is prominent before the tube starts stretching. Contrariwise, as can be seen from Figure 3.2., the MLD "toy" model, similar to DEMG model, could not predict the extension thinning behavior of the monodisperse melt (Mead et al., 2015). From this one may conclude that CCR effect may not be the physics to define the extension thinning observed at high deformation rates.

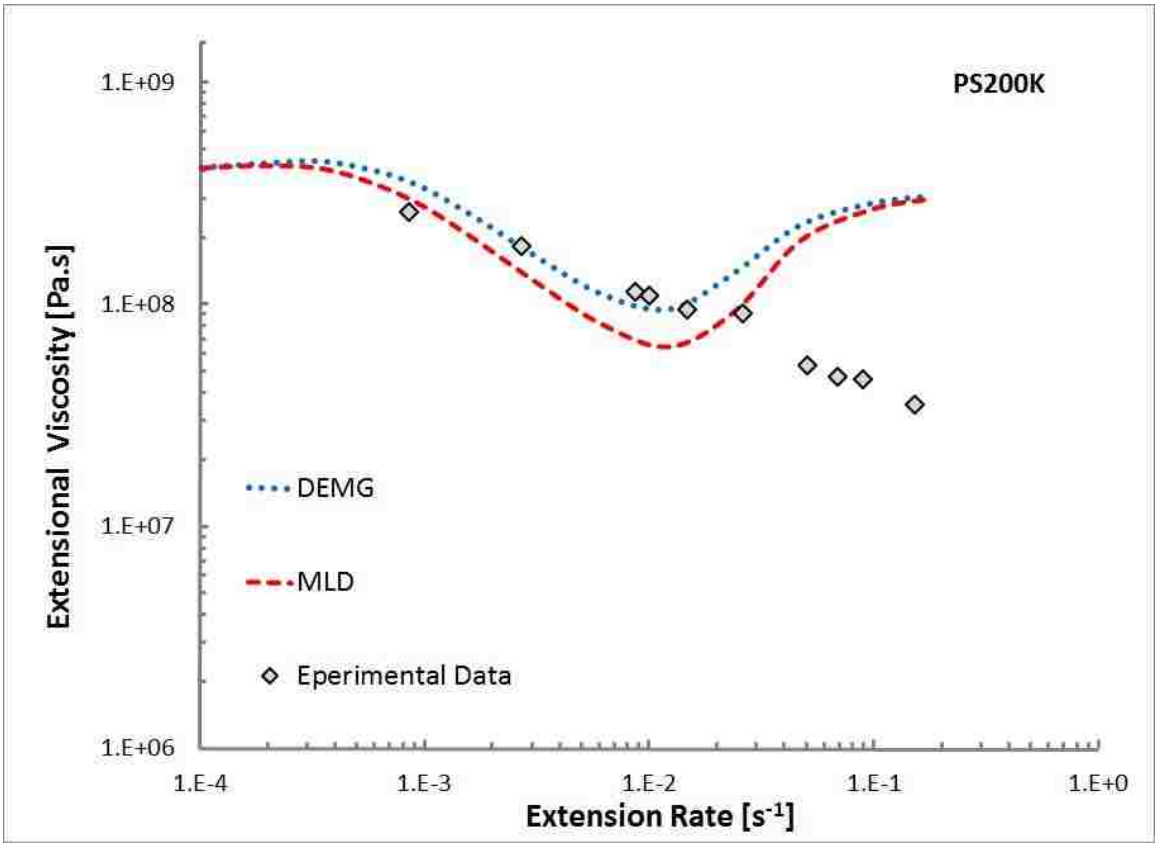

Figure 3.2. Steady extensional viscosity vs extension rate curve showing DEMG, MLD, and experimental results for 200KPS monodisperse melt. Both DEMG and MLD predict an extension thickening behavior under high extension conditions, where experiments show an extension thinning behavior (Mead et al., 2015).

Though the steady shear behavior has been explained using the MLD model by incorporating CCR, the steady extension melt thinning related issues have not yet been dealt with. In 2012, two independent research groups working on two completely different approaches to tackle the extensional entanglement polymer rheology issues (Park and group using stochastic simulation and Yaoita et al. using the tube theory way (Park et al., 2012; Yaoita et al., 2012)), proposed similar concept called the configuration dependent friction coefficient (CDFC).

The idea of CDFC was initially developed by Ianniruberto et al. when it was proposed that when the stretch and orientation of the chain occurs, there will be a loss of monomeric friction ζ (Ianniruberto et al., 2012). MD simulations and recent experimental studies have also validated the presence of reduction in the friction factor when the polymer system is highly stretched and oriented (Andreev et al., 2013; Wingstrand et al., 2015). Yaoita et al. then validated that the friction coefficient as a function of stretch/orientation factor $\zeta(F_{SO})$ remains at equilibrium when (F_{SO}) is increased to a certain threshold value ($\approx$ 0.15), after which it starts steeply decreasing with a further increase in the stretch/orientation factor. Here $(F_{SO}) = \overline{\lambda^2}\bar{S}$, where $\bar{\lambda} = \frac{\lambda}{\lambda_{max}}$ and $\bar{S}$ are the averaged anisotropic orientation of all components (Yaoita et al., 2012, 2014).

When incorporated in the constitutive MLD equation, they showed that a reduction in the friction coefficient can very much be the reason for the observed steady extension thinning behavior in linear polymer melts when the system is highly stretched and orientated (Yaoita et al., 2014). In their stochastic simulation, Park et al. also verified that CDFC is definitely the key to the extension thinning behavior of the linear polymer melts at high extension rates (Park et al., 2012). Further discussion on CDFC and how the concept is incorporated in describing the constitutive equations is taken up in Paper II.

The new constitutive "toy" model called the Mead-Banerjee-Park (MBP) monodisperse model and developed by the authors, is a modification of the MLD "toy" with the incorporation of two major concepts: a) CDFC and b) entanglement dynamics (ED). Until now, all the major modified tube models that have been developed were based on the assumption of a constant number of entanglements, irrespective of the flow.

The models assumed that with CCR when the entanglements get destroyed new entanglements take its place and thus the total number of equilibrium entanglements remain fixed. But under fast deformation when the strands are unraveling, orienting and getting stretched, the number of entanglements on the chain cannot remain fixed. The same phenomenon was also observed by Baig et al. (2009) in their Brownian dynamic simulation of entangled linear polymers. Thus the above assumption was modified in the new model to define an idea of entanglement dynamics where the number of equilibrium entanglements on the chain alters with deformation (Mead et al., 2015). Details regarding the model development, simulations, and results are presented in Paper II.

4. HISTORY OF POLYDISPERSE SYSTEM CONSTITUTIVE "TOY" MODEL DEVELOPMENT

Similar to the model development discussed for the monodisperse systems the polydisperse constitutive "toy" model development also starts with Doi and Edwards' tube model as the base. The DE model failed to describe the polydisperse conditions because of its assumption that the constraint matrix around the test chain is fixed (single reptation of only the test chain). This implies that the movement either by reptation or chain retraction occurs only in the primary chain (Doi & Edwards, 1986). As pointed out earlier, in a polydisperse system, more than one molecular weight component is blended together; consequently, there will be complex entanglements of shorter and longer chains. Each of these chains will have its own reptation and Rouse time of motion, and thus, the entanglements will also have different lifetimes. The entanglements of long-short chains will dissolve much faster than long-long entanglements as the short chain moves faster than the long chains. Thus, this will allow the long chains to relax faster by constraint release (Larson, 1999; Auhl et al., 2009; Mishler & Mead, 2013a, 2013b). In such a scenario it is erroneous to assume that the matrix chain that creates the constraint around the test chain is constant.

A semi-empirical concept of "double reptation" was proposed and implemented by multiple researchers to overcome the incongruity of Doi and Edwards' model (Rubinstein & Colby, 1988; Tsenoglou, 1987, 1991; des Cloizeaux, 1988, 1990). Applications of monodisperse models to polydisperse systems have always proven to be difficult, due to their inherent complexities, and the double reptation model has proven to be one of the most successful models to describe polydispersity in recent times.

The idea in a simplistic approach can be thought of as a combination of reptation and constraint release. According to this proposed theory, the test chain and the surrounding chains are allowed to reptate together. The proposed theory provides accurate predictions of G' and G'' for a specified molecular weight distribution, for both bidisperse and polydisperse systems (Wasserman & Graessley, 1992). Another positive feature of this model is that it has no added parameters over the original DE model (single reptation). The inversion of the double reptation mixing rule could also be used to generate the molecular weight distribution of the system, analytically and numerically, from its rheological behavior as described by Mead (1994).

The MLD "toy" model for monodisperse systems was modified based on binary interaction theory and generalized double reptation with a slip-link entanglement survival probability equation to account for polydispersity (Mead et al., 1998; Mead, 2007). Although the model could successfully predict some of the polydisperse rheology behavior, the physics behind the system was not sound. It was mostly based on the idea that the basic underlying physics in monodisperse and polydisperse systems are same and thus can be easily generalized without adding any new mechanism. The complexities behind the entanglements present and their probable effects on the entire system were not considered important (Mishler & Mead, 2013a).

In 2009, Auhl et al. made an effort to explain the behavior of bidisperse polyisoprene (PI) systems under uniaxial extension using a concept of nested tube (Auhl et al., 2009). The major motivation behind the theory is the fact that in polydisperse system, multiple constrain release rates exist and that the elongation hardening that is observed (deviation from linear viscoelastic behavior) is related to the long chain component's

stretch relaxation. Consider a bi-blend (same material) system of widely separated molecular weights mixed together such that there are two types of chains in the blend: long chains and short chains. This implies that there are four major types of entanglements present in the system: a) long-long, b) long-short, c) short-long and d) short-short. Thus, for the long chains, the two types of entanglements will have two different constraint release rates, and the long-short will dissolve faster than long-long.

Thus, one can imagine (see Figure 4.1.), two tubes around the long chains with the thin tube defined by all the entanglements and the thick tube given by only the long-long entanglements. The presence of the short chain component is considered to create a dilution effect, and thus their entanglement effects are not considered. The long chain component and the effect of short chain dilution on the stretch relaxation are analyzed and are believed to be responsible for the stress generated in the system. The presence of short chains and the stress related to them are neglected as they are considered to provide the dilution effect only (Auhl et al., 2009).

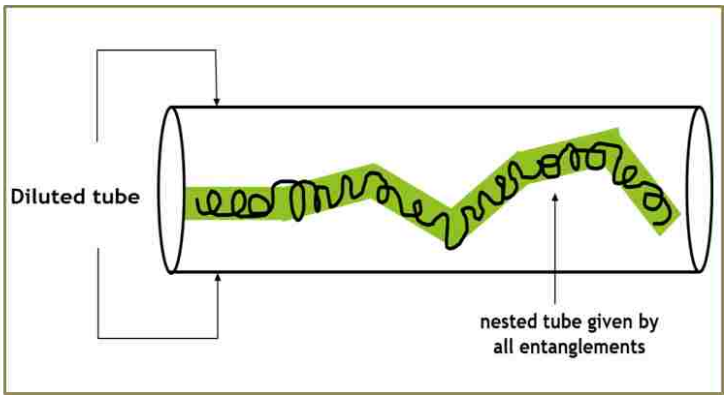

Figure 4.1. Nested tube model proposed by Auhl et al. (2009). The primary tube is defined by all the entanglements whereas the diluted tube is given by only the long entanglements

Similar to nested tube model of Auhl et al., the "diluted stretch tube model" was defined by Mishler and Mead to describe polydispersity (Mishler & Mead, 2013a). The difference between the two models is how the tubes are defined and the generated stress calculation method. According to the diluted stretch tube model, the primary tube (or the thin tube) is given by all the entanglements that exist in the system. If we consider the same system as Auhl et al. (2009), which has long and short chain components with long-long, long-short, short-long, and short-short entanglements, then the primary/thin tube is defined by all four types of entanglements (see Figure 4.2.). On the other hand, to define the diluted tube, there is a criterion. All those entanglements, that have a reptation time that is much larger than the Rouse time of the primary chain are considered viable $\frac{{\tau_{s_i}}^{eff}}{\tau_{d_j}} \ll 1$, $({\tau_{s_i}}^{eff} = \frac{{\tau_{s_i}}^{1}(t)}{\Psi_i})$. The diluted tube is defined only by the viable entanglements.

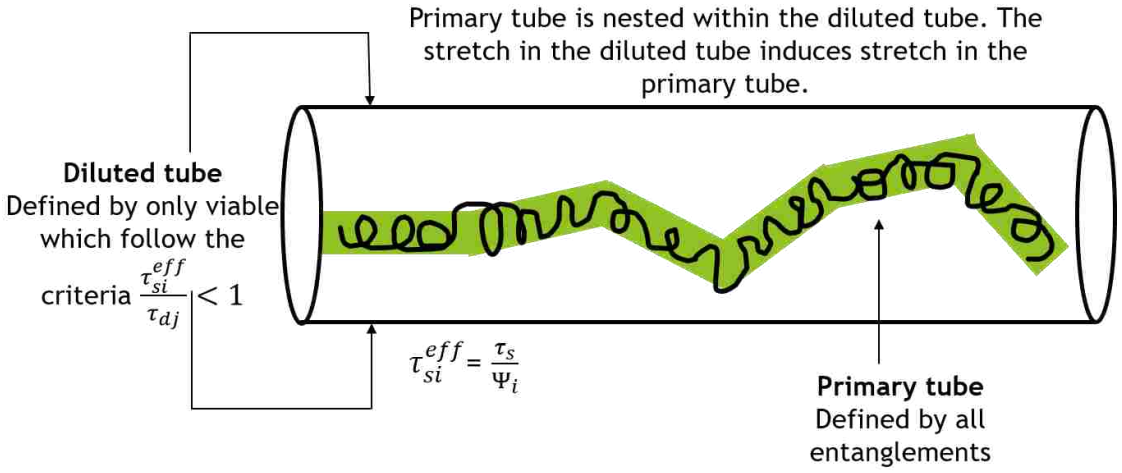

Figure 4.2. Diluted stretch tube model proposed by Mishler & Mead 2013a. [Redrawn from Mishler and Mead, 2013a]. The primary tube is defined by all the entanglements whereas the diluted tube is given by viable entanglements given by the criterion. The unviable entanglements behave like solution.

Those entanglements that have an average lifetime less than the effective Rouse time of the test chain $\frac{\tau_{s_i}{}^{eff}}{\tau_{d_j}} > 1$, ($\tau_{s_i}{}^{eff} = \frac{\tau_{s_i}{}^{1}(t)}{\Psi_i}$) act as a solvent with respect to the stretch relaxation process. The major factor behind the criteria is that the chains have different lifetimes, and there are constraints that move away much faster than the primary chain Rouse motion, thus not effecting the stretch dynamics of the primary chain. The stretch generated in the diluted tube is coupled with that of the primary tube, and the stress is given by all the entanglements that are present in the system, and not only by the ones that define the diluted tube (Mishler & Mead, 2013a, 2013b).

The MBP polydisperse model is based on the concept of “diluted stretch tube” theory incorporated in the MBP monodisperse model. Thus the MBP “toy” model for the polydisperse system will have the same physics of CCR, ED and CDFC as that of the monodisperse condition along with stretch tube dilution. The details regarding the constitutive model development, simulation, and results are discussed in Paper III.

PAPER

I. Modeling and simulation of biopolymer networks: Classification of the cytoskeleton models according to multiple scales

Abstract

We reviewed numerical/analytical models for describing rheological properties and mechanical behaviors of biopolymer networks with a focus on the cytoskeleton, a major component of a living cell. The cytoskeleton models are classified into three categories: the cell-scale continuum-based model, the structure-based model, and the polymer-based model, according to the length scales of the phenomena of interest. The criteria for classification of the models are modified and extended from those used by Mofrad [M. R. K. Mofrad, *Annual Rev. Fluid Mech*. 41, 433 (2009)]. The main principles and characteristics of each model are summarized and discussed by comparison with each other. Since the stress-deformation relation of cytoskeleton is dependent on the length scale of stress elements determines, our model classification helps systematic understanding of biopolymer network modeling.

INTRODUCTION

Recent studies in the field of medicine have elucidated the need to understand how the structures of biopolymers and the various physical forces acting on them contribute to the synthesis, growth, transportation, information processing and functioning of living cells and tissues. Many of these forces and their effects have been identified and studied, such as hemodynamic shear stress on vascular tissues, inspiratory pressure on lung functions, tension on skin ageing etc. [1]. In addition, numerous diseases, including tumours, lung cancer, emphysema, neuro-degeneration, pulmonary fibrosis, etc. [2-4], have been associated with the change of these physical forces and, subsequently, the biopolymer structures. These physical forces have also been found to be vital for cellular and genetic regulation in the living body [5].

Living cells dynamically respond to any mechanical perturbations in their environment solely by altering the cytoskeleton configuration and functioning [6, 7]. The cytoskeleton is a network of protein tubules present inside a cell, and is responsible for cellular structure, shape, movement and growth. Cells are adhered to a scaffold called the extra-cellular matrix. During the process of cell growth and movement, the cellular forces in the scaffold and inside the cell are balanced by the cytoskeleton [8-11]. Even the interactions between two adjacent cells are affected by the mechanical behavior of the cytoskeleton [12]. Thus it is imperative to identify the various mechanical forces and analyze their effects on the structure and behaviors of the cytoskeleton in order to understand cell functioning and abnormalities. This knowledge will lead to a better understanding of the causes of disease and corresponding cures.

There have been numerous efforts to model the relationships between the structure of the cytoskeleton and its rheological properties and mechanical behaviors. However, due to the cytoskeleton's complex structure and heterogeneous components, no single approach has been able to accurately encompass all of its various behaviors. As shown in Figure 1, the cytoskeleton network is composed of three main highly entangled protein structures: actin filaments, microtubules and intermediate filaments. These components together are responsible for the properties and mechanics of the cells [13].

The actin filament (or F-actin), a filamentous form of monomeric G-actin protein, is the major component of the cytoskeleton, comprising up to 10% of the total cellular protein mass [14]. It has a persistent length about 15 – 17 μm [15]. The F-actin further cross-links to create a bundle or an orthogonal cytoskeleton network structure by the cross-linking of actin binding proteins [15-21]. The F-actin filaments are also continuously undergoing polymerization and depolymerization, leading to an active network structure [15, 22-24]. These cross-linkers and the degree of crosslinking also lead to strain stiffening behavior exhibited by the F-actin [13, 25].

Microtubules, the second major component of the cytoskeleton network, exhibit hollow cylindrical shapes composed of monomers α and β – tubulin with persistent lengths of 6 mm [13,15]. They have higher bending stiffness, are more active in nature than actin filaments, and continuously undergo polymerization and depolymerisation [25, 26]. The microtubules are known to be the compressive load-bearing component of the network as balanced against the tensed actin and intermediate filaments [27].

The intermediate filaments (persistence length ~ 1 μm) are the least well studied of the three components of cytoskeleton [13,15]. They, along with F-actin, act as the tension-bearing components under deformation and have a rope-like structure consisting of different proteins [12-13, 25]. They are more stable compared to F-actin and microtubules and can withstand higher stresses and strains before rupture [25].

The dynamics and properties of the cytoskeleton result from the collective actions of the aforementioned components at various time and length scales. Therefore, successful modeling of the cytoskeleton requires proper approximation of the behaviors and properties of those structural elements for the time and length scales of the phenomena of interest. The length scale is important for thermal and mechanical effects. However, biological effects or structural reorganization (including polymerization/depolymerization) must consider both length and time scales. For example, the stress-deformation behaviors within a time scale range where there is no structural reorganization or polymerization/depolymerization are referred as "passive dynamics," whereas "active dynamics" are related to biological responses at longer time scales [13].

This review paper classifies numerous analytical and numerical models used to analyze cytoskeleton behaviors and properties into three groups according to length scales: *cell-scale continuum-based models*, *structure-based models*, and *polymer-based models*, as shown in Figure 1. We focus on models used to analyze the passive dynamics of the cytoskeleton. Length scales of individual cell mechanical properties range from atomistic to the macroscopic cell level. It is also noteworthy that we exclude models that work at the scale of collective cell motions (> 10 μm).

Our classification is adapted from that used by Mofrad's review in 2009 [13]. Models, which describe the dynamic behaviors of a single cell as an elastic continuum medium, are classified as "cell-scale continuum-based models". Mofrad named similar models "continuum-based models", but we add "cell-scale" (typically around 10 μm [28]) to distinguish them from continuum approaches at smaller scales [28]. "Structure-based models" elucidate cytoskeleton properties with discrete representative volume elements (RVE) which approximate the stress-deformation relationship among structural components (typically between 1 and 10 μm [28]). As this model name was used in Chen's review in 2014 [29], these models encompass the groups of "tensegrity models" as classified in Mofrad [13], the models reviewed by Chen and co-workers in 2012 [30], and the continuum polymer network models summarized in a review by Unterberger and Holzapfel in 2014 [28]. The "polymer-based model" explains the cytoskeleton properties in terms of polymer network structures (typically around 1 μm [28]) or a single polymer molecule (less than 10 nm [28]), as in Mofrad [13].

Many reviews have summarized various models for cellular and cytoskeleton dynamics using different approaches. As mentioned, Mofrad provided a unified insight into the overall cytoskeleton rheology and experimental techniques [13]. However, additional structure-based and polymer-based models have subsequently been added to other reviews. Chen and co-workers summarized models by focusing particularly on the structure-based models [30]. Chen's review classified models into continuum-based and structure-based models. However, the author specifically arranged continuum-based models related to indentation experiments into another separate group: nanoindentation models. [29]. Nava and co-workers [31] and Moeendarbary and Harris [32] have unified various models

ranging from cell mechanics (>10 μm) to cytoskeleton behaviors (~1 μm). The former, which is mostly related to mechanics of adherent cells, proposed a model classification that included only continuum-based models and structure-based models (they used terms of continuum model and microstructural model). The latter models depict various cell phenomena at different time scales and length scales (but do not provide much detail on cytoskeletons). There were other reviews [28, 33, 34] which mainly emphasized polymer-based models (from molecular level to network scale), but did not provide much discussion of cell-scale and structure-based models.

Our aim is to provide a systematic understanding of cytoskeleton models in terms of length scales, which determine the stress-deformation relation of the cytoskeleton. This paper summarizes the underlying principle, main application, and advantages and disadvantages of cytoskeleton models in each classified length scale group.

CELL-SCALE CONTINUUM-BASED MODELS (~10 μM)

The cell-scale continuum-based models describe the mechanical/rheological behaviors and properties of a cell at cellular length scales (typically ~10 μm), which is larger than the typical distance between different cell components [28]), by assuming that cell cytoplasm is a homogeneous and continuous medium. These models are usually used for the simulation of cell motions (migration, spreading, etc.) or experiments for cell property measurements [35]. Based on the level of simplification and the behaviors of interest, these models can be further classified into elastic/viscoelastic models, multi-phasic models and soft glassy models.

1. Elastic/Viscoelastic Models

Elastic/viscoelastic continuum-based models utilize Cauchy's momentum equation as well as constitutive equations that represent the stress-strain behavior of the cytoskeleton as a homogeneous elastic or viscoelastic medium [13]. A cell cytoplasm is discretized into small computational units (mesh) to solve those model equations by the finite element method with necessary boundary conditions. The major application of this approach is for analysing and evaluating the cells' experimentally measured *in vivo* and *in vitro* force levels and their effects on cell behaviors [36]. It gives adequate results when measuring the cell deformation macroscopically [37, 38].

These models are classified into elastic models or viscoelastic models depending on the dynamic time scale of the cellular behavior of interest [13]. An elastic model is sufficient to describe small deformations following Hook's law, whereas a nonlinear elastic

model, such as the Gaussian model, is required for larger deformations [29]. However, the elastic models are only suitable for modeling cell material properties and cell dynamic behaviors at limited time scales (near equilibrium) due to their oversimplification [29, 31].

The time-dependent stress-strain behaviors can be described by the viscoelastic models that utilize typical viscoelastic constitutive equations, such as typical or modified Maxwell model [31, 32]. Viscoelastic models have been able to predict the cellular mechanics for blood cells, which are under continuous shear and high mechanical perturbations, as well as for adherent cells such as epithelial and endothelial cells [39]. Recently, a 2D viscoelastic model was used to simulate cell migration in a microchannel [39]. A recent 3D constitutive model was extended to simulate lipid bilayer-cytoskeleton coupling in an erythrocyte membrane [40].

2. Multiphasic Model

The multiphasic continuum model was first proposed by Guilak and co-workers, based on the idea that the viscoelastic behaviors of cells can be attributed to the intrinsic viscoelastic property of the cytoskeleton (solid phase in cytoplasm), the fluid viscosity of the interstitial fluid (cytosol: water with ions), and the solid-fluid interaction within a cell [41]. The basic approach of the biphasic cell model [42] can be extended to a more realistic physical representation of a cell by adding more phases. Therefore, the biphasic approach requires constitutive stress-strain equations in each phase as well as additional momentum and mass conservation equations over those phases. For example, the triphasic model considers a viscous liquid phase, an elastic solid phase, and an ionic phase, where two

stress-deformation equations are required for the liquid and solid phases and an additional equation exists for the osmotic pressure in the ionic phase [43, 44].

Time or deformation rate-dependent response to stress can be described by the poro-elastic or poro-viscoelastic concept, which views the cytoplasm as a wetted porous solid [45-47]. Under this context, the cell viscoelasticity is a measure of the time scale (function of the poro-diffusivity, which is proportional to a combined variable of elastic modulus of the solid phase, porous size, and the fluid phase viscosity) needed for redistribution of the intracellular fluids and cell response under mechanical perturbations. As the poro-diffusivity increases, the relaxation of the cell gets faster [32].

Combination of the above models with the structure-based models can be used to study the phase interactions and cell mechanics. The multiphasic approach can more accurately predict the cell rheological behaviors, such as creep response of the cell [48] and the chondrocyte mechanics [49]. However, one of the major disadvantages of these models is the increased number of estimated parameters and the increase in complexity of the model [32,41].

3. Soft Glassy Models

The soft glassy rheology model [50, 51] (also referred as power-law rheology [29]) was initially proposed by Sollich and co-workers [52, 53], describing soft glassy materials with weak dependence of storage (G') and loss (G") moduli on frequency, ω. Soft glassy materials generally have a disordered structure of aggregated discrete components (e.g. foams, pastes, and colloids, etc.) that interact weakly. They usually have low moduli in the

range of Pa to kPa, and are not thermodynamically stable. Based on the above observations of the resemblance of the cytoskeleton to soft glassy materials, the soft glassy rheology was proposed as another interpretation of the continuum-based cytoskeleton model to elucidate how the macroscopic cellular response is related to the localized structural rearrangements caused by meta-stability and disordered structure [32, 50, 51]. This model can adequately predict the frequency dependency of elastic and loss moduli for all animal tissue types, including the smooth muscles in human airway, endothelial and epithelial cells, for a wide time range of ~0.001 – 100 sec using a universal parameter called a noise temperature. However, microscopic interpretation of this parameter has not been performed [50].

4. Discussion of the Cell-scale Continuum-based Models

The aforementioned cell-scale continuum-based models have been widely used for simulation of whole cell behaviors as well as for cell material property experiments. According to the conditions of the behaviors of interest, different models can be chosen. For example, even for simulation of the same micropipette aspiration experiments, different models have been chosen according to the ranges of deformation and time [48,54,55].

There are some major disadvantages with all of the above continuum-based models. Firstly, these models emphasize macroscopic cellular behaviors and dynamics. Microstructure and individual cytoskeleton component behaviors are not considered by approximation at the continuum level. For example, the effects of actin cross-linkers, thermal fluctuations, and polymerization/depolymerization are neglected. Therefore, the

interpretation of the molecular level interactions is not allowed. Additionally, the macroscopic models cannot predict and understand the pre-stressed phenomenon observed in the cytoskeleton network [56]. The structure-based models and the polymer-based models, which will be discussed in the subsequent sections, portray a better understanding of cytoskeleton properties and behaviors from a microstructural point of view.

STRUCTURE-BASED MODEL (1~10 μM)

Structure-based models utilize discrete structural elements, which represent the individual stress-strain relationships among the microstructural components of the cytoskeleton, to describe the rheological properties and mechanical behaviors of the cytoskeleton [29, 32]. Since the heterogeneity of the cytoskeleton is considered through the microstructural stress elements, these models can describe some cell behaviors that cannot be simulated by the cell-scale continuum-based models, such as stability of the cell shape and cell stiffness [56]. The structure-based models can be further categorized into two groups: the pre-stress (pre-existing tensile stress) models and the semi-flexibility models. Pre-stress models, which include the cortical membrane model, the tensed cable nets model, and the tensegrity (cable and strut) models, consider pre-stress in the intercellular force balance to predict cell shape [56]. Note here that some reviews, such as by Mofrad [13], named all pre-stress models as tensegrity models. Semi-flexibility models include open cell foam models, the semi-flexible network element model ('element' is added to be distinguished from other polymer-based network models), and continuum polymer network models, which utilize RVE to the represent coarse-grained semi-flexible actin network [30]. The pre-stress model is important because it is known that the pre-stress is related to the cell shape stability and the cell stiffness [56]. The semi-flexibility model relates the bending ability of actin filaments with cell behaviors, such as strain hardening [30, 31]. Since the stress elements of these models consider the cytoskeleton components, the element length scales are considered to be smaller than cell scale (<10 μm) [28]. However, since the stress element is still an imaginary representation of the actual polymer network, the element length scale is considered to be larger than the polymer network scale

(>1 μm) [31, 56]. These models consider affine approximation (local deformation is the same as the macroscopic deformation) of the discrete elements, allowing continuum interpretations of the deformations, resulting in less numerical and computational complexity than the polymer-based models [56].

1. Cortical Membrane Model

This model assumes that the stress bearing elements of the cytoskeleton are restricted within a thin or several thin distinctive cortical layers with the stress balanced either completely by the pressurized cytoplasm itself, or by the cytoplasm and extracellular matrix together [57]. This model can also predict the linear stress and cell stiffness relationship and give a good approximation for suspended cell (e.g. blood cells) and non-adherent cell behavior [58, 59]. The major disadvantage of this model is that its primary assumption, that the resistance to cell shape alteration is provided by a thin cortical layer, cannot be applied to adherent cells [60]. Thus, the limitation of this model inspired the shell-like 3D pre-stress models in the next section [30, 56].

2. Tensed Cable Nets Models

This concept models a network completely constituted of tensile cable elements (linear-elastic springs) without the balanced compression in the microtubules. The pre-stress is maintained and supported by the external extracellular matrix. The model predicts a linear relationship between stiffness and stress when the cable tension is constant; otherwise, the trend is non-linear [56]. As in the cortical membrane model, the pre-stress in the cortical membrane can be simulated with 2D tensed cable nets [59, 61, 62]. One

example of a typical 2D cable net (reinforced squared net) is shown in Figure 2. In the case of the behavior of suspended cells, such as blood cells, this model provides very good agreement with the experimental observations; however, the behaviors of adherent cells, such as cell spreading and cell migration, require more complicated 3D models for better simulation [30, 56].

The 3D tensed cable nets models construct 3D cable networks with uncrossed free-sliding joints as well as pin joints [63, 64]. The pre-stress is equal to the sum of all the tensile forces in the cables across a cross-sectional area [63, 65]. This model is also able to predict some of the mechanical properties, such as Young's modulus, of the cytoskeleton and has good accordance with micropipette aspiration experiments. It also provides better interpretations of cell mechanics compared to the open cell foam models, which will be introduced later. [30]. Major disadvantages with the model are that they do not include anything about compressed microtubules and still have limited ability to predict the behavior for adherent cells [27, 31, 56].

3. Tensegrity (Cable-strut) Models

The tensional integrity, or tensegrity, model employs a discrete network of self-stabilizing pre-stressed tension bearing components (actin and intermediate tubules) which are balanced by locally compressed units (microtubules), each subjected to mechanical equilibrium and geometric deformation [10, 27, 66]. *In vivo* probing has elucidated that the actin filaments are the stiffest of all cytoskeleton components with a linear shape, whereas the microtubules appear curved. Thus, the principal assumption of this model is that actin and intermediate tubules are the stress bearing components but the microtubules resist

compression, which is in accordance with the above observations [10, 67, 68]. The stress element of this model is based on variations of R. Buckminster Fuller's tensional integrity structure, proposed in 1961 [69]. This model describes a network system stabilized by continuous tension rather than continuous compression units [27]. Thus, the mechanical stability of the network depends on the arrangements and re-arrangements of these components. One of the most typical tensegrity elements, the octahedral structure, is shown in Figure 3. This basic structure consists of six rigid struts (compression-resisting elements) and 24 elastic cables (tensile-bearing elements). Depending on the experimental conditions, more complicated structures [70], viscoelastic cables [71], additional tensegrity elements and cables for nucleus and intermediate filaments [10, 72], and multimodal or additional tensegrity elements [10, 73, 74] can be added.

The model correctly predicts the linear increase in stiffness of the network with that of the applied stress in accordance with experimental results [27, 56]. This model can also predict both static and dynamic behavior of various cell types (e.g., human airway smooth muscle cells and the adherent cells) and has confirmed that the cells maintain their shape by redistributing and balancing the stress between the cytoskeleton and the extracellular matrix [31, 32, 56]. The pre-stress and subsequent increase in cell stiffness as predicted by this model can probably also explains the high elasticity and non-linear viscoelastic behaviors observed in cells [32]. In contrast, this model still has the disadvantage in the prediction of the elastic modulus greater than experimentally measured values and the limitation in the description of cell viscoelastic behaviors, which requires consideration of polymer structure at smaller scales [28, 30].

4. Open Cell Foam Model

In this model, the actin network is a rigid cross-linking of beam-like structures, of which shape is either cuboid, dodecahedron, tetrakaidecahedron, or icosahedron, with bending and twisting of the struts as the major stress-generating component. One of the typical stress units is a cuboid as shown in Figure 4a. [30, 75]. This model has a major application when studying endothelial cells. It can also predict the strain hardening under compression for the adherent cells exposed to local mechanical perturbations [31]. The open cell foam model does not include pre-stress and thus does not elucidate the effect of stress on cell stiffness. The rigidity of the cross-link is a major disadvantage of the model, as in reality the actin cross-links are not rigid [12]. Overall, this model may not be able to provide as much information regarding cytoskeleton mechanics compared to the other models [30, 31].

5. Semi-flexible Network Element Model

We named this model as “semi-flexible network element model” because this model describes the cytoskeleton rheological properties using an RVE-based approach to represent the structure of a semi-flexible polymer network [76]. As shown in Figure 4b., the RVE of this model consists of four equal-length strings and elastic springs, which simplifies the complex network structure. This model can predict Young’s modulus as well as the shear modulus in terms of the relative ratio between the bending stiffness and the axial stiffness as well as the cross-link density. Although this model relates the microstructure of the cytoskeleton network to cell mechanical properties, it is not suitable

for the simulation of cell dynamics due to the lack of structural information at larger scales (3D structure and microtubules) [30].

6. Continuum Polymer Network Model

The concept of this model is based on rubber elasticity in continuum mechanics; however, it also considers the force-extension relation of polymer chains, which is not directly included in the cell-scale continuum-based models. The RVE of this model is a continuous medium with principal stretch axes, as shown in Figure 4c. Different shaped RVEs have been used for describing polymer networks [77-80]. The eight-chain model or all-direction model was used for actin-filament networks [20, 81].

This type of model has recently been improved to overcome the limitation of affine approximation and to include the prediction of negative normal stress behaviors. Van Oosterwyck and co-workers considered inextensibility of chain and sliding cross-links for non-affine deformation [82]. Recently, two nonlinear springs connected in series were used to show the effect of the linker stiffness on the rheological properties [83]. Unterberger and co-workers' nonaffine homogenization method can show the negative normal stress behavior [84, 85]. A different approach, where a rigid rod connected to the surrounding elastic medium by cross-linkers, was reported to show the effect of the flexibility of the cross-link on the rheological properties [86].

Using a proper application of this model to the finite element method, the cell behavior, such as that observed in a microindentation experiment, can be simulated.

However, only qualitative agreement was achieved, which is conjectured to be due to the lack of larger scale information as in the semi-flexible network element model [84, 85].

7. Discussion on the Structure-based Models

The structure-based models provide a better understanding of the cytoskeleton behaviors and properties related to microstructural information, such as pre-stress and semi-flexibility, which are neglected in the cell-scale continuum-based models. But it is still an affine continuum approach and thus does not provide information about thermal fluctuations, network morphology, actin polymerization and cross-linking effects. The polymer-based model has been used to overcome those limitations, which will be discussed in the next section.

Although the structure-based models are more suitable for describing the cytoskeleton properties rather the cell behaviors because the RVE approach is usually used when averaging over the cell and cannot be used for local fluctuations of deformations in a cell. However, proper choice of finite element method and multiscale simulation can allow structure-based models to simulate cell behaviors. For example, Chen used the tensegrity models to simulate cell spreading [87], and Unterberger used the continuum polymer network model to simulate micropipette aspiration [84, 85]. However, the computational time is generally longer than that for continuum-based models due to the more complex calculations for each RVE.

Among the pre-stress models, the tensegrity model seems to be the best because it considers the actin networks as well as the microtubules, whereas other models do not

consider the microtubules. Compared to the semi-flexibility models, the pre-stress models are generally better at describing larger cell scale behaviors due to the inclusion of the pre-stress. However, the semi-flexibility models are better in the sense that more microstructural information (semi-flexibility) can be incorporated in simulating the cytoskeleton properties.

POLYMER-BASED MODELS (<1 μM)

We classify models, which consider the structure of polymer molecules (actin filaments) or the morphology of polymer networks to predict cytoskeleton material properties as polymer-based models. The models in this type are further categorized into the discrete polymer network model (a.k.a. Mikado model) and the single polymer chain model. The original classification of the polymer-based model can be found in a review by Mackintosh (2006) [88] as well as in a review by Mofrad (2009) [13]. Recently, Unterberger and Holzapfel published a thorough review on polymer-based models in 2014 [28]. However, they also included the continuum polymer network model in their review. Here, we classify the continuum polymer network model as a structure-based model because actin network structure is simplified into a RVE with chains in principal axes in a continuous medium.

The structure-based models utilize many imaginary microstructural units, which have been proposed to model the complex physical properties of cells. However, these models still lack actual information on the detailed structure and behaviors of the cytoskeleton at polymer molecular-level scales, such as cytoskeleton network morphology, cross-linker properties, and thermal fluctuation. Since the cytoskeleton is a complex structure of biopolymers, such as actin filaments, modeling the cytoskeleton structure at smaller polymer scales (~1 μm for polymer networks and <10 nm for single chains [28]) is essential to understand the origin of the unusual physical behaviors of cells. The polymer-based models have been used to elucidate the nonlinear mechanical response of the cytoskeleton to external forces in terms of collective behaviors (the effects of

connectivity for networks and entanglements for solutions) as well as single chain properties (semi-flexibility and finite extensibility) of actin filaments.

The single polymer chain models provide the force-extension relationship of an actin filament, which is a fundamental aspect of all the models at larger scales. The discrete polymer network models are used to elucidate the interplay between the polymer network structure and the semi-flexibility of individual actin filaments. One of the distinguishing unusual behaviors of the cytoskeleton is the negative normal stress effect [89], which is explained only by polymer-based models that consider semi-flexibility.

1. Discrete Network Models

In this model, the RVE is a simulation box filled with cross-linked polymer chains. Each simulation method is different in how it simulates semi-flexible polymer chains, the properties of cross-linkers, and how to construct the network structure.

Simpler approaches include the 2D network models. Head and co-workers used random 2D networks of worm-like chains to derive the scaling of the bulk modulus and the affine/non-affine elastic deformation regime as a function of the concentration and contour length of an actin filament [90, 91]. An elastic beam was used as the network element to predict the scaling of shear modulus [92]. A network of Euler-Bernoulli beams was employed to identify the elastic deformation regime according to the magnitude of strains [93]. The same network model was also used to explain the negative normal stress phenomenon with an asymmetric force-extension relation of actin filaments [94]. This model was also combined with a kinetic Monte Carlo method to show the strain

dependence of the cross-link rupture and stiffness [95]. Alonso and co-workers proposed a model based on the flocking theory. Polymer chains are considered as point particles, while cross-linkers are represented as potential functions [96, 97]. This model can simulate strain hardening, viscoelastic creep, stress relaxation, network rupture, and network reformation. Fallquivt and co-workers also used a 2D network model to study the effect of the filament length dispersion and the cross-linker compliance on the network material properties. It is noteworthy that they also performed a simulation using the continuum polymer network model to connect the effect of the cross-linker properties to a larger scale model [98].

Although 2D network approaches have been used for many studies, their limitations, such as the inability to represent the effect of 3D morphologies of cross-linkers on the actin network structure, have inspired the development of 3D network models. Huisman and co-workers have used the 3D network of Euler-Bernoulli beams [99] and an inextensible worm-like chain model [100, 101] to study the strain-stiffening and scaling of elastic moduli. Brownian dynamics (BD) simulation method was used to study similar cytoskeleton network properties. Polymerization/depolymerization was simulated using actin monomers represented as rod-like units, which results in a 3D network structure [16, 102, 103]. It is noteworthy that both the model by Huisman and the BD model [102] discovered that stress is concentrated in a few chains at high strain. The BD model was also used for extensive study of actin network behaviors, such as identification of distinctive regimes and mechanisms of creep, as well as the origin and control of viscous flows in cortical cells [104]. The BD simulations and the dynamic cross-linking of the actin filaments can also be studied to understand behaviors of cancerous cells [105]. Whereas many models assume isotropic deformation, some models can predict the different

morphologies of cytoskeleton networks, such as bundled filaments. The aforementioned BD model demonstrated the different morphologies as a function of cross-linker properties. Cyron and co-workers used stochastic governing equations to demonstrate different morphologies [106]. A recent study, which proposed a form-finding model (a 2D model was used earlier [107]), found that cells create parallel rather than disordered bundles of actin filaments during cell motion and cell adhesion. The parallel bundles align in the stretched direction, increasing the stiffness of the cell [108].

2. Single Polymer Chain Model

The single polymer chain model describes the most fundamental physical behaviors and properties of the cytoskeleton in the polymer molecule scale (<10 nm). Modeling the nonlinear force-stretch relationship of a single polymer chain is one the main issues in this type of model.

Molecular dynamics (MD) simulations are used for the smallest atomic scale. Matsushita and co-workers simulated a single F-action filament with a full atomic structure to estimate its extensional stiffness [109]. Coarse-grained MD (CGMD) simulations were also performed by Chu and Voth to estimate the persistence length [110]. CGMD was also used to identify the heterogeneous mechanical properties of F-actin according to G-actin subunit structural differences [111-113].

The dynamics features of a single filament can be modelled at a larger scale (polymer chain level: ~10 nm) than atomistic scale (~1 nm) in MD simulations. These types of models are called wormlike chain models. Although the atomic scale information

can be scaled up [114] or modelled as an elastic rod that incorporates the helical structure of the filaments, the worm-like chain model [115, 116] has been widely used. Based on the previous analyses [88, 90, 91], although a short filament with a length scale that is much smaller than its persistence length, its longitudinal response is determined by transverse thermal fluctuation. The model equation for the relationship between the force and the extension was later developed by Holzapfel and Ogden [117], and the Monte Carlo simulation was developed by Blundell and Terentjev [118]. There is also an approach using the finite element method to solve the Langevin equation for wormlike chain dynamics, which is also extended to model 2D network behaviors [119].

3. Discussion on the Polymer-based Models

Consideration of polymer structure in models made it possible to predict or elucidate cytoskeleton properties/behaviors, which was not possible using larger scale models. For example, the frequency dependence of shear moduli, can be predicted by considering the polymer network structure, whereas the soft glassy model predicted that behavior by adjusting a parameter [50]. The effects of cross-linkers are essential in determining the overall actin physical properties and the consequent cytoskeleton properties. The affinity of the actin binding proteins to the actin filament, the resulting network morphology (bundle or orthogonal), the degree of cross-linking, concentration, and the molecular weight affect the non-linear viscoelastic response of the cytoskeleton [120, 121].

However, the general disadvantages of considering microstructural information at smaller scales are heavy computational cost for larger scale simulation and the neglect of

structural information at larger scales. Due to computational limits, the frequency dependence of shear moduli cannot be investigated for longer time ranges, and some filaments that are larger than the simulation box cannot be modelled [102]. Simulation of active behaviors, including polymerization/depolymerization of actin filaments, requires longer time scales. Polymerization/depolymerization can be considered only in the generation of a 3D network structure but not in the simulation of active behaviors [102, 122]. However, Alonso and co-workers simulated active behaviors such as network reconstruction using a 2D model, which is computationally less expensive [123].

It is understood that the behavior of the cytoskeleton network is not a function of one single component but is interdependent on the behaviors of all of the three major components together [10, 68]. Considering that, a model based solely on actin cannot predict and analyze the true cytoskeleton behavior. Similarly, these models also do not consider the compression in microtubules and the importance of intermediate filaments in bearing stress.

DISCUSSION/SUMMARY

We classified many mathematical and numerical models for mechanical behaviors and rheological properties of the cytoskeleton of a cell, which have been published up to 2014. The categories used are adapted from those used in a review by Mofrad in 2006: the cell-scale continuum-based model (originally continuum-based model), the structure-based model (tensegrity models and other RVE-based models), and the polymer-based model. These categories may be further classified into five groups by dividing the structure-based models into the pre-stress model and the semi-flexibility model as well as by dividing the polymer-based models into the single polymer chain model and the discrete polymer network model. Table 2.5.1 briefly summarizes the models we classified and discussed in this paper. The length scale classification is expected to promote more systematic identification of principles and characters of models.

The polymer-based models consider the stress elements, single polymer chain and polymer network at the smallest scales among the models in those categories. These models describe the relation between the cell properties and the molecular structure of the cytoskeleton. However, high computational load prevents use of those models to simulate cell behaviors. For example, the BD model [102] showed the limitations in the simulation of polymer chains longer than the simulation box, frequency range in the shear modulus prediction, and the simulation of structural rearrangement by polymerization/depolymerization. Additionally, the effects of the microtubules and the intermediate filaments, which are larger scale cellular components than actin filaments, are not included in the simulation box of actin networks.

The structure-based models describe the cytoskeleton properties and dynamic behaviors using RVE of imaginary stress elements, which coarse-grain the polymer chain and network behaviors. The semi-flexibility models connect the effects of semi-flexibility and the stiffness of polymer chains to cytoskeleton behaviors at larger scales. The pre-stress models can explain the cell shape stability and the cell stiffness in terms of the pre-stress of the cytoskeleton, which is not considered in the cell-scale continuum-based model. The structure-based model can generally be used to model cytoskeleton material properties with better computational efficiency than the polymer-based models. However, they can also be used for cell dynamics with proper multi-scale numerical schemes. We also conjecture that models or studies which connect the pre-stressed model and the semi-flexibility model would make up for the disadvantages of both models.

The cell-scale continuum-based model, which handles the largest length scales among those model categories, can be used for modeling cell dynamics or behaviors, which are associated with experiments on cell property measurements. The coarse-grained mathematical constitutive models cannot give information on cytoskeleton microstructure.

As we have reviewed, the cytoskeleton modeling presents different challenges compared to usual entangled polymer system modeling, where smaller scale models based on microstructural information can describe polymer behaviors and properties with more detail [124, 125]. Due to the heterogeneity of the cytoskeleton network, models at smaller scales may lose larger scale structural information, such as the effects of pre-stress and microtubules. Therefore, proper choice of models, especially for the structure-based models, as well as for multi-scale modeling or studies connecting models in different scales

is important. Furthermore, development of a model using a new approach that employs coarse-graining to include more information from smaller scale studies to connect models should also be considered. For example, the mean-field approach used in stochastic models for simulating of complex entangled polymer systems is being explored as a new interpretation of the cross-linking and rearrangement of networks [125].

In this review, we focused mainly on models based on the passive dynamics associated with pure mechanical/rheological responses. However, there are models based on different approaches, such as the gel-like model: it was proposed by Pollock that the cell movement and shape alteration can be described by the phase-transition mechanism of a gel-like structure [126]. There have been models that consider the active behaviors which are related with biological responses or structural rearrangement by polymerization/depolymerization. For example, the granular model considered microtubule rearrangement to describe cell crawling [127]. There have been models which described active behaviors of motor proteins [128] and growth and remodeling [129]. Although many reviews have pointed out the need to improve models for active dynamics [28, 30, 31], apparent barriers to that development are the inherent complexity of the models for passive dynamics and the need for broader interdisciplinary research including biomedical engineering, medical science, biophysics, biology, chemistry, materials science, and chemical engineering, etc.

CONCLUDING REMARKS

The objective of this review is to provide a framework for approaching and understanding the plethora of biopolymer network models in terms of length scales, which are related to the stress components and the phenomena of interest. Identifying the length scale categories of a model can give a quick insight into the advantages and disadvantages of the model, and the types of behaviors and properties described. Conversely, models can be selected based on the length scale of the phenomena of interest. The correct prediction of biopolymer network mechanical/rheological properties is important in many biomedical applications associated with biopolymer networks [1, 130, 131]. Therefore, the framework provided by this review is expected to promote various studies on biopolymer networks.

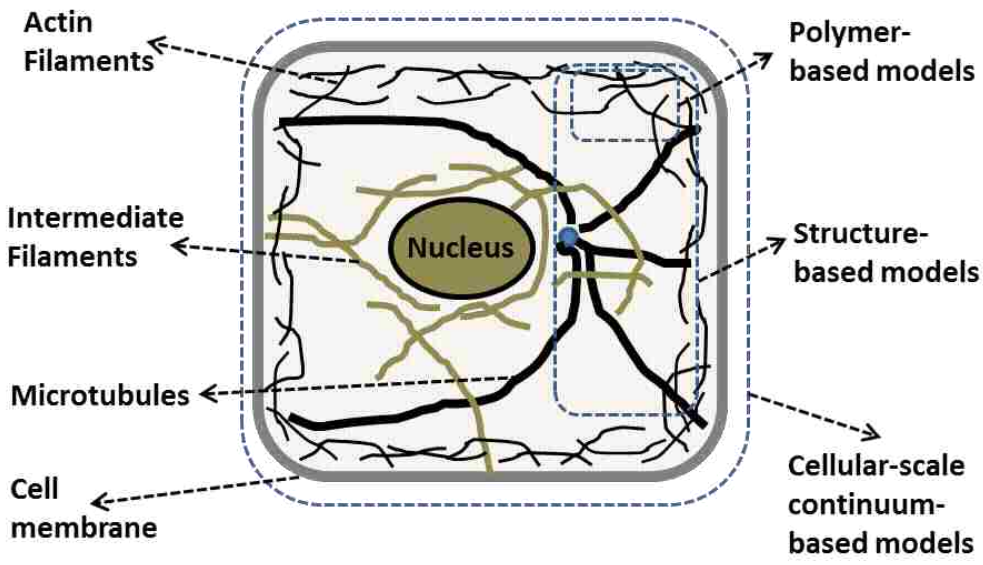

Fig. 1. **Schematic diagram which shows the structural components of the cytoskeleton in a typical eukaryotic cell and the length scales for each group of models.**

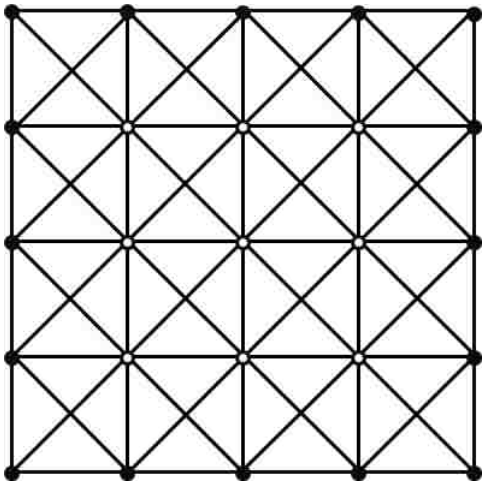

Fig. 2. A typical example of 2D tensed cable nets models: reinforced squared nets. (redrawn from [Coughlin and Stamenovic (2003); Paul et al, (2008)]).

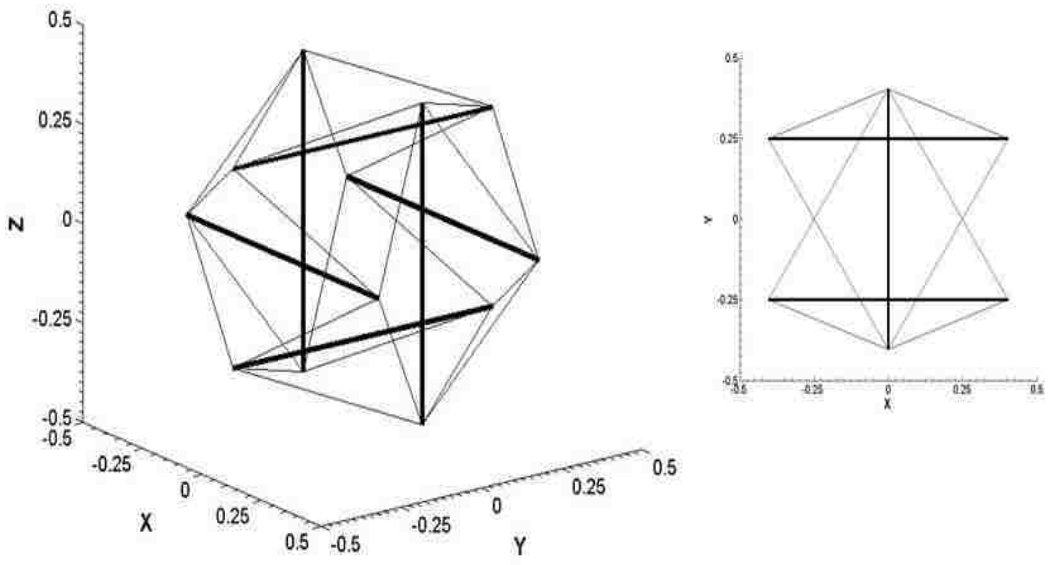

Fig. 3. A typical octahedron tensegrity element structure. The inset is a view from the xy-plane, which looks identical to the views from the zx-plane and the yz-plane. (Redrawn from [Canadas *et al.*, (2002)]).

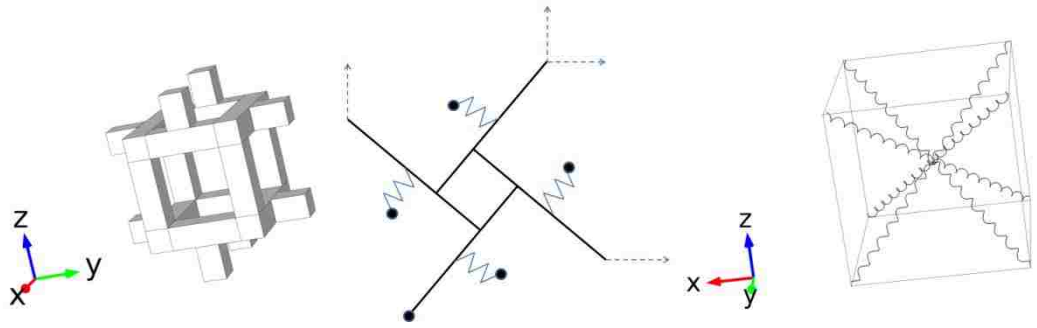

(a) (b) (c)

Fig. 4. The RVEs of (a) a typical open cell foam model (cuboid), (b) the semi-flexible polymer network model, and (c) the continuum polymer network models (8-chain model). (More details of each model are available in each original reference. Images were also redrawn [75,76, 81]).

Table 1. Summary of the cytoskeleton models

Models		Principle (how to model)		Advantage/Disadvantage		Ref
Cell-Scale Continuum Model (~ 10 μm)	Elastic/Viscoelastic Model	Cytoplasm as continuous media	Constitutive rheological equation	Good for cell dynamics simulation/ No microstructural information	Computationally efficient enough to describe the near equilibrium/transient behaviors of cell dynamics.	[13,36]
	Multiphasic Model		Constitutive rheological equations in each phase		More accurate at the cost of computational cost	[41]
	Soft Glassy Model		Sollich's equation		Prediction over large time scale ranges	[51]
Structure-based Pre-Stress Model (4~10 μm)	Cortical Model, Cable Nets Model	Pre-stressed stress unit	Cable networks	Pre-stressed is considered. Possibility for both cell dynamics and cell properties. Lack of polymer structural information (semi-flexibility)	Lack of microtubule and intermediate filament information	[57,56]

Table 1. Summary of the cytoskeleton models (cont.)

	Tensegrity Model	Pre-stressed stress unit	Cable-Strut networks	Pre-stressed is considered. Possibility for both cell dynamics and cell properties. Lack of polymer structural information (semi-flexibility)	Considers all actin filaments, microtubules, and sometimes intermediate filaments. Versatility of the model	[56]
Structure-based Semi-Flexibility Model (1~4 μm)	Open Cell Foam Model	Stress unit with semi-flexibility	Rigid beam structure	Semi-flexibility or bending is considered. Lack of microtubule and polymer molecule information (network morphology). Generally, not good for cell dynamics	Prediction of bending dominated deformation. Some structural information is not correct.	[30,31]
	Semi-flexibility Network Element Model		Simplified Polymer Network		Complex network behavior is well simplified. Lack of 3D structural information	[30]
	Continuum Polymer Network Model		Continuous medium with principal axes		Continuum mechanics and microstructural strain-stretch relation are connected. Possibility for cell dynamics	[81,84]

Table 1. Summary of the cytoskeleton models (cont.)

Polymer-based Discrete Network Model (10 nm~ 1 μm)	2D Networks	Actin filament network	2D Networks of semi-flexible chains	Polymer morphology and collective network motions are considered. Not god for cell dynamics	Simpler than 3D. Active dynamics may be possible. Lack of 3D morphological information	[90,96]
	3D Networks		3D Networks of semi-flexible chains		Details of microstructural information are considered. Computational load limits active dynamics.	[16,99]
Polymer-based Single Chain Model (<10 nm)	Worm-like Chain Model	Single actin filament chain	Continuous chain	Basic chain stretch dynamics. Not good for network properties and cell dynamics	Chain stretch dynamics considering semi-flexibility and finite inextensibility can be obtained	[117]
	Molecular Dynamics simulation		G-actin monomer units		Basic parameters, persistence length and finite extensibility can be obtained	[109, 110]

ACKNOWLEDGEMENT

The partial financial support from the Energy Research & Development Center of Missouri University of Science & Technology is gratefully acknowledged.

REFERENCES

1. D. Discher, C. Dong, J. J. Fredberg, F. Guilak, D. Ingber, P. Janmey, R. D. Kamm, G. W. Schimd-Scho and S. Weinbaulam, *Ann. Biomed. Eng.*, **37,** 847 (2009).

2. J. R. Stehn, N. K. Haass, T. Bonello, M. Desouza, G. Kottyan, H. Treutlein, J. Zeng, P. R. B. B. Nascimento, V. B. Sequeira, T. L. Butler, M. Allanson, T. Fath, T. A. Hill, A. McCluskey, G. Schevzov, S. J. Palmer, E. C. Hardeman, D. Winlaw, V. E. Reeve, I. Dixon, W. Weninger, T. P. Cripe, and P. W. Gunning, *Cancer Res*, **73**, 5169 (2013).

3. S. D. Bernal, S. B. Baylin, J. H. Shaper, A. F. Gazdar, and L. B. Chen *Cancer Res*, **43**, 1798 (1983).

4. F. C. S. Ramaekers and F. T. Bosman, *J. Pathol.*, **201**, 351 (2004).

5. B. Geiger, J. Spatz, and A. Bershadsky, *Nat. Rev. Mol. Cell Biol*., **10**, 21 (2009).

6. M. Mehrbod and M. R. K Mofrad , *PLoS ONE*, **6**, 10, e25627 (2011).

7. E. M. Huisman, in *Introduction, Simulation of biopolymer networks under shear*, Leiden University, Leiden (2011).

8. M. E. Chicurel, C. S. Chen, D. E. Ingber, *Curr. Opin. Cell Biol.*, **10**, 232 (1998).

9. N. Wang, K. Naruse, D. Stamenovic, J. J. Fredberg, S. M. Mijailovich, I. M. Tolic-Norrelykke, *P. Natl. Acad. Sci. USA*, **98**, 7765 (2001).

10. D. E. Ingber, *J. Cell Sci.*, **116**, 1157 (2003)

11. C. Galli, S. Guizzardi, G. Passeri, G. M. Macaluso, R. Scandroglio, *Acta Biomedica.*, **76**, 5 (2005).

12. T. J. Chen, C. C. Wub, F. C. Su, *Med. Eng. Phys.*, **34**, 1375 (2012).

13. M. R. K. Mofrad, *Annu. Rev. Fluid Mech*. **41**, 433 (2009).

14. H. Lodish, A. Berk, S. L. Zipursky, P. Matsudaira, D. Baltimore, and D Darnell, *Molecular Cell Biology*, W.H. Freeman Co. publications, New York (1999).

15. F. Gittes, B. Mickey, J. Nettleton, and J Howard, *J. Cell Biol*., **120**, 923 (1993).

16. T. Kim, W. Hwang and R.D. Kamm, *Exp. Mech.*, **49**, 91 (2009).

17. M. L. Gardel, J. H. Shin, F. C. MacKintosh, L. Mahadevan, P. A. Matsudaira, and D. A. Weitz, *Science*, **304**, 1301 (2004).

18. M. L. Gardel, J. H. Shin, F. C. MacKintosh, L. Mahadevan, P. A. Matsudaira, and D. A. Weitz, *Phys. Rev. Lett.*, **93**, 188102 (2004).

19. F. C. MacKintosh, J. Kas, and P. A. Janmey, *Phys. Rev. Lett.*, **75**, 4425 (1995).

20. C. Storm, J. J. Pastore, F. C. MacKintosh, T. C. Lubensky and P. A. Janmey, *Nature*, **435**, 191 (2005).

21. J. Xu, Y. Tseng, and D. Wirtz, *J. Biol. Chem*. **275**, 35886 (2000).

22. O. Lieleg, M. M. A. E. Claessen, and A. R. Bausch, *Soft Matter*, **6**, 218 (2010).

23. B. Alberts, D. Bray, A. Johnson, J. Lewis, M. Raff, K. Roberts, P. Walter, in *Essential cell biology : An introduction to the molecular biology of the cell*, Garland Publishing, New York (1998).

24. I. Fujiwara, S. Takahashi, H. Tadakuma, T. Funatsu, S. Ishiwata, *Nat. Cell Biol.*, **4**, 666 (2002).

25. G. A. Buxton, N. Clarke, P. J. Husse, *Express Polym. Lett.*, **3**, 579 (2009).

26. T. Mitchison and M. Kirschner, *Nature*, **312**, 237 (1984).

27. D. Stamenović, *FME Transactions*, **34**, 57 (2006).

28. M. J. Unterberger and G. A. Holzapfel, *Biomech. Model Mechanobiol.*, **13**, 1155 (2014)

29. J. Chen, *Interface Focus*, **4**, 20130055 (2014)

30. T.J. Chen, C.C. Wu, and F.C. Su, *Med. Eng. Phys*., **34**, 1375 (2012)

31. M. M. Nava, M. T. Raimondi, and R. Pietrabissa, *Biomech. Model Mechanobiol.*, **13**, 929, (2014).

32. E. Moeendarbary, and A. R. Harris, *WIREs Syst. Biol. Med*., **6**, 371, (2014).

33. S.S. Andrews, *Phys. Biol*., **11**, 011001 (2014)

34. E. Roberts, *Cur. Opin. Struc. Biol*., **25**, 86 (2014)

35. P. A. Janmey, and C. Schmidt, in *Cytoskeletal Mechanics - Models and Measurements in Cell Dynamics*, M. R. K. Mofrad, and R. D. Kamm Eds., Cambridge University Press (2006).

36. M. R. K. Mofrad, H. Karcher, and R. D. Kamm, in *Cytoskeletal Mechanics - Models and Measurements in Cell Dynamics*, M. R. K. Mofrad, and R. D. Kamm Eds., Cambridge University Press (2006).

37. B. Fabry, G. Maksym, J. Butler, M. Glogauer, D. Navajas, J Fredberg, *Phys. Rev. Lett.*, **87**, 148102 (2001).

38. A. R Bausch, F. Zeimann, A. A. Boulbitch, K. Jacobson, E. Sackmann, *Biophysics*, **75**, 2038 (1998).

39. D. Aubry, H. Thiam, M. Piel, and R. Allena, *Biomech. Model. Mechanobiol*., DOI 10.1007/s10237-014-0595-3 (2014)

40. I. Pajic-Lijakovic and M. Milivojevic, *Biomech. Model Mechanobiol*., **13**, 1097 (2014)

41. F. Guilak, M. A. Haider, L. A. Setton, T. A. Laursen, and F. P.T. Baaijens, in *Cytoskeletal Mechanics - Models and Measurements in Cell Dynamics*, M. R. K. Mofrad, and R. D. Kamm Eds., Cambridge University Press (2006).

42. V.C. Mow, S.C. Kuei, W.M. Lai, and C.G. Armstrong, *J. Biomech. Eng*., **102**, 73 (1980).

43. W.M. Lai, J.S. Hou, and V.C. Mow, *J. Biomech. Eng*., **113**, 245 (1991).

44. W.Y. Gu,W.M. Lai, and V.C. Mow, *J. Biomech. Eng*., **120**, 169 (1998).

45. M. Biot, *J. Appl. Phys*. **12**, 155 (1941).

46. A.F. Mak, *J. Biomech. Eng*., **108**, 123 (1986).

47. M.R. DiSilvestro and J.K. Suh, *An. Biomed. Eng.*, **30**, 792 (2002).

48. F.P.T. Baaijens, W.R. Trickey, T.A. Laursen, and F. Guilak, *An. Biomed Eng*., **33**, 494 (2005)

49. L. Cao, F. Guilak, and L. Setton, *Cell. Mol. Bioeng*., **2**, 306 (2009).

50. B. Fabry and J. J. Fredberg in *Cytoskeletal Mechanics - Models and Measurements in Cell Dynamics*, M. R. K. Mofrad, and R. D. Kamm Eds., Cambridge University Press (2006).

51. B. Fabry and J. J. Fredberg, *Respir. Physiol. Neurobiol*, **137**, 109 (2003).

52. P. Sollich, F. Lequeux, P. Hebraud and M. Cates, *Phys. Rev. Lett.*, **78**, 2020 (1997).

53. P. Sollich, *Phys. Rev. E,* **58**, 738 (1998).

54. Haider M, Guilak F, *J Biomech Eng*., **122**, (3), 236 (2000)

55. Haider M, Guilak F, *J Biomech Eng* **124,** (5), 586 (2002)

56. D. Stamenović in *Cytoskeletal Mechanics - Models and Measurements in Cell Dynamics*, M. R. K. Mofrad, and R. D. Kamm Eds., Cambridge University Press (2006).

57. D. V. Zhelev, D. Needham, R. M. Hochmuth, *Biophys. J.*, **67**, 696 (1994).

58. D.E. Discher, D.H. Boal, and S.K. Boey, *Biophys. J*., **75**, 1584 (1998).

59. S.K. Boey, D.H. Boal, and D.E. Discher, *Biophys. J*., **75**: 1573 (1998).

60. D. Stamenovic´, D. E. Ingber, *Biomech. Model Mechanobiol*., **1**, 95 (2002).

61. M. F. Coughlin and D. Stamenović, *Biophys J,* **84**, 1328 (2003).

62. R. Paul, P. Heil, J. P. Spatz, and U. S. Schwarz US, *Biophys J,* **94**, 1470 (2008).

63. K. Y. Volokh, and O. Vilnay, *Int. J. Solids Struct.*, **34**, 1093 (1997).

64. D.E. Ingber, L. Dike, L. Hansen, S. Karp, H. Liley, and A. Manitos, *Int. Rev. Cytol*., **150**, 173 (1994).

65. D. Stamenović, and M. F. Coughlin, *J. Theor. Biol.*, **201,** 63 (1999).

66. F. J. Alenghat, B. Fabry, K. Y. Tsai, W. H. Goldmann and D. E. Ingber, *Biochem. Biophys. Res. Commun.*, **277**, 93 (2000)

67. J. M. Vasiliev, *J. Cell Sci. Suppl*., **8**, 1 (1987).

68. D. E. Ingber, *Annu. Rev. Physiol.,* **59**, 575 (1997).

69. B. Fuller, *Portfolio & ARTnews Annual*, **4**, 112 (1961).

70. H. Baudriller, B. Maurin, P. Canadas, P. Montcourrier, A. Parmerggiani, and N. Betache, *C R Mecanique,* **334**, 662 (2006).

71. P. Canadas, V.M. Laurent, C. Oddou, D. Isabey, and S. Wendling, *J Theor Biol*., **218**, 155 (2002).

72. N. Wang and D. Stramenovic, *Am. J. Physiol. Cell Physiol.,* **279**, C188 (2000).

73. D.E. Ingber, *FASEB J*., **20**, 811 (2006).

74. Y.Z. Luo, X. Xu, T. Lele, S. Kumars, and D.E. Ingber, *J. Biomech*., **41**, 2379 (2008).

75. R. Satcher, C. F. Dewey Jr, and J. H. Hartwig, Microcirculation, **4**, 439 (1997).

76. S. Roy and H. J. Qi, *Phys. Rev. E*., **77**, 061916 (2008).

77. P.J. Flory and J. Rehner Jr, *J. Chem Phys*., **11**, 512 (1943).

78. L.R.G. Treloar, *Trans. Far. Soc*., **42**, 83 (1946).

79. E.M. Arruda, and M.C. Boyce, *J. Mech. Phys. Solids*, **41**, 389 (1993).

80. P.D. Wu and E. Giessen, *J. Mech. Phys. Solids*, **41**, 427 (1993).

81. J.S. Palmer and M.C. Boyce, *Acta Biomater*, **4**, 597 (2008)

82. H. Van Oosterwyck, J.F. Rodriguez, M. Doblare, J.M. Garcia, *Comput. Methods Biomech. Biomed. Eng.*, **16**, 1002 (2013).

83. G.A. Holzapfel, M.J. Unterberger, R.W. Ogden, *J. Mech. Behav. Biomed. Mater*., **38**, 78 (2014)

84. M.J. Unterberger, K.M.Schmoller, A.R. Bausch, G.A. Holzapfel, *J. Mech. Behav. Biomed. Mater*., **22**, 95 (2013)

85. M.J. Unterberger, K.M.Schmoller, C. Wurm, A.R. Bausch, G.A. Holzapfel, *Acta Biomater.*, **9**, 7343 (2013)

86. C.P. Broederz, C. Storm, F.C. MacKintosh, *Phys. Rev. let.*, **101**, 118103 (2008).

87. T.J. Chen, C.C. Wu, M.J. Tang, J.S. Huang, and F.C. Su, *PloS One*, **5**, e14392 (2010).

88. F.C. MacKintosh, in *Cytoskeletal Mechanics - Models and Measurements in Cell Dynamics*, M. R. K. Mofrad, and R. D. Kamm Eds., Cambridge University Press (2006).

89. P. A. Janmey, M. E. McCormick, S. Rammensee, J. L. Leight, P. C. Georges, and F. C. MacKintosh, *Nature Mater.*, **6**, 48 (2007).

90. D. A. Head, A. J. Levine, and F. C. MacKintosh, *Phys. Rev. Lett.*, **91**, 108102 (2003).

91. D. A. Head, A. J. Levine, and F. C. MacKintosh, *Phys. Rev. E Stat. Nonlin. Soft Matter Phys.*, **68**, 061907 (2003).

92. J. Wilhelm and E. Frey, *Phys. Rev. Lett.*, **91**, 108103 (2003).

93. P.R. Onck, T. Koeman, T. van Dillen, and E. van der Giessen, *Phys. Rev. Lett.*, **95**, 178102 (2005).

94. E. Conti and F.C. MacKintosh, *Phys. Rev. Lett.*, **102**, 088102 (2009).

95. A.S. Abhilash, P.K. Purohit, and S.P. Joshi, *Soft Matter*, **8**, 7004 (2012).

96. R. Alonso, J. Young, and Y. Cheng, *Cell. Mol. Bioeng.*, **7,** 58 (2014)

97. F. Cucker, F., and S. Smale. *IEEE Trans. Automat. Control*, **52,** 852 (2007).

98. B. Fallqvist, A. Kulachenko, and M. Kroon, *J. Theor. Biol.*, **350**, 57 (2014)

99. E.M. Huisman, T. van Dillen, P.R. Onck, and E. van der Giessen, *Phys. Rev. Lett.*, **99**, 208103 (2007).

100. E.M. Huisman, C. Storm, G.T. Barkema, *Phy. Rev. E*, **78**, 051801 (2008).

101. E.M. Huisman, C. Storm, G.T. Barkema, *Phys. Rev. E*, **82**, 061902 (2010).

102. T. Kim, W. Hwang, H. Lee, R. D. Kamm, *PLoS Comput. Biol.*, **5**, e1000439 (2009).

103. T. Kim, in *Thesis: Simulation of Actin cytoskeleton structure and rheology*, Massachusetts Institute of Technology, Massachusetts, (2007).

104. T. Kim, M.L. Gardel, and E. Munro, *Biophys. J.*, **106**, 526 (2014).

105. M. Mak, M. Zaman, and R. Kamm, *Med. Phys.*, **41**, 164 (2014).

106. C. Cyron, A.R. Baush, K.W. Muller, and W.A. Wall, *J. Comput. Phys.*, **244**, 236 (2013).

107. J. Gong, D. Zhang, Y. Tseng, B. Li, D. Wirtz, and B.W. Scahfer, *PLoS ONE*, **8**, e77417 (2013).

108. B. Li, Y. Wang, and J. Gong, J. Zhejiang *Univ-Sci. A*, **15**, 732 (2014)

109. S. Matsushita, T. Adachi, Y. Inoue, M. Hojo, and M. Sokabe, *J. Biomech.*, **43**, 3162 (2010).

110. J-W. Chu and G. A. Voth, *Biophys. J.*, **90**, 1572 (2006).

111. O.N. Yogurtcu, J.S. Kim, and S.X. Sun, *Biophys. J.*, **103**, 719 (2012).

112. J. Fan, M.G. Saunders, and G.A. Voth, *Biophys. J.*, **103**, 1334 (2012).

113. J. Fan, M.G. Saunders, E.J. Haddadian, K.F. Ffreed, E.M. de la Cruz, and G.a. Voth, *J. Mol. Biol.*, **425**, 1225 (2013).

114. D. Ming, Y. Kong, Y. Wu, and J. Ma, *PNAS*, **100**, 104 (2003).

115. O. Kratky and G. Porod, *Recl. Trav. Chim. Pays-Bas.*, **68**, 1106 (1949).

116. M. Fixman and J. Kovac, *J. Chem. Phys.*, **58**, 1564 (1973)

117. G.A. Holzapfel and R.W. Ogden, *J. Elast.*, **104**, 319 (2011).

118. J.R. Blundell and E.M. Terentjev, *Macromolecules*, **42**, 5388 (2009)

119. Y. Lin, X. Wei, J. Qian, K.Y. Sze, and V.B. Shenoy, *J. Mech. Phys. Solids*, **62**, 2 (2014)

120. B. Wagner, R. Tharmann, I. Haase, M. Fischer, and A. R. Bausch, *PNAS*, **103**, 13974 (2006).

121. H. Hatami-Marbini and M. R. K. Mofrad, *Stud. Mechanobiology Tissue Eng. Biomater.*, **4**, 3 (2011).

122. G.A. Buxton, N. Clarke, and P.J. Hussey, *eXPRESS Pol. Lett*., **3**, 579 (2009).

123. R. Alonso, J. Young, and Y. Cheng, *Cell. Mol. Bioeng*., **7**, 58 (2014).

124. A. E. Likhtman, *J. Non-Newtonian Fluid Mech*. **157**, 158 (2009).

125. J. Park, D.W.Mead, and M.M. Denn, *J. Rheol*. **56**, 1057 (2012).

126. G. H. Pollack, in *Cytoskeletal Mechanics - Models and Measurements in Cell Dynamics*, M. R. K. Mofrad, and R. D. Kamm Eds., Cambridge University Press (2006).

127. B. Maurin, P. Canadas, H. Baudriller, P. Montcourrier, and N. Bettache, *J. Biomech.*, **41**, 2036 (2008).

128. P. Chen and V.B. Shenoy, *Soft Matter*, **7**, 355 (2011).

129. S. Na, G.A. Meininger, and J.D. Humphrey, *J. Theor. Biol*., **246**, 87 (2007).

130. Y. Jang, S. Park, and K.Char, Kor. *J. Chem. Eng*., **28**, 1149 (2011).

131. Y. Jeong and I.S. Kang, Kor. *J. Chem. Eng.*, **12**, 540 (1995)

II. A constitutive model for entangled polymers incorporating binary entanglement pair dynamics and a configuration dependent friction coefficient

Synopsis

Following recent work [e.g. Park *et al.* (2012) J. Rheol. 56: 1057-1082, Yaoita *et al.* (2012) Macromolecules 45: 2773-2782, Ianniruberto *et al.* (2012) Macromolecules 45: 8058-8066] we introduce the idea of a conFig.uration dependent friction coefficient (CDFC) based on the relative orientation of Kuhn bonds of the test and surrounding matrix chains. We incorporate CDFC into the "toy" model of Mead *et al*. (1998) [Macromolecules 31: 7895-7914] in a manner akin to Yaoita *et al*. (2014) [Nihon Reoroji Gakkaishi, 42: 207-213]. Additionally, we incorporate entanglement dynamics (ED) of discrete entanglement pairs into the new Mead-Banerjee-Park (MBP) model in a way similar to Ianniruberto and Marrucci, (2014) [J. Rheol. 58: 89-102]. The MBP model predicts a deformation dependent entanglement microstructure which is physically reflected in a reduced modulus that heals slowly following cessation of deformation. Incorporating ED into the model allows "shear modification" to be qualitatively captured. The MBP model is tested against experimental data in steady and transient extensional and shear flows. The MBP model captures the monotonic thinning of the extensional flow curve of entangled monodisperse polystyrene (PS) melts [Bach *et al.* (2003) Macromolecules 36: 5174-5179] while simultaneously predicting the extension hardening found in PS semi-dilute solutions where CDFC is diluted out [Bhattacharjee *et al.* (2002) Macromolecules 35: 10131-10148].

The simulation results also show that the rheological properties in nonlinear extensional flows of PS melts are sensitive to CDFC but not to convective constraint release (CCR) while those for shear flows are influenced more by CCR. The monodisperse MBP “toy” model is generalized to arbitrary polydispersity.

I. INTRODUCTION

The idea of a configuration dependent friction coefficient (CDFC), which is based on the relative orientation of a test chain *segment* to the surrounding matrix chain segments, was previously introduced by [Park *et al.* (2012)]. Although related through a Kuhn-Grün analysis [e.g. Larson (1988)], a better, more fundamentally based proposition is to base CDFC on the relative orientation of the Kuhn bonds of the test and matrix chains respectively [Ianniruberto *et al.* (2011, 2012); Yaoita *et al.* (2012, 2014)]. Since CDFC impacts both the stretch (Rouse) and terminal relaxation times equally, CDFC can in principle capture the monotonic thinning of the extensional flow curve of entangled monodisperse polystyrene (PS) melts [Bach *et al.* (2003)] while simultaneously predicting the extension hardening found in entangled monodisperse PS solutions where the effects of CDFC is negligible due to dilution [Bhattacharjee *et al.* (2002); Desai and Larson (2014)].

In addition to altering the form of CDFC employed we shall also address other fundamental issues in molecular modelling the rheology of polymer melts. In particular, the mono and polydisperse MLD models (Mead-Larson-Doi model [Mead *et al.* (1998)]) assume a *constant* entanglement density in all flow situations. This fundamental assumption is almost certainly *wrong*. Theoretically, the assumption of a constant entanglement density is reflected in the fact that the equilibrium plateau modulus is used to scale the stress in all tube models, i.e. the GLaMM model [Graham *et al.* (2003)], all Doi-Edwards type models such as the MLD model [Mead *et al.* (1998); Mead (2007)], and the pom-pom model [McLeish and Larson (1998)]. It's difficult to understand how the

equilibrium plateau modulus can be used to scale stress levels in the highly nonlinear flow regime since reductions in the entanglement density have been demonstrated in non-equilibrium molecular dynamics simulations of shear flow [Baig *et al.* (2010)] and detailed molecular models [Andreev *et al.* (2013)]. Additionally, interrupted transient step shear rate rheological data on linear and long-chain branched (LCB) polyethylene melts by Dealy and Tsang (1981) [and references therein] strongly support the idea of a dynamic entanglement network. These theoretical and experimental results suggest that a fundamental re-appraisal is appropriate for the formulation of molecular constitutive models that span the full range of flows from linear viscoelasticity to the nonlinear fast flow regime of linear and LCB polymer melts.

In this paper we develop a new molecular model based on the dynamics of discrete entanglement pairs (entanglement dynamics: ED) as opposed to traditional mean field tube descriptions [Desai and Larson (2014)]. Adopting this description is supported by recent atomistic simulations which reveal the nature of an entanglement to be that of a topological coupling of a discrete pair of chains [Everaers *et al.* (2004); Tzoumanekas and Theodorou (2006); Baig *et al.* (2010)]. Both the modulus and the terminal disengagement time are functions of the entanglement density and changes to the entanglement density will directly impact these quantities. This paper seeks to incorporate a quantitative description of entanglement pair dynamics and a Kuhn bond based CDFC into the mono and polydisperse MLD "toy" models. This will yield a general molecular constitutive model at the theoretically and computationally simple "toy" level that can handle arbitrary polydispersity in arbitrarily fast flows.

This paper is organized as follows: In Sec. II, we introduce a toy dynamical equation for entanglement pairs in monodisperse systems. In Sec. IIA we define the specific form of CDFC we shall use for monodisperse systems. Section III reviews aspects of the Desai-Larson modified DEMG model (Doi-Edwards-Marrucci-Grizzuti [Pearson et al. (1991), Mead and Leal (1995), Mead et al (1995)]) which will serve as a base case for the current work. Section IV introduces two new effects we anticipate will impact the dynamics of highly oriented systems. Section V summarizes the new monodisperse toy molecular model incorporating all the features presented in Secs. II-IV. Steady and transient uniaxial extension is simulated and compared with experimental data in Sec. VI. Steady and transient simulations are also performed for shear flow in Sec. VIA. The results of our new molecular model are discussed and summarized in Sec. VII.

II. MODELLING THE ENTANGLEMENT PAIR DYNAMICS FOR MONODISPERSE SYSTEMS

We begin by constructing a toy dynamical equation for the number of entanglements on a chain in a monodisperse melt. This is inspired by analogy to the slip-link entanglement dynamics in the stochastic simulator [Park *et al.* (2012)] and the discrete slip-link model of Andreev *et al.* (2013) and is similar in spirit to transient network models [Mewis and Denn (1983)]. Ianniruberto and Marrucci (2014) have independently pursued conceptually similar arguments to those presented below to construct a dynamical equation for the entanglement density.

$$\dot{N}(t) = \underbrace{\frac{N_e - N(t)}{\tau_d^1(t)}}_{\substack{test\ \ chain\ tip\ \ diffusion}} \underbrace{-\beta\left[\left(\underline{\underline{\kappa}} : \underline{\underline{S}}_{tube}\right) - \frac{\dot{\Lambda}(t)}{\Lambda} + \frac{\dot{\alpha}(t)}{\alpha}\right]N(t)}_{\substack{convective\ \ destruction\\ of\ \ entanglements}} + \underbrace{\frac{N_e - N(t)}{\tau_d^1(t)}}_{matrix\ tip\ diffusion} \tag{1}$$

Here, $N(t)$, represents the number of entanglement pairs per polymer chain at the current time, t while $N_e \equiv \frac{M}{M_e}$ represents the average equilibrium number of entanglement pairs per chain of molecular weight M with entanglement molecular weight M_e. The non-equilibrium tube disengagement time is $\tau_d^1(t)$. In the second term on the RHS, β is a parameter that reflects the "efficiency" of the convective constraint release mechanism (CCR). The velocity gradient is given by $\underline{\underline{\kappa}}$ and the orientation tensor is defined by $\underline{\underline{S}}_{tube} \equiv \left\langle \widehat{R}\widehat{R} \right\rangle$, where $\widehat{R}$ is the unit end-to-end vector of a tube segment. The relative stretch of the "partially disentangled" chain variable is defined by $\Lambda(t) \equiv \frac{L(t)}{L_{eq}(t)}$ where $L(t)$

is the current tube contour length and $L_{eq}(t)$ is the equilibrium length. Note here that $\Lambda(t)$ is different from the relative stretch of a "fully entangled" chain relative to the initial equilibrium length, which is defined as $\lambda(t) \equiv \frac{L(t)}{L_{eq}}$. Additionally, the ratio between the maximum stretch ratios of both relative stretches is defined as $\alpha(t) \equiv \frac{\Lambda_{\max}(t)}{\lambda_{\max}}$.

What equation (1) represents is the idea that entanglements are destroyed by CCR in proportion to the current entanglement density, $N(t)$, times the fractional rate at which they are destroyed via convection. Entanglements are created by tip diffusion/fluctuations of the test chain and the matrix chains at a rate in proportion to the difference between the entanglement density and its equilibrium value, a driving force, divided by the time scale for the process, $\tau_d^1(t)$.

We now derive the entanglement destruction term in (1), more specifically the expression for the fractional rate of convective destruction of entanglements: $\left[\left(\underline{\underline{\kappa}} : \underline{\underline{S}}_{tube}\right) - \frac{\dot{\Lambda}(t)}{\Lambda} + \frac{\dot{\alpha}(t)}{\alpha}\right]$. Since $L_{eq}(t)$ is a function of the entanglement density $N(t)$, i.e. $L_{eq}(t) \sim \sqrt{N(t)}$ (See equation A1.3 of Appendix A), differentiating $\Lambda(t) \equiv \frac{L(t)}{L_{eq}(t)}$ with respect to time and simplifying yields:

$$\frac{\dot{L}(t)}{L(t)} = \underbrace{\frac{\dot{L}_{eq}(t)}{L_{eq}(t)}}_{\substack{\text{Internal rearrangements of the chain contour due to CR driven disentanglement}}} + \underbrace{\frac{\dot{\Lambda}(t)}{\Lambda(t)}}_{\substack{\text{Fractional rate of tube stretch via all mechanisms}}} = \frac{1}{2}\frac{\dot{N}(t)}{N(t)} + \frac{\dot{\Lambda}(t)}{\Lambda(t)} \qquad (2)$$

The fractional rate of change of the tube contour length $\frac{\dot{L}(t)}{L(t)}$ has two separate contributions. The first term on the RHS of (2) is new and represents the fractional tube shortening/lengthening rate due to constraint release (CR) driven disentanglement. The second term on the RHS represents the fractional rate of tube stretching due to affine stretch, chain retraction of the chain tips into interior parts of the chain and CCR driven tube shortening. All of the effects contained within the second term on the RHS have been presented in Mead et al 1998 and discussed in detail there. Only the disentanglement term, $\frac{\dot{L}_{eq}(t)}{L_{eq}(t)} = \frac{1}{2}\frac{\dot{N}(t)}{N(t)}$, is new. However, even this term is discussed in Sec. II.A.2 of Mead et al 1998. Note that in the original MLD model the entanglement density was assumed to be *constant*, $\dot{N} = 0$.

From equation (16) or (29) we determine that $\frac{\dot{\alpha}(t)}{\alpha} = -\frac{1}{2}\frac{\dot{N}(t)}{N(t)}$ so we finally have an expression for $\frac{\dot{L}(t)}{L(t)}$ in terms of MBP model terms,

$$\frac{\dot{L}(t)}{L(t)} = \frac{1}{2}\frac{\dot{N}(t)}{N(t)} + \frac{\dot{\Lambda}(t)}{\Lambda(t)} = -\frac{\dot{\alpha}(t)}{\alpha} + \frac{\dot{\Lambda}(t)}{\Lambda(t)} \tag{3}$$

Thus, calculating $\frac{\dot{L}(t)}{L(t)}$ is straightforward in the MBP model. Equation (3) for $\frac{\dot{L}(t)}{L(t)}$ can be used directly in equation (9) defining *k* of the MLD paper (Mead *et al.* 1998 pg. 7901);

$$k \equiv \left(\underline{\underline{\kappa}} : \underline{\underline{S}}\right) - \frac{\dot{L}(t)}{L(t)} = \left[\left(\underline{\underline{\kappa}} : \underline{\underline{S}}\right) - \frac{\dot{\Lambda}(t)}{\Lambda} + \frac{\dot{\alpha}(t)}{\alpha}\right] \approx \left[\left(\underline{\underline{\kappa}} : \underline{\underline{S}}\right) - \frac{\dot{\Lambda}(t)}{\Lambda}\right] \tag{4}$$

Generally, $\left|\left(\underline{\underline{\kappa}}:\underline{\underline{S}}\right)-\frac{\dot{\Lambda}(t)}{\Lambda}\right| >> \left|\frac{\dot{\alpha}(t)}{\alpha}\right|$ which when valid reduces (4) to the same CCR expression in the original MLD model. We use the expression for *k* (4) in the convective destruction of entanglements term in (1) as well as in the stretch equation and orientational relaxation equation, both of which include CCR, in the MBP model.

Note that we have ignored factors of Λ^2 in the denominator of the reptative diffusion entanglement creation/destruction terms in (1). We ignore this factor in light of the fact that we are not considering contour length fluctuations explicitly. Contour length fluctuations have no such factor scaling the diffusive creation/destruction of entanglements. Tip contour length fluctuations are presumably responsible for most of the diffusive entanglement creation/destruction processes. However, for the newly created tip entanglement to diffuse into the interior of the chain it takes the reptation time. Hence using the bare reptation time as a characteristic time scale for entanglement creation is a compromise in this simple toy version of the model. A tube coordinate is needed to have a proper description of the entanglement creation/destruction processes. The model of Andreev *et al.* (2013) provides just such a description in a detailed way. Experimentally, studies of the re-entanglement kinetics/dynamics from virgin (unentangled), nascent polymer melts provide a viable means to quantitatively determine the appropriate time scale for the re-entanglement processes described in equation (1) [Yamazaki *et al* (2006); Rastogi *et al* (2003); Wang *et al* (2009)].

The factor β scaling the convective destruction of entanglements term represents a CCR "efficiency" factor related to the number of constraint release events required to generate a single disentanglement [Ianniruberto and Marrucci (1996)].

This interpretation suggests that $0 < \beta < 1$. The factor β was originally introduced by Ianniruberto and Marrucci (1996, 2001) to ensure a stable monotonic steady shear stress vs. shear rate curve and β retains this interpretation in the current work.

The non-equilibrium tube disengagement time $\tau_d^1(t)$ is a function of the entanglement density, $N(t)$. Physically this arises because the absolute distance for the chain to diffuse shortens as the number of entanglements decreases. In Appendix A we derive the result:

$$\tau_d^1(t) = \left(\frac{N(t)}{N_e}\right)\tau_{d,0}(t) \tag{5}$$

Here $\tau_d^1(t)$ is the terminal tube disengagement time for arbitrary $N(t)$ relative to the non-equilibrium tube disengagement time, $\tau_{d,0}(t)$, which will be lowered in fast flows by CDFC and hence is also a function of time (Sec. IIA).

Using (5) in (1) the expression for the entanglement dynamics can now be simplified and re-written as:

$$\dot{N}(t) = \underbrace{\frac{2N_e}{\tau_{d,0}(t)}\left[\frac{N_e}{N(t)} - 1\right]}_{\substack{entanglement\ creation \\ via\ tip\ diffusion}} - \underbrace{\beta\left[\left(\underline{\underline{\kappa}} : \underline{\underline{S}}_{tube}\right) - \frac{\dot{\Lambda}(t)}{\Lambda} + \frac{\dot{\alpha}(t)}{\alpha}\right]N(t)}_{CCR\ induced\ entanglement\ destruction} \tag{6}$$

Note that the MLD "toy" model for ED does not explicitly contain tip fluctuations which are undoubtedly very important in the re-entanglement process [Mead (2011b);

Andreev *et al.* (2013)]. A more detailed model at the tube coordinate level is needed to properly capture the effects of tip fluctuations versus reptational effects.

The modulus scales the stress in molecular models and is a function of the entanglement density. It can be written as [Dealy and Wissbrun (1989)]:

$$G_N(t) \equiv \frac{\rho RT}{M_e(t)} = \frac{\rho RT}{\left(\frac{M}{N(t)}\right)} = \frac{N(t)}{N_e} G_N^0 \tag{7}$$

Here, G_N^0 is the equilibrium plateau modulus. ρ, R, and T are density, gas constant, and absolute temperature, respectively. If the entanglement density is significantly lower than equilibrium the modulus will be directly impacted (lowered) for an extended period of time following deformation. This could explain the phenomena of "shear modification" which is still unexplained theoretically [Rokudai (1979); Yamaguchi and Wagner (2006); Leblans and Bastiaansen (1989)]. Shear modification is a deformation-induced reversible reduction in the dynamic moduli for high molecular weight polydisperse linear and LCB entangled polymers [Dealy and Wissbrun (1989)]. Shear modification is one of the last great unsolved theoretical problems in nonlinear molecular rheology.

One of the conundrums with the above entanglement dynamics model is that in very fast extension virtually all the entanglements are convected away leaving a modulus that approaches zero. Not surprisingly the discrete slip-link model by Andreev *et al.* (2013) has similar issues. When all entanglements are stripped from the chain the Peterlin modulus will be applicable [Desai and Larson (2014)]. The Peterlin modulus is that of an unentangled ensemble of stretched chains in a flow field.

A. Formulation of the expression for Kuhn bond based CDFC on the stretch and terminal orientational relaxation times

Here we briefly outline how to calculate the net fractional Kuhn bond orientation and the reformulated expression for the decrease in the friction coefficient due to net Kuhn relative bond alignment of the test chain with respect to the matrix chains. Note here that structural parameters of PS are used since the experimental data of PS melts and solutions are compared with the predictions by various models studied in this paper.

We start by denoting the net Kuhn bond orientation in the polydisperse MLD "toy" model single segment as $\underline{\underline{S}}_{Kuhn}$. The net Kuhn bond orientation of the matrix is proportional to the birefringence which, using the freely jointed chain model in a Kuhn-Grün analysis, yields:

$$\underline{\underline{S}}_{Kuhn} = \left(1 - \frac{3x}{\mathrm{L}^{-1}(x)}\right)\underline{\underline{S}}_{tube} + isotropic\ terms = \left(1 - \frac{3x}{\mathrm{L}^{-1}(x)}\right)\left\langle \hat{R}\hat{R} \right\rangle + isotropic\ terms \tag{8}$$

Where $\underline{\underline{S}}_{tube}$ is the single tube segment orientation. The inverse Langevin function term, $\mathrm{L}^{-1}(x)$, in (8) can be accurately approximated within 1% [Treloar (1975) pg. 178] for easy calculation,

$$\left(1 - \frac{3x}{\mathrm{L}^{-1}(x)}\right) \approx \frac{3}{5}x^2 + \frac{1}{5}x^4 + \frac{1}{5}x^6 \tag{9}$$

where x is the fractional chain extension:

$$x \equiv \frac{\lambda}{\lambda_{\max}} \tag{10}$$

Note here that Yaoita *et al.* (2012) use the simplest approximation $\left(1-\frac{3x}{\mathrm{L}^{-1}(x)}\right)\approx x^2$ in their work. It is also noted that the definition of *x* will be altered, $x\equiv\frac{\Lambda}{\Lambda_{\max}}$, for models that include entanglement density dynamics.

The maximum relative stretch $\lambda_{\max}$ is calculated as [Mead (2011b)],

$$\lambda_{\max}=n^{1/2}=0.82\left[\frac{M_e}{C_\infty M_0}J\right]^{1/2}. \tag{11}$$

Here *J* is the number of carbon-carbon sigma bonds in the backbone, *J*=2 for PS, M_e is the equilibrium average entanglement molecular weight (13333 Da for PS). In non-equilibrium flow situations the entanglement molecular weight is a function of concentration and the dynamic entanglement density along the chain. C_∞ is the characteristic ratio, 9.8 for PS [Flory (1969)] and M_0 is the monomer molecular weight, 104 Da for PS. n is the number of Kuhn bonds in an entanglement segment. Note that for PS melts $\lambda_{\max}=4.2$, a relatively small maximum stretch. The maximum stretch will be much larger ($\lambda_{\max}>25$) for the entangled high MW entangled PS solutions considered by Bhattacharjee *et al.* (2002).

Ianniruberto *et al.* calculated the functional form of the reduced friction versus matrix Kuhn bond orientation for monodisperse PS melts in their 2012 paper [Ianniruberto *et al.* (2012) see Fig. 4]. We use the Ianniruberto *et al.* (2012) CDFC calculation as a guide.

$$\frac{\varsigma(t)}{\varsigma_{eq}} = \frac{\tau_{d,0}(t)}{\tau_{d,eq}} = \frac{\tau_s(t)}{\tau_{s,eq}} = 0.02239\left(S_{Kuhn}(t)\right)^{-1.65} \qquad S_{Kuhn} > 0.1 \tag{12}$$

Where ς is the monomeric friction coefficient, τ_d is the reptation time, and τ_s is the longest Rouse relaxation time. Subscript "*eq*" indicates equilibrium value and "0" means a value for a fully entangled chain.

The true form of the dependence of the accelerated relaxation rate can in principle be determined by the nonlinear extensional stress relaxation experiments of Yaoita *et al.* (2012) which are of fundamental importance with respect to CDFC. These experiments are discussed in detail in Section III and Fig. 7.

Following Yaoita *et al.* (2012) we define the scalar net fractional Kuhn bond alignment S_{Kuhn} as,

$$S_{Kuhn} \approx \phi_p\left(\frac{3}{5}x^2 + \frac{1}{5}x^4 + \frac{1}{5}x^6\right)\left|\underline{\underline{S}}_{tube}\right| \qquad 0 < S_{Kuhn} < 1 \tag{13}$$

The fractional Kuhn bond orientation, S_{Kuhn}, varies between zero and one for perfect orientation. The anisotropic tube orientation in uniaxial extension is denoted by $\left|\underline{\underline{S}}_{tube}\right| = \left(S_{xx} - S_{yy}\right)$. For shear deformation the principal values must be used, $\left|\underline{\underline{S}}_{tube}\right| = \left[\left(S_{xx} - S_{yy}\right)^2 + 4S_{xy}^2\right]^{\frac{1}{2}}$. The mass fraction of polymer scales the fractional Kuhn bond orientation and is represented by ϕ_p such that CDFC for both melts, $\phi_p = 1$, and entangled solutions, $\phi_p < 1$, can be modelled.

III. MODIFICATION OF THE DESAI-LARSON TOY DEMG MODEL TO INCORPORATE ED, CDFC AND CCR

Here we briefly outline how to incorporate the new results in Sections II and IIA into the Desai-Larson modified DEMG model [Desai and Larson (2014)]. We eliminate the Desai and Larson tube dilation effect and replace it with the CDFC and entanglement dynamics results presented in Sections II and IIA above. This allows *both* the disengagement time and the stretch time to be modified by CDFC which should in principle allow an accurate modeling of steady state extensional viscosity data for *both* melts and solutions.

One of the key theoretical developments in the Desai-Larson model is the derivation of a new stretch dynamics equation for the partially disentangled chain that incorporates the fact that the maximum extension is a function of the entanglement density [Mead (2011b)]. When $M_e(t) = \frac{M}{N(t)}$ changes (increases) with deformation induced disentanglement, the maximum stretch also increases as described below.

$$\Lambda_{\max}(t) = n^{1/2} = 0.82\left[\frac{M_e(t)}{C_\infty M_0} J\right]^{1/2} = 0.82\left[\frac{M}{C_\infty M_0 N(t)} J\right]^{1/2} \tag{14}$$

There is one new stretching effect to account for in the stretch equation: stretch shortening due to removal of chain back folds. The stretch dynamical equation for the diluted (partially disentangled) chain, generalized to include constraint release effects, is [Desai and Larson (2014), Mead *et al.* (1998)].

$$\dot{\Lambda}(t) = \underbrace{-\left[\frac{\dot{\alpha}(t)}{\alpha}\Lambda\right]}_{\substack{\text{stretch reduction}\\ \text{due to disentanglement}}} + \underbrace{\left(\underline{\underline{\kappa}} : \underline{\underline{S}}_{tube}\right)\Lambda}_{\text{affine stretch}} - \underbrace{k_s\left(\frac{\Lambda-1}{\tau_s}\right)}_{\text{chain retraction}} - \underbrace{\frac{1}{2}(\Lambda-1)\left[\underline{\underline{\kappa}} : \underline{\underline{S}}_{tube} - \frac{\dot{\Lambda}}{\Lambda} + \frac{\dot{\alpha}(t)}{\alpha} + \frac{1}{\Lambda^2\tau^1{}_d(t)}\right]}_{\text{CCR driven tube shortening}} \tag{15}$$

where, $\alpha(t) = \dfrac{\Lambda_{\max}(t)}{\lambda_{\max}} = \left[\dfrac{N_e}{N(t)}\right]^{\frac{1}{2}}$ and $\dot{\alpha}(t) = -\dfrac{1}{2}\left[N_e\right]^{\frac{1}{2}}\left[N(t)\right]^{-\frac{3}{2}}\dot{N}(t)$ (16)

and the nonlinearity of the spring is incorporated in a single factor denoted by k_s [Cohen (1991), Desai and Larson (2014)]:

$$k_s(t) \equiv \frac{\mathrm{L}^{-1}\left(\dfrac{\Lambda(t)}{\Lambda_{\max}(t)}\right)}{3\dfrac{\Lambda(t)}{\Lambda_{\max}(t)}} \approx \frac{\left(3\lambda_{\max}^2\alpha^2 - \Lambda^2\right)/\left(\lambda_{\max}^2\alpha^2 - \Lambda^2\right)}{\left(3\lambda_{\max}^2\alpha^2 - 1\right)/\left(\lambda_{\max}^2\alpha^2 - 1\right)} \tag{17}$$

We have added a CCR tube shortening term to the Desai-Larson stretch equation (15) that requires discussion. This is done in Section IV below.

The above generalized expression of the stretch dynamics is principally what we take from the Desai-Larson diluted tube model. We use the entanglement dynamics model presented in Section II to replace the tube dilation dynamics expressions in the Desai-Larson model.

IV. MODIFICATION OF THE NEW CDFC-ED "TOY" MLD MODEL TO ACCOUNT FOR REDUCED LEVELS OF CCR FOR HIGHLY ALIGNED SYSTEMS

In this Section we outline the manner in which the previously presented model can be modified to account for the idea that CCR effects are different (greatly reduced) in systems of slightly oriented versus highly oriented chains. These effects will impact CCR driven re-orientation as well as CCR driven stretch relaxation (tube shortening) in fast flows [Mead *et al.* (1998)]. These ideas are partly motivated by the work of Desai and Larson (2014) that showed that CCR appears not to be important to capture the salient features of fast nonlinear extensional flows. This is a conclusion that we affirm in calculations with our new model.

The specific effect we wish to incorporate in our model is that CCR effects do not strongly impact highly aligned chains. For example, in the limit of perfectly aligned chains in fast flow there are no dynamical (topological) constraints and consequently CCR will have no effect on the orientation or stretch of the test chain even though $\underline{\underline{\kappa}} : \underline{\underline{S}}_{tube}$ is very large [Desai and Larson (2014)]. Of course this ideal limiting situation can only be approached in any finite deformation rate flow. We propose an ad hoc empiricism that smoothly transits between the Gaussian and highly oriented extreme situations. A sketch of these ideas for CCR driven stretch relaxation is shown in Fig.s 1 and 2.

We propose the following empirical changes to the stretch and orientation dynamical equations to account for the ideas presented in the above thought experiment. CCR in stretching flows relaxes $\frac{1}{2}(\Lambda - 1)$ of the stretch associated with a given

entanglement [Mead (2011a)]. Using the above ideas, we construct an empirical function that smoothly transits between the Gaussian and highly oriented cases.

$$\underbrace{\frac{1}{2}(\Lambda-1)}_{\substack{Gaussian\ \ tube\\ shortening}} \underbrace{-\frac{1}{2}\left(\left|\underline{\underline{S}}_{tube}\right|\right)(\Lambda-1)}_{\substack{highly\ \ oriented\ \ biased\\ tube\ \ shortening}} = \frac{1}{2}\left(1-\left|\underline{\underline{S}}_{tube}\right|\right)(\Lambda-1) \tag{18}$$

We have included a new empirical term to the tube shortening expression, $\left(1-\left|\underline{\underline{S}}_{tube}\right|\right)$. Fig. 1 illustrates the physical ideas underlying this empirical factor multiplying the tube shortening term. Note that for $\left|\underline{\underline{S}}_{tube}\right| \approx 1$ we assume the chain is unraveled and linear rather than a zig-zagged cat's cradle (back folded) conformation. The new term effectively wipes out tube shortening stretch relaxation for fast flows where the tube is highly oriented. Desai and Larson (2014) have shown that this is a desirable feature to have in the model for fast uniaxial extension and this underlies the motivation for this ad hoc factor in the stretch equation.

Incorporating the new proposed physics into the stretch equation yields:

$$\dot{\Lambda}(t) = -\left[\frac{\Lambda}{\alpha}\dot{\alpha}(t)\right] + \left(\underline{\underline{\kappa}} : \underline{\underline{S}}_{tube}\right)\Lambda - k_s\left(\frac{\Lambda-1}{\tau_s}\right) - \frac{1}{2}\left(1-\left|\underline{\underline{S}}_{tube}\right|\right)(\Lambda-1)\left[\underline{\underline{\kappa}} : \underline{\underline{S}}_{tube} - \frac{\dot{\Lambda}}{\Lambda} + \frac{\dot{\alpha}(t)}{\alpha} + \frac{1}{\Lambda^2\tau^1{}_d(t)}\right] \tag{19}$$

Thus, at high fractional extensions the effect of CCR on stretch smoothly disappears as $\left|\underline{\underline{S}}_{tube}\right|$ monotonically increases. Thus, CCR can effectively reduce stretch in shear flows where the orientation is lower than it is in extensional flows.

We also propose an ad hoc modification to the orientation dynamics equation to account for biased (reduced) re-orientation due to nematic (molecular packing) effects in highly aligned systems. Nematic effects are well established in cross-linked rubbers and polymer melts [Doi *et al.* (1989)]. In such highly oriented systems the switch function, $\frac{1}{\Lambda}$, already diminishes the effect of CCR on the re-orientation process. We add to this effect with an ad hoc empirical nematic re-orientation suppression factor $(1-S_{Kuhn})$.

$$\frac{1}{\tau(t)} = (1-S_{Kuhn})\left[\frac{1}{\Lambda^2(t)\tau^1{}_d(t)} + \frac{1}{\Lambda}\left[\underline{\underline{\kappa}} : \underline{\underline{S}}_{tube} - \frac{\dot{\Lambda}}{\Lambda} + \frac{\dot{\alpha}(t)}{\alpha} + \frac{1}{\Lambda^2\tau^1{}_d(t)}\right]\right] \tag{20}$$

The factor $(1-S_{Kuhn})$ empirically accounts for the idea that the re-orientation process will be biased (reduced) by nematic packing effects due to the net Kuhn bond orientation of the matrix. Note that we are actually not including a biased re-orientation but rather an increased orientational relaxation time which has a similar effect on the orientation level. Another way to look at this effect is that constraint release effects will be ineffectual in highly aligned systems i.e. when S_{Kuhn} is large (see Fig.s 1 and 2). Including the new factor of $(1-S_{Kuhn})$ along with the switch function will effectively reduce all CCR driven re-orientation in fast stretching flows where S_{Kuhn} is large.

Note that there will be a sharp distinction between uniaxial extension and shear with the above two modifications. In uniaxial extension the orientation and stretch is severe and the above two modifications will both kick in. Conversely, in shear flows the orientation and stretch is weak and $(1-S_{Kuhn}) \approx 1$ such that there are no nematic effects in melts or solutions.

V. SUMMARY OF THE EQUATIONS IN THE EDS - KUHN BOND CDFC RE-FORMULATION OF THE MONODISPERSE MLD TOY MODEL

Here we briefly summarize the equation set for the new monodisperse MLD "toy" model [see Desai and Larson (2014) equations 31-37 and note the differences]. We are only considering the monodisperse case here. Generalizing the results to polydisperse systems is an important goal of this work. This is straightforward and is done in Appendix B.

We start with the deterministic differential evolution equation for the entanglement pair orientation, $\underline{\underline{S}}_{tube}$ [Desai and Larson (2014), Mead (2007), Larson (1984), Marrucci (1984)]. We choose the differential approximation to the orientation evolution for coding simplicity and speed in computing. Here, $\hat{\underline{\underline{S}}}_{tube}$ represents the upper convected time derivative.

$$\hat{\underline{\underline{S}}}_{tube}(t) + 2\left(\underline{\underline{\kappa}}(t) : \underline{\underline{S}}_{tube}(t)\right)\underline{\underline{S}}_{tube} + \left(\frac{1 - S_{Kuhn}}{\tau(t)}\right)\left(\underline{\underline{S}}_{tube}(t) - \frac{1}{3}\underline{\underline{\delta}}\right) = 0 \tag{21}$$

Relaxation time
$$\frac{1}{\tau(t)} = \frac{1}{\Lambda^2(t)\tau^1{}_d(t)} + \left(\frac{1}{\Lambda}\right)\left[\underline{\underline{\kappa}} : \underline{\underline{S}}_{tube} - \frac{\dot{\Lambda}}{\Lambda} + \frac{\dot{\alpha}(t)}{\alpha} + \frac{1}{\Lambda^2\tau^1{}_d(t)}\right] \tag{22}$$

where,
$$\tau^1{}_d(t) = \left(\frac{N(t)}{N_e}\right)\tau_{d,0}(t) \tag{23}$$

and CDFC
$$\frac{\varsigma(t)}{\varsigma_{eq}} = \frac{\tau_{d,0}(t)}{\tau_{d,eq}} = \frac{\tau_s(t)}{\tau_{s,eq}} = 0.02239\left(S_{Kuhn}(t)\right)^{-1.65} \qquad S_{Kuhn} > 0.1 \tag{24}$$

$$S_{Kuhn} = \phi_p \left(1 - \frac{3x_i}{\mathrm{L}^{-1}(x_i)}\right)\left|\underline{\underline{S}}_{tube}\right| \approx \phi_p \left(\frac{3}{5}x^2 + \frac{1}{5}x^4 + \frac{1}{5}x^6\right)\left|\underline{\underline{S}}_{tube}\right| \tag{25}$$

where $x \equiv \frac{\Lambda}{\Lambda_{\max}}$ and for uniaxial stretch $\left|\underline{\underline{S}}_{tube}\right| = \left(S_{xx} - S_{yy}\right)$ while for shear deformation

$$\left|\underline{\underline{S}}_{tube}\right| = \left[\left(S_{xx} - S_{yy}\right)^2 + 4S_{xy}^2\right]^{\frac{1}{2}} \tag{26}$$

Entanglement dynamics $\dot{N}(t) = \frac{2N_e}{\tau_{d,o}(t)}\left[\frac{N_e}{N(t)} - 1\right] - \beta\left[\underline{\underline{\kappa}} : \underline{\underline{S}}_{tube} - \frac{\dot{\Lambda}}{\Lambda} + \frac{\dot{\alpha}(t)}{\alpha}\right]N(t)$ (27)

Stretch dynamics

$$\dot{\Lambda}(t) = -\left[\frac{\Lambda}{\alpha}\dot{\alpha}(t)\right] + \left(\underline{\underline{\kappa}} : \underline{\underline{S}}_{tube}\right)\Lambda - k_s\left(\frac{\Lambda - 1}{\tau_s}\right) - \frac{1}{2}\left(1 - \left|\underline{\underline{S}}_{tube}\right|\right)(\Lambda - 1)\left[\underline{\underline{\kappa}} : \underline{\underline{S}}_{tube} - \frac{\dot{\Lambda}}{\Lambda} + \frac{\dot{\alpha}(t)}{\alpha} + \frac{1}{\Lambda^2 \tau^1{}_d(t)}\right] \tag{28}$$

$$\alpha(t) \equiv \frac{\Lambda_{\max}(t)}{\lambda_{\max}} = \left[\frac{N_e}{N(t)}\right]^{\frac{1}{2}} \quad \text{And} \quad \dot{\alpha}_i(t) = -\frac{1}{2}\left[N_e\right]^{\frac{1}{2}}\left[N(t)\right]^{-\frac{3}{2}}\dot{N}(t) \tag{29}$$

Nonlinear spring $k_s(t) \equiv \frac{\mathrm{L}^{-1}\left(\frac{\Lambda(t)}{\Lambda_{\max}(t)}\right)}{3\frac{\Lambda(t)}{\Lambda_{\max}(t)}} \approx \frac{\left(3\lambda_{\max}^2\alpha^2 - \Lambda^2\right)/\left(\lambda_{\max}^2\alpha^2 - \Lambda^2\right)}{\left(3\lambda_{\max}^2\alpha^2 - 1\right)/\left(\lambda_{\max}^2\alpha^2 - 1\right)}$ (30)

Stress calculator $\underline{\underline{\sigma}}(t) = 3G_N(t)\left[\frac{\mathrm{L}^{-1}\left(\frac{\Lambda(t)}{\Lambda_{\max}(t)}\right)}{3\frac{\Lambda(t)}{\Lambda_{\max}(t)}}\right]\Lambda^2\,\underline{\underline{S}}_{tube} \approx 3G_N(t)k_s(t)\Lambda^2(t)\underline{\underline{S}}_{tube}(t)$ (31)

where the partially disentangled modulus is defined as:

$$G_N(t) \equiv \frac{\rho RT}{\left(\frac{M}{N(t)}\right)} = \frac{N(t)}{N_e} G_N^0 \tag{32}$$

The fact that the modulus is a function of time, $G_N(t) = \frac{N(t)}{N_e} G_N^0$, clearly demonstrates that the new model will predict "shear modification". For high molecular weight systems or systems with LCB the entanglement microstructure will take an extended time to heal during which the measured dynamic moduli will be lower than their equilibrium values, $G^*(\omega,t) < G^*(\omega,\infty)$. This shear modification can be quite large and last for an extended period of time as the entanglement microstructure slowly heals via the diffusive process of reptation [Rastogi et al (2003), Rokudai (1979)]. The entanglement microstructure will heal on a time scale of the disengagement time, $\tau_{d,0}$, which can be very long indeed for high molecular weight or LCB systems.

VI. SIMULATION OF MONODISPERSE LINEAR PS MELTS AND ENTANGLED SEMIDILUTE SOLUTIONS IN STEADY AND TRANSIENT UNIAXIAL EXTENSION

In this Section we explore the properties of the new MBP entanglement dynamics model for monodisperse systems by numerically solving the system of equations (21) - (32) summarized in Sec. V. Although the equation set appears complex and formidable they are all ordinary differential equations that can be stepped forward in time using the simple Euler method. Because the Euler method is first order in time care must be taken to take small enough time step sizes to ensure convergence. Using the Euler method makes the code simple to write and fast to execute. Computational speed becomes an issue when polydispersity is introduced particularly so when the integral form of the orientation evolution equation is used [Mishler and Mead (2013a), (2013b)].

We will execute our study by including/excluding various physical effects to isolate their significance. The physics we are interested in understanding are CCR, ED (through β), and CDFC. The simulation software allows us to turn the specific physics "on"/"off" and to thereby quantify the impact of the specific physics on rheology. We shall be particularly interested in the following basic models summarized in Table I. The experimental data sets, which are used to compare with the calculated prediction results, are summarized in Table II.

The first simulations we perform are for the flow curves for steady uniaxial extension of monodisperse PS melts. For these simulations we shall choose a value of $\beta = 0.12$ (ED "on") in equation (27). This value is chosen such that the shear stress – shear rate curve is monotonic (see Fig. 10 of Section VIA).

A monotonic shear stress – shear rate curve is necessary for stable shear flow [Ianniruberto and Marrucci (2001)]. All values of $\beta < 0.12$ yield monotonic shear stress – shear rate curves. The first system we shall study is PS200K (130 ^{o}C monodisperse PS melt by Bach *et al.*'s (2003)) in steady state extensional flow. The average equilibrium number of entanglements per chain in this system is 15. The results of a variety of simulations are shown in Fig. 3 along with the experimental data. The base case for comparison is the DEMG model which has no ED, CCR or CDFC. The DEMG line in Fig. 3 shows a ladle shaped flow curve. The upturn in viscosity is associated with the onset of chain stretching and occurs when the stretch Weissenberg number is about unity, $\dot{\varepsilon}\tau_{s,eq} \approx 1$. Complimentary to the DEMG model is the MLD "toy" model which is simply the DEMG model with CCR switched "on". Here again we see the ladle shaped flow curve, lowered relative to the DEMG model by the additional relaxation mechanism of CCR. The predicted flow curves of both the DEMG and MLD models are qualitatively and quantitatively at odds with the experimental data.

The next simulation we execute is the base DEMG model with CDFC now turned "on" (DEMG-cdfc). Its flow curve is now monotonic extension thinning and closely mimics the experimental data both before and after $\dot{\varepsilon} \approx \frac{1}{\tau_{s,eq}}$. This result, and those presented in what follows, strongly suggest that CDFC is the essential feature needed to achieve a monotonic thinning extensional flow curve for monodisperse PS melts [Desai and Larson (2014)].

The simulation results are sensitive to the details of the specific expression for CDFC used. In particular, the details of the form of the expression for S_{Kuhn} used matter in the simulations. The shape of the flow curve is determined by the specific functional form of CDFC used (see equations (24-26)). In particular, to achieve a monotonic flow curve CDFC must be activated slightly before $\dot{\varepsilon} \approx \frac{1}{\tau_{s,eq}}$. If CDFC is activated later than $\dot{\varepsilon} \approx \frac{1}{\tau_{s,eq}}$, a "kink" will occur in the flow curve. Precisely when CDFC is activated depends on the specific functional form of the CDFC we use.

The next simulation we perform is to include ED in the simulation. In this case, we choose $\beta = 0.12$ with both CCR "on" and CDFC "on", i.e. the MBP model. ED is "on" for any $1 > \beta > 0$. This generates the black solid curve in Fig. 3. Here for $\dot{\varepsilon} < \frac{1}{\tau_{s,eq}}$, we observe excessive thinning with lower viscosity values relative to those for DEMG-cdfc which is caused by CCR. The curve also shows an upturn around $\dot{\varepsilon} \approx \frac{1}{\tau_{s,eq}}$ due to the onset of stretch. However, for $\dot{\varepsilon} > \frac{1}{\tau_{s,eq}}$, it becomes a thinning curve again, approximately parallel to the DEMG-cdfc case. This thinning effect is due to the effects of CDFC being activated. Hence, the results especially at $\dot{\varepsilon} > \frac{1}{\tau_{s,eq}}$ are approximately *equivalent* to the DEMG-cdfc model when we add ED despite the fact that the internal workings of the two models are entirely *different*. In particular the average number of entanglements is dramatically lower when ED is turned "on" resulting in a lower modulus. The lower modulus implies a

different entanglement microstructure relative to the DEMG model with CDFC now turned "on" which predicts a constant entanglement density.

The final simulation we perform is with $\beta = 0.12$, ED "on", CCR "off" and CDFC "on" (MBP-xccr). This is shown as the blue dashed line curve in Fig. 3. As with the DEMG-cdfc model, the MBP-xccr model generates results very close to the experimental data. The flow curve shows a much smaller "kink" right after $\dot{\varepsilon} \approx \frac{1}{\tau_{s,eq}}$ than that of the MBP curve and closely mimics the experimental data. The small "kink" is the result of stretch being activated prior to CDFC being activated. Choosing a different functional form for CDFC can in principle eliminate this "kink" by modifying precisely when CDFC is activated relative to $\dot{\varepsilon} \approx \frac{1}{\tau_{s,eq}}$. Precisely when CDFC is activated is impacted by whether ED and CCR are "on" or "off". The details of the models, including when CDFC is activated, are displayed in the Fig.s of Appendix C.

We now address the perplexing question of why the simulations of the "straight" DEMG-cdfc are very similar to the new MBP-xccr model with $\beta = 0.12$, i.e. although the details of the two models, such as the number of entanglements and the modulus, are profoundly different, they nevertheless yield approximately equivalent extensional flow curves in close agreement with experimental data. Fig. 4 plots the average number of entanglements per chain versus extension rate for $\beta = 0.12$ with CCR "off" and CDFC "on" (MBP-xccr model). We see that for fast extensional flows the average number of entanglements per chain is approximately half that at equilibrium. Physically, the modulus is the manifestation of the entanglement microstructure (see equation (32)) and hence the

modulus drops off proportionately. Thus, the new MBP-xccr model predicts significant changes in the entanglement microstructure in fast extensional flow.

Figure 5 plots the steady state relative stretches, λ and Λ, for the two different models (DEMG-cdfc and MBP-xccr) versus extension rate. Clearly the relative stretch of the MBP simulations, Λ, is significantly larger than the relative stretch of the DEMG-cdfc simulation, λ. The reason that these two simulations yield approximately equivalent extensional flow curves is that the effect of ED on the modulus, equation (32), is effectively canceled by the corresponding increase in stretch. Using the expression for the stress (31) we argue that for the two models the following products are proportional to the extensional stress and are approximately equal even though $\Lambda \neq \lambda$:

$$G_N(t)\Lambda^2_{MBPxccr}(t) \approx G^0_N \lambda^2_{DEMGcdfc}(t) \tag{33}$$

Here we have made the assumption that orientation has effectively saturated when stretch commences. The saturated orientation cancels on both sides of (33). We have also assumed that the non-Gaussian factors k_s are both close to unity and cancel. Note that for any given model with ED the following equality holds;

$$G_N(t)\Lambda^2_{ED}(t) = G^0_N\left(\frac{N(t)}{N_e}\right)\lambda^2_{ED}(t)\left(\frac{N_e}{N(t)}\right) = G^0_N \lambda^2_{ED}(t) \tag{34}$$

Here, $\lambda^2_{ED}(t)$ represents the stretch relative to the equilibrium extension in any model with ED. Hence, another way to see the approximation in (33) is to note that both the DEMG-cdfc and MBPxccr models yield similar expressions for the extensional stress

in fast steady extension, (34). However, note that $\lambda_{ED}^2(t)$ and $\lambda_{DEMG}^2(t)$ are calculated differently in each model and hence are *not* equal.

The argument underlying equation (33) may very well explain the apparent "success" of the mono and polydisperse MLD models in predicting nonlinear flows despite the fact that all MLD models assume a *constant* entanglement density [Mead (1998), Mead (2011a), Mishler and Mead (2013a,b)].

In Fig. 6 we examine the transient extensional viscosity versus time for the PS200K melt. Transient extensional viscosities are more typical of what one encounters in practice since steady state (Hencky strains greater than ~3) extensional viscosities are very difficult to achieve experimentally. The specific case that we examine is for an extension rate of 0.01 sec^{-1} which corresponds to a stretch Weissenberg number of $\dot{\varepsilon}\tau_{s,eq} \approx 1$. Note the broad maximum in the MBP curve at a Hencky strain of ~1.5. The cause of the maximum is that entanglement dynamics [$N(t)$] is controlled by ED and lags the stress, only slowly approaching its steady state value. As in the case for the steady uniaxial flow curves, the DEMG-cdfc and MBP-xccr models provide the best fit to the data.

The next transient extensional experiment we examine is stress relaxation after imposing 3 Hencky strain units on a PS145K at 120°C. These experiments were performed by Yaoita *et al.* (2012) and provide definitive, hard experimental evidence for the existence of CDFC. Fig. 7 displays the results of our simulations along with the experimental data. Fig. 7 experimentally demonstrates that CDFC accelerates the relaxation following cessation of stretch. The higher the initial stress, the higher the net Kuhn bond orientation and the larger the CDFC effect and hence the faster the initial relaxation rate. The

systematic increase in the initial rate of relaxation strongly supports the existence of CDFC and this effect is quantitatively captured in the MBP model. Additionally, for the MBP model, the entanglement density relaxes on a time scale of $\tau_d \approx 7800 \text{ sec}$, much slower than the time scale shown in Fig. 7. Hence the modulus is lowered relative to the equilibrium state and persists even though the deformation has ceased and this effect does not impact the relaxation processes in Fig. 7. This phenomenon is "shear modification".

Finally, we examine another PS melt, PS545k studied by Huang *et al.* (2013). The principal difference between this set of experiments/simulations and Fig. 3 is that the average number of entanglements per chain is very large, Z~41. Hence the separation between the equilibrium stretch and orientational relaxation times is correspondingly large since $\tau_d \approx 3Z\tau_s$. However, despite this distinction the salient features of Fig. 8 are largely similar to those discussed for the PS200K melt in Fig. 3. In particular, we see an enhanced sensitivity as to precisely when CDFC is activated relative to the onset of stretch. This sensitivity manifests itself in the size of the "kink" in the flow curve as discussed above with respect to Fig. 3. These simulations provide a severe test for the precise functional form of CDFC used.

Figure 9 shows the steady state experimental extensional flow curves for 20 wt.% 1.95M PS solution at 21°C showing monotonic thinning before, and hardening after, $\dot{\varepsilon}\tau_{s,eq} \approx 1$ [Acharya *et al.* (2008)]. The new MBP model qualitatively captures the salient ladle shape features of the flow curve data as does the straight DEMG model without ED, CDFC or CCR. Once again, the DEMG-cdfc and MBP-xccr provide the best fits to the experimental data.

Thus the new MBP-xccr model, which includes ED and CDFC, captures *both* the monotonic thinning behavior of monodisperse PS melts and the thinning/hardening behavior observed for entangled PS solutions. For solutions, CDFC is effectively diluted out and is ineffective due to the factor of ϕ_p in (13) a point which is also discussed by Yaoita *et al.* (2012). Hence, the results from the DEMG and DEMG-cdfc models are almost identical since CDFC is diluted out and is essentially inactive in semi-dilute solutions.

A. Simulation of monodisperse linear PS melts and solutions in steady and transient shear flow

Since we are interested in a generally applicable "toy" molecular model, we examine the predictions of the new MBP model in steady and transient shear flow. Here the orientations will be lower than in fast extensional flows and we anticipate that CCR will be more important than it is in fast extensional flows.

The first issue we address is determining the range of allowable values for β. We do this by demanding that the shear stress vs. shear rate curve be monotonic such that, consistent with most experiments, shear flow of melts is stable [McLeish & Ball (1986)]. Fig. 10 displays the derivative of several shear stress vs. shear rate curves for different values of β. It is evident that the shear stress-shear rate curves are monotonic (all positive slopes) for all $\beta < 0.12$ and exhibit a broad maximum for $\beta > 0.12$. Hence for our simulations we choose the maximum allowable value for $\beta = 0.12$.

In Fig. 11. we compare the calculated shear flow curve for a 7 wt. % 8.42M PS solution with experimental data [Pattamaprom and Larson (2001)]. We also compare the first normal stress difference with data in Fig. 12. In both cases all the models

approximately mimic the data. The MBP model improves the agreement with the experimental viscosity at high shear rates whereas the normal stress differences are under predicted. Note that the results from the DEMG and DEMG-cdfc models were very similar, which indicates the effect of CDFC is very weak for solutions as was the case in the extensional flows of semi-dilute solutions. The flow curve of MBP-xccr in Fig. 12 is very similar to those of DEMG models but the discrepancy from the experimental data is a little lower than that of DEMG models.

Figure 13 shows the simulation results of transient shear viscosity of a PS200K-S melt [Schweizer et al (2004)]. All the models display similar trends to those found in steady shear flow of solutions with the DEMG-cdfc and MBP-xccr models performing best. The shear stress overshoot is missed by all models in fast shear flows, $\dot{\gamma} = 30\ \text{sec}^{-1}$. This is caused by the differential form of the orientation evolution equation used in this work rather than the rigorous integral formulation [Larson (1984), Marrucci (1984)]. Using the original Doi-Edwards integral evolution equation employing the universal orientation tensor will significantly improve these fast transient shear simulations at the expense of more complex simulation software.

VII. DISCUSSION/SUMMARY

We have constructed a mathematically and computationally simple "toy" molecular model that includes ED, CDFC and CCR into the base DEMG "toy" model: the MBP model. This model is a natural next step in the systematic progression of increasingly detailed and complex molecular models for entangled linear flexible polymers. This point can be seen by noting that there are three essential components to the constitutive equation for a monodisperse polymer melt or an entangled semi-dilute solution. This can be seen by referencing the stress calculator equation (31). (Note that equations (31) or (35) can be generated directly from the stress-optical rule which is valid in both the linear and *nonlinear* flow regions [Larson (1988)].)

$$\underline{\underline{\sigma}}(t) = 3 \underbrace{G_N(t)}_{\substack{Entanglement \\ dynamics}} \underbrace{\Lambda^2(t)}_{\substack{Stretch \\ dynamics}} \underbrace{\underline{\underline{S}}_{tube}(t)}_{\substack{Orientation \\ dynamics}} \tag{35}$$

The three fundamental components of any monodisperse constitutive relationship are; 1) A quantitative description of the orientation dynamics (21), 2) A quantitative description of the stretch dynamics (28) and 3) A quantitative description of the entanglement dynamics (27) (which are manifested in (35) through the nonlinear modulus $G_N(t)$ eq. (32)). The three essential constitutive equation components are, of course, all coupled and nonlinear. They also incorporate effects like CDFC in the time scales in their descriptions.

The original Doi-Edwards model assumed no stretch and no entanglement dynamics only considering the orientation dynamics in (35) [Doi-Edwards (1986)]. Consequently, the original family of Doi-Edwards tube and reptation models is restricted

to the linear viscoelastic region. To access more general, nonlinear flow situations, the Doi-Edwards model evolved naturally and systematically by next including the stretch dynamics to generate the DEMG model [Pearson et al (1991), Mead et al (1995), Mead and Leal (1995)]. The next step in the evolutionary progression was the MLD model which considered entanglement dynamics in the form of constraint release (CCR) in the restricted context of a *constant* net entanglement density [Mead et al (1998)]. The new MBP model relaxes the final restriction of a constant entanglement density in order to access nonlinear flow phenomena far from equilibrium. In the above manner we can see the logical and systematic progression/evolution of molecular models starting from the seminal work of de Gennes and Doi-Edwards.

The new MBP model generates extensional flow curves that are monotonic thinning (with a small "kink" near $\dot{\varepsilon}\tau_{s,eq} \approx 1$) for monodisperse PS melts qualitatively consistent with experiment. The results are sensitive to the specific functional form of CDFC used and the predictions could potentially be improved by modifying the expression for CDFC to fit the flow curve data (equations 24-26). We have not performed this exercise but could do so in principle. We have used a shifted version of the specific functional form of CDFC calculated by Ianniruberto *et al.* (2012) which has a sound theoretical basis underlying it. For monodisperse PS solutions the effects of CDFC are effectively diluted out and the classical tube model ladle shaped extensional flow curve is generated. The simulation results strongly suggest that CDFC is important in the prediction of rheological properties in nonlinear extensional flows of monodisperse PS melts. CCR is detrimental to the predictions in extensional flows but is important for the rheological properties in shear flows.

We have also provided a plausible explanation as to why the DEMG-cdfc model yields a monotonic thinning flow curve of monodisperse PS melts that are approximately equivalent to those predicted by the new MBP-xccr model, i.e. DEMG with ED "on", CDFC "on" and CCR "off". This may partially explain the previous apparent "success" of the mono and polydisperse MLD models in predicting phenomena such as the Cox-Merz rule even though the flow curves calculated assume a *constant* entanglement density [Mead (2011b)]. This suspicious coincidence masks the underlying details that are actually occurring in fast nonlinear flows of entangled polymers. Our new model simultaneously captures nonlinear flows and the entanglement microstructure modification that occurs in these fast flows.

Incorporating ED into the model allows the nonlinear phenomenon of "shear modification" to be captured by the model [Dealy and Wissbrun (1989)]. Shear modification manifests itself in linear polymer melts with broad, high MWD and melts with LCB. Direct measurement of the reduced modulus during or after shear or extension would provide an excellent test of the new ED model [Mead (2013)]. Note that current molecular constitutive models for polymer systems with LCB do not predict "shear modification" despite the fact that this is a prominent nonlinear property [McLeish and Larson (1998)].

Generalizing the new MBP model to polydisperse systems is straightforward and is performed in Appendix B. Having a generally applicable model for polydisperse systems that is easy to code and fast to execute has many practical applications in analytic rheology.

We shall pursue applications such as MWD determination from transient extensional rheology experiments in future work.

Finally, knowledge of the melt entanglement density following polymer shaping operations (finite deformations) is crucially important with respect to determining the ultimate mechanical properties of the part. Specifically, crystallization processes are severely impacted by the entanglement density of the melt [Yamazaki *et al*. (2006), Wang *et al*. (2009), Eder *et al*. (1990)]. The morphology of the resulting crystallites determines the physical and mechanical properties of the final product [Rastogi *et al*. (2003)]. Hence, the information gleaned from molecular models with ED, such as the MBP model, is directly relevant to polymer processing operations.

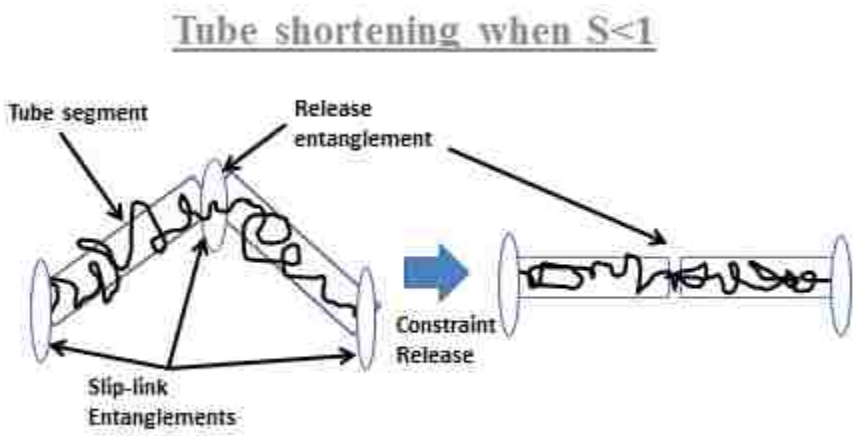

FIG. 1. Schematic diagram for tube shortening when $S_{=tube} < 1$: The tube is crinkled and constraint release shortens the tube and relaxes stretch and orientation [Mead *et al.* (1998), Mead (2011a)].

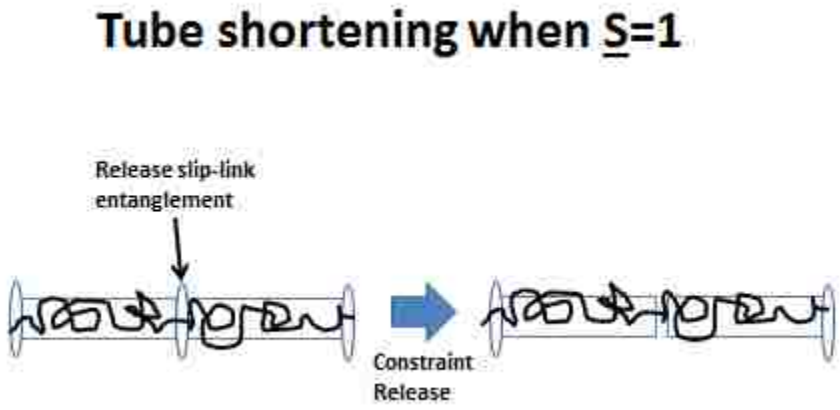

FIG. 2. Schematic diagram for tube shortening when $S_{=tube} \approx 1$: Constraint release does not relax any stretch. Note that the tube is unraveled and linear rather than in a zig-zag cat's cradle (back folded) conformation ($S_{=tube} \approx 1$ in both cases). Fast, large deformations unravel the chain and generate highly extended nearly linear conformations [Desai and Larson (2014) see Fig. 1].

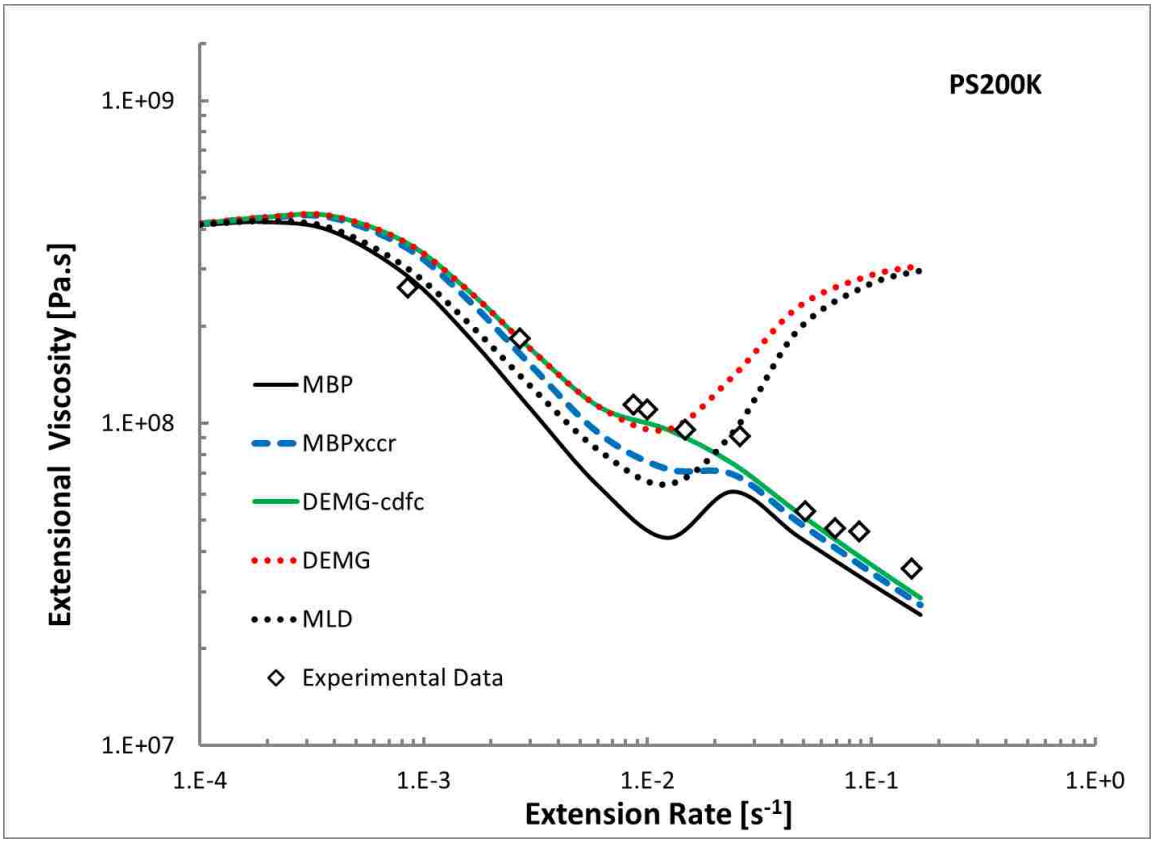

FIG. 3. Steady state extensional viscosity as a function of extension rate: Experimental data is for monodisperse PS200K at 130ºC [Bach *et al.* (2003)]. Predictions are from various options of the family of models (see Fig. legend and Table 1). This allows us to determine that CDFC is the essential ingredient required to capture the monotonic extensional flow curve of monodisperse PS melts. The "kink" in the MBP flow curve begins at $\dot{\varepsilon}\tau_{s,eq} \approx 1$.

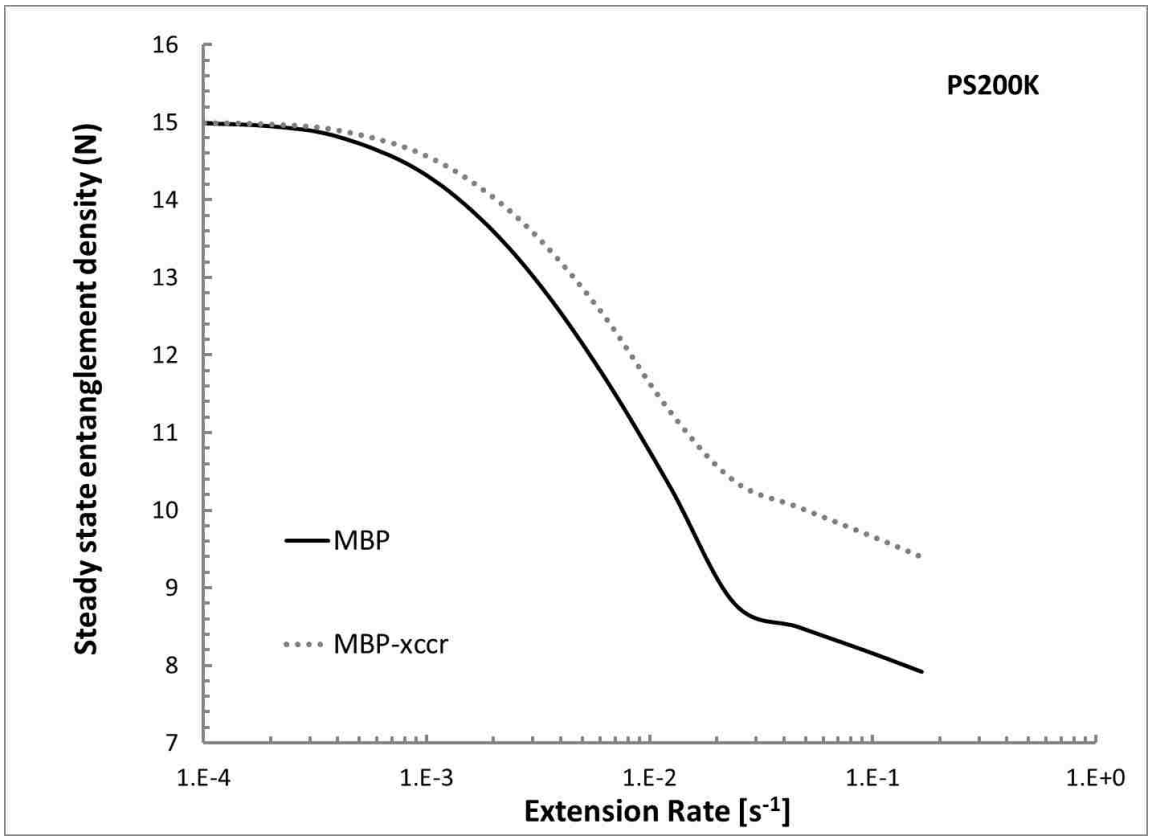

FIG. 4. The steady state entanglement density, $N(\dot{\varepsilon})$, versus extension rate, $\dot{\varepsilon}$, for the MBP model and the MBP-xccr model. The system simulated is monodisperse PS200K at 130ºC. For the case where ED is turned "off", i.e. DEMG-CDFC the entanglement density is a *constant* equal to the equilibrium value of 15 (Data not shown).

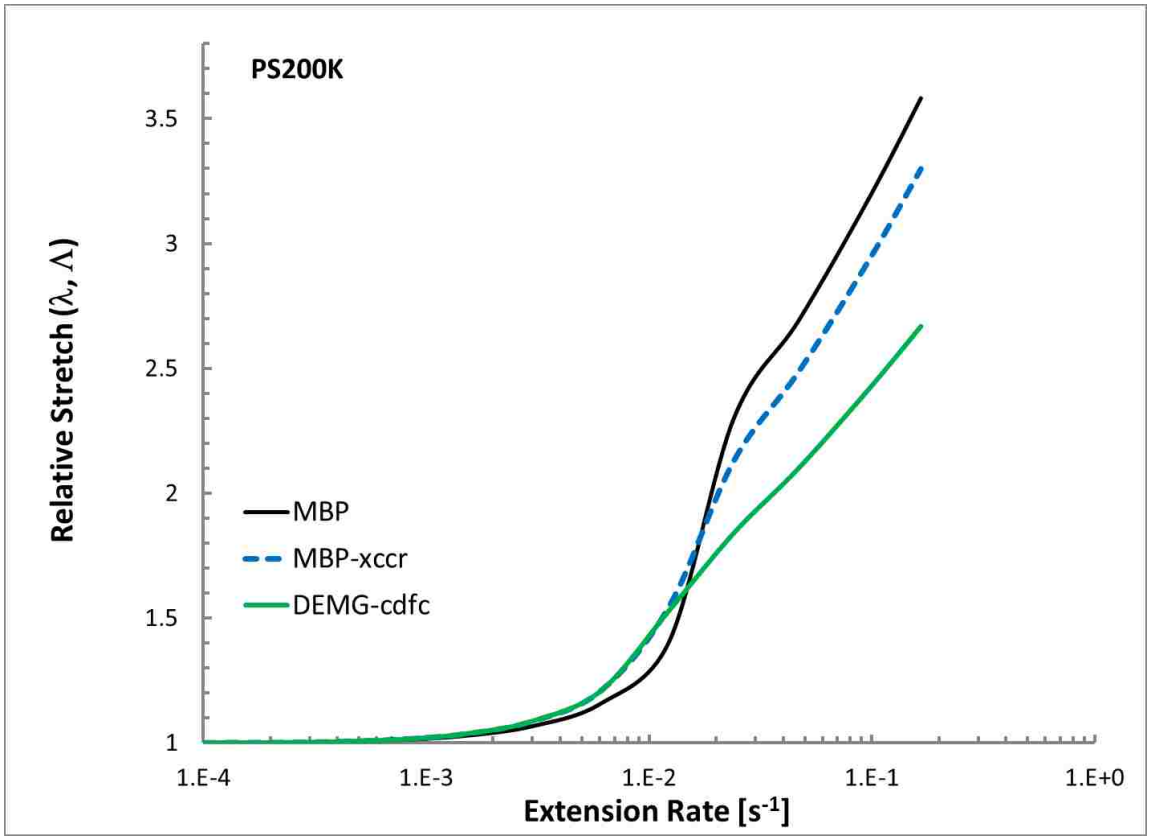

FIG. 5. The relative stretches for MBP, MBP-xccr, and DEMG-cdfc. The respective curves are: $\lambda(\dot{\varepsilon})$ vs. $\dot{\varepsilon}$ (DEMG-cdfc) and $\Lambda(\dot{\varepsilon})$ vs. $\dot{\varepsilon}$ (MBP and MBP-xccr) for the monodisperse PS200K melt. The relative stretch $\Lambda(\dot{\varepsilon})$ is *increased* relative to the base DEMG-cdfc case by virtue of the unraveling of back folds that occurs in the new model [Desai and Larson (2014)].

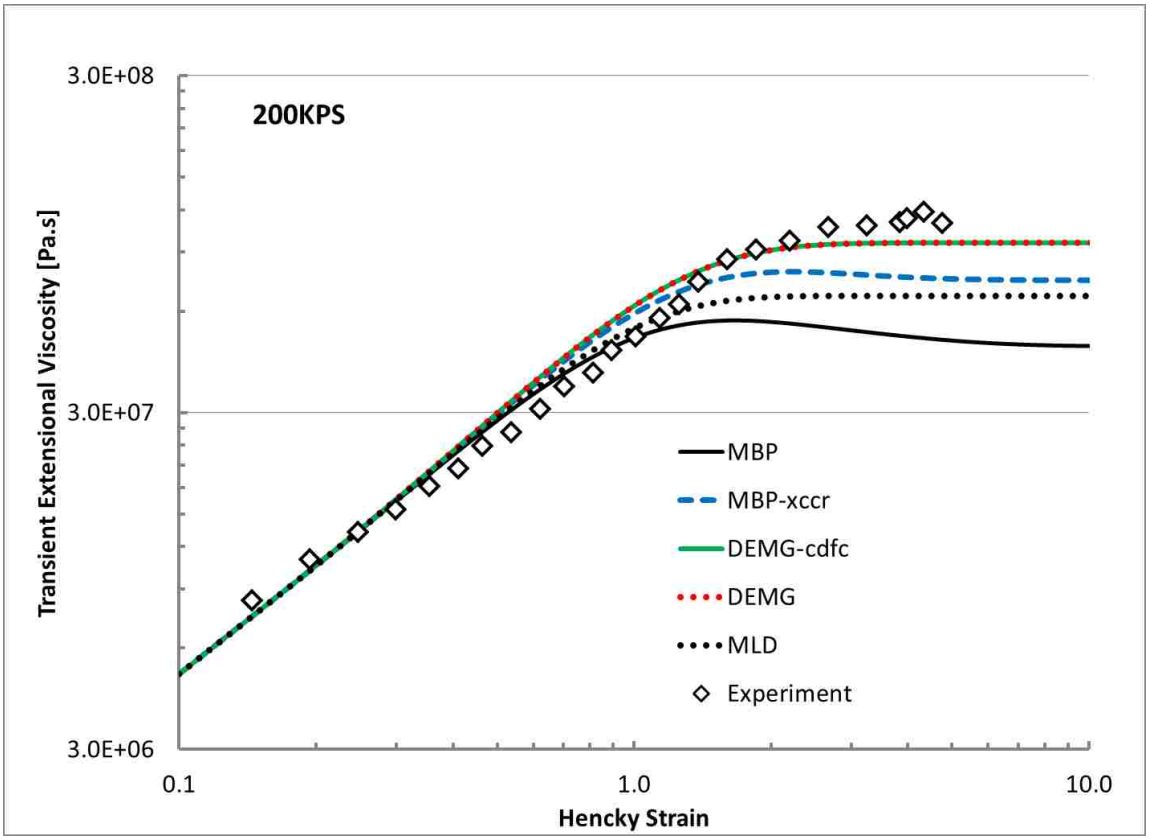

FIG. 6. Transient extensional viscosity, $\eta_e(t)$ versus t , for monodisperse PS200K at an extension rate of 0.01 sec^{-1} ($\dot{\varepsilon}\tau_{s,eq} \approx 1$). Note the small and broad maximum in the transient viscosity at a Hencky strain of ~1.5 for the MBP model. This is caused because ED lags the stress, i.e. it takes many Hencky strain units to partially disentangle the melt. Note that the results from the DEMG and DEMG-cdfc models are effectively on top of each other since this extension rate is below the onset of CDFC threshold.

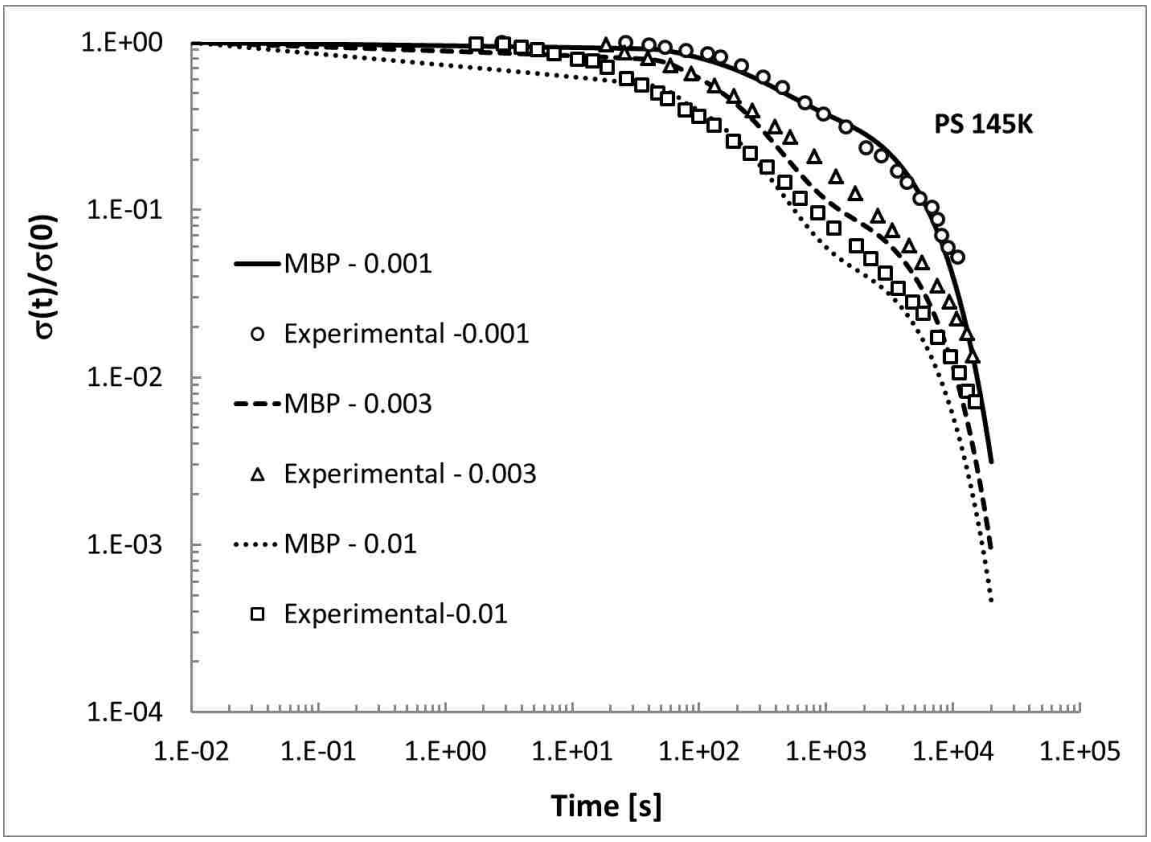

FIG. 7. Normalized stress relaxation after imposing 3 Hencky strain units for a monodisperse PS145K melt at 120^{o}C at three different steady extension rates. The higher the extension rate, the higher the net Kuhn bond orientation and the greater the effect of CDFC on the initial rate of stress relaxation. The MBP model captures this effect.

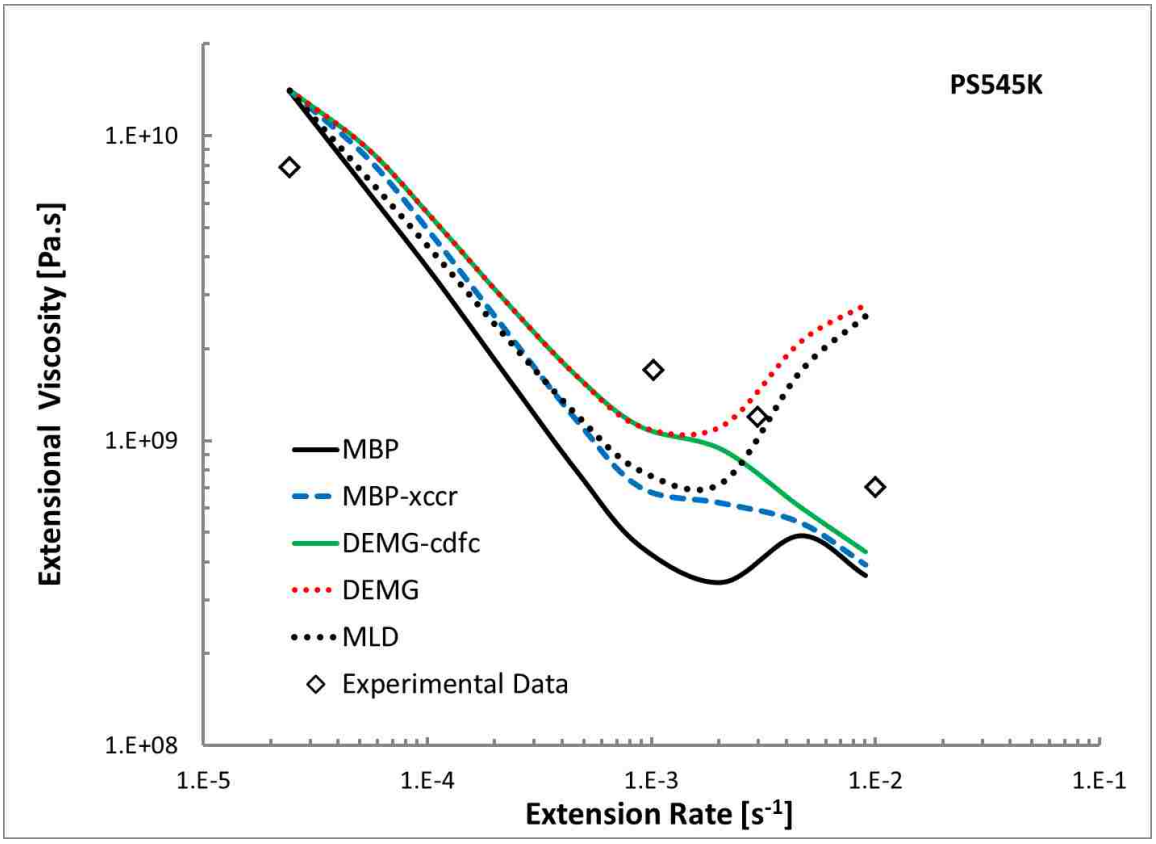

FIG. 8. Steady state extensional viscosity as a function of extension rate. Experimental data is for monodisperse PS545K melt at 130°C [Huang *et al.* (2013)]. Predictions are from various options of the family of models (see Fig. legend and Table 1). Once again the DEMG-CDFC and MBPxccr models perform best.

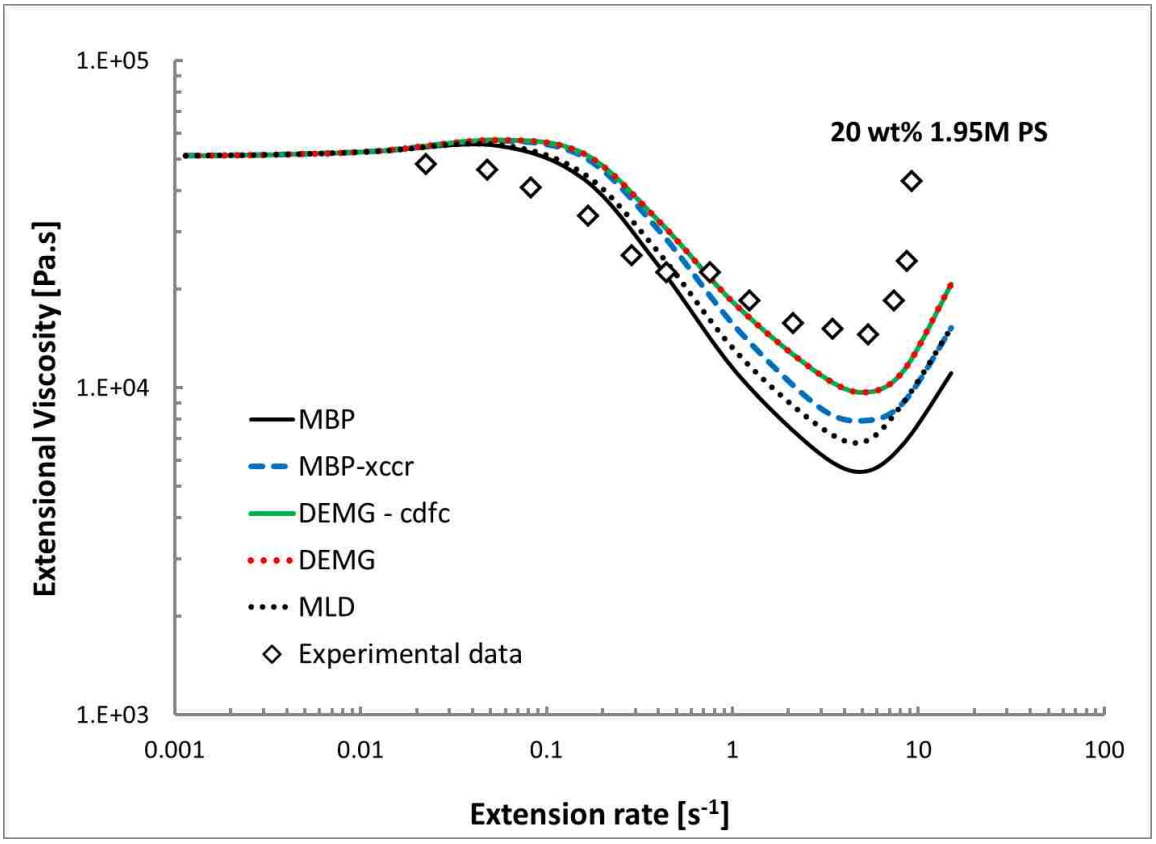

FIG. 9. Steady state extensional viscosity as a function of extension rate. Experimental data is for a monodisperse 20% 1.95M PS solutions at 21°C [Acharya *et al.* (2008)]. Predictions are from various options of the family of models (see Fig. legend and Table 1). Note that the results from DEMG and DEMG-cdfc are on top of each other.

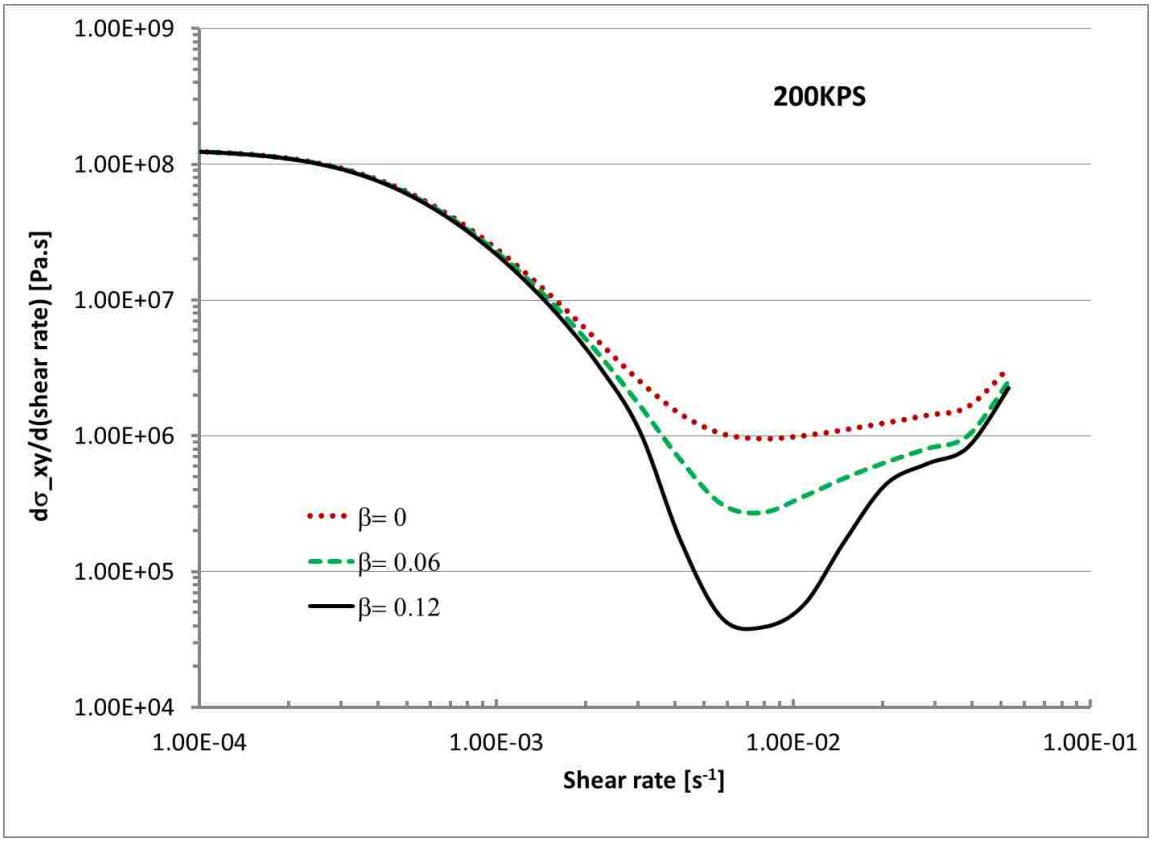

FIG. 10. The (slope of shear stress-shear rate curve) derivative of steady shear stress with respect to $\dot{\gamma}$, $\frac{d\sigma_{xy}}{d\dot{\gamma}}$ versus $\dot{\gamma}$ for a family of β values. For stable shear flow the shear stress vs shear rate curve must be monotonic (positive slope everywhere). The maximum value of β that yields a monotonic curve of stress-shear rate is $\beta = 0.12$. The results from $\beta = 0.13$ showed *negative* values around shear rate of $0.01 s^{-1}$ (curve not shown).

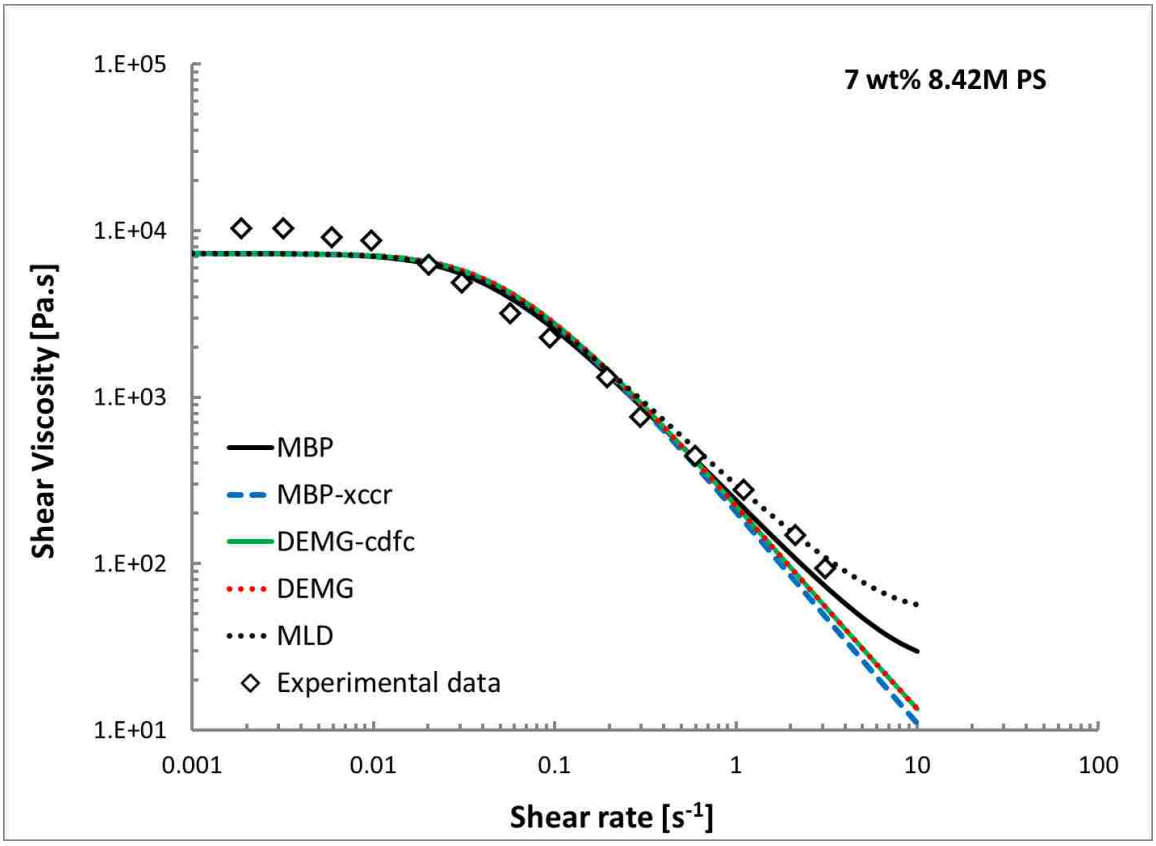

FIG. 11. The shear flow curve, η vs. $\dot{\gamma}$, for a monodisperse PS solution 7% 8.42M PS. Predictions are from various options of the family of models (see Fig. legend and Table 1). Note that the results from the DEMG and DEMG-cdfc models effectively superpose since CDFC is diluted out of this semi-dilute system.

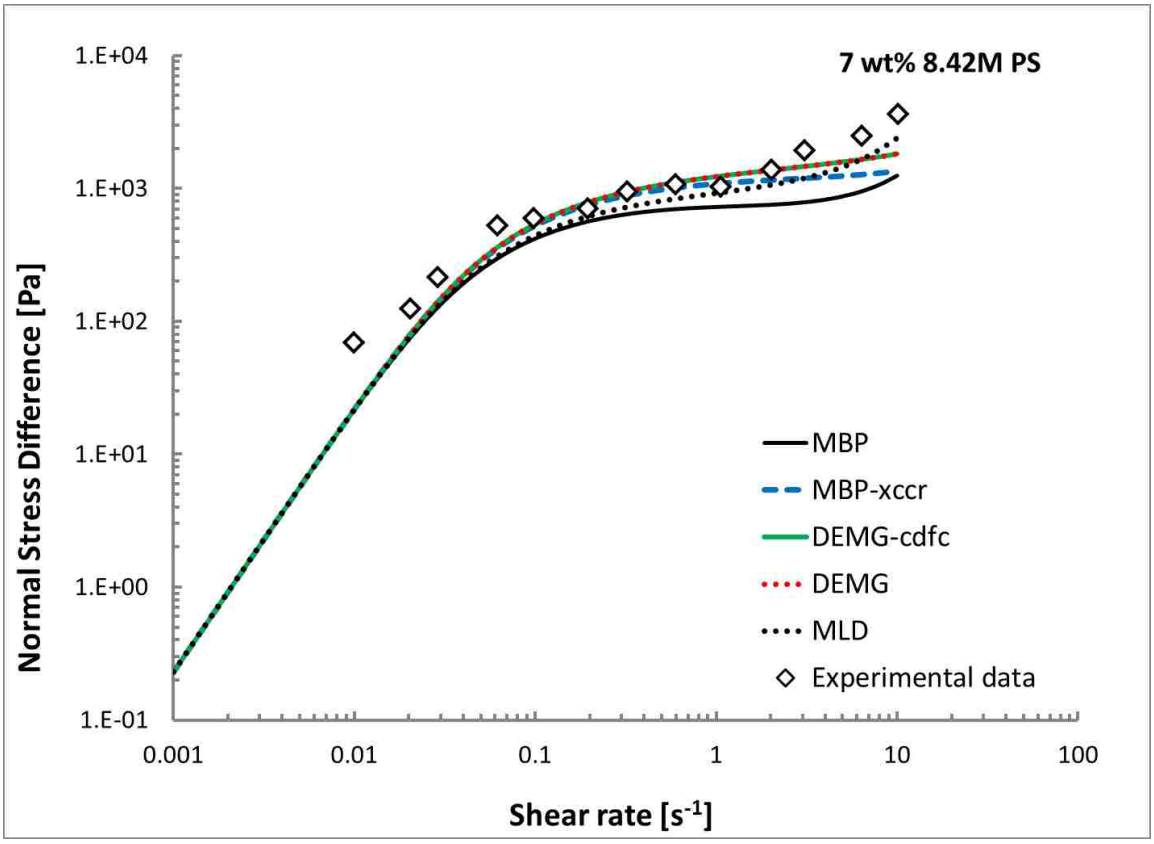

FIG. 12. The first normal stress difference for a monodisperse PS solution 7% 8.42M PS is shown, N_1 vs. $\dot{\gamma}$. Predictions are from various options of the family of models (see Fig. legend and Table 1). Note that the results from the DEMG and DEMG-cdfc models are on top of each other since CDFC is diluted out of this system.

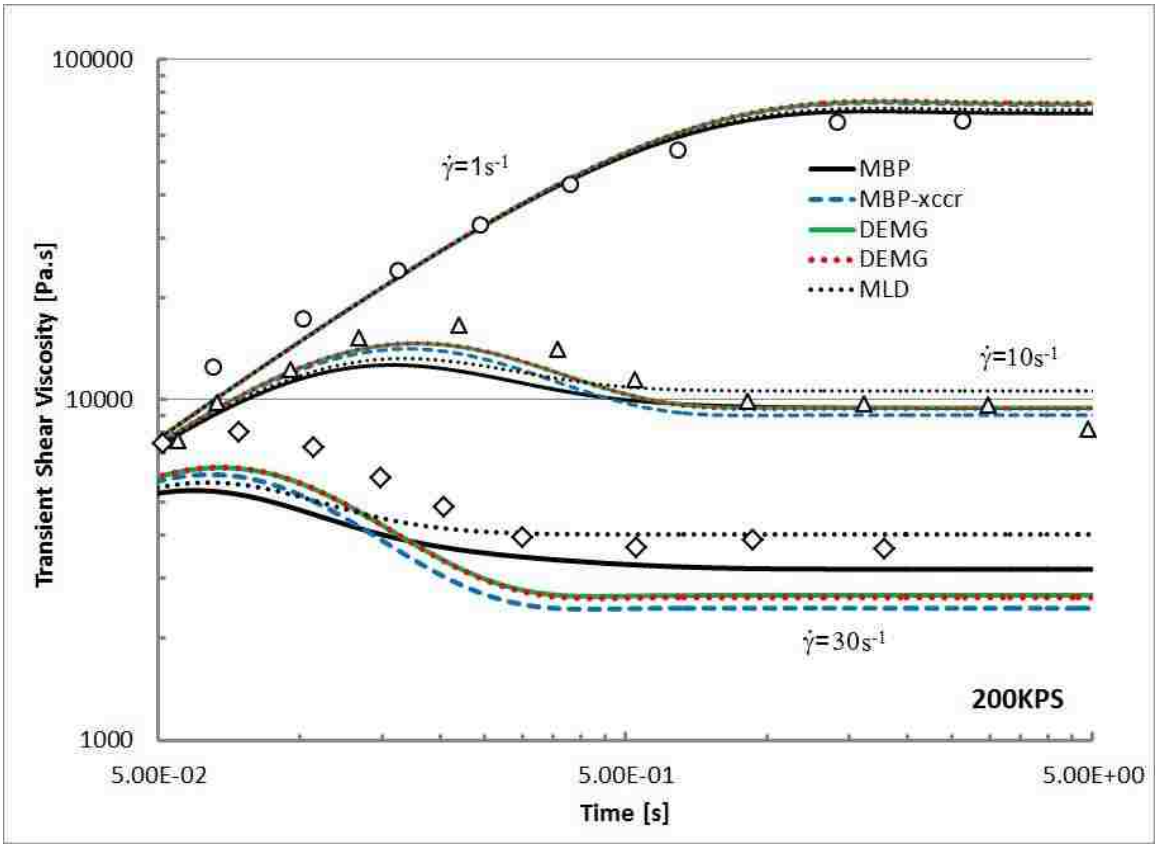

FIG. 13. Transient monodisperse 200K-S PS melt at shear rates of $1s^{-1}$, $10s^{-1}$ and $30s^{-1}$. Since the net Kuhn bond orientation is low the effect of CDFC is negligible and the DEMG-cdfc model is approximately equal to the DEMG model. The poor agreement with data at 30 sec^{-1} is due to the use of the differential form of the orientation evolution equation.

TABLE I: Summary of the family of toy molecular models studied.

Model	CCR	ED	CDFC
DEMG	**off**	**off ($\beta = 0$)**	**Off**
DEMG-cdfc	**off**	**off ($\beta = 0$)**	**On**
MLD	**on**	**off ($\beta = 0$)**	**Off**
MBP	**on**	**on($\beta \neq 0$)**	**On**
MBP-xccr	**off**	**on($\beta \neq 0$)**	**On**

TABLE II: Experimental data sets compared (Input parameter estimations were referred to Desai and Larson (2014) and Likhtman and McLeish (2002). M_e=13333 Da is used for all PS melts to give λ_{max}=4.2 whereas M_e for solutions are evaluated by dividing by $\Phi_p^{1.2}$. The values of $\tau_{d,f}$ given below include the effect of double reptation.)

Sample	G_N^0 (kPa)	$\tau_{d,f}$ (s)	$\tau_{S,eq}$ (s)	N_{eq}	Ref
PS200K	200	1610	94.3	15	Bach *et al.* (2003)
PS200K-S	200	1.33	0.065	15	Schweizer *et al*. (2004)
PS545K	250	54418	779	41	Huang *et al.* (2013)
PS145K	290	7839	1134	10.7	Yaoita *et al.* (2012)
20% 1.95M PS	6.8	6.26	0.17	30.4	Acharya *et al.* (2008)
7% 8.42M PS	0.52	31.65	0.6	44.3	Pattamaprom & Larson (2001)

ACKNOWLEDGMENTS

The authors acknowledge Dr. Morton M. Denn's helpful comments and use of the computational facilities at the City College of New York. Partial financial support from the Materials Research Center and the Energy Research & Development Center of Missouri University of Science & Technology is also gratefully acknowledged.

APPENDIX A: DERIVATION

In this Appendix we derive equation (5) in the main text, the relationship between the non-equilibrium tube disengagement time $\tau_d^1(N)$, the number of entanglements N and the equilibrium terminal disengagement time, $\tau_{d,0}$. We start with the relationship between the tube length b and the Kuhn bond length a [Doi and Edwards (1986)]:

$$Nb^2 = M_k a^2 \tag{A1}$$

Here, N is the number of entanglements (tube segments). The end-to-end distance of the tube segments and Kuhn bonds within them must be equal. M_k is the number of Kuhn segments of length a. Hence, the tube length b is related to the number of entanglements through:

$$b = \frac{M_k^{\frac{1}{2}}}{N^{\frac{1}{2}}} a \tag{A2}$$

The equilibrium tube contour length, $L_{eq} = Nb$, is a function of the number of entanglements N,

$$L_{eq} = Nb = N^{\frac{1}{2}} \left(M_k^{\frac{1}{2}} a \right) \tag{A3}$$

Note that L_{eq} is a monotonically increasing function of N.

The terminal tube disengagement time τ_d is related to the tube length through [Doi and Edwards (1986)],

$$\tau_d = \frac{{L_{eq}}^2}{\pi^2 D_c} \tag{A4}$$

Here $D_c = \frac{kT}{M\varsigma_o}$ is the curvilinear diffusion coefficient and ς_o is the monomeric friction coefficient. We define the equilibrium terminal disengagement time as $\tau_{d,0} = \frac{L_{eq}^2}{\pi^2 D_c} = \frac{N_e M_k b^2}{\pi^2 D_c}$ where N_e is the equilibrium number of entanglements. Substituting these expressions into equation (A1.4) above yields the result (5):

$$\tau_d^1(N) = \left(\frac{N}{N_e}\right)\tau_{d,0} \tag{A5}$$

APPENDIX B: GENERALIZATION OF THE NEW EDS – CDFC MLD TOY MODEL TO POLYDISPERSE SYSTEMS

In this Appendix we outline the manner in which the ideas presented in the main text can be generalized to describe polydisperse systems. In this Section i-j subscripts denote components of the MWD and not tensor components [Mead (2007)].

The ij entanglement pair dynamics are described by the following equation which generalizes eq. (1):

$$\dot{N}_{ij}(t) = \underbrace{\frac{N_{ij}^0 - N_{ij}(t)}{\tau_{d,i}^1(t)}}_{i-chain\ tip\ \ diffusion} \underbrace{-\beta\left[\left(\underline{\underline{\kappa}}:\underline{\underline{S}}_{i,tube}\right) - \frac{\dot{\Lambda}_i(t)}{\Lambda_i} + \frac{\dot{\alpha}_i(t)}{\alpha_i}\right]N_{ij}(t)}_{convective\ \ destruction\ of\ ij\ entanglements} + \underbrace{\frac{N_{ij}^0 - N_{ij}(t)}{\tau_{d,j}^1(t)}}_{j\ matrix\ tip\ \ diffusion} \tag{B1}$$

Here, $N_{ij}(t)$ represents the number of j entanglements on an i chain and $N_{ij}^0 = w_j N_{e,i} = w_j \frac{M_i}{M_e}$ represents the equilibrium number of j entanglements on an i-chain and $N_{e,i} = \frac{M_i}{M_e}$ is the total equilibrium number of net entanglements on an i chain. $N_{e,i}$ is a function of molecular weight and the molecular weight between entanglements which is assumed not to be affected by polydispersity.

The reptation time of an i-chain is modified by the number of current entanglements of all other chains on the i-chain (eq. 5 and Appendix I),

$$\tau_{d,i}^1(t) = \left(\frac{N_i(t)}{N_{e,i}}\right)\tau_{d,i}(t) = \left(\frac{\sum_j N_{ij}(t)}{N_{e,i}}\right)\tau_{d,i}(t) \tag{B2}$$

Of course, CDFC as described in Section IIA will also be present which will reduce $\tau_{d,i}(t)$ in fast flows.

The first approximation to try for the functional form of the reduced friction CDFC is that used in our first paper [Park *et al.* (2012)]:

$$\frac{\varsigma(t)}{\varsigma_{eq}} = \frac{\tau_{s,i}(t)}{\tau_{s,i}^{0}} = \frac{\tau_{d,i}(t)}{\tau_{d,i}^{0}} = 1 - k \underbrace{\underline{\underline{S}}_{=Kuhn,i}}_{\substack{test\ chain \\ Kuhn\ bond \\ orientation}} : \underbrace{\sum_j w_j \underline{\underline{S}}_{=Kuhn,j}}_{\substack{net\ matrix\ Kuhn \\ bond\ orientation}} \tag{B3}$$

The above expression is written for a polydisperse system where the components are denoted by subscripts and w_j represents the weight fraction of MW component *j*. The effect of Kuhn bond concentration is accounted for in the weight fraction of matrix polymers and/or solvent. The relative orientation of the test chain and the matrix is quantified by the double dot product of the two orientations.

This is one possible algorithm that we propose for CDFC of the polydisperse MLD model. Other functional forms for the dependence of the friction factor on relative test chain – matrix Kuhn bond alignment can be tried too. For example by generalizing (24) we see that:

$$\frac{\varsigma(t)}{\varsigma_{eq}} = \frac{\tau_{s,i}(t)}{\tau_{s,i}^{0}} = \frac{\tau_{d,i}}{\tau_{d,i}^{0}} = f\left(\underline{\underline{S}}_{=Kuhn,i} : \sum_j w_j \underline{\underline{S}}_{=Kuhn,j}\right) = 0.02239\left[\underline{\underline{S}}_{=Kuhn,i} : \sum_j w_j \underline{\underline{S}}_{=Kuhn,j}\right]^{-1.65} =$$

$$= 0.02239\left[x_i^2 \underline{\underline{S}}_{=tube,i} : \sum_j w_j x_j^2 \underline{\underline{S}}_{=tube,j}\right]^{-1.65} \tag{B4}$$

This function approximates the monodisperse case, equation (24). Note that for most common commercial molecular weight distributions the effects of CDFC will largely disappear due to the lower overall level of Kuhn bond orientation in polydisperse systems under ordinary flow conditions. The low MW components effectively act as solvent for the high MW components [Mead (2011b)].

The i-component partially disentangled chain stretch equation remains unchanged:

$$\dot{\Lambda}_i(t) = \underbrace{-\left[\frac{\dot{\alpha}_i(t)}{\alpha_i(t)}\right]\Lambda_i(t)}_{\substack{\text{stretch reduction}\\ \text{due to disentanglement}}} + \underbrace{\left(\underline{\underline{\kappa}} : \underline{\underline{S}}_i\right)\Lambda_i}_{\text{affine stretch}} - \underbrace{k_{s,i}(t)\left(\frac{\Lambda_i - 1}{\tau_{s,i}(t)}\right)}_{\text{chain retraction}} + \underbrace{\frac{1}{2}\left(1 - \left|\underline{\underline{S}}_{tube,i}\right|\right)(\Lambda_i - 1)\dot{\Phi}}_{\text{CCR tube shortening}} \tag{B5}$$

where $\dot{\Phi}$ is the fractional rate of matrix entanglement renewal, $\dot{\Phi} \equiv \sum_j w_j \left(\left(\underline{\underline{\kappa}} : \underline{\underline{S}}_{tube,j}\right) - \frac{\dot{\Lambda}_j(t)}{\Lambda_j} + \frac{\dot{\alpha}_j(t)}{\alpha_j} + \frac{1}{\Lambda_j^2 \tau_{d,j}} \right)$ and $\left|\underline{\underline{S}}_{tube,i}\right|$ is the magnitude of the i-chain tube orientation, $\left|\underline{\underline{S}}_{tube,i}\right| = \sum_j w_j \left|\underline{\underline{S}}_{tube,ij}\right|$. The nonlinear spring factor $k_{s,i}(t)$ is defined by (30) for each i chain.

The maximum stretch ratio factor $\alpha_i(t) \equiv \frac{\Lambda_{i,\max}(t)}{\lambda_{\max}}$ needs to be calculated to solve the stretch equation. The easiest way to accomplish this is using the definition of $\alpha_i(t)$ along with the known entanglement pair dynamics, $N_{ij}(t)$,

$$\alpha_i(t) \equiv \frac{\Lambda_{i,\max}(t)}{\lambda_{\max}} = \left[\frac{N_{e,i}}{\sum_j N_{ij}(t)}\right]^{\frac{1}{2}} \tag{B6}$$

The factor $\dot{\alpha}_i(t)$ in (B6) can be calculated numerically at each time step rather than solving the ordinary differential equation for $\alpha_i(t)$.

Similarly, the orientation of the ij entanglement pairs obeys the following differential equation [Mead (2007)]:

$$\hat{\underline{\underline{S}}}_{tube,ij}(t) + 2\left(\underline{\underline{\kappa}}(t) : \underline{\underline{S}}_{tube,ij}(t)\right)\underline{\underline{S}}_{tube,ij} + \left(\frac{1 - S_{Kuhn}}{\tau_{d,ij}(t)}\right)\left(\underline{\underline{S}}_{tube,ij} - \frac{1}{3}\underline{\underline{\delta}}\right) = 0 \tag{B7}$$

Where the ij entanglement disengagement time $\tau_{d,ij}$ is:

$$\frac{1}{\tau_{d,ij}(t)} = \frac{1}{\Lambda_i^2(t)\tau_{d,i}(t)} + \left(\frac{1}{\Lambda_i}\right)\left[\left(\underline{\underline{\kappa}} : \underline{\underline{S}}_{tube,j}\right) - \frac{\dot{\Lambda}_j(t)}{\Lambda_j} + \frac{\dot{\alpha}_j(t)}{\alpha_j} + \frac{1}{\Lambda_j^2(t)\tau_{d,j}(t)}\right] \tag{B8}$$

And S_{Kuhn} is the net matrix Kuhn bond orientation, $S_{Kuhn} = \sum_i w_i S_{Kuhn,i} \approx \sum_i w_i x_i^2 \left|\underline{\underline{S}}_{tube,i}\right|$.

Of course, the Kuhn bond conformation dependence (CDFC) of the disengagement and stretch times is applicable. This is why we write both $\tau_{d,i}(t)$ and $\tau_{s,i}(t)$ as functions of time. Additionally, the effect of "solvent like" entanglements with respect to stretch processes needs to be accounted for in polydisperse systems. This can be accomplished in the manner described in Mishler and Mead (2013a,b) where entanglements with an average lifetime less than the Rouse time act as solvent with respect to stretch relaxation processes.

The expression for the stress is more involved and requires some discussion. Consider the expression for the stress from the polydisperse MLD model without entanglement dynamics:

$$\underline{\underline{\sigma}}(t) = 3\sum_i \left(w_i G_N^0\right) k_{s,i} \Lambda_i^2 \underline{\underline{S}}_{tube,i} = 3\sum_i \underbrace{\left(w_i G_N^0\right)}_{\substack{i\ chain \\ \text{modulus}}} k_{s,i} \Lambda_i^2 \underbrace{\sum_j w_j \underline{\underline{S}}_{tube,ij}(t)}_{\underline{\underline{S}}_{tube,i}} \tag{B9}$$

Here $G_N^0 \equiv \frac{\rho RT}{M_e}$ represents the equilibrium value of the modulus and M_e is the molecular weight between entanglements which for the MLD model is a constant. The factor $k_{s,i}$ represents the effects of the i-component finitely extensible nonlinear spring, eq. (30). In (A2.9) we have assumed that $G_N = \sum_i G_{N,i} = \sum_i \frac{\rho_i RT}{M_e}$. However $\rho_i = w_i \rho$ so that $G_{N,i} = w_i \frac{\rho RT}{M_e} = w_i G_N^0$, hence (A2.9).

We need to generalize this expression to allow for varying degrees of deformation induced disentanglement where the molecular weight between entanglements varies from component to component in the MWD. The non-equilibrium modulus can be written as $G_{N,i} \equiv \frac{\rho_i RT}{M_{e,i}(t)}$. Here, $M_{e,i}(t)$ is the molecular weight between entanglements on the i-component. In the polydisperse case with varying degrees of disentanglement two things in the expression for G_N change: $\rho_i = w_i \rho$ the number of i-strands per unit volume and the molecular weight between entanglements on i-component chains $M_e(t) \equiv \frac{M_i}{N_i(t)}$.

With these two changes in mind we can write the non-equilibrium i-chain modulus $G_{N,i}$ by analogy to the monodisperse equilibrium case.

$$\frac{\rho_i RT}{M_{e,i}(t)} = w_i \left(\frac{N_i(t)}{N_{e,i}} \right) G_N^0 = \underbrace{w_i G_N^0 \left(\frac{\sum_k N_{ik}(t)}{N_{e,i}} \right)}_{\substack{i \ \ chain \\ modulus}} \tag{B10}$$

So, using the above expression for the i-chain modulus we can write the stress for a system with arbitrary polydispersity as:

$$\underline{\underline{\sigma}}(t) = 3 \sum_i \underbrace{\left(w_i \left(\frac{\sum_k N_{ik}(t)}{N_{e,i}} \right) G_N^0 \right)}_{i \ \ chain \ \ modulus} k_{s,i}(t) \Lambda_i^2(t) \underbrace{\sum_j w_j \underline{\underline{S}}_{tube,ij}(t)}_{\underline{\underline{S}}_{tube,i}} \tag{B11}$$

As with the monodisperse case, polydisperse systems are predicted to display shear modification since $N_{ik}(t)$ will recover its equilibrium entanglement density $N_{e,i}$ on reptation time scales which can be extremely long for high molecular weight entanglement pairs.

We anticipate that for typical commercial polydisperse polymer melts most of the effects of CDFC discussed in this paper will disappear since the average level of Kuhn bond orientation will be low. However, this will not be the case for the entanglement dynamics effects. The effects of ED such as “shear modification” will manifest themselves for broad polydisperse melts with high molecular weight tails [Dealy and Tsang (1981), Rokudai (1979)].

APPENDIX C: INTERNAL DETAILS OF THE MODEL CALCULATIONS

In this Appendix we detail the inner model workings underlying Fig. 3. In this way the mechanisms responsible for the observed uniaxial flow curves can be readily understood. In Fig. 14 the steady state orientation as a function of extension rate is displayed for the system described in Fig. 3. Similarly, Fig. 15 displays the steady state Kuhn bond orientation as a function of extension rate. An inflection point is seen in the curves at $\dot{\varepsilon}\tau_{s,eq} \approx 1$ corresponding to the onset of significant stretch. CDFC effects set in for Kuhn bond orientations greater than 0.1. Finally, Fig. 16 displays CDFC, $\frac{\varsigma}{\varsigma_{eq}} = \frac{\tau_{s,i}}{\tau_{s,i}^{0}}$, as a function of extension rate and the onset of CDFC effects is clearly shown. All of the above Fig.s can be correlated to the extensional viscosity flow curve shown in Fig. 3 and obvious conclusions concerning the causes for the various features can be drawn. In particular, precisely when CDFC is activated relative to $\dot{\varepsilon} \approx \frac{1}{\tau_{s,eq}}$ is impacted by whether ED and CCR are "on" or "off". Choosing a different functional form for CDFC can in principle modify precisely when CDFC is activated relative to $\dot{\varepsilon} \approx \frac{1}{\tau_{s,eq}}$.

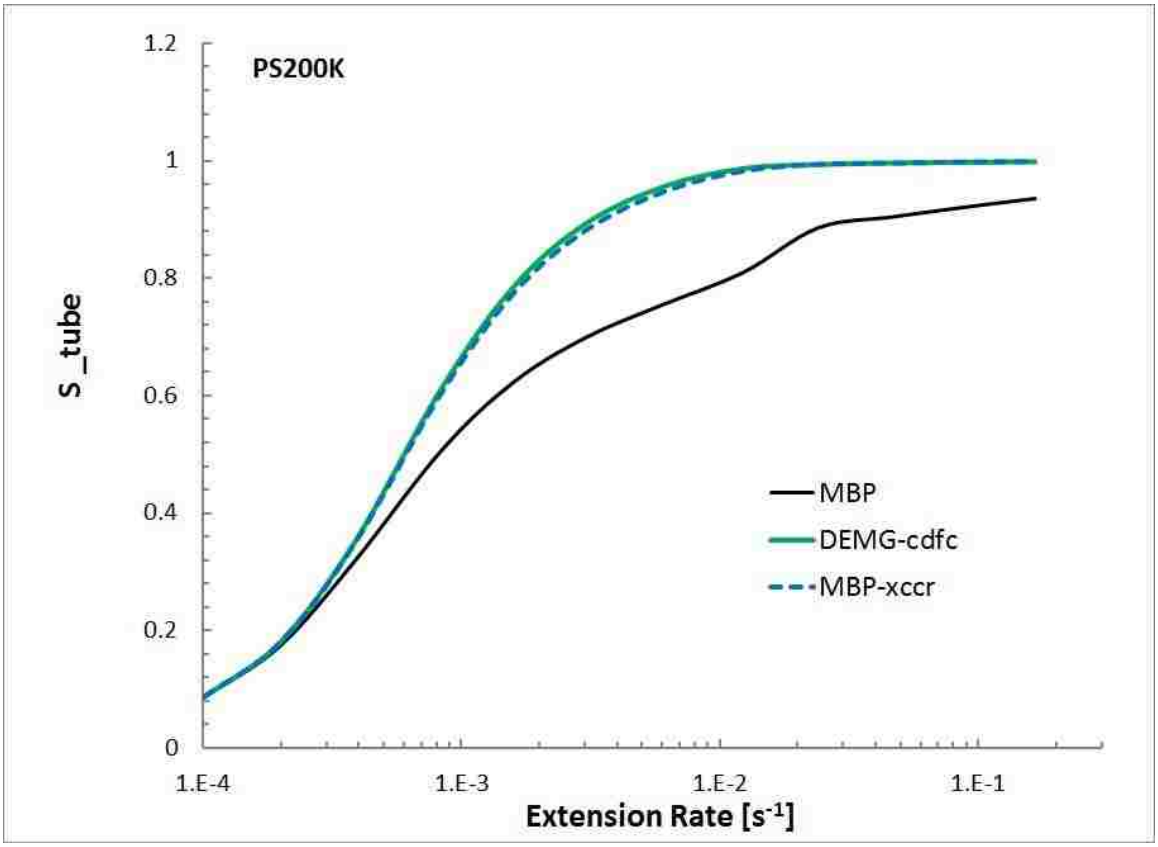

FIG. 14. Steady state orientation as a function of extension rate for monodisperse PS200K at 130ºC [Bach *et al.* (2003)]. Predictions are from various options of the family of models (see Fig. legend and Table 1). This allows us to determine the orientation levels when stretch and CDFC commence. The equilibrium stretch relaxation time is $\tau_{s,eq} \approx 94$ sec which doesn't include the effects of CDFC.

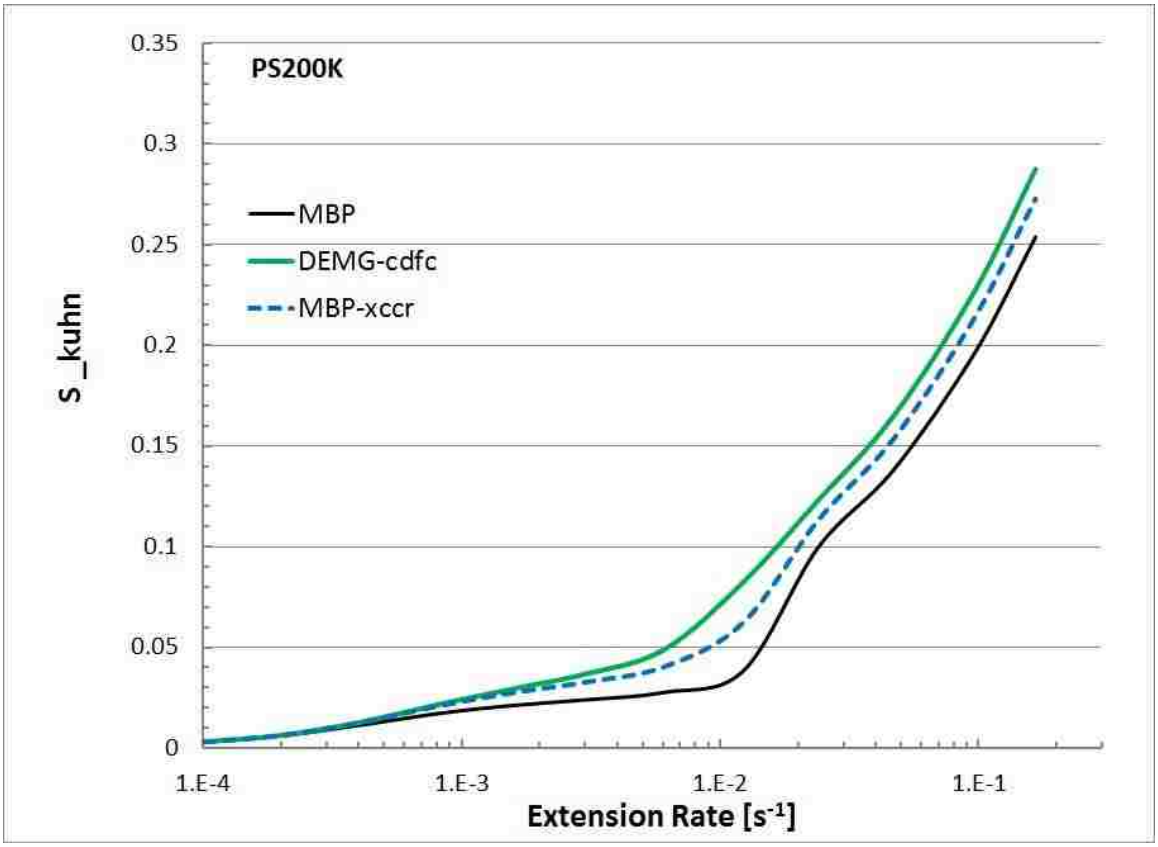

FIG. 15. Steady state Kuhn bond orientation as a function of extension rate for monodisperse PS200K at 130°C. Predictions are from various options of the family of models (see Fig. legend and Table 1). The equilibrium stretch relaxation time is $\tau_{s,eq} \approx 94$ which doesn't include the effects of CDFC. CDFC commences when Kuhn bond orientation is greater than 0.10.

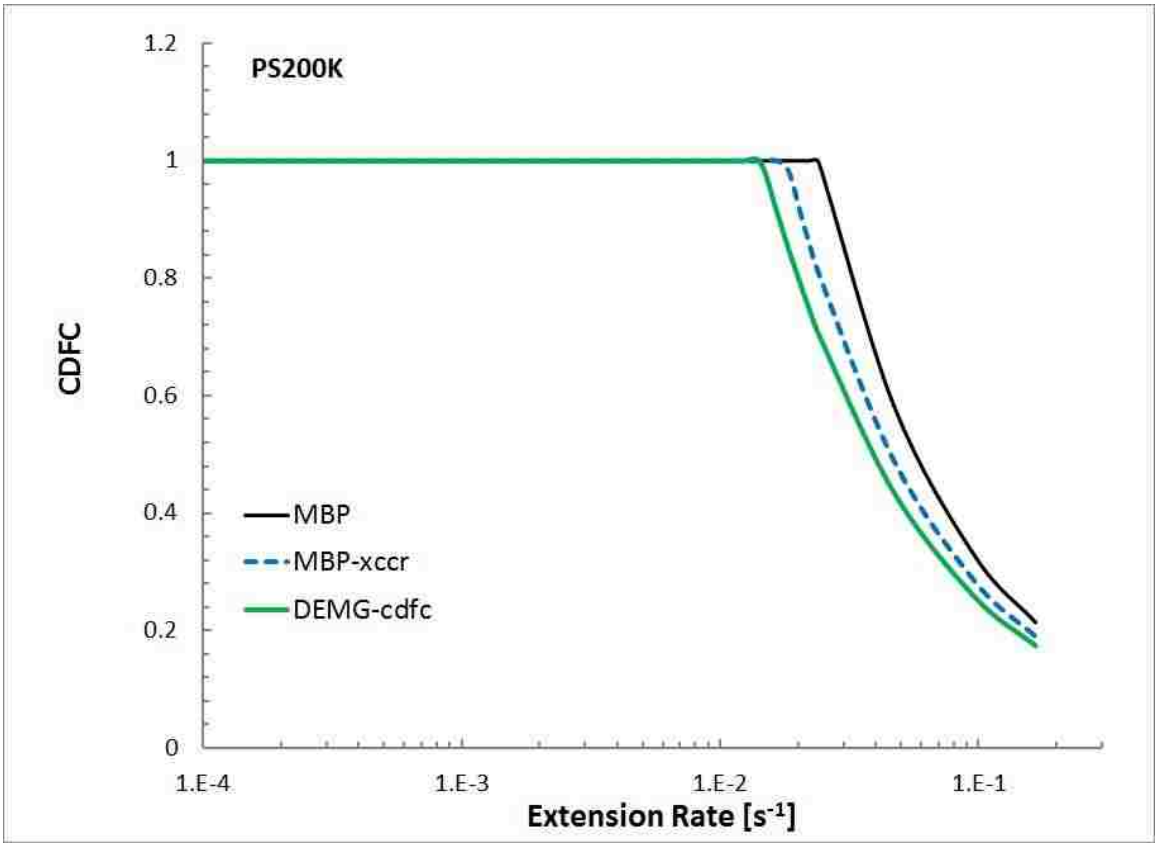

FIG. 16. Steady state ratio of $\frac{\varsigma}{\varsigma_{eq}} = \frac{\tau_{s,i}}{\tau_{s,i}^{0}}$ as a function of extension rate for monodisperse PS200K at 130°C. The equilibrium stretch relaxation time is $\tau_{s,eq} \approx 94$ sec which doesn't include the effects of CDFC. Predictions are from various options of the family of models (see Fig. legend and Table 1).

References

Acharya, M. V., P.K. Bhattacharjee, D.A. Nguyen and T. Sridhar, "Are Entangled Polymeric Solutions Different from Melts?" AIP Conf. Proc. **1027**, 391-393 (2008).

Andreev, M., R.N. Khaliullin, R.J.A. Steenbakkers and J.D. Schieber, "Approximations of the discrete slip-link model and their effect on nonlinear rheology predictions", J. Rheol. **57**, 535-557 (2013).

Bach, A., K. Almal, O. Hassager and H.K. Rasmussen, "Elongational viscosity of narrow molar mass distribution polystyrene", Macromolecules **36**, 5174-5179 (2003).

Baig, C., V.G. Mavrantzas and M. Kroger, "Flow effects on melt structure and entanglement network of linear polymers: Results from a non-equilibrium molecular dynamics study of a polyethylene melt in steady shear", Macromolecules **43**, 6886-6906 (2010).

Bhattacharjee, P.K., J.P. Oberhauser, G.H. McKinley, L.G. Leal and T. Sridhar, "Extensional rheometry of entangled solutions", Macromolecules **35**, 10131-10148 (2002).

Cohen, A., "A Padé approximant to the inverse Langevin function", Rheol. Acta **30**, 270-273 (1991).

Dealy, J.M. and WM. K.-W. Tsang, "Structural time dependency in the rheological behavior of molten polymers", J. Appl. Poly. Sci. **26**, 1149-1158 (1981).

Dealy, J.M. and K.F. Wissbrun, *Melt Rheology and its Role in Plastics Processing* Van Norstrand Reinhold (1989).

Desai, P.S. and R.G. Larson, "Constitutive model that shows extension thickening for entangled solutions and extension thinning for melts", J. Rheol. **58**, 255-279 (2014).

Doi, M., and S.F. Edwards, *The Theory of Polymer Dynamics*, Oxford Science Publications, (1986).

Doi, M., D.S. Pearson, J. Kornfield and G.G. Fuller, “Effect of nematic interaction in the orientational relaxation of polymer melts”, Macromolecules **22**, 1488-1490 (1989).

Eder, G., H. Janeschitz-Kriegl, and S. Liedauer, “Crystallization processes in quiescent and moving polymer melts under heat transfer conditions”, Progress Polymer Sci. **15**, 629–714(1990).

Everaers, R., S.K. Sukumaran, G.S. Grest, C. Svaneburg, A. Sivasubramanian and K. Kremers, “Rheology and microscopic topology of entangled polymeric liquids”, Science **303**, 823-827 (2004).

Flory, P. J., *Statistical Mechanics of Chain Molecules* Interscience, New York, (1969).

Graham, R.S., A.E. Likhtman, T.C.B. McLeish and S.T. Milner, “Microscopic theory of linear, entangled polymer chains under rapid deformation including chain stretch and convective constraint release”, J. Rheol. **47**, 1171-1200 (2003).

Huang, Q., O. Mednova, H.K. Rasmussen, N.J. Alvarez, A. L. Skov, K. Almdal, and O. Hassager, “Concentrated Polymer Solutions are Different from Melts: Role of Entanglement Molecular Weight”, Macromolecules **46**, 5026-5035 (2013)

Ianniruberto, G, A. Brasiello, G. Marrucci, “Friction Coefficient Does Not Stay Constant in Nonlinear Viscoelasticity”, Proceedings of the 7th Annual European Rheology Conf., pg. 61, (2011).

Ianniruberto, G., A. Brasiello and G. Marrucci, “Simulation of fast shear flows of PS oligomers confirm monomeric friction reduction in fast elongational flows of monodisperse PS melts as indicated by rheooptical data”, Macromolecules **45**, 8058-8066 (2012).

Ianniruberto, G., and G. Marrucci, “On compatibility of the Cox-Merz rule with the model of Doi and Edwards”, J. Non-Newtonian Fluid Mech. **65**, 241–246 (1996).

Ianniruberto, G., and G. Marrucci, “A simple constitutive equation for entangled polymers with chain stretch”, J. Rheol. **45**, 1305-1318 (2001).

Ianniruberto, G., and G. Marrucci, “Convective constraint release revisited”, J. Rheol. **58**, 89-102 (2014).

Larson, R.G., *Constitutive Equations for Polymer Melts and Solutions*, Butterworths (1988).

Larson, R.G., “A constitutive equation for polymer melts based on partially extending strand convection”, J. Rheology **28**, 545-572(1984).

Leblans, P.J.R., and C. Bastiaansen, “Shear modification of low density polyethylene: Its origin and its effect on the basic rheological functions of the melt”, Macromolecules **22**, 3312-3317 (1989).

Likhtman, A. E., and T. C. B. McLeish, ‘‘Quantitative theory for linear dynamics of linear entangled polymers,’’ Macromolecules **35**, 6332–6343 (2002).

Marrucci, G.G., in *Advances in Transport Processes* Vol. V A.S. Majumdar and R.A. Mashelkar, Eds. John Wiley & Sons (1984).

McLeish, T.C.B. and R.C. Ball, "A molecular approach to the spurt effect in polymer melt flow", J. Poly. Sci. Poly. Phys. Ed. **24**, 1753-1745 (1986).

McLeish, T.C.B. and R.G. Larson, “Molecular constitutive equations for a class of branched polymer: the pom-pom polymer”, J. Rheol. 42, 81-110 (1998).

Mead, D.W., D. Yavich and L. Leal, "The reptation model with chain stretching I) Basic equations and general properties", Rheologica Acta **34**, 339-360(1995).

Mead, D.W. and L. Leal, "The reptation model with chain stretching II) Steady flow properties", Rheologica Acta **34**, 360-383(1995).

Mead, D.W., R.G. Larson and M. Doi, “A molecular theory for fast flows of entangled polymers”, Macromolecules **31**, 7895-7914 (1998).

Mead, D.W., "Development of the "Binary Interaction" Theory for Entangled Polydisperse Linear polymers", Rheol. Acta **46**, 369-395 (2007).

Mead, D.W., "Derivation of the "Switch Function" in the Mead-Larson-Doi Theory", Rheologica Acta **50**, 631-643 (2011a).

Mead, D.W. , "Analytic Derivation of the Cox-Merz Rule Using the MLD "Toy" Model for Polydisperse Linear Polymers", Rheol. Acta **50**, 837-866 (2011b).

Mead, D.W., "Small Amplitude Oscillatory Shear Flow Superposed on Parallel or Perpendicular Steady Shear of Polydisperse Linear Polymers: The MLD Model", J. Non-Newtonian Fluid Mech. **195**, 99-113 (2013).

Mewis, J., and M.M. Denn, "Constitutive equations based on the transient network concept", J. Non-Newtonian Fluid Mech. **12**, 69-83 (1983).

Mishler, S.D. and D.W. Mead, "Application of the MLD "Toy" Model to Extensional Flows of Broadly Polydisperse Linear Polymers: Model Development", J. Non-Newtonian Fluid Mech. **197**, 61-79 (2013a).

Mishler, S.D. and D.W. Mead, "Application of the MLD "Toy" Model to Extensional Flows of Broadly Polydisperse Linear Polymers: Comparison to Experimental data Sets", J. Non-Newtonian Fluid Mech. **197**, 80-90 (2013b).

Park, J., D.W. Mead, and M.M. Denn, "Stochastic Simulation of Entangled Polymeric Liquids in Fast Flows: Microstructure Modification", J. Rheol. **56**, 1057-1082 (2012).

Pattamaprom, C. and R.G. Larson, "Constraint release effects in monodisperse and bidisperse polystyrenes in fast transient shearing flows", Macromolecules **34**, 5229-5237 (2001).

Pearson, D. S., E. A. Herbolzhiemer, N. Grizzuti, and G. Marrucci, "Transient behavior of entangled polymers at high shear rates", J. Polymer Sci., Part B: Polymer Phys. Ed. **29**, 1589-1597 (1991).

Rastogi, R., L. Kurelec, J. Cuijpers, D. Lippits, M. Wimmer, P. J. Lemstra, "Disentangled State in Polymer Melts; A Route to Ultimate Physical and Mechanical Properties", Macromolecular Materials Eng. **288**, 964–970 (2003).

Rokudai, M., "Influence of shearing history on the rheological properties and processability of branched polymers", J. Appl. Poly. Sci. **23**, 463-471 (1979).

Schweizer, T., J. van Meerveld, and H. C. Ottinger, "Nonlinear shear rheology of polystyrene melt with narrow molecular weight distribution—Experiment and theory," J. Rheol. **48**, 1345–1363 (2004).

Treloar, L.R.G., *The Physics of Rubber Elasticity* 3rd Edition, Oxford University Press (1975).

Tzoumanekas, C., and Theodorou, D. N., "Topological Analysis of Linear Polymer Melts: A Statistical Approach", Macromolecules **39**, 4592-4604 (2006).

Wang, X., R. Liu, M. Wu, Z. Wang, Y. Huang, "Effect of chain disentanglement on melt crystallization behavior of isotactic polypropylene", Polymer **50**, 5824–5827(2009)

Yamaguchi, M., and M.H. Wagner, "Impact of processing history on rheological properties for branched polypropylene", Polymer **47**, 3629-3635 (2006).

Yamazaki, S., F. Gu, K. Watanabe, K. Okada, A. Toda, M. Hikosaka, "Two-step formation of entanglement from disentangled polymer melt detected by using nucleation rate", Polymer **47** 6422-6428(2006).

Yaoita, T., T. Isaki, Y. Masubuchi, H. Watanabe, G. Ianniruberto and G. Marrucci, "Primitive chain network simulation of elongational flows of entangled linear chains: Stretch/orientation induced reduction of monomeric friction", Macromolecules **45**, 2773-2782 (2012).

Yaoita, T., Y. Masubuchi and H. Watanabe, "Concept of stretch/orientation reduction tested with a simple constitutive equation", Nihon Reoroji Gakkaishi, **42**, 207-213 (2014).

III. Constitutive model for polydisperse entangled polymers incorporating binary entanglement pair dynamics and a configuration dependent friction coefficient

Synopsis

The concepts of entanglement dynamics (ED) and configuration dependent friction coefficient (CDFC) in our previous monodisperse Mead-Banerjee-Park (MBP) "toy" constitutive model [Mead *et al*., J. Rheol. **59**, 335-363 (2015)] have been combined with that of diluted stretch tube theory of Mishler and Mead [J. Non-Newtonian Fluid Mech. (2013)] to develop the polydisperse MBP "toy" constitutive model. The model is first used in the "forward" direction to predict the nonlinear viscoelastic material properties of model polydisperse systems. The polydisperse MBP toy model accurately predicts the material properties in the forward direction for transient and steady uniaxial extension and shear flow melt and solution conditions. The model can correctly generate the long and short chain component contributions to the rheological property measured.

I. INTRODUCTION

In our previous paper we developed the Mead-Banerjee-Park (MBP) "toy" constitutive model for entangled monodisperse linear flexible polymers that displayed considerable promise in predicting both extensional and shear flow properties in the highly nonlinear flow regime [Mead *et al* (2015)]. In this paper we continue our study of the MBP model by examining model polydisperse systems in fast extensional and shearing flows. We shall consider both model and general molecular weight distributions with P discrete weight fractions, $\sum_{j=1}^{P} w_j = 1$. Here and throughout this paper subscripts denote discrete molecular weight components *not* tensor component indices.

As pointed out by Mishler and Mead (2013a and b), construction of a naïve polydispersity model is straightforward given the monodisperse MBP model developed in Appendix B of Mead *et al*., (2015). However, this naïve construction does not take account of the fact that for systems with broad polydispersity low molecular weight components may have an orientational relaxation time less than the stretch relaxation time of the high molecular weight component (See Figure 1).

In this case, the low molecular weight components act effectively as "solvent" with respect to the stretch processes of the long chains. This fact necessitates the construction of a "diluted stretch tube" to describe stretching processes for polymer systems with broad molecular weight distribution (MWD) in nonlinear flows [Mishler and Mead (2013a and b)].

Hence, we incorporated the dilute tube theory into the monodisperse MBP to develop a new "toy" constitutive model for the improved prediction of viscoelastic material properties of polydisperse systems. Note here that our new model for polydisperse system is called as "MBP" model whereas the previous model for monodisperse system is distinguished as "monodisperse MBP". The model by Mishler and Mead (2013a and b) will be abbreviated as "MM" model.

In this paper, as in our previous work [Mead *et al*., (2015)], we use the term "tube" despite the fact that we believe that defining entanglements as discrete pair-wise couplings between two chains is a more accurate physical description of chain-chain interactions. Indeed, the traditional "tube" is an unhelpful concept in nonlinear rheology. Invoking a "tube" effectively fixes the entanglement density at a prescribed level consistent with the "tube diameter". Thus the tube concept is not conducive to simple descriptions of entanglement dynamics since this would necessitate a continuously varying dynamic tube diameter.

We believe that a simpler and more natural approach is to describe the viscoelastic properties in terms of the pair-wise entanglement dynamics as the conceptual paradigm rather than a mean field "tube". Hence, when we use the term "tube" in this paper we mean a series of discrete, oriented ij entanglement couplings along the test chain.

This paper is organized in the following manner; In Section II we outline how the dilute tube theory of MM model is combined with the monodisperse MBP model to result in MBP model. Section III.A uses the MBP model to simulate transient uniaxial extension for validation against the experimental data and to be compared with the MM model

prediction. Similarly, Section III.B predicts the transient shear flows. Section IV discusses the effect of polydisperse components on the rheological properties. Section V summarizes and concludes our results.

II. THE POLYDISPERSE MBP "TOY" MODEL FOR LINEAR POLYMERS

A. Incorporation of dilute tube theory into the monodisperse MBP model

In this Section we outline the manner in which the entanglement dynamics ideas proposed by Mead *et al*., (2015) and Mishler and Mead (2013a, b) can be generalized to describe polydispersity within the MBP "toy" model framework (See Appendix B of Mead *et al*., (2015)). As alluded in the introduction, in the general MWD case we shall have to consider the possibility that some components of the MWD act like "solvent" with respect to stretch of the i-component. As we shall see, such situations manifest themselves for MWD's with polydispersity indices (PI) greater than around 2. Specifically, solvent-like entanglements with respect to stretch occur when there is *overlap* in the stretch and orientational relaxation spectra (Figure 2).

Generalizing the i-component toy stretch equation for polydisperse systems with broad MWD's requires discussion. As proposed in previously published work by Mishler and Mead, entanglements with a lifetime less than the Rouse (stretch) relaxation time effectively act as solvent with respect to stretch processes of the test chain. The criteria $\frac{\tau_{s,i}}{\Psi_i(t)\tau_{d,j}} > 1$ defines a "cut-off" molecular weight, M_j, relative to the test chain molecular weight, M_i, splitting the MWD into solvent-like and full entanglement

fractions with respect to stretch relaxation processes of the i-chain[†], see Figure 2. Auhl *et al* have demonstrated that the effective (experimentally observed) stretch relaxation $\tau_{s,i}^{eff}$ is altered from the bare Rouse time $\tau_{s,i}$ by "stretch tube dilution" such that $\tau_{s,i}^{eff} = \frac{\tau_{s,i}}{\Psi_i}$. Here, $1-\Psi_i(t)$ is the "dilution" level of solvent like entanglements with respect to stretch of the long chains defined by the cutoff criteria $\frac{\tau_{s,i}}{\Psi_i \tau_{d,j}} > 1$ (see Figure 2);

$$\Psi_i(t) = \frac{\sum_{j>cut} N_{ij}(t)}{\sum_{j} N_{ij}(t)} = \frac{\sum_{j>cut} N_{ij}(t)}{N_i(t)} \tag{1}$$

Physically, Eq (1) represents the fraction of viable stretch entanglements. Note that entanglement densities replace weight fractions in the definition of $\Psi_i(t)$. Note that we have had to generalize the definition of $\Psi_i(t)$ to account for the ij entanglement dynamics which were not considered in the work of Mishler and Mead (2013).

[†] In order to calculate $\Psi_i(t) = \frac{\sum_{j>cut} N_{ij}(t)}{\sum_{j} N_{ij}(t)} = \frac{\sum_{j>cut} N_{ij}(t)}{N_i(t)}$ self consistently an iterative procedure is required. For the first iteration we choose $\Psi_i = 1$ and determine a new dilution level and cut-off molecular weight. The new value of Ψ_i is then fed into the cut-off criteria and this iterative process is repeated until convergence is achieved (Figure 2). This procedure is necessary to generate a dilution level that is self-consistent with the definition of the effective stretch relaxation time we use in the diluted stretch tube, $\tau_{s,i}^{eff} = \frac{\tau_{s,i}}{\Psi_i}$. Note that the position of the j-cut *changes* with time and must be updated accordingly.

Similar modifications have to be made in the definition of $\underline{\underline{S}}_{i,d}(t)$, Eq (6) below. These are essentially elaborate bookkeeping measures; counting ij entanglement pairs on the chain when entanglement dynamics and stretch tube dilution are operational (see Figure 3. for a qualitative illustration of the model, identification of variables and the hierarchy of "tubes").

The main polydispersity ideas and equations are detailed by Mead *et al*., (2015) Appendix B. We summarize the MBP model equations previously described by Mead *et al*., (2015) and the diluted stretch tube model of Mishler and Mead (2013a) in Section II.B.

As described in Mishler and Mead, the purpose of creating a diluted stretch tube is to calculate the i-chain stretch in systems with broad MWDs where some of the entanglements are solvent-like with respect to stretch processes of a given test chain (see Figure 2). Subsequent work by Mead *et al*., (2015) revealed that entanglement dynamics reduce the entanglement density and this effect also needs to be factored into the i-chain stretch dynamics equation. The result is that we calculate the stretch in the diluted and partially disentangled stretch "tube" (see Figure 3.). This stretch, $\Lambda_{i,d}(t)$, is then related to the stretch in the partially disentangled "tube", $\Lambda_i(t)$, through the stretch coupling Eq (9). Stress is then calculated in the partially disentangled tube, Eq (11). We note that the expression for the stress, Eq (11), collapses to the correct linear viscoelastic limit after complete relaxation of the system. In the following section we will take a look at the equations that have been developed to study the polydisperse systems, both solutions and melts under shear and extension conditions.

B. Summary of the polydisperse MBP "toy" model equations

1) The ij disentangled "tube" entanglement density evolution equation;

$$\dot{N}_{ij}(t)=\frac{N_{ij}^{0}-N_{ij}(t)}{\tau_{d,i}^{1}(t)}-\beta\left[\underline{\underline{\kappa}}:\underline{\underline{S}}_{i,tube}-\frac{\dot{\Lambda}_i(t)}{\Lambda_i}+\frac{\dot{\alpha}_i(t)}{\alpha_i}\right]N_{ij}(t)+\frac{N_{ij}^{0}-N_{ij}(t)}{\tau_{d,j}^{1}(t)} \tag{2}$$

2) The ij entanglement pair orientation evolution equation;

The orientation tensor $\underline{\underline{S}}_{tube,ij}(t)$ for the slow relaxing stretch entanglements ($j > cut$) evolves as;

$$\hat{\underline{\underline{S}}}_{tube,ij}(t)+2\left(\underline{\underline{\kappa}}(t):\underline{\underline{S}}_{tube,ij}(t)\right)\underline{\underline{S}}_{tube,ij}+\left(\frac{1-S_{Kuhn}}{\tau_{d,ij}(t)}\right)\left(\underline{\underline{S}}_{tube,ij}-\frac{1}{3}\underline{\underline{\delta}}\right)=\underline{\underline{0}} \tag{3a}$$

And the orientation tensor $\underline{\underline{S}}_{tube,ij}(t)$ for the fast relaxing ij stretch entanglements ($j < cut$) evolves as;

$$\hat{\underline{\underline{S}}}_{tube,ij}(t)+2\left(\underline{\underline{\kappa}}(t):\underline{\underline{S}}_{tube,ij}(t)\right)\underline{\underline{S}}_{tube,ij}+\left(\frac{1-S_{Kuhn}}{\tau_{d,ij}(t)}\right)\left(\underline{\underline{S}}_{tube,ij}-\underline{\underline{I}}_{ij}(t)\right)=\underline{\underline{0}} \tag{3b}$$

Where the tension induced orientation tensor, $\underline{\underline{I}}_{ij}(t)$, in the fast relaxing entanglements ($j < cut$) is defined as [Mead and Mishler (2013) Eq. (12)]:

$$\underline{\underline{I}}_{ij}(t)\equiv\left(1-\frac{3x_{i,d}(t)}{L^{-1}\left(x_{i,d}(t)\right)}\right)\underline{\underline{S}}_{i,d}(t)+\frac{3x_{i,d}(t)}{L^{-1}\left(x_{i,d}(t)\right)}\frac{1}{3}\underline{\underline{\delta}} \tag{3c}$$

where $x_{i,d}(t) = \dfrac{\Lambda_{i,d}(t)}{\Lambda_{i,d\max}(t)}$ is the fractional extension of the partially diluted and disentangled i-tube and the corresponding orientation, $\underline{\underline{S}}_{i,d}(t)$, is defined below Eq (6).

3) The i chain diluted and disentangled stretch tube segmental stretch equation;

$$\dot{\Lambda}_{i,d}(t) = \underbrace{-\left[\frac{\dot{\alpha}_{i,d}(t)}{\alpha_{i,d}(t)}\right]\Lambda_{i,d}(t)}_{\substack{\text{stretch reduction}\\ \text{due to disentanglement}}} + \underbrace{\left(\underline{\underline{\kappa}} : \underline{\underline{S}}_{i,d}\right)\Lambda_{i,d}}_{\substack{\text{affine stretch}\\ \text{of viable}\\ \text{entanglement}}} - \underbrace{k_{d,i}(t)\left(\frac{\Lambda_{i,d}-1}{\tau_{s,i}(t)}\right)}_{\text{chain retraction}} - \underbrace{\frac{1}{2}\left(1-\left|\underline{\underline{S}}_{tube,i}\right|\right)\left(\Lambda_{i,d}-1\right)\dot{\Phi}_i}_{\text{CCR tube shortening}} \tag{4}$$

where $$\alpha_{i,d}(t) \equiv \frac{\Lambda_{i,d\max}(t)}{\lambda_{\max,i}} = \left[\frac{N_{e,i}}{\sum_{j>cut} N_{ij}(t)}\right]^{\frac{1}{2}} = \left[\frac{N_{e,i}}{N_{i,d}(t)}\right]^{\frac{1}{2}} \tag{5}$$

and $$\underline{\underline{S}}_{i,d}(t) \equiv \frac{\sum_{j>cut} \frac{N_{ij}(t)}{N_i(t)} \underline{\underline{S}}_{tube,ij}(t)}{\Psi_i(t)} \tag{6}$$

with $$\dot{\Phi}_i(t) = \frac{\sum_{j>cut}\left[\underline{\underline{\kappa}} : \underline{\underline{S}}_{j,d} - \frac{\dot{\Lambda}_{j,d}(t)}{\Lambda_{j,d}} + \frac{\dot{\alpha}_{j,d}(t)}{\alpha_{j,d}} + \frac{1}{\Lambda_{j,d}^2(t)\tau_{d,j}(t)}\right]}{\Psi_i(t)} \tag{7}$$

$$k_{d,i}(t) \equiv \frac{\mathrm{L}^{-1}\left(\frac{\Lambda_{i,d}(t)}{\Lambda_{\max,id}(t)}\right)}{3\frac{\Lambda_{i,d}(t)}{\Lambda_{\max,id}(t)}} \approx \frac{\left(3\lambda_{\max,i}^2\alpha_{i,d}{}^2 - \Lambda_{i,d}{}^2\right)/\left(\lambda_{\max,i}^2\alpha_{i,d}{}^2 - \Lambda_{i,d}{}^2\right)}{\left(3\lambda_{\max,i}^2\alpha_{i,d}{}^2 - 1\right)/\left(\lambda_{\max,i}^2\alpha_{i,d}{}^2 - 1\right)} \tag{8}$$

4) Diluted and partially disentangled i-stretch tube – partially disentangled i-tube stretch coupling relationship;

$$\Lambda_i\left(\frac{\Lambda_{\max,i}}{3}\right)L^{-1}\left(\frac{\Lambda_i}{\Lambda_{\max,i}}\right)= \\ =\left(1-\Psi_i\right)\left[\Lambda_i\left(\frac{\Lambda_{\max,i}}{3}\right)L^{-1}\left(\frac{\Lambda_i}{\Lambda_{\max,i}}\right)\frac{3x_i}{L^{-1}\left(x_i\right)}\right]+\Psi_i\left[\Lambda_{i,d}\left(\frac{\Lambda_{\max,id}}{3}\right)L^{-1}\left(\frac{\Lambda_{i,d}}{\Lambda_{\max,id}}\right)\right] \tag{9}$$

where $x_i=\dfrac{\Lambda_i}{\Lambda_{\max,i}}$ is the fractional extension of the partially disentangled i-tube.

5) The ij partially disentangled tube entanglement pair relaxation time equation;

$$\frac{1}{\tau_{d,ij}(t)}=\frac{1}{\Lambda_i^2(t)\tau_{d,i}(t)}+\left(\frac{1}{\Lambda_i}\right)\left[\underline{\underline{\kappa}}:\underline{\underline{S}}_{tube,j}-\frac{\dot{\Lambda}_j(t)}{\Lambda_j}+\frac{\dot{\alpha}_{j,d}(t)}{\alpha_{j,d}}+\frac{1}{\Lambda_j^2(t)\tau_{d,j}(t)}\right] \tag{10}$$

6) The general non-Gaussian stress calculated in the partially disentangled tube

$$\underline{\underline{\sigma}}(t)=\sum_{i=1}^{P}w_i\,\underline{\underline{\sigma}}_{d,i}(t)=3\sum_i\underbrace{\left(w_i\left(\frac{\sum_k N_{ik}(t)}{N_{e,i}}\right)G_N^0\right)}_{i\quad chain\ modulus}k_{s,i}(t)\Lambda_i^2(t)\underbrace{\sum_j\frac{N_{ij}(t)}{N_i(t)}\underline{\underline{S}}_{tube,ij}(t)}_{\underline{\underline{S}}_{tube,i}} \tag{11}$$

where $$k_{s,i}(t)\equiv\frac{\mathrm{L}^{-1}\left(\dfrac{\Lambda_i(t)}{\Lambda_{\max,i}(t)}\right)}{3\dfrac{\Lambda_i(t)}{\Lambda_{\max,i}(t)}}\approx\frac{\left(3\lambda_{\max,i}^2\alpha_i{}^2-\Lambda_i{}^2\right)/\left(\lambda_{\max,i}^2\alpha_i{}^2-\Lambda_i{}^2\right)}{\left(3\lambda_{\max,i}^2\alpha_i{}^2-1\right)/\left(\lambda_{\max,i}^2\alpha_i{}^2-1\right)} \tag{12}$$

and $$\alpha_i(t) \equiv \frac{\Lambda_{\max,i}(t)}{\lambda_{\max,i}} = \left[\frac{N_{e,i}}{\sum_j N_{ij}(t)}\right]^{\frac{1}{2}} = \left[\frac{N_{e,i}}{N_i(t)}\right]^{\frac{1}{2}} \tag{13}$$

Since the stress is calculated by Eq. (11) in the partially disentangled tube (see Figure 3 tube (B)) a reference modulus must be invoked in order to do quantitative calculations. This is done with the plateau modulus G_N^o which is referenced to the equilibrium entanglement state where the modulus is known (see Figure 3 tube (A)). Similarly, the partially disentangled tube orientation $\underline{\underline{S}}_{tube,i}$ is related to the orientation of its constituent ij-entanglement pairs which requires a weighting based on the entanglement composition present.

These important points explain the presence of the two new factors in the expression for the stress, Eq. (11). Specifically, the j-entanglement fraction on an i-chain factor, $\frac{N_{ij}(t)}{N_i(t)}$, appears in the calculation of the partially disentangled tube orientation $\underline{\underline{S}}_{tube,i}$. For the equilibrium entanglement microstructure, the factor $\frac{N_{ij}(t)}{N_i(t)}$ is equal to the weight fraction $w_j = \frac{N_{ij}}{N_{e,i}}$ and the Mishler and Mead expression for $\underline{\underline{S}}_{tube,i}$ is recovered. Hence the factor $\frac{N_{ij}(t)}{N_i(t)}$ is a correction to account for non-equilibrium entanglement microstructure in the partially disentangled tube. The factor $\frac{N_{ij}(t)}{N_i(t)}$ accounts for differing

amounts of Kuhn bonds oriented per entanglement pair as the entanglement microstructure is modified.

In a similar manner the i-chain modulus is corrected from its equilibrium entanglement microstructure reference value with a similarly motivated factor, $\left(\frac{\sum_k N_{ik}(t)}{N_{e,i}}\right)G_N^0$. Hence there are two effects that account for the modified entanglement microstructure in a deforming melt one to account for the modification of the chain modulus and another to account for varying numbers of Kuhn bonds per entanglement pair.

C. Numerical simulation

Numerical solution of equations (2) - (13) was obtained by integration using Euler method. We confirmed that a small step size of $\Delta t=5\times10^{-11}$s gives convergent results including trace of $\underline{\underline{S}}_{tube,ij}(t)=1.0000$ of in Eq. (3). The value of β (CCR efficiency) in Eq. (2) was set as 0.12, same as monodisperse MBP model [Mead *et al*., (2015)]. The experimental data sets used for comparison with the model predictions are summarized in Table I. Input parameters for each experimental data are summarized in Table II, Table III, Table V, Table VI and Table VII.

III. COMPARISON TO EXPERIMENTAL DATA

A. Uniaxial extensional flow of polydisperse PS melts and solutions

In this section, our model is used to simulate transient uniaxial extensional flows of polydisperse polystyrene (PS) melts and solutions. The results are compared to the experimental data as well as the results from the MM model.

The experimental data for the uniaxial extension of bidisperse melts and solutions are chosen for PS melt with PI<2 [Read *et al*., (2012)], PS melt with PI>2 [Minegishi et al.], and PS solution [Ye *et al*., (2002)]. The PS melt with PI>2 (PSM2), is a wide molecular weight distribution system of 20 components and spiked with a high molecular weight component of 3.2×10^6. The PSM1 and PSS1 are both bidisperse systems. The simulation input parameters and the abbreviations for each experimental data are summarized in Table II and Table III.

Figure 4 shows the transient uniaxial extensional viscosity of the PSM2, which has broad MWD spiked by small portion of longer chain component (see Table III for data), at extension rates of $\dot{\varepsilon}$=0.013, 0.097, and 0.572 s^{-1}. All the predictions by MM model and MBP model show excellent agreement with the experimental data up to t~40s, where experimental data is available. At t >40s, the steady state viscosity predicted by MBP model is lower than that by MM model. Due to the lack of steady state experimental data for PSM2 data set, the difference between MM model and MBP model predictions could not be validated. Therefore, we chose an experimental set of which steady state data are available (PSM1: Table II).

Figure 5 shows the transient uniaxial extensional viscosity of the PSM1 (see Table II for data) at extension rates of $\dot{\varepsilon}$ =0.00015, 0.01, and 0.3 s^{-1}. Compared to the prediction by MM model, MBP model shows the improved agreement with the experimental data. Since our model incorporated ED and CDFC to the MM model, we performed simulations by including/excluding the physical effects to isolate each contribution to the improved agreement. Table IV summarizes which physical effect is included/excluded in each model compared in Figure 6. Note here again that exclusion of both ED and CDFC from our model is equivalent to the MM model (MBP $_{-ED\text{-}CDFC}$ is equivalent to MM). Exclusion of ED alone (MBP $_{-ED}$ or MM $_{+CDFC}$) resulted in slight reduction of the discrepancy from the experimental data and its result is similar to that of MM model. However, the results from the model without CDFC only (MBP $_{-CDFC}$ or MM $_{+ED}$) show similarity to those from our model with only slightly larger values. This comparison indicates that the effect of ED on rheological properties of polydisperse polymer melts under uniaxial extension is more important than that of CDFC. In contrast to our previous monodisperse MBP model, which showed prominent effect of CDFC but not much effect of ED, the observed trend is opposite. This can be explained by that shorter chains behave like solvent to longer chains, which resulted in diminished CDFC effect as in entangled polymer solution [Mead et al. (2015)]. In this case the polydisperse melt under extension condition shows similar behavior as that of the monodisperse solution system under high extension, where too we observed a weakening of CDFC due to the presence of the solvent.

Next we simulate uniaxial extension of PSS1 (see Table II for details) to extend the validation to solutions. Figure 7 shows the transient extensional viscosity vs strain curves at extension rates of 0.5 and 1.0 s^{-1}. The MBP results also show the similar trends as

predicted in extension of melts: lower viscosity values than those predicted by MM model and excellent agreement with the experimental data. Even in case of solutions, ED is an important physics to scale the system, whereas CDFC is not. The effect of CDFC is further reduced due to the presence of solvent.

B. Shear flow of polydisperse PS melts and solutions

In this Section we simulate transient shear flows of polydisperse polymer systems using the MBP model. The results are compared to the prediction by MM model and the experimental data for validation. A data set (PSS2) from Pattamaprom and Larson (2001) was chosen for shearing of PS solution and a data set (PSM3) from Ye and Sridhar (2005) for shearing of PS melts. Input parameters for numerical calculation are summarized in Tables.

Figures 8 and 9 shows the transient shear viscosities and transient normal stress differences of 7% bidisperse PS solution (PSS2) at shear rates 0.01, 1.0 and 100 sec^{-1} respectively. As in the results for uniaxial extensions in Section III.A, the predictions by MBP model show good agreement with the experimental data. All the rheological properties are also predicted to have lower values than those by MM model. Figure 10 also shows the same trend for transient shear viscosities of PS melt (PSM3).

IV. INVESTIGATION ON THE EFFECT OF POLYDISPERSITY

In this section, we discuss the effects of each polymer component on rheological properties. We go back to the PSM1 and examined the contributions of short and long polymer components to transient extensional viscosity. The results are shown in Fig 11. At a low extension rate of 0.00015 s^{-1}, short components mainly contribute to the transient extensional viscosity up to around 1000s. After that time, long components start to become dominant in the viscosity contribution. At an intermediate extension rate of 0.01 s^{-1}, the transient viscosity trend is mainly due to the long components. At a high extension rate of 0.3 s^{-1}, both curves of long and short components show similar trend as the transient viscosity curve.

The differences in the contributions by each component are due to the differences in relaxation times which are different according to polymer chain lengths. For example, the extension rate of 0.01s^{-1} is large enough to stretch the long components ($\dot{\varepsilon}\tau^{0}{}_{r,long} = 4.2 > 1$) whereas the short components are still under orientation ($\dot{\varepsilon}\tau^{0}{}_{r,short} = 0.29 < 1$). Figure 12 also shows how much each component is stretched at each extension rate in terms of the fractional stretch, $x(t)=\Lambda(t)/\Lambda_{max}$. At the low rate of 0.00015s^{-1}, both components are not stretched. At the intermediate rate of 0.01s^{-1}, it is clearly seen that only the long component is stretched to contribute to the transient extensional flow curve. At the high rate of 0.3s^{-1}, both components are stretched. The short components show smaller steady state value of x than that of the long components due to the difference between each relaxation time. Figure 13 shows the stretches of each component in terms of relative

stretch $\Lambda(t)=_L(t)/L_{eq}(t)$. While x(t) reached at steady state values, the curves of $\Lambda(t)$ show increasing trends.

This is due to the reduction of $\underline{L_{eq}}(t)$ by the reduced $N_{ij}(t)$. The transient behaviors of $N_{ij}(t)$ are shown in Fig. 14. As the extension is applied, polymer chains get disentangled with different rates for each pair. It is observed that long-long entanglements were rapidly disentangled compared to others. This is because the re-entanglement or formation of new entanglements in case of long-long entanglements is much slower compared to others due to their larger reptation/orientation time. Thus when the chains are getting disentangled, new entanglements are not forming fast enough for the long-long component. The number of long-short and short-long entanglements reduces to the same extent, as they have comparable characteristic time scales. The number of short-short entanglements falls the least, may be because the reduction in the equilibrium number of entanglements is compensated by faster formation of new entanglements. It can be deducted that the polydispersity enhances ED to relax orientation more than in monodisperse system, which results in the lower values of rheological properties than predicted by the previous MM model.

Finally, we also investigated the effects of polymer components with different lengths by applying MBP model to simulate extension of a model polydisperse system of MWD of Wesslau's log-normal 10 components of systems with average molecular weight of 2.4×10^5 and PI 2.33 (see Table VII). Figure 15 shows the relative stretch of each component at an extension rate of $10s^{-1}$. Clearly, the longest component is stretched first before shorter. Thus we can firmly conclude that the strain hardening observed in the

polydisperse system, causing the deviation from linear viscoelastic envelope (LVE) is due to the stretching in longer chain components. This is true till the time when the shorter chains do not start stretching. As for the PSM1 [Read et al., (2012)] it can be seen, that at very high extension rates, when both the long and the short chains are getting stretched, then the viscosity is equally scaled by both the short and the long chains.

V. CONCLUSION

The MBP monodisperse model and Mishler and Mead's (2013a, 2013b) "diluted stretch tube" theory is combined together to develop the MBP polydisperse model. The concepts of CDFC and ED are sustained in the MBP polydisperse "toy" model. We verified our new constitutive model for polydisperse system against the experimental data and compared with the previous model (Mishler and Mead (2013a and 2013b). The MBP polydisperse model can correctly predict the PS bi-blend both melt and solution behavior under uniaxial extension, defining each component's effect on the overall system.

We found that the ED effect is more important in polydisperse system than the CDFC effect in the monodisperse system. This observation is not unpredictable as the entanglement structure is very complex for a polydisperse system. With different time scales, the strong effect of ED is imperative. The polydispeprsity enhances disentanglements to result in more relaxed orientation than in monodisperse system. Further due to the solution-like behavior of some of the entanglements, the CDFC effect weakens and is not important in defining the overall viscosity of the system. The CDFC effect is similar to what observed in case of monodisperse solution systems (Mead et al., 2015).

We also examined to confirm that the effects of longer components are dominant in rheological properties. The model can predict the individual effects due to the short and the long components of the system. It is observed, that the deviation that occurs in the transient viscosity from LVE (strain hardening), is due to the commencement of stretch in

the long chain component. Further increase in extension rates causes the shorter chain to start stretching and then the overall viscosity is scaled both by longer and shorter chain.

The wide MWD PS 686, and the model generated Wesslau's log-normal MWD are simulated to understand the effect of the high molecular weight component on the overall viscosity of the system. The model can predict the experimental behavior for PS 686 very accurately. For both the PS 686 and Wesslau's log-normal MWD, the strain hardening is observed exactly at the point when the high molecular weight component begins stretching. The model can also correctly predict the shear flow transient and steady state (shear viscosity, shear stress and first normal stress difference) behavior for both the bidisperse solution and large MWD melt, again confirming that ED is important to both qualitatively and quantitatively describe the properties. Even in shear melt and solution systems, CDFC is found to be inconsequent.

It has long been known that a polymer melt's rheological properties reflect the underlying fluid microstructure [Dealy and Saucier (2000), Dealy and Larson (2006)]. Microstructure here refers to the MWD, entanglement density and long chain branching. Consequently, rheology is commonly used in industry to characterize polymer resins using relatively crude rheological criteria such as the Melt Flow Index (MFI) [Bremner et al., (1990)]. Such rheological criteria were until recently largely based on empiricism rather than sound theory. However, molecular rheology has advanced to the point where it is now possible to definitively and quantitatively characterize commercial polymer resins from their rheology alone. These ideas form the motivation and basis of Analytic Rheology as a science.

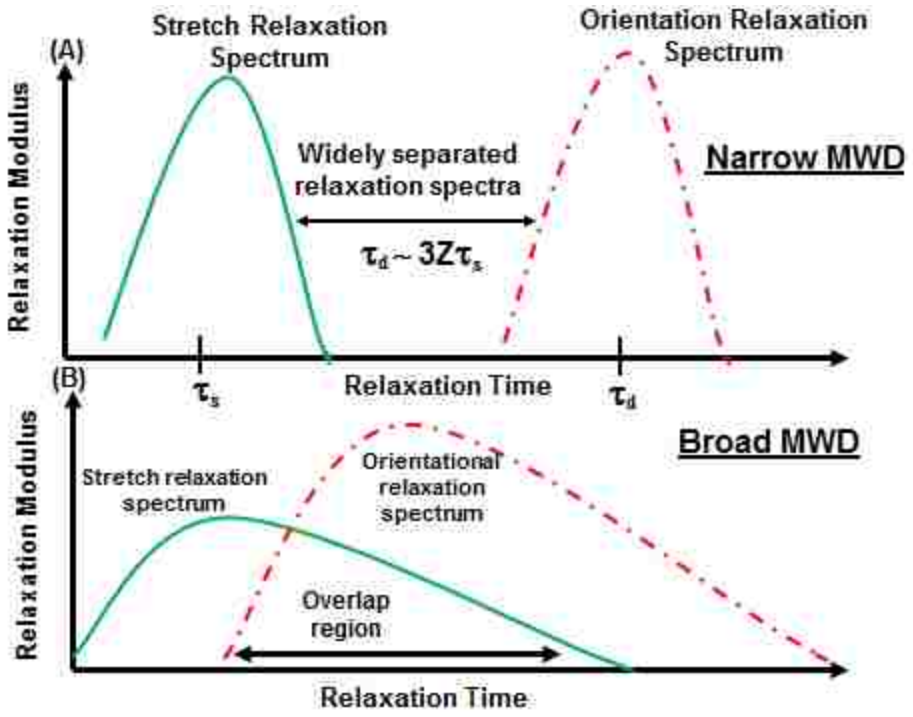

FIG. 1. Qualitative sketch of the orientational and stretch relaxation spectra for two hypothetical molecular weight distributions. A) A narrow MWD $\left(\frac{M_w}{M_n} <\sim 2\right)$ where the stretch and orientational relaxation spectra are widely separated as envisioned in the original Doi-Edwards model. B) A broad MWD $\left(\frac{M_w}{M_n} >\sim 2\right)$ typical of most commercial polymer systems where there is a wide *overlap* of the stretch and orientational relaxation spectra. Dispersion in the MWD and dispersion in the stretch and orientational relaxation spectra go hand in hand. Entanglement constraints that do not survive longer than the stretch relaxation time of the test chain do not impact the stretch dynamics of the high molecular weight components of a polydisperse system.

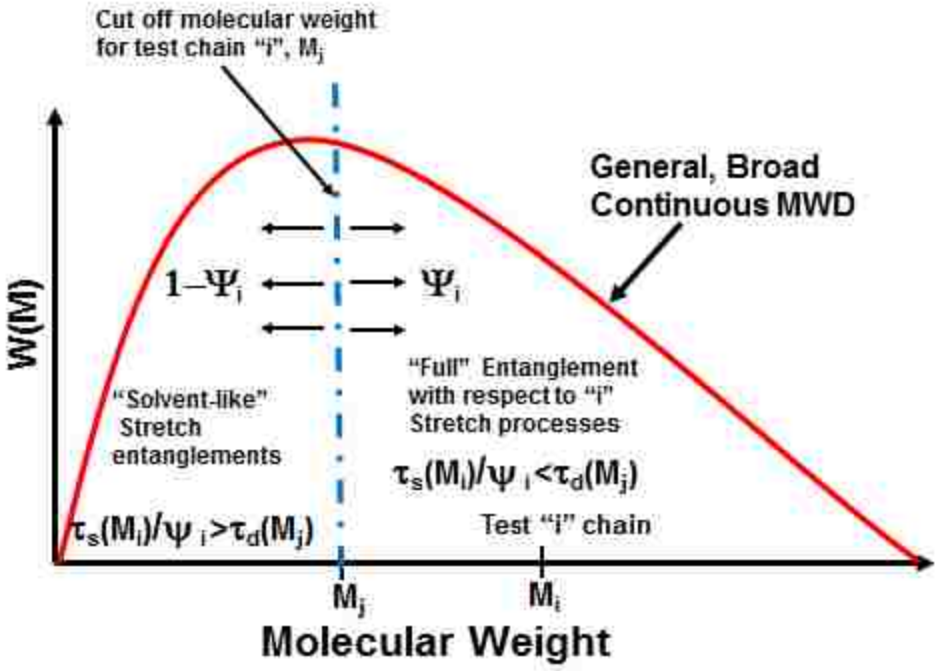

FIG. 2. Sketch of a typical broad MWD for a commercial polymer system with orientational and stretch relaxation spectra overlap. A given test chain of molecular weight, M_i, is chosen and the self-consistent cut-off criteria $\frac{\tau_{s,i}(M_i)}{\Psi_i(M_i)\tau_{d,j}(M_j)}=1$ is applied which defines a conjugate molecular weight chain, M_j, that demarcates the boundary between "solvent-like" chains with respect to stretch processes of the i chain and "full" entanglements with respect to i chain stretch processes.

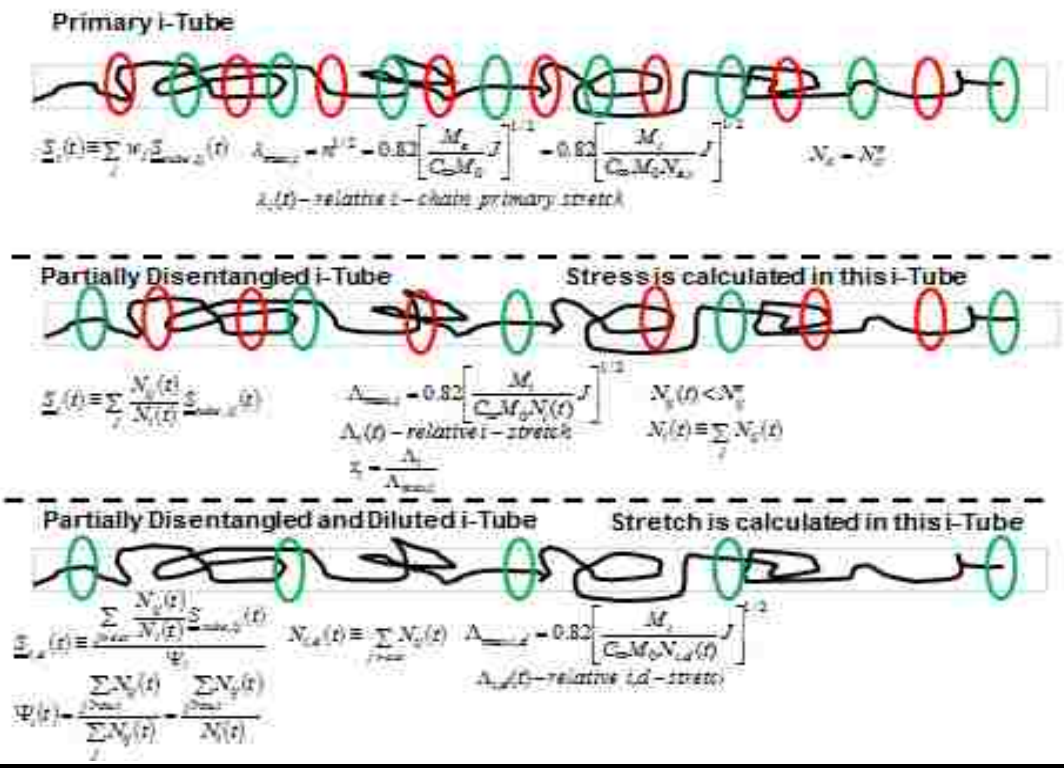

FIG. 3. Sketch of the three distinct unraveled "tubes" used in the polydisperse MBP model and their interrelationships. The construction of these tubes is motivated by the need to calculate the chain stretch in the presence of "solvent-like" entanglements and entanglements lost by deformation (convection off the chain ends). The lengths of the tubes are not in general equal (as they are drawn). We draw them as such for illustrative simplicity. The sketch illustrates a bi-disperse system of fast relaxers (red entanglements) and slow relaxers (green (i) entanglements) relative to the stretch relaxation time of the green (i) chains. The disentangled tube has fewer red and green entanglements. The disentangled and diluted stretch tube has no red (fast) stretch entanglements. Careful attention to the ij entanglement bookkeeping must be made.

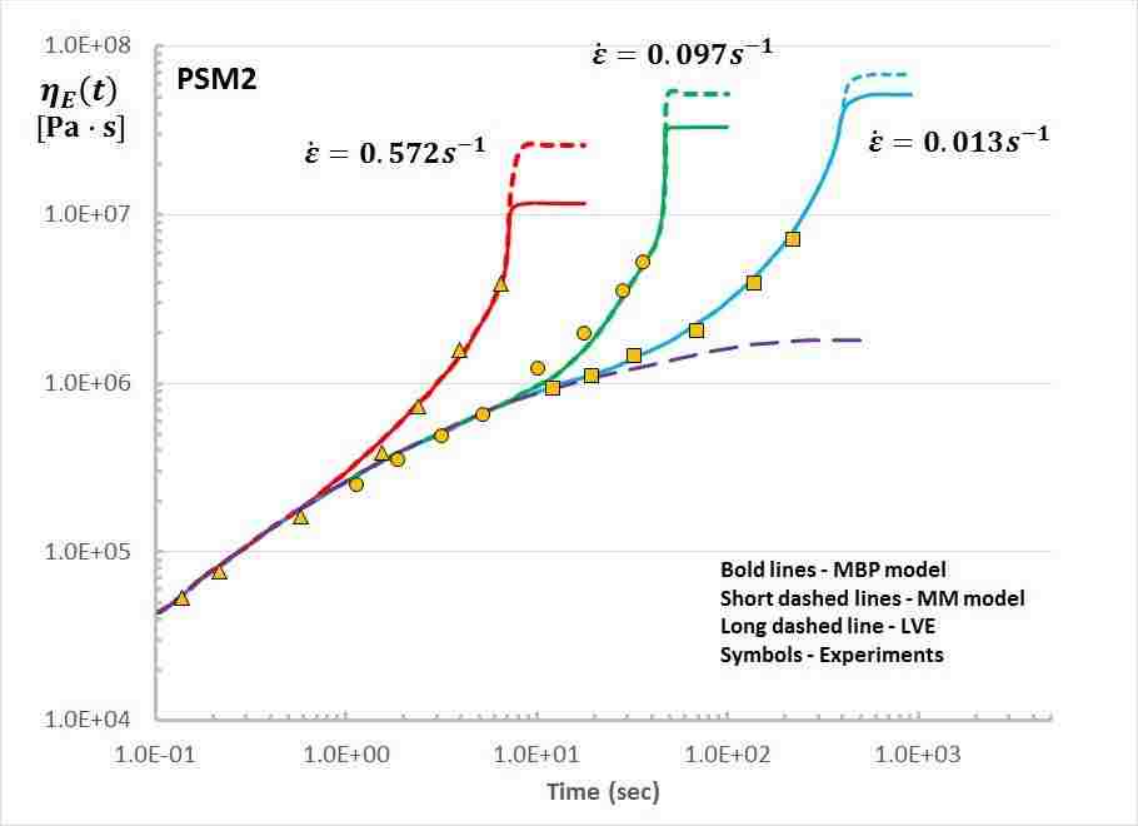

FIG. 4. Transient extensional viscosity curves for PSM2 (see Table III for the data) at $\dot{\varepsilon}$=0.013, 0.097, and 0.572s^{-1}. Predictions by MM and MBP, experimental data, and LVE curves are compared.

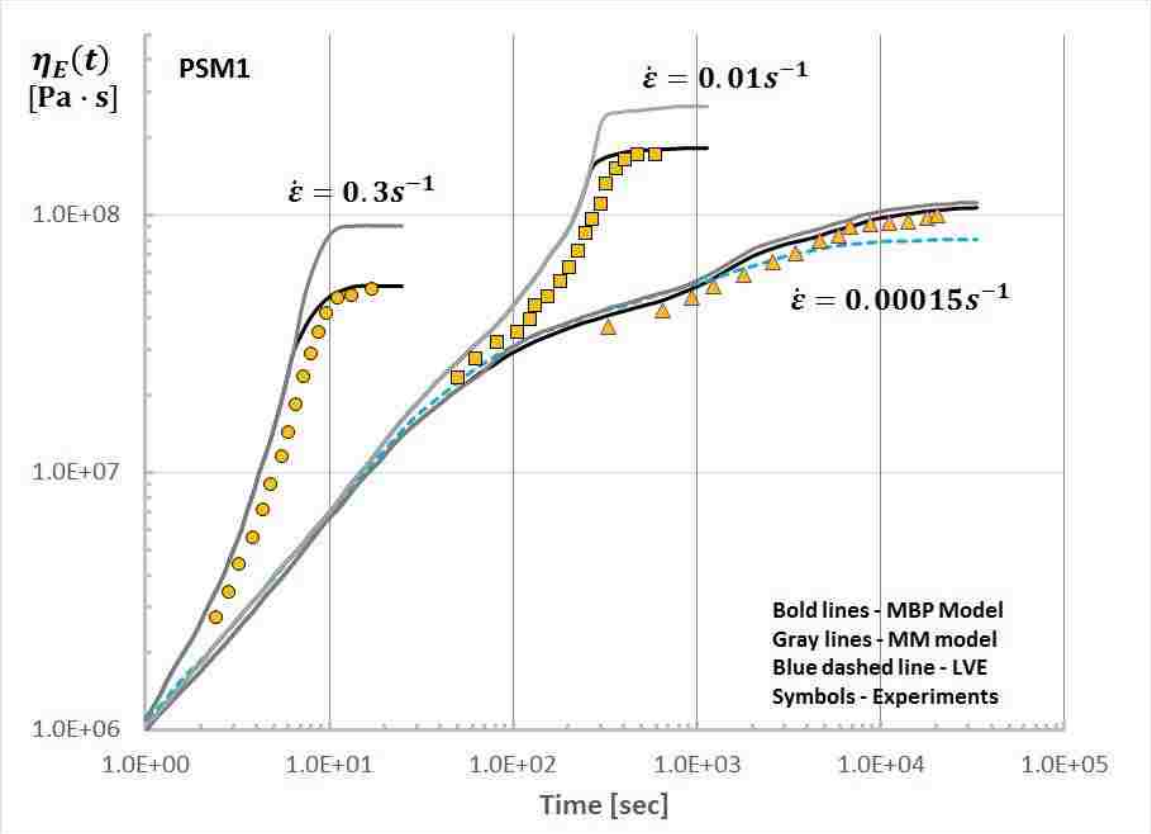

FIG. 5. Transient extensional viscosity curves for PSM1 (see Table II for the data) at $\dot{\varepsilon}$=0.00015, 0.01, and 0.3 s^{-1}. Predictions by MM and MBP, experimental data, and LVE curves are compared.

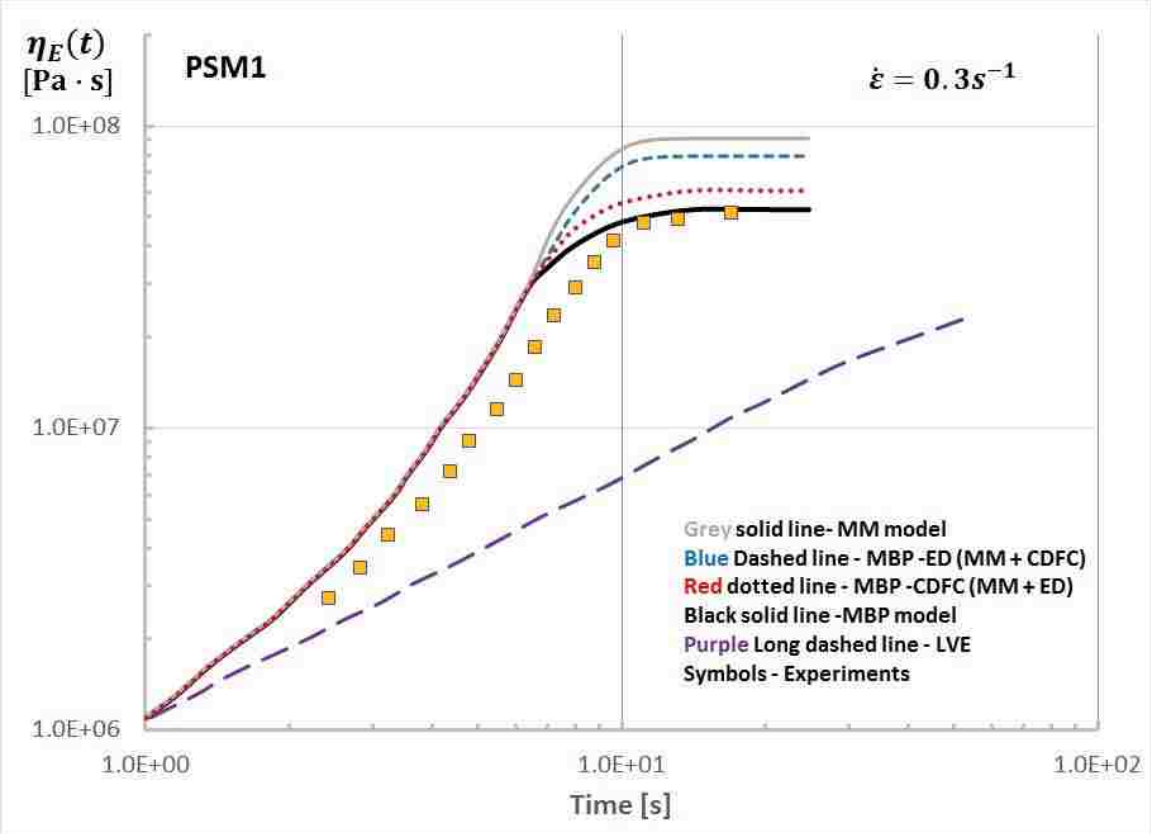

FIG. 6. Transient extensional viscosity curves for PSM1 (see Table II for the data) at $\dot{\varepsilon}$=0.3 s^{-1}. Predictions from different models are compared (see Table III for the details).

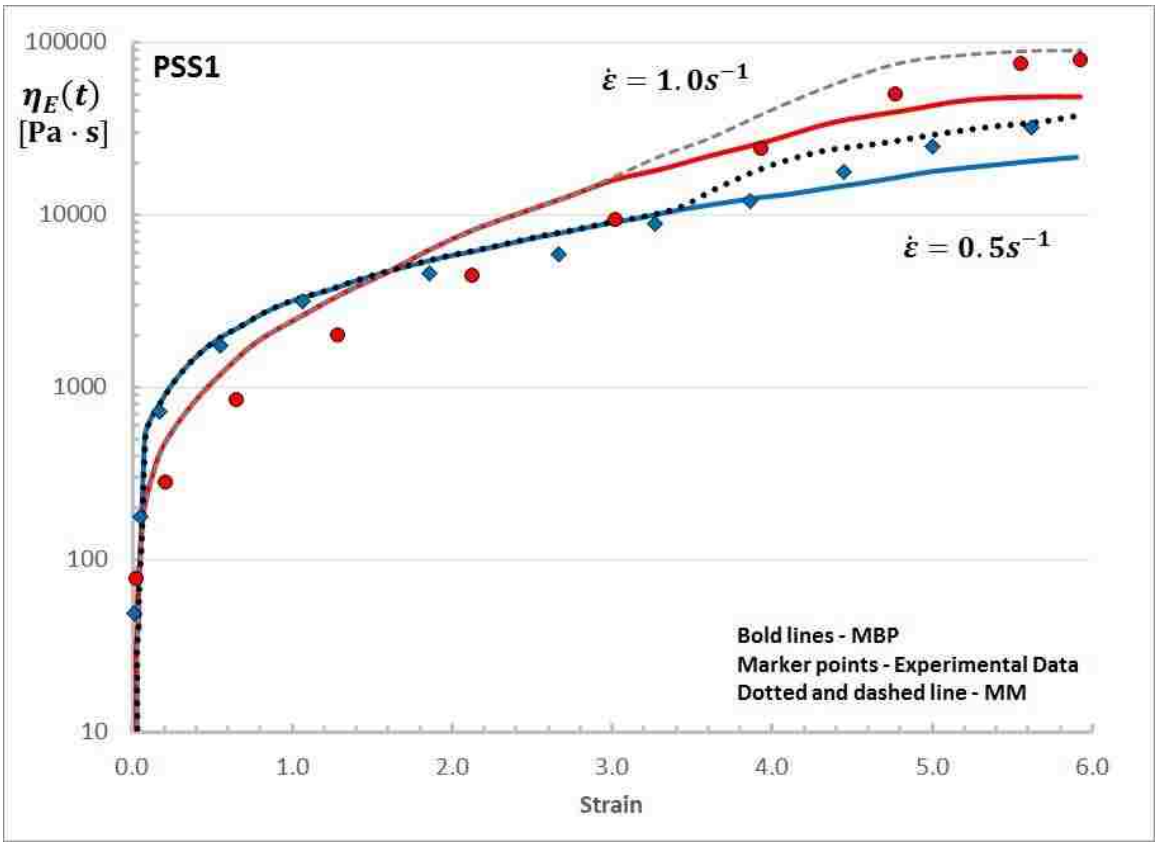

FIG. 7. Transient extensional viscosities for PSS1 (see Table II for the data) at $\dot{\varepsilon}$=0.5 and 1.0 s^{-1}. Predictions by MM and MBP, experimental data [Ye et al. (2003)], and LVE curves are compared.

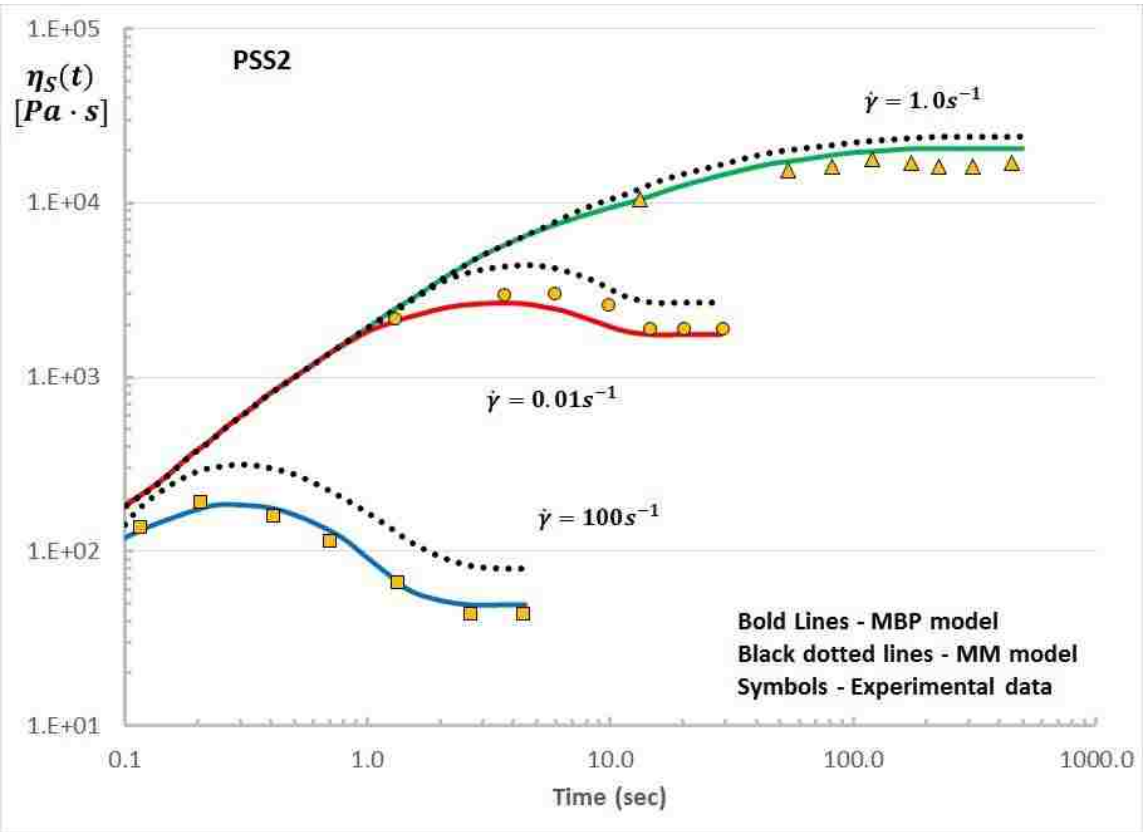

FIG. 8. Transient shear viscosities for 7% PS blend solution (PSS2 see Table V for details) at $\dot{\gamma}$ 0.01, 0.1 and 100 sec^{-1}. Predictions by MM and MBP and experimental data [Pattamaprom and Larson (2001)] are compared with each other.

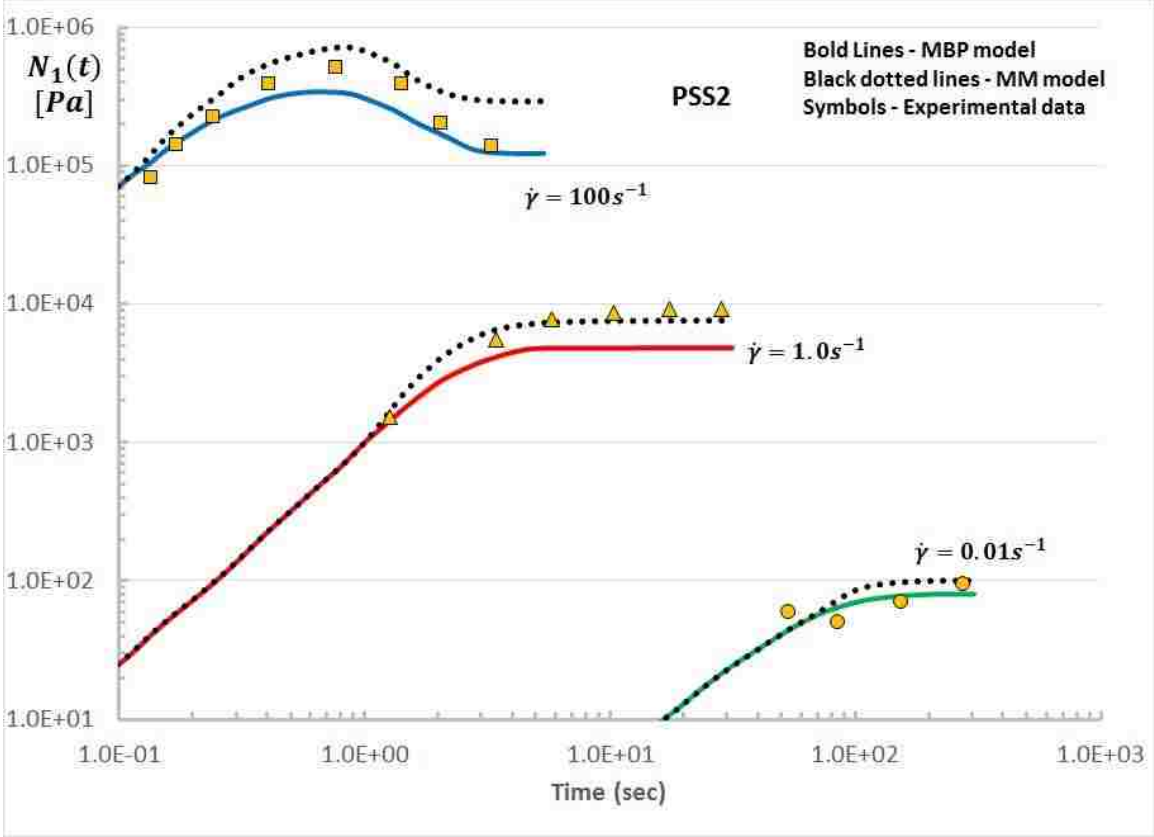

FIG. 9. Transient normal stress differences for 7% PS blend solution (PSS2 see Table V for details) at $\dot{\gamma}$ 0.01, 0.1 and 100 sec^{-1}. Predictions by MM and MBP and experimental data [Pattamaprom and Larson (2001)] are compared with each other.

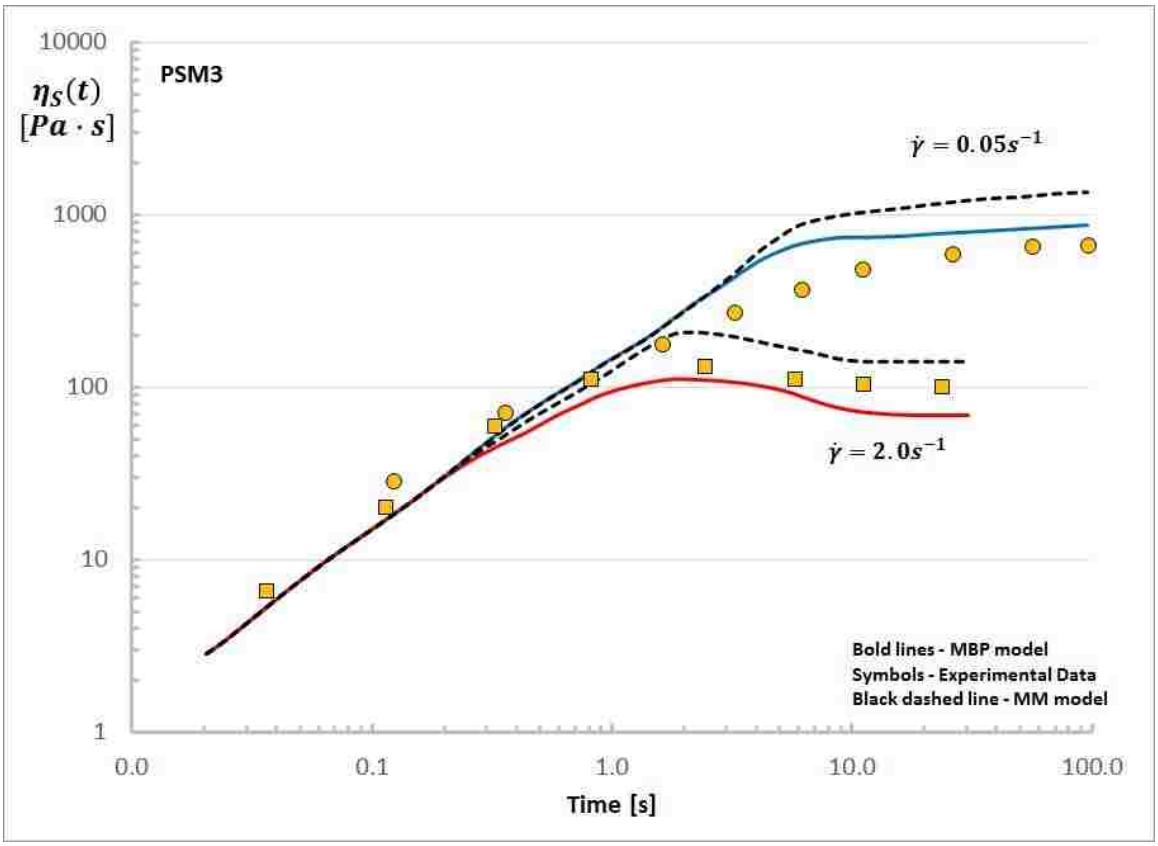

FIG. 10. Transient shear viscosity for PS melt (PSM3) (PI = 3.2) (see Table VI for details) at $\dot{\gamma}$ 0.05 and 2.0 sec^{-1} respectively. The experimental data given by markers are taken from Ye and Sridhar (2005).

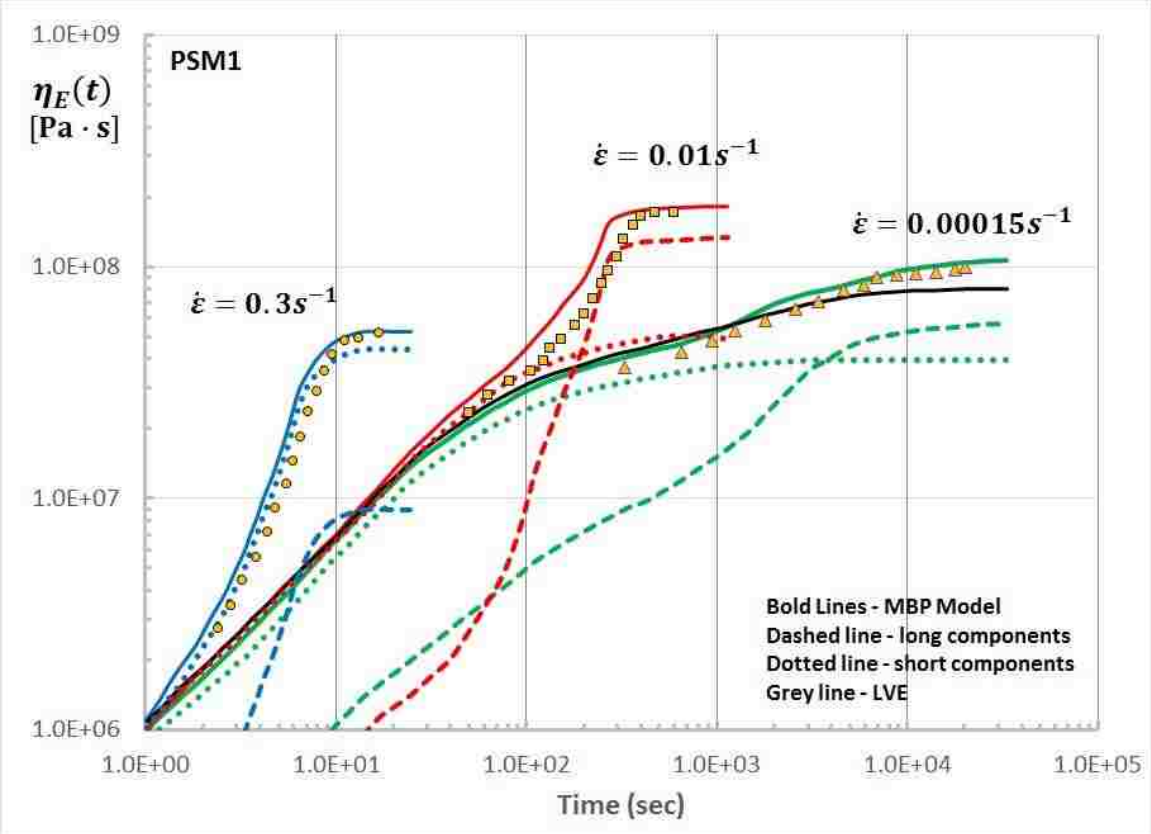

FIG. 11. Transient uniaxial extensional viscosity curves of each polymer component for PS bidisperse melt, PSM1 [Read *et al*. (2012)], at $\dot{\varepsilon}$=0.00015, 0.01 and 0.3 s^{-1}, predicted by MBP model.

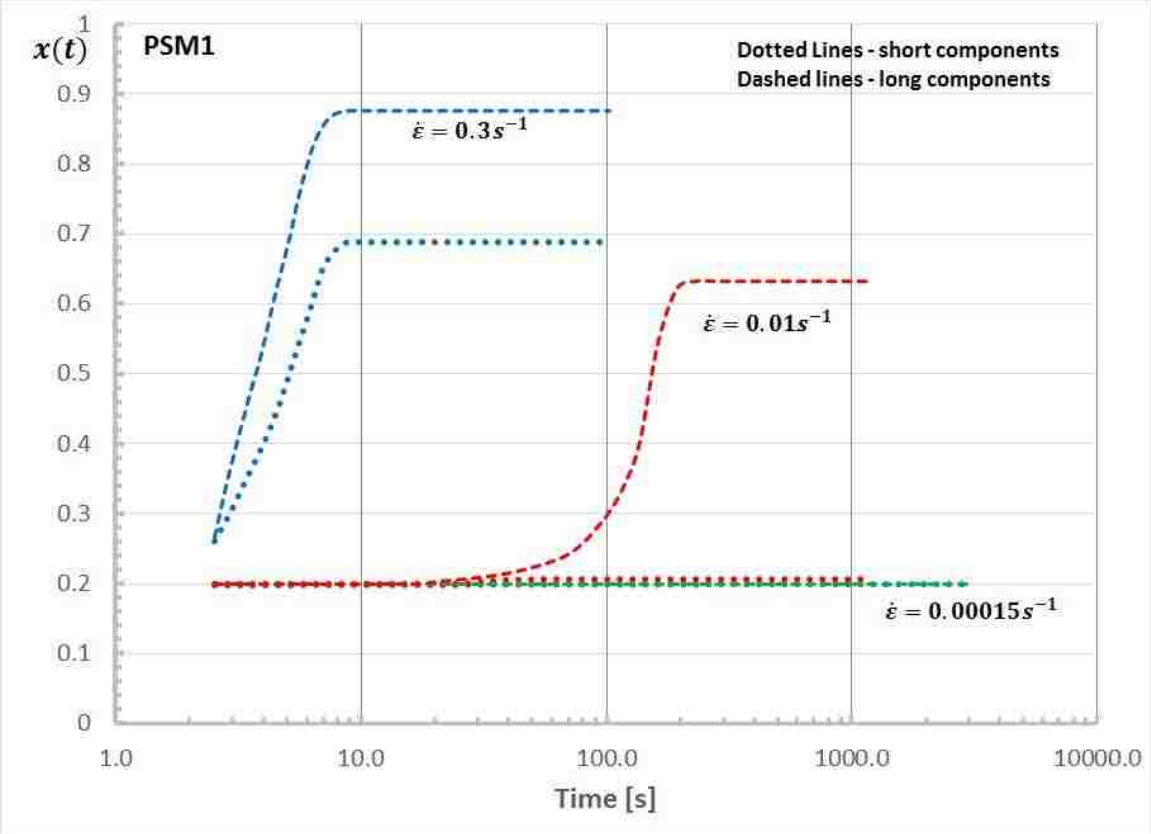

FIG. 12. Transient fractional stretch, $x(t)=\Lambda(t)/\Lambda_{max}$, curves of each polymer component for PS bidisperse melt, PSM1 [Read *et al*. (2012)], at $\dot{\varepsilon}$=0.00015, 0.01 and 0.3 s^{-1}, predicted by MBP model.

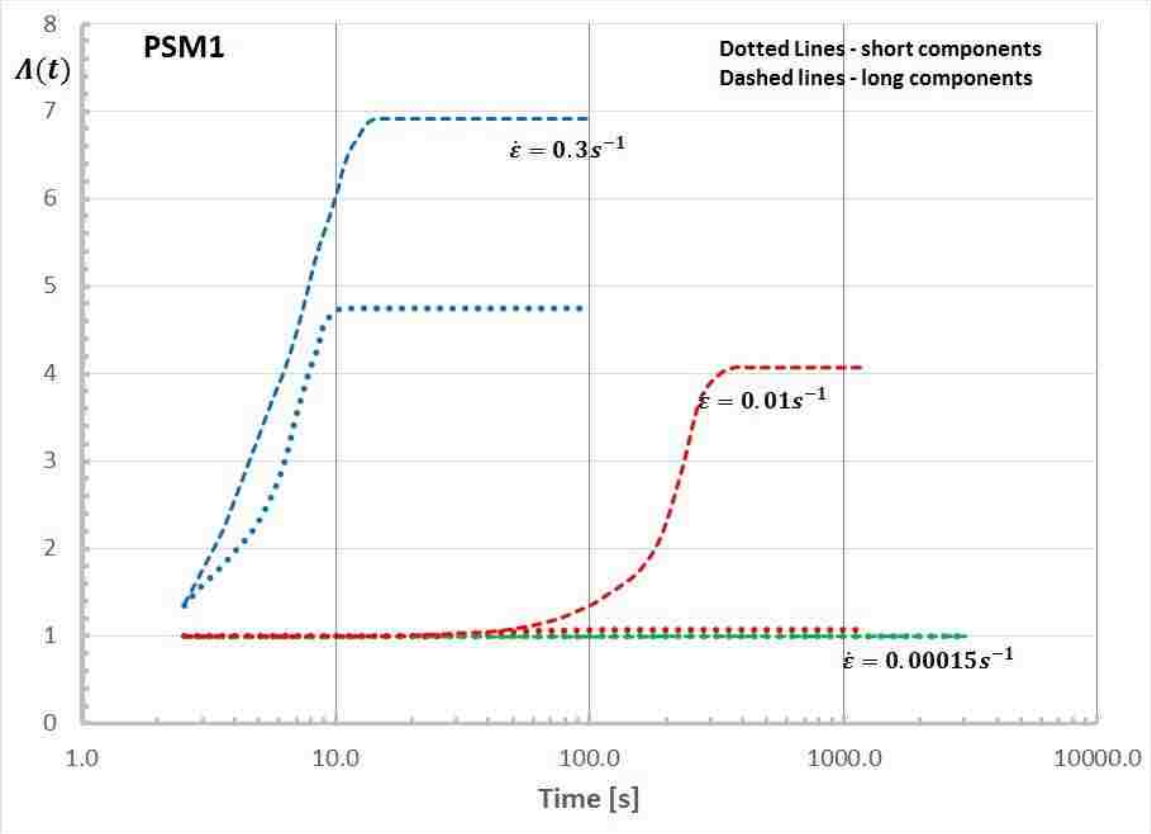

FIG. 13. Transient relative stretch, $\Lambda(t)=L(t)/L_{eq}(t)$, curves of each polymer component for PS bidisperse melt, PSM1 [Read *et al*. (2012)], at $\dot{\varepsilon}$=0.00015, 0.01 and 0.3 s^{-1}, predicted by MBP model.

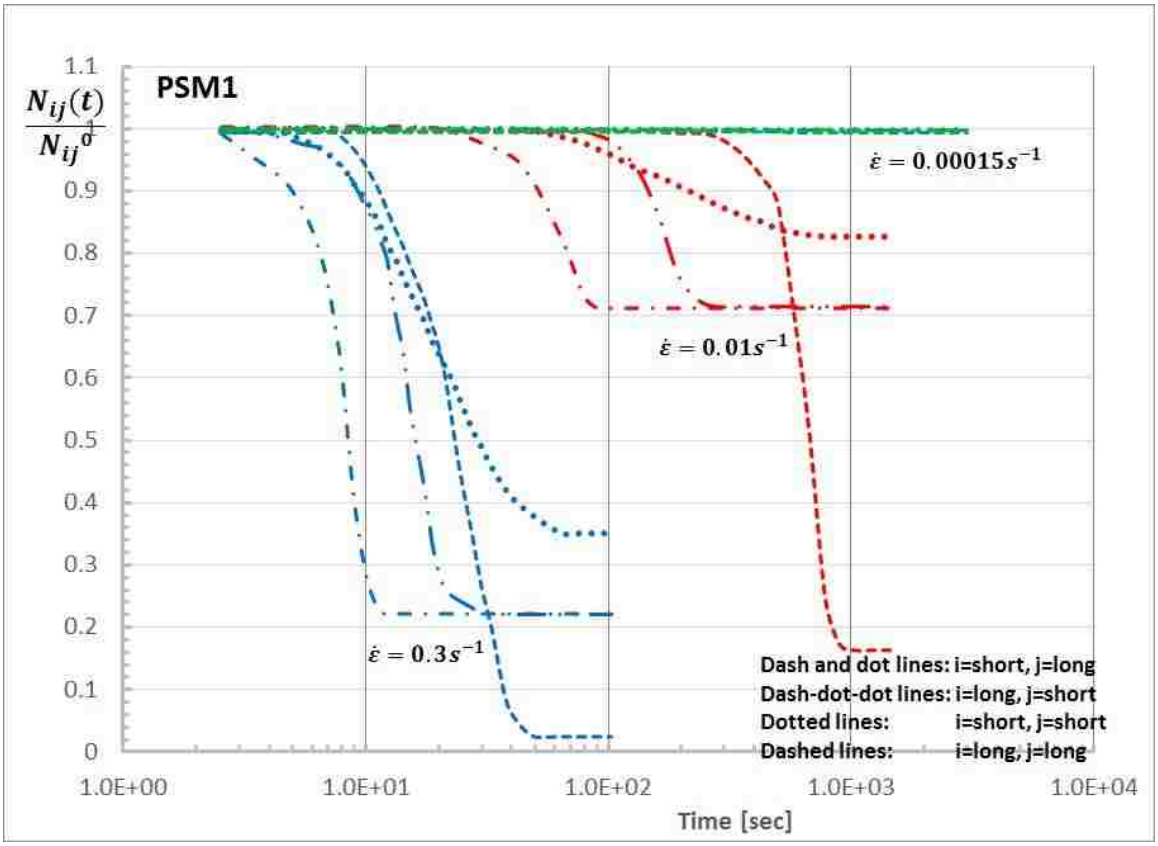

FIG. 14. Transient normalized entanglement dynamics curves of each entanglement pair for PS bidisperse melt, PSM1 [Read *et al*. (2012)], at $\dot{\varepsilon}$=0.00015, 0.01 and 0.3 s^{-1}, predicted by MBP model.

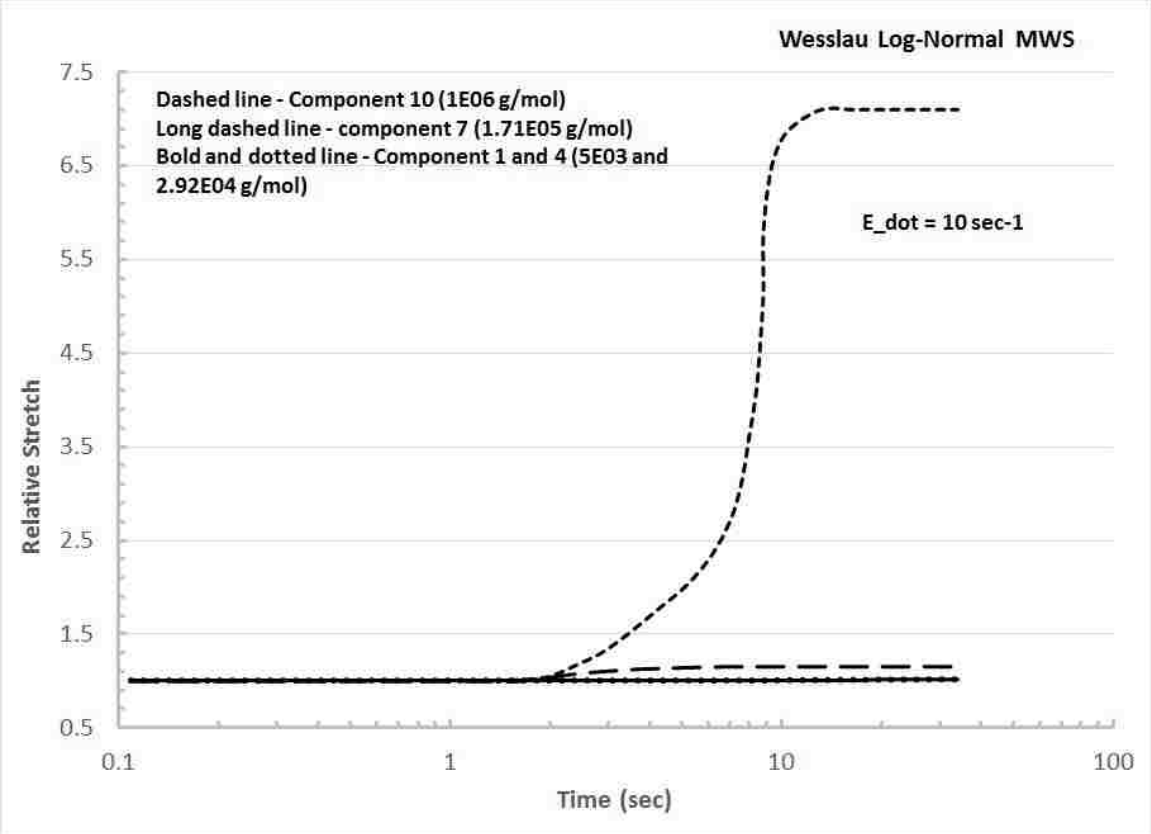

FIG. 15. Transient relative stretch curves for Wesslau's log-normal MWD, for components 1, 4, 7, and 10, at $\dot{\varepsilon}$=10 s^{-1}, predicted by MBP model.

TABLE I. Summary of the experimental data sets used in this study. (PSMW* is not an experimental data set but a model MWD with log distribution).

Symbol	Melt/Solution	Section used in	Input parameters	Reference
PSM1	Melt	III.A, IV	Table II	Read et al. (2012)
PSM2	Melt	III.A	Table III	Minegishi et al.
PSM3	Melt	III.B	Table V	Ye & Sridhar (2005)
PSS1	Solution	III.A	Table II	Ye et al. (2003)
PSS2	Solution	III.B	Table VI	Pattamaprom & Larson (2003)
PSMW*	Melt	IV	Table VII	*Model MWD system

TABLE II. Simulation input values for the uniaxial extension of bidisperse PS melt with PI = 1.248 (PSM1) [Read *et al*., (2012)] and bidisperse 7% PS solution (PSS1) [Ye *et al*., (2003)].

Symbol	G_N^o [Pa]	Molecular weight [kg/mol]	Weight fraction	$\tau^0_{d,i}$ [s]	$\tau^0_{r,i}$ [s]	N_e
PSM1	2.46×10^5	390	0.1402	2.564×10^4	420.84	20.31
		103	0.8598	4.696×10^2	29.24	5.354
PSS1	6.13×10^2	2890	0.8	9.40	0.765	12.33
		8420	0.2	189.60	5	35.93

TABLE III. Simulation input values for the data set PSM2 (PS 686 spiked with MW 3.2×10^6 component; PI=2.33) directly taken from [Mishler and Mead (2013b)], which was originally obtained from Minegishi et al.

Weight fraction	**G_N^o [Pa]**	**Molecular weight (kg/mol)**	**$\tau^0_{d,i}$ [s]**	**$\tau^0_{r,i}$ [s]**	**N_e**
0.0186	3.00×10^5	22.9	1.37×10^{-3}	1.37×10^{-3}	1.762
0.0415		42.3	6.27×10^{-3}	4.69×10^{-3}	3.254
0.0687		67.2	3.02×10^{-2}	1.18×10^{-2}	5.169
0.0961		83.0	0.110	2.53×10^{-2}	0.638
0.117		137	0.340	4.92×10^{-2}	10.538
0.127		184	0.928	8.87×10^{-2}	14.154
0.123		241	2.320	0.152	18.538
0.108		310	5.470	0.252	23.846
0.0879		392	12.100	0.403	30.154
0.0665		490	25.900	0.629	37.692
0.0474		605	53.100	0.959	46.538
0.0321		740	105.000	1.430	56.923
0.0208		897	203.000	2.110	69.000
0.0129		1080	381.000	3.060	83.077
0.00777		1290	697.000	4.360	99.231
0.00452		1530	1.24×10^3	6.130	117.692
0.00255		1810	2.20×10^3	8.580	139.231
0.0014		2130	3.83×10^3	11.900	163.846
7.54×10^4		2500	6.61×10^3	16.400	192.308
3.96×10^4		2910	1.11×10^4	22.200	223.846
0.015		32000	1.53×10^4	26.800	246.154

TABLE IV. Summary of which physical effects are included/excluded in each model, compared in Figure 5.

Model Symbol	Equivalent Symbol	ED	CDFC
MBP	MM $_{+ED+CDFC}$	On	On
MBP $_{-ED}$	MM $_{+CDFC}$	Off	On
MBP $_{-CDFC}$	MM $_{+ED}$	On	Off
MBP $_{-ED\ -CDFC}$	MM	Off	Off

TABLE V. Simulation input values for shear 7% bidisperse PS solution (PSS2) [Pattamaprom and Larson (2001)].

Symbol	G_N^o [Pa]	Molecular weight (kg/mol)	Weight fraction	$\tau^0_{d,i}$ [s]	$\tau^0_{r,i}$ [s]	N_e
PSS 2.9/8.4	5.20×10^2	2890	0.6	1.53	0.13	15.21
		8420	0.4	31.65	0.6	44.30

TABLE VI. Simulation input values for shear PSM3 [PS melt (P1) (PI=3.5)] [Ye and Sridhar (2005)].

Weight fraction	G_N^o [Pa]	Molecular weight (kg/mol)	$\tau^0_{d,i}$ [s]	$\tau^0_{r,i}$ [s]	N_e
0.002	6.19×10^2	52.6	1.46×10^{-4}	2.16×10^{-4}	0.225
0.003		76.5	4.47×10^{-4}	4.56×10^{-4}	0.327
0.004		100	1.01×10^{-3}	7.86×10^{-4}	0.429
0.004		120	1.73×10^{-3}	1.13×10^{-3}	0.513
0.01		147	3.17×10^{-3}	1.69×10^{-3}	0.627
0.032		218	1.03×10^{-3}	3.71×10^{-3}	0.930

Table VI. Simulation input values for shear PSM3 [PS melt (P1) (PI=3.5)] [Ye and Sridhar (2005)] (cont.)

0.009		284	2.29×10^{-2}	6.29×10^{-3}	1.212
0.049		344	4.05×10^{-2}	9.21×10^{-3}	1.467
0.02		442	8.62×10^{-2}	1.52×10^{-2}	1.886
0.122		601	2.17×10^{-1}	2.82×10^{-2}	2.566
0.087		869	6.55×10^{-1}	5.89×10^{-2}	3.708
0.035		978	9.34×10^{-1}	7.46×10^{-2}	4.174
0.179		1410	2.80	1.55×10^{-1}	6.018
0.041		2070	8.83	3.34×10^{-1}	8.826
0.141		2460	1.49×10^{1}	4.72×10^{-1}	10.504
0.123		4200	7.38×10^{1}	1.37	17.909
0.123		8190	5.48×10^{2}	5.23	34.938
0.016		29640	2.60×10^{4}	68.5	126.504

TABLE VII. Simulation input values for model generated Wesslau's log-normal PS melt MWD with PI = 2.33 and weight avg. MW = 2.4×10^5 (PSMW).

Weight fraction	**G_N^o [Pa]**	**Molecular weight (kg/mol)**	**$\tau^0_{d,i}$ [s]**	**$\tau^0_{r,i}$ [s]**	**N_e**
3.53×10^{-4}	2.46×10^5	5.00	2.64×10^{-6}	3.38×10^{-6}	2.60×10^{-1}
2.69×10^{-3}		9.01	1.95×10^{-5}	1.39×10^{-5}	4.69×10^{-1}
0.014		16.2	1.44×10^{-5}	5.67×10^{-5}	8.44×10^{-1}
0.0499		29.2	1.06×10^{-3}	2.33×10^{-4}	1.52
0.123		52.7	7.92×10^{-3}	9.62×10^{-4}	2.74
0.209		94.9	5.85×10^{-2}	3.95×10^{-3}	4.94
0.247		171	0.43	1.62×10^{-2}	8.91
0.2009		308	3.20	6.66×10^{-2}	16.0
0.111		555	23.73	2.74×10^{-1}	28.9
0.0422		1000	175.65	1.12	52.1

References

Andreev, M., R.N. Khaliullin, R.J.A. Steenbakkers and J.D. Schieber, "Approximations of the discrete slip-link model and their effect on nonlinear rheology predictions," J. Rheology **57**, 535-557 (2013).

Auhl, D., P. Chambon, T.C.B. McLeish and D.J. Read, "Elongational Flow of Blends of Long and Short Polymers: Effective Stretch Relaxation Time," Phys. Rev. Lett. **103**, Article 136001 (2009).

Baig, C., V.G. Mavrantzas and M. Kroger, "Flow effects on melt structure and entanglement network of linear polymers: Results from a non-equilibrium molecular dynamics study of a polyethylene melt in steady shear," Macromolecules **43**, 6886-6906 (2010).

Bremner, T., A. Rudin, and D. G. Cook. "Melt flow index values and molecular weight distributions of commercial thermoplastics," Journal of Applied Polymer Science **41**, 7-8 1617-1627 (1990).

Dealy, J. M., and P. C. Saucier. Rheology in plastics quality control. Hanser Publishers, (2000).

Dealy, J.M. and R.G. Larson, "Structure and rheology of molten polymers: From structure to flow behavior and back again," Hanser, Munich (2006).

Dealy, J.M. and WM. K.-W. Tsang, "Structural time dependency in the rheological behavior of molten polymers," J. Appl. Poly. Sci. **26**, 1149-1158 (1981).

Doi, M., and S.F. Edwards, "The Theory of Polymer Dynamics," Oxford Science Publications, (1986).

Eder, G., H. Janeschitz-Kriegl, and S. Liedauer, "Crystallization processes in quiescent and moving polymer melts under heat transfer conditions," Progress Polymer Sci. **15**, 629–714 (1990).

Everaers, R., S.K. Sukumaran, G.S. Grest, C. Svaneburg, A. Sivasubramanian and K. Kremers, "Rheology and microscopic topology of entangled polymeric liquids," Science **303**, 823-827 (2004).

Graham, R.S., A.E. Likhtman, T.C.B. McLeish and S.T. Milner, "Microscopic theory of linear, entangled polymer chains under rapid deformation including chain stretch and convective constraint release," J. Rheology **47**, 1171-1200 (2003).

Huang, Q., O. Mednova, H.K. Rasmussen, N.J. Alvarez, A. L. Skov, K. Almdal, and O. Hassager, "Concentrated Polymer Solutions are Different from Melts: Role of Entanglement Molecular Weight," Macromolecules **46**, 5026-5035 (2013).

Ianniruberto, G., and G. Marrucci, "Convective constraint release revisited," J. Rheol. **58**, 89-102 (2014).

Larson, R. G., "Constitutive Equations for Polymer Melts and Solutions," Butterworths, Boston, (1988).

Likhtman, A. E., and T. C. B. McLeish, ''Quantitative theory for linear dynamics of linear entangled polymers,'' Macromolecules **35**, 6332–6343 (2002).

Mead, D.W., "Derivation of the "Switch Function" in the Mead-Larson-Doi Theory," Rheologica Acta **50**, 631-643 (2011).

Mead, D.W., "Development of the "Binary Interaction" Theory for Entangled Polydisperse Linear polymers," Rheol. Acta **46**, 369-395 (2007).

Mead, D.W., and L. Leal, "The reptation model with chain stretching I) Basic equations and general properties," Rheologica Acta **34**, 339-360 (1995).

Mead, D.W., D. Yavich and L. Leal, "The reptation model with chain stretching II) Steady flow properties," Rheologica Acta **34**, 360-383 (1995).

Mead, D.W., N. Banerjee and J. Park, "Constitutive model for entangled polymers incorporating binary entanglement pair dynamics and a configuration dependent friction coefficient," J. Rheol **59**, 335-363 (2015).

Mead, D.W., R.G. Larson and M. Doi, "A molecular theory for fast flows of entangled polymers," Macromolecules **31**, 7895-7914 (1998).

Milner, S. T., and T. C. B. McLeish. "Parameter-free theory for stress relaxation in star polymer melts." Macromolecules **30**, 7 2159-2166 (1997).

Minegishi, A., A. Nishioka, T. Takahashi, Y. Masubuchi, J. Takimoto and K. Koyama, "The effect of ultrahigh molecular weight polymers on the non-linear response in uniaxial elongational viscosity," J. Soc. Rheology Japan **25**, 215-216 (1997).

Minegishi, A., A. Nishioka, T. Takahashi, Y. Masubuchi, J. Takimoto and K. Koyama, "Uniaxial elongational viscosity of PS/a small amount of UHMW-PS blends," Rheologica Acta **40**, 329-338 (2001).

Minegishi, A., Y. Naka, T. Takahashi, Y. Masubuchi, J. Takimoto and K. Koyama, "Strain hardening property of polystyrene (PS)/ultrahigh molecular weight (UHMW)-PS blends," AIP Conference Proceedings **499**, 649-650 (1999).

Mishler, S.D. and D.W. Mead, "Application of the MLD "Toy" Model to Extensional Flows of Broadly Polydisperse Linear Polymers: Model Development," J. Non-Newtonian Fluid Mech. **197**, 61-79 (2013a).

Mishler, S.D. and D.W. Mead, "Application of the MLD "Toy" Model to Extensional Flows of Broadly Polydisperse Linear Polymers: Comparison to Experimental data Sets," J. Non-Newtonian Fluid Mech. **197**, 80-90 (2013b).

Park, J., D.W. Mead, and M.M. Denn, "Stochastic Simulation of Entangled Polymeric Liquids in Fast Flows: Microstructure Modification," J. Rheology **56**, 1057-1082 (2012).

Pattamaprom, C. and R. G. Larson, "Constraint Release Effects in Monodisperse and Bidisperse Polystyrenes in Fast Transient Shearing Flows," Macromolecules **34**, 5229-5237 (2001).

Press, W. H., S. A. Teukolsky, and B. P. Flannery 3rd. "Cambridge University Press; New York," Numerical Recipes: The Art of Scientific Computing (2007).

Read, D. J., K. Jagannathan, S. K. Sukumaran and D. Auhl, "A full-chain constitutive model for bidisperse blends of linear polymers," J. Rheol. **56**, (4), 823-873 (2012).

Rokudai, M., "Influence of shearing history on the rheological properties and processability of branched polymers," J. Appl. Poly. Sci. **23**, 463-471 (1979).

Watanabe, H., and T. Kotaka, "Viscoelastic properties and relaxation mechanisms of binary blends of narrow molecular weight distribution polystyrenes." Macromolecules **17**, 11 2316-2325 (1984).

Ye, X. and T. Sridhar, "Effects of the Polydispersity on Rheological Properties of Entangled Polystyrene Solutions", Macromolecules **38**, 3442-3449 (2005).

Ye, X., R. G. Larson, C. Pattamaprom, and T. Sridhar, "Extensional properties of monodisperse and bidisperse polystyrene solutions", J. Rheol. **47**, (2) 443-468 (2003).

SECTION

5. CONCLUSION

This dissertation has successfully elucidated the importance of the knowledge of entangled polymer rheological properties in both the fields of biological science and polymer processing. The write-up has been organized in three major sections. Firstly, a review on the mathematical models developed to quantify cytoskeleton mechanical behavior has been presented; followed by development of constitutive “toy” models to describe the rheological properties of both monodisperse and polydisperse linear entangled polymer systems under various deformation conditions.

In the review on mathematical models to study cytoskeleton mechanical properties, a framework for approaching and understanding the plethora of biopolymer network models in terms of length scales has been provided. The length scales and their proper description are important as they are related to the stress components and the phenomena of interest. Identifying the length scale categories of a model also can give a quick insight into the advantages and disadvantages of the model and the types of behaviors and properties described. Conversely, models can be selected based on the length scale of the phenomena of interest. Models mainly based on the passive dynamics associated with pure mechanical/rheological responses were focused on. However, there are models based on different approaches, such as the gel-like model: it was proposed by Pollock that the cell movement and shape alteration can be described by the phase-transition mechanism of a gel-like structure (Pollock, 2006). There have been models that consider the active behaviors which are related with biological responses or structural

rearrangement by polymerization/depolymerization. For example, the granular model considered microtubule rearrangement to describe cell crawling (Maurin et al., 2008). There have been models which described active behaviors of motor proteins (Chen & Shenoy, 2011) and growth and remodeling (Na et al., 2007). Although many reviews have pointed out the need to improve models for active dynamics (Unterberger & Holzapfel, 2014; Chen et al., 2012; Nava et al., 2014), apparent barriers to that development are the inherent complexity of the models for passive dynamics and the need for broader interdisciplinary research including biomedical engineering, medical science, biophysics, biology, chemistry, materials science, and chemical engineering, etc. The correct prediction of biopolymer network mechanical/rheological properties is important in many biomedical applications associated with biopolymer networks. Therefore, the framework provided by this review is expected to promote various studies on biopolymer networks (Banerjee & Park, 2015).

Moving on from the field of medicine to that of polymer processing, the research attempted to understand and answer some of the persisting questions regarding linear monodisperse entangled polymer systems under fast non-linear deformation conditions.

In that effort a mathematically and computationally simple “toy” molecular model that incorporates ED, CDFC, and CCR into the base DEMG “toy” model, the MBP model for monodisperse entangled polymers was constructed. This model is a natural next step in the systematic progression of increasingly detailed and complex molecular models for entangled linear flexible polymers. The constitutive equation developed for monodisperse polymer melt or an entangled semi-dilute solution has three

major components (see equation (1)): 1) A quantitative description of the orientation dynamics, 2) a quantitative description of the stretch dynamics, and 3) a quantitative description of the entanglement dynamics (which are manifested through the nonlinear modulus $G_N(t)$). All the three components are coupled together and nonlinear. The effect of CDFC has been incorporated in the description of the time scales (Mead et al., 2015).

$$\underline{\underline{\sigma}}(t) = 3 \underbrace{G_N(t)}_{\substack{Entanglement \\ dynamics}} \underbrace{\Lambda^2(t)}_{\substack{Stretch \\ dynamics}} \underbrace{\underline{\underline{S}}_{tube}(t)}_{\substack{Orientation \\ dynamics}} \tag{1}$$

The new MBP model generates extensional flow curves that are monotonically thinning (with a small "kink" near $\dot{\varepsilon}\tau_{s,eq} \approx 1$) for monodisperse PS melts that are qualitatively consistent with the experiment. The results are sensitive to the specific functional form of the CDFC used. For monodisperse PS solutions, the effects of CDFC are effectively diluted out and the classical tube model ladle shaped extensional flow curve is generated. The simulation results strongly suggest that CDFC is important in the prediction of rheological properties in nonlinear extensional flows of monodisperse PS melts. CCR is detrimental to the predictions in extensional flows but is important for the rheological properties in shear flows (Mead et al., 2015).

A plausible explanation as to why the DEMG-cdfc model yields a monotonically thinning flow curve of monodisperse PS melts that are approximately equivalent to those predicted by the new MBP-xccr model (i.e. DEMG with ED "on", CDFC "on" and CCR "off") is also provided. This suspicious coincidence masks the underlying details that are actually occurring in fast nonlinear flows of entangled polymers. The new model

simultaneously captures nonlinear flows and the entanglement microstructure modification that occurs in these fast flows (Mead et al., 2015).

Furthermore, the knowledge of the melt entanglement density following polymer shaping operations (finite deformations) is crucially important with respect to determining the ultimate mechanical properties of the part. Hence, the information gleaned from molecular models with ED, such as the MBP model, is directly relevant to polymer processing operations (Mead et al., 2015).

The next endeavor is to generalize the new MBP model to polydisperse systems. Having a generally applicable model for polydisperse systems that is easy to code and fast to execute has many practical applications in analytic rheology. The MBP monodisperse model and Mishler and Mead's (2013a, 2013b) "diluted stretch tube" theory is combined together to develop the MBP polydisperse model. The concepts of CDFC and ED are sustained in the MBP polydisperse "toy" model.

The MBP polydisperse model can correctly predict the PS bi-blend both melt and solution behavior under uniaxial extension, defining each component's effect on the overall system. It can be concluded that due to the solution-like behavior of some of the entanglements, the CDFC effect weakens and is not important in defining the overall viscosity of the system. The CDFC effect is similar to what observed in case of monodisperse solution systems (Mead et al., 2015).

Entanglement dynamics (ED), on the other hand, proved to be very important physics in defining the system. This observation is not unpredictable as the entanglement

structure is very complex for a polydisperse system. With different time scales, the strong effect of ED is imperative. The model can also predict the individual effects due to the short and the long components of the system. It is observed, that the deviation that occurs in the transient viscosity from LVE (strain hardening), is due to the commencement of stretch in the long chain component. Further increase in extension rates causes the shorter chain to start stretching and then the overall viscosity is scaled both by longer and shorter chain.

The wide MWD PS 686, a most probable MWD and the model generated Wesslau's log-normal MWD are simulated to understand the effect of the high molecular weight component on the overall viscosity of the system. The model can predict the experimental behavior for PS 686 very accurately. For both the PS 686 and Wesslau's log-normal MWD, the strain hardening is observed exactly at the point when the high molecular weight component begins stretching. The model can also correctly predict the shear flow transient and steady state (shear viscosity, shear stress and first normal stress difference) behavior for both the bidisperse solution and large MWD melt, again confirming that ED is important to both qualitatively and quantitatively describe the properties. Even in shear melt and solution systems, CDFC is found to be inconsequent.

It has long been known that a polymer melt's rheological properties reflect the underlying fluid microstructure (Dealy and Saucier, 2000; Dealy and Larson, 2006). Microstructure here refers to the MWD, entanglement density and long chain branching. Consequently, rheology is commonly used in industry to characterize polymer resins

using relatively crude rheological criteria such as the Melt Flow Index (MFI) (Bremner et al., 1990).

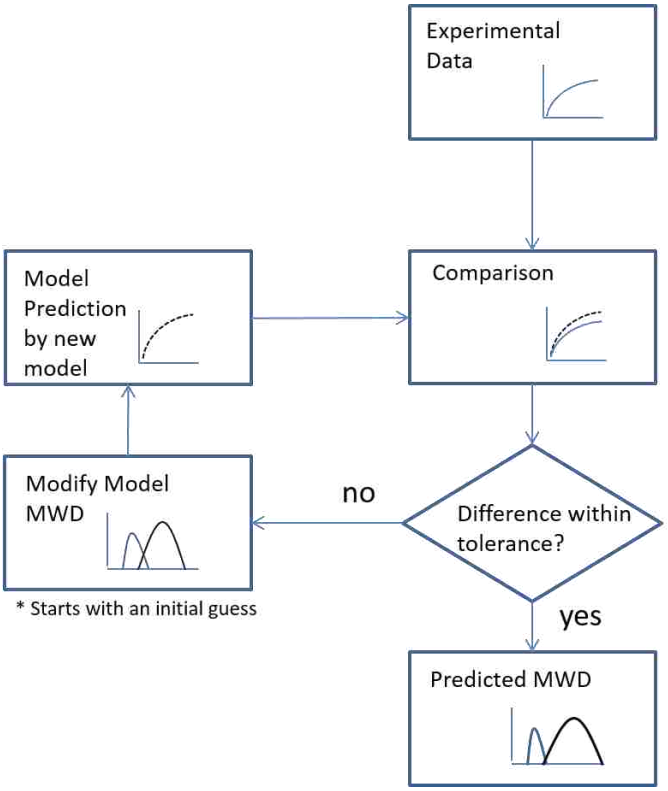

Figure 5.1. Analytic rheology scheme.

Such rheological criteria were until recently largely based on empiricism rather than sound theory. However, molecular rheology has advanced to the point where it is now possible to definitively and quantitatively characterize commercial polymer resins from their rheology alone. These ideas form the motivation and basis of Analytic Rheology as a science. Thus, having a generally applicable model for polydisperse

systems that is easy to code and fast to execute has many practical applications in analytic rheology. Analytic rheology is the prediction of the molecular weight distribution of the system from the viscosity and stress data. Figure 5.1, gives a glimpse of the analytic rheology procedure.

APPENDIX A.

TRACE OF ORIENTATION TENSOR ($\underline{\underline{S}}_{tube,ij}(t)$) FOR THE MBP POLYDISPERSE "TOY" MODEL

TRACE OF ORIENTATION TENSOR ($\underline{\underline{S}}_{tube,ij}(t)$)

The trace of orientation tensor $\underline{\underline{S}}_{tube,ij}(t)$=1.00, is a method of validation for the numerical analysis of polydisperse system. The ij entanglement pair orientation evolution equations (3a and 3b) in paper III, are checked for their trace values.

$$\underline{\underline{S}}_{tube,ij}(t) = \begin{bmatrix} S_{xx} & S_{xy} & 0 \\ S_{yx} & S_{yy} & 0 \\ 0 & 0 & S_{zz} \end{bmatrix}$$

Trace (tr) of $\underline{\underline{S}}_{tube,ij}(t) = S_{xx} + S_{yy} + S_{zz}$ (sum of the diagonals of the matrix).

For extension deformation condition at extension rate $0.01s^{-1}$ the trace of $\underline{\underline{S}}_{tube,ij}(t)$= 0.999998 at $\Delta t=5\times10^{-11}$s. For shear deformation condition at shear rate $1.0s^{-1}$ the trace of $\underline{\underline{S}}_{tube,ij}(t)$= 0.999999 at $\Delta t=5\times10^{-11}$s. Under other deformation rates the trace of $\underline{\underline{S}}_{tube,ij}(t)$ also show same level of convergence, hence, the values for only single extension and shear rates are discussed in here.

The above results validate that the numerical analysis for the MBP polydisperse constitutive “toy” model using Euler’s method is accurate and shows a convergence for a step size of $\Delta t=5\times10^{-11}$s.

APPENDIX B.

ADDITIONAL FIGURES AND TABLES FOR THE MBP POLYDISPERSE "TOY" MODEL

B.1. Component entanglement dynamics results:

The importance of entanglement dynamics (ED) to describe the polydisperse system has been discussed in detail in paper III (Sections III.A and IV). Figure B.1 shows the transient normalized entanglement dynamics curve for the short and the long chain components, for PSM1 (see Table 2., in paper III Section III.A for details) at extension rates ἑ 0.00015, 0.01 and 0.3 sec^{-1}. This shows the drop in the number of entanglements in long and short chains w.r.t to the equilibrium number of entanglements.

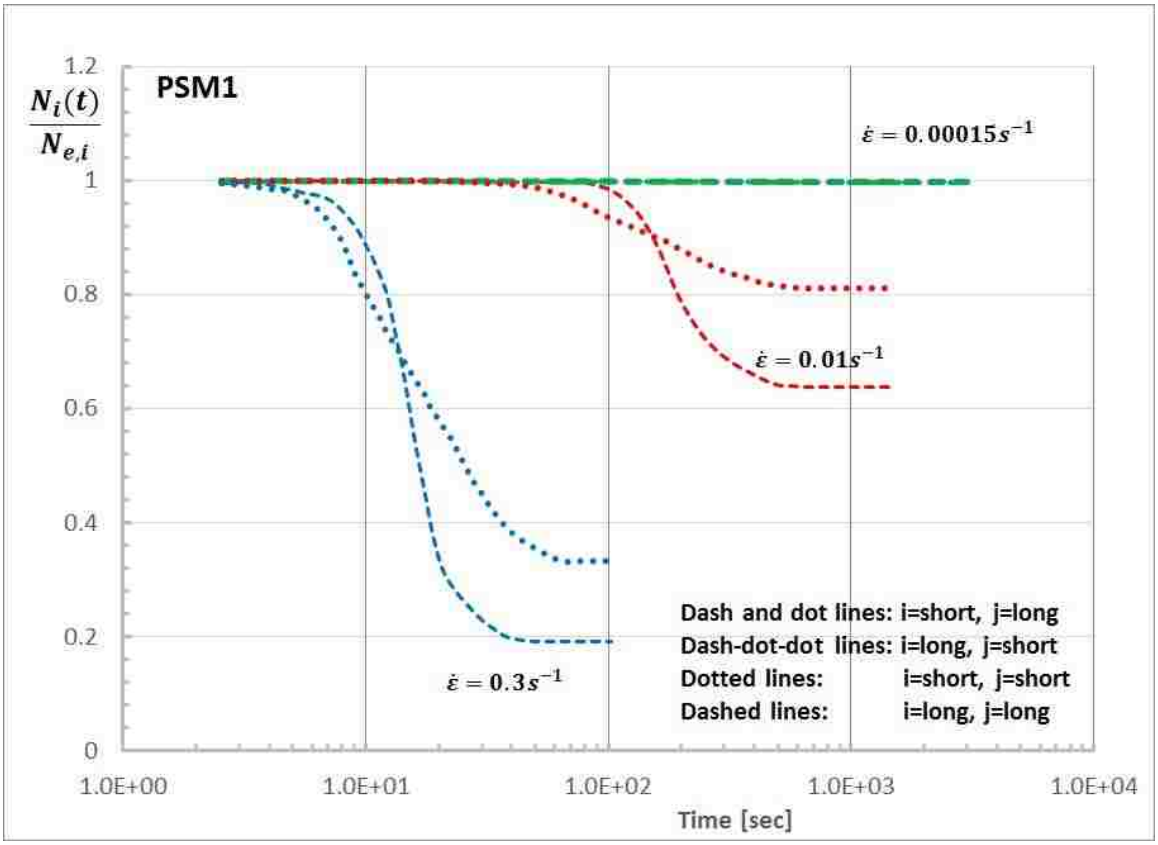

Figure B.1. Transient normalized entanglement dynamics curve for PSM1 at ἑ 0.00015, 0.01 and 0.3 sec^{-1} showing the short and long chain entanglement dynamics.

As can be seen from Figure B.1, the number of entanglements on the longer chain component falls of more than the short chain components. This is because the entanglements on long-long components fall off to a larger extend compared to the long-short, short-short and short-long which can be seen from Figure 14, in Paper III. The reason behind the faster disentanglement of long-long components as discussed is due to the reduced re-entanglement or formation of new entanglements for the long-long components.

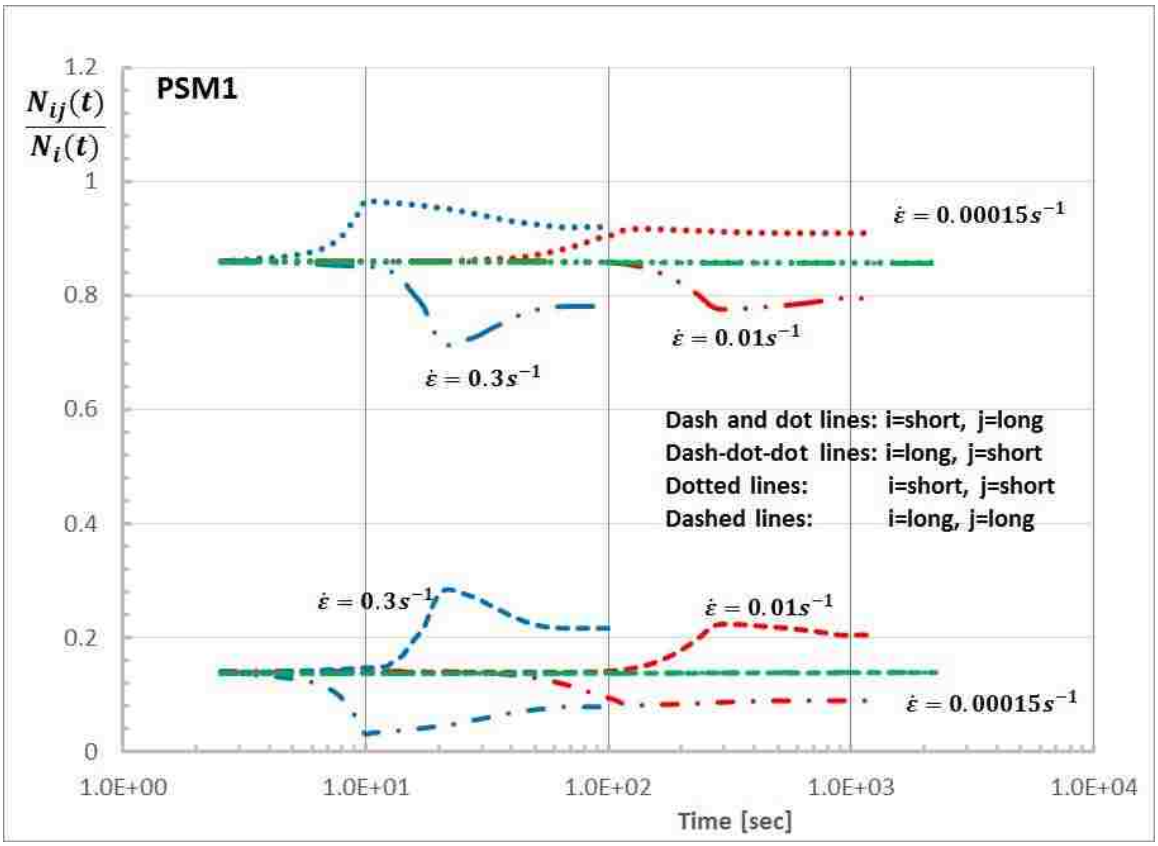

Figure B.2. Transient normalized entanglement dynamics curve $(N\_ij\ (t))\ /\ N\_i$)for PSM1 at ἑ 0.00015, 0.01 and 0.3 sec^{-1} showing the short and long chain entanglement dynamics.

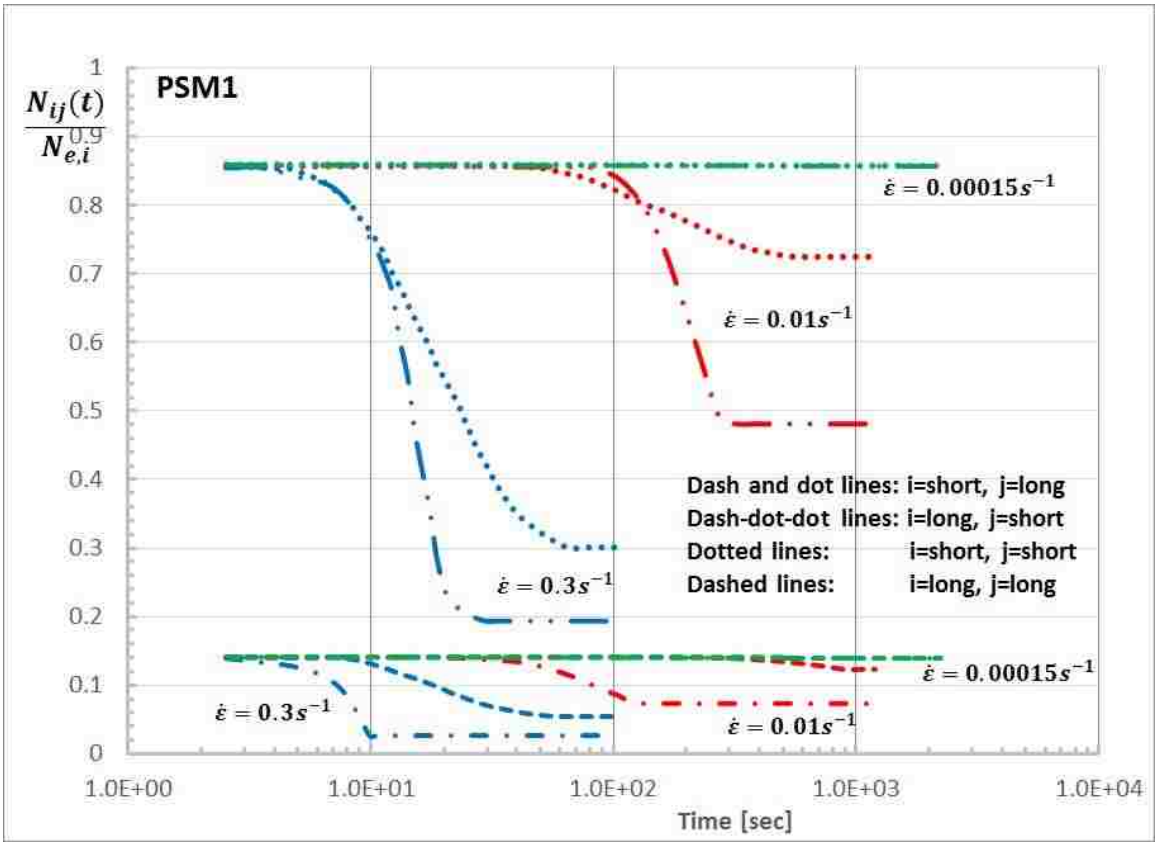

Figure B.3. Transient normalized entanglement dynamics curve $(N\_ij\ (t))\ /\ N\_ei$)for PSM1 at ἑ 0.00015, 0.01 and 0.3 sec^{-1} showing the short and long chain entanglement dynamics.

In order to investigate the entanglement dynamics behavior of each of the individual components at different extension rates, different normalized curves have been plotted. Figure B.2. shows the Transient normalized entanglement dynamics curve $(N\_ij\ (t))\ /\ N\_i$)for PSM1 at ἑ 0.00015, 0.01 and 0.3 sec^{-1}. Similarly, Figure B.3 and B.4 show the Transient normalized entanglement dynamics curve $(N\_ij\ (t))\ /\ N\_ei$) and $(N\_ij\ (t))\ /\ ((N\_i\ (t) * w\_j))$ or PSM1 respectively. Each of these curves show how the number of entanglements on the chain is changing with time.

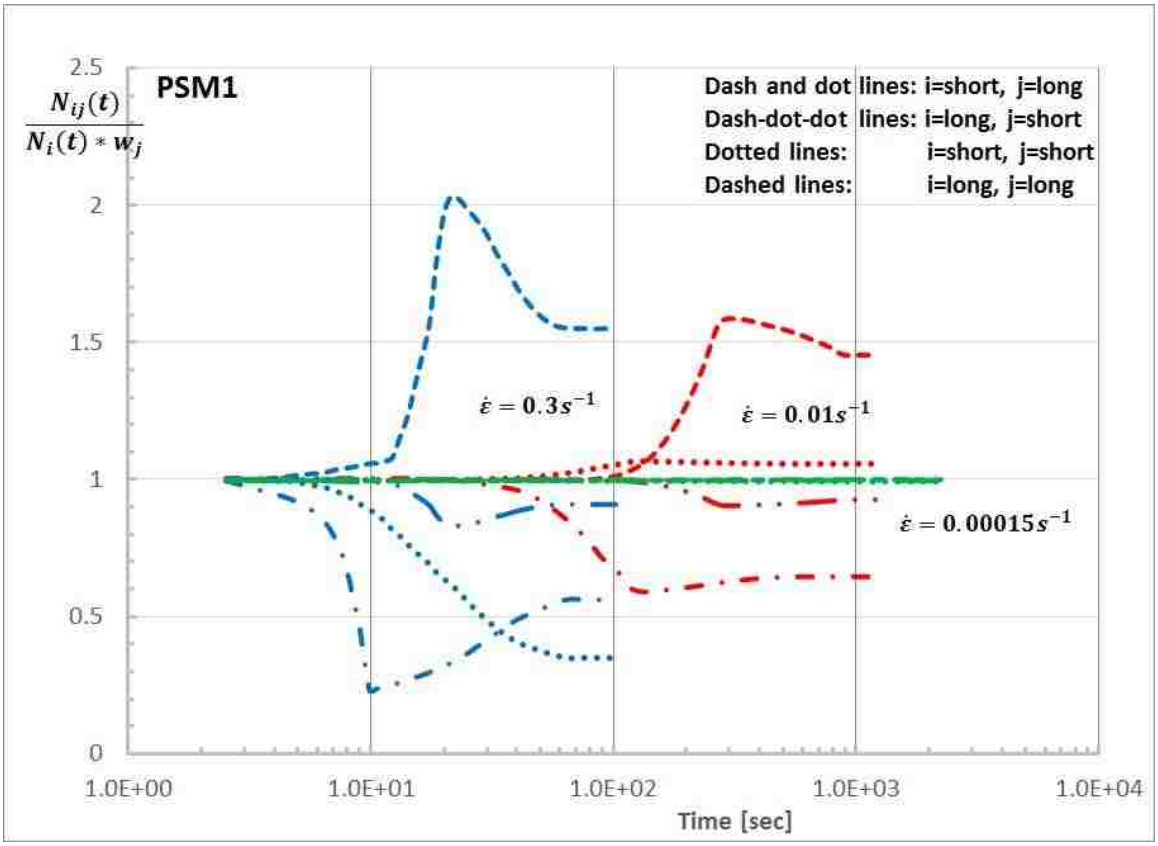

Figure B.4. Transient normalized entanglement dynamics curve $(N\_ij\ (t))\ /\ ((N\_i\ (t) * w\_j))$ or PSM1 at ἐ 0.00015, 0.01 and 0.3 sec^{-1} showing the short and long chain entanglement dynamics.

B.2. Steady state uniaxial extension melt and shear solution results:

Along with the transient behavior, the steady state behavior of PSM1 under uniaxial extension and of PSS2 under shear is of interest. Figure B.5 gives the steady uniaxial extensional viscosity curve for PSM1 (see Table 2., in paper III for details) along with the short chain and the long chain contributions. The observations in close agreement with the experimental results from Read et al. (2012). One can again see that with increase in extension rates, the contributions of the long chains increases as the it

starts stretching at $\dot{\varepsilon} > \sim 0.002 = \frac{1}{\tau_{r-long}}$. On further increasing the extension rates, the short chain starts stretching $\dot{\varepsilon} > \sim 0.04 = \frac{1}{\tau_{r-short}}$, and its contribution becomes more prominent. For high extension rate condition both the short and the long chains contribute equally to the overall viscosity of the system. The stretching effects of the individual components have been more clearly described in paper III, Section IV.

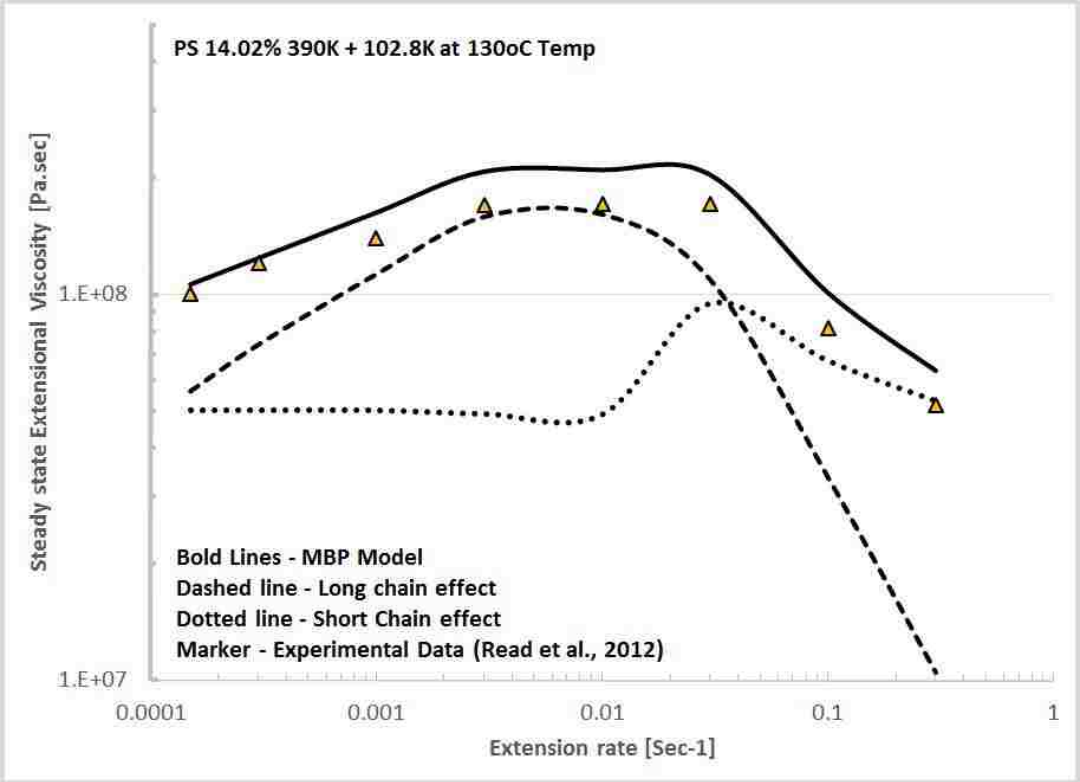

Figure B.5. Steady state extensional viscosity curve for PS bidisperse melt (see Table 2., in paper III for details). The long and short chain component effects are given by dashed and dotted lines respectively. The experimental data given by markers are taken from Read et al. (2012).

Figure B.6 shows the steady state shear viscosity and first normal stress difference vs shear rate curve, for PSS2 (see Table 5., in paper III for details). The MBP predictions are in close agreement with the experimental results from Pattamaprom and Larson (2001). As expected, the shear viscosity for polydisperse solution system monotonically reduces with increase in shear rate, whereas the first normal stress difference shows a monotonic increase with shear rate.

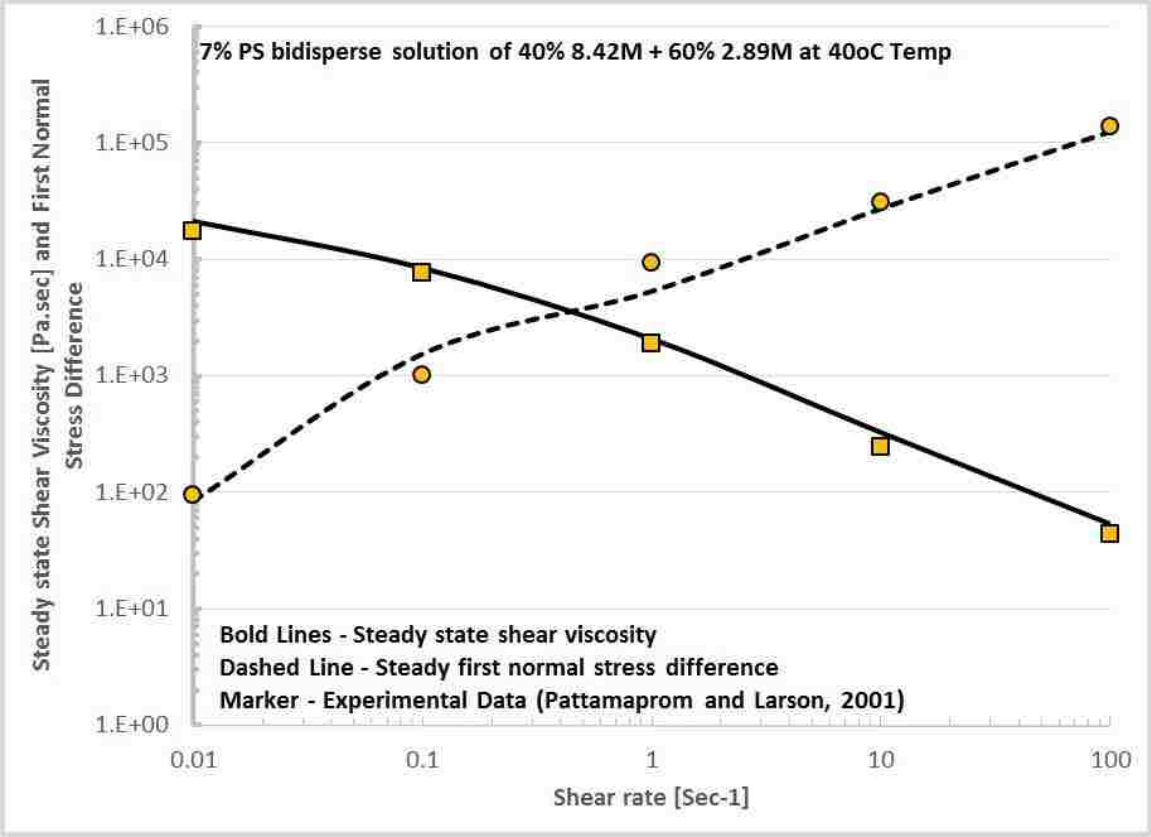

Figure B.6. Steady state shear viscosity and first normal stress difference vs shear rate curve difference for 7% PS bidisperse solution (see Table 5., in paper III for details). The experimental data given by markers are taken from Pattamaprom and Larson (2001).

B.3. [PS 686] and PSMW [Wesslau's log-normal] MWD under uniaxial extension results:

The effect of higher molecular weight component, on the overall viscosity of the system, for wide molecular weight distribution (MWD), is of interest. The PSM2 (PS 686 melt system spiked with 3.2×10^6 MW component (Mishler & Mead, 2013)) (see Table 3., in paper III for details) is simulated and the results (see Figure 4) are discussed in paper III, Section III.A. Figure B.7, shows the transient relative stretch curves for components, 9, 13, and 21 (see Table 3., in paper III for details) at extension rate 0.572sec^{-1}.

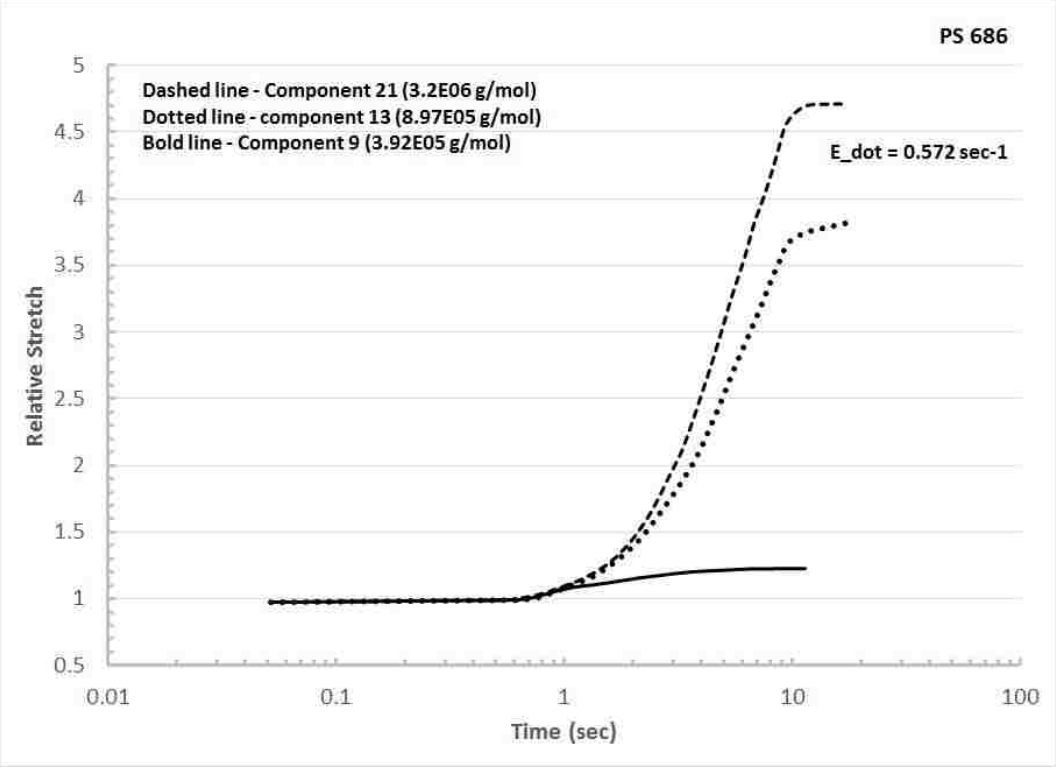

Figure B.7. Relative stretch curve for PSM2 (PS 686, for components (9, 13 and 21)) (see Table 3., in paper III for details) at ἑ 0.572 sec^{-1}.

It can be clearly seen that the strain hardening observed in the system (see Figure 4., in paper III for the transient viscosity curve) is due to stretch occurring in the high molecular weight component.

The PSMW (Wesslau's log-normal 10 components PS melt MWD (PI = 2.33)) for uniaxial extension deformation (see Table 7., in paper III for details) is a model generated MWD which is simulated to validate the stretching effects of high molecular weight components on the overall viscosity of the system under high uniaxial extension deformation.

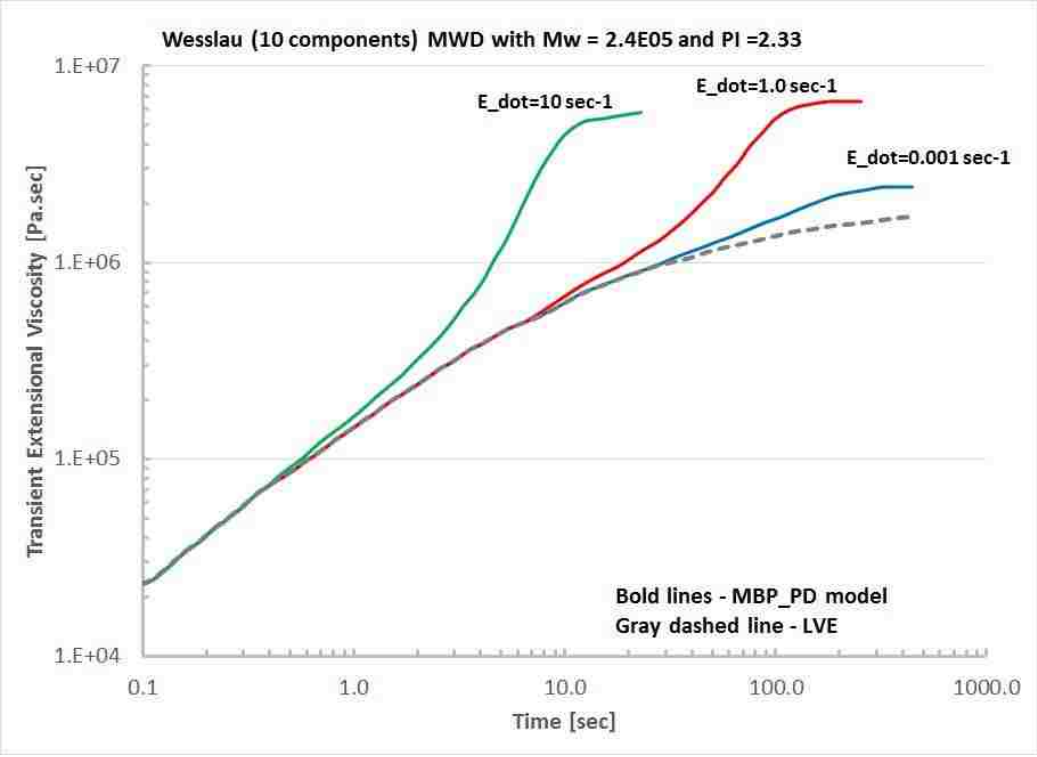

Figure B.8. Transient extensional viscosity curve for PSMW (Wesslau's log-normal PS melt MWD) (see Table 7., in paper III for details) at extension rates 0.001, 1.0 and 10 sec^{-1}. The LVE is given by grey dashed line.

Figure B.8. shows the transient extensional viscosity curves at extension rates 0.001, 1.0 and 10 sec^{-1} respectively. The effects of the stretching in the high molecular weight components have been discussed in paper III, Section IV (see Figure 14).

B.4. Most probable MWD results:

The most probable two components MWD is generated using the code. Figure B.9. shows the transient extensional viscosity curve at extension rates 0.001, 1.0 and 10 sec^{-1} respectively.

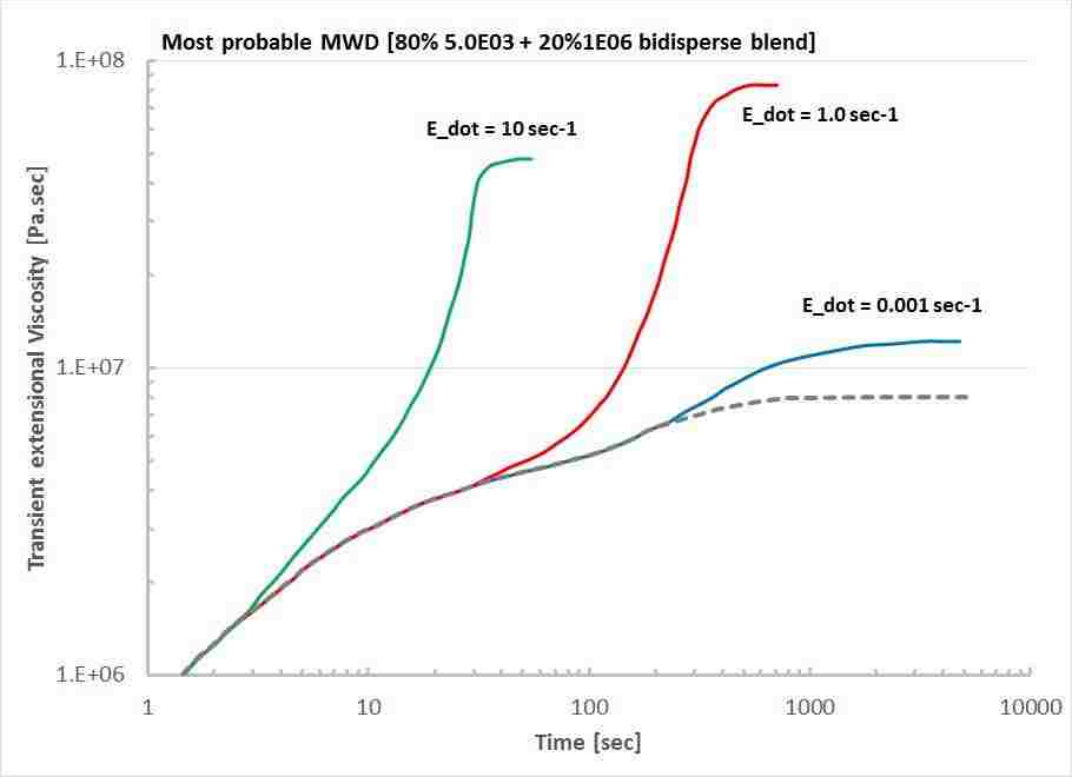

Figure B.9. Transient extensional viscosity curve for most probable PS melt MWD (see Table B.1. for details) at extension rates 0.001, 1.0 and 10 sec^{-1}. The LVE is given by grey dashed line.

The simulation is performed to validate the numerical analysis of the MBP polydisperse model. Table B.1. gives the simulation inputs for the most probable MWD melt. The system is simulated for uniaxial extension. Again the strain hardening behavior is observed. As this is a model generated data to just check the code, it has not been validated against experimental results.

Table B.1. Simulation input values for model generated most probable MWD bidisperse PS melt.

G_N^o [Pa]	Weight fraction	Molecular weight (kg/mol)	$\tau^0_{d,i}$ [s]	$\tau^0_{r,i}$ [s]	N_e
2.46×10^5	0.8	5.00	2.64×10^{-6}	3.38×10^{-6}	0.26
	0.2	1000	175.65	1.12	52.08

B.5. CCR effect in polydisperse system:

For the monodisperse extension system it was observed that the effect of (convective constraint release) CCR on the system depended on the deformation condition. Shear deformation requires CCR to describe the shear thinning observed for high shear rates, on the other hand, CCR caused over prediction og relaxation in casee of extension. The effect of CCR or even the persence of it and its requirement to define a system have always been controvertial. This made it improtant to study its effect.

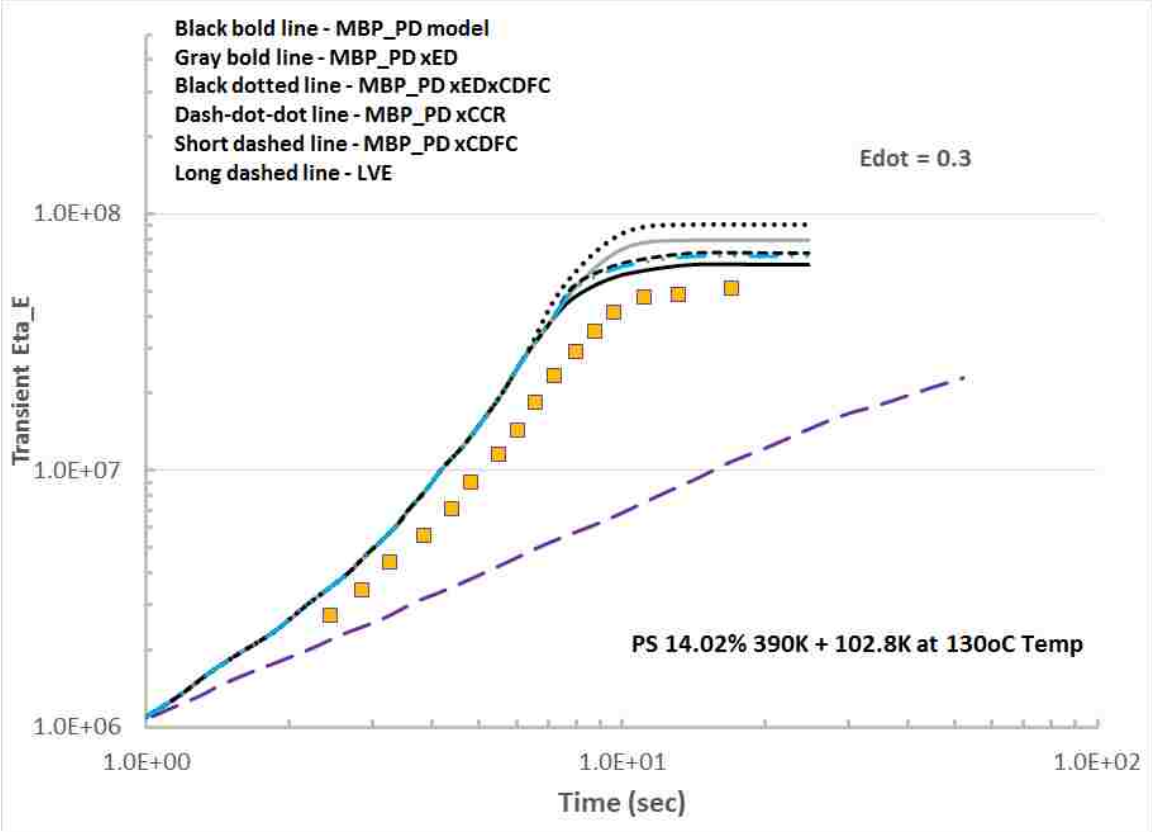

Fig B.10. Transient extensional viscosity for PS melt (PSM1) at 0.3 s^{-1} extension rate for different simulation combinations to check the effect of the individual physics.

To check the effect of CCR in case of polydisperse melt extension (PSM1) and see how CCR is effecting the system MBP $_{xCCR}$. Figure B.10 shows the individual effect of ED, CDFC and CCR. The effects of ED and CDFC have been discussed in detail in Paper III. On turning "off" CCR, it can be seen that the curve deviates from the experimental results and the behavior is similar to that of MBP without CDFC. Thus one can conclude that CCR again have a week effect on the overall behavior of the system. The behavior is thus similar to that of the monodisperse extension melt systems when

CCR becomed ineefective due to the loss of ttopological constraint when the system gets highly oriented.

B.6. Diluted tube Stretch, Maximum relative stretch and CDFC

Figure B.11 shows the comparison bbetween the relative stretch in the primary and the diluted tube for bidisperse PS melt (PSM1) under extension rates ἑ 0.00015, 0.01 and 0.3 sec^{-1}. It can be seen that as the extension rates increases, the stretching in the diluted tube becomes more prominent compared to that of the primary tube.

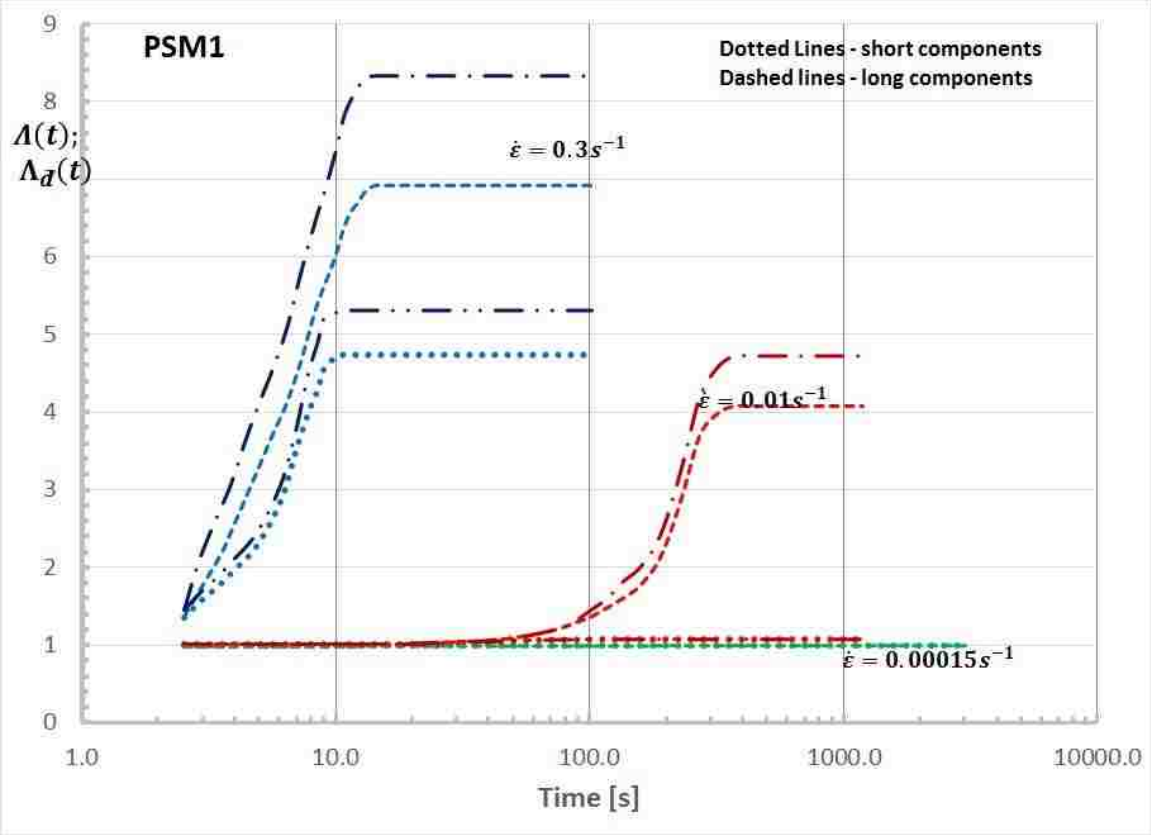

Figure B.11. Transient normalized entanglement dynamics curve $(N\_ij\ (t))\ /\ N\_ei$)for PSM1 at ἑ 0.00015, 0.01 and 0.3 sec^{-1} showing the short and long chain entanglement dynamics.

The diluted tube for the longer chain component is stretched more than the primary tube. This may be becarse the siluted tube is defined by only viable components whereas, the primary tube is defined by all the entanglements present in the sytem. This allows the diluted tube to unravel more and get stretched.

Figure B.12. shows the maximum relative stretch for diluted tube for bidisperse PS melt (PSM1) under extension rates ἑ 0.00015, 0.01 and 0.3 sec^{-1}. Here one can see that the diluted tube starts unravelling under high extension rates. The chain start to stretch and the back bends and loops in the chain gets straightened.

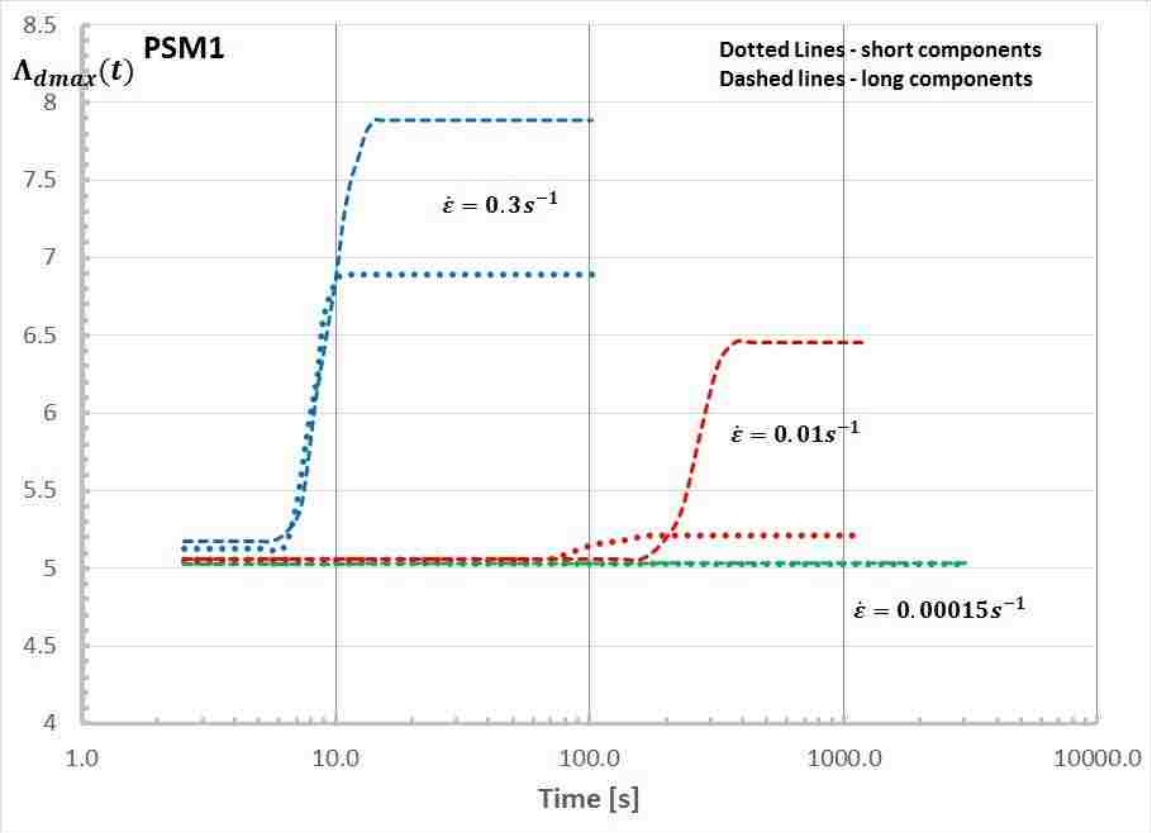

Figure B.12. Transient maximum relative stretch for diluted tube for PSM1 at ἑ 0.00015, 0.01 and 0.3 sec^{-1} showing the short and long chain entanglement dynamics.

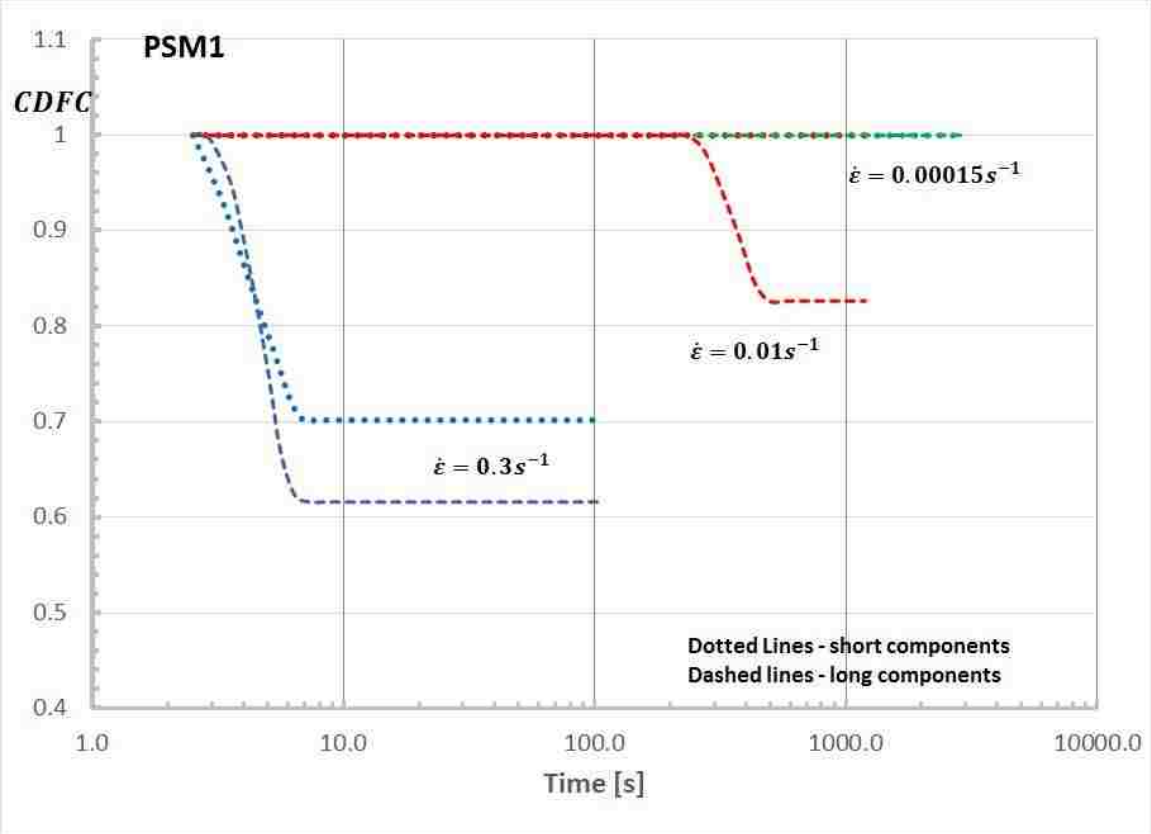

Figure B.13. Transient CDFC for PSM1 at ἐ 0.00015, 0.01 and 0.3 sec^{-1} showing the short and long chain entanglement dynamics.

Figure B.13. shows the transient CDFC effect PSM1 at ἐ 0.00015, 0.01 and 0.3 sec^{-1}. From this curve one can observe that the with increase in extension rate, the long chain gets effected first, then both long and short chains showing CDFC due to orientation. Though CDFC effect is there, the reduction due to CDFC is not high and thus their effect on the overall behavior of the system is not prominent.

REFERENCES

Andreev, M., Khaliullin, R. N., Steenbakkers, R. J. A., and Schieber J. D. "Approximations of the discrete slip-link model and their effect on nonlinear rheology predictions," Journal of Rheology, 57, 2 (2013) 535-557.

Auhl, D., Chambon, P., McLeish, T. C. B., and Read, D. J. "Elongational flow of blends of long and short polymers: Effective stretch relaxation time," Physical review letters, 103, 13 (2009) 136001(4).

Baig, C., V.G. Mavrantzas and M. Kroger, "Flow effects on melt structure and entanglement network of linear polymers: Results from a non-equilibrium molecular dynamics study of a polyethylene melt in steady shear", Macromolecules 43, (2010) 6886-6906.

Banerjee, N., and Park, J. "Modeling and simulation of biopolymer networks: Classification of the cytoskeleton models according to multiple scales," Korean Journal of Chemical Engineering, 32, 7 (2015) 1207-1217.

Barkema, G. T., Panja, D., Van Leeuwen, J. M. J. "Structural modes of a polymer in the repton model," The Journal of Chemical Physics, 134, 15 (2011) 154901.

Bremner, T., A. Rudin, and D. G. Cook. "Melt flow index values and molecular weight distributions of commercial thermoplastics," Journal of Applied Polymer Science 41, 7-8 (1990) 1617-1627.

Chen, P., and V. B. Shenoy. "Strain stiffening induced by molecular motors in active crosslinked biopolymer networks," Soft Matter, 7 (2011) 355-358.

Chen, T. J., C. C. Wu, and F. C. Su. "Mechanical models of the cellular cytoskeletal network for the analysis of intracellular mechanical properties and force distributions: A review," Medical engineering & physics, 34, 10 (2012) 1375-1386.

De Gennes, P. G. "Reptation of a Polymer Chain in the Presence of Fixed Obstacles," Journal of Chemical Physics, 55, 2 (1971) 572-579.

De Gennes, P. G. "Reptation of stars," Journal de Physique, 36, 12 (1975) 1199-1203.

Dealy, J. M., and P. C. Saucier. Rheology in plastics quality control. Hanser Publishers, (2000).

Dealy, J.M. and R.G. Larson, "Structure and rheology of molten polymers: From structure to flow behavior and back again," Hanser, Munich (2006).

Des Cloizeaux, J. "Double reptation vs. simple reptation in polymer melts," EPL (Europhysics Letters), 5, 5 (1988) 437-442.

Des Cloizeaux, J. "Relaxation and viscosity anomaly of melts made of long entangled polymers: time-dependent reptation," Macromolecules, 23, 21 (1990) 4678-4687.

Doi M., and Kuzuu, N. Y. "Rheology of star polymers in concentrated solutions and melts," Journal of Polymer Science: Polymer Letters Edition, 18, 12 (1980) 775-780.

Doi, M. and Edwards, S. F. The theory of polymer dynamics. Oxford University Press, New York, (1986).

Doi, M., and Edwards, S. F. "Dynamics of concentrated polymer systems. Part 1. - Brownian motion in the equilibrium state," Journal of the Chemical Society, Faraday Transactions 2: Molecular and Chemical Physics, 74 (1978a) 1789-1801.

Doi, M., and Edwards, S. F. "Dynamics of concentrated polymer systems. Part 2. - Molecular motion under flow," Journal of the Chemical Society, Faraday Transactions 2: Molecular and Chemical Physics, 74 (1978b) 1802-1817.

Doi, M., and Edwards, S. F. "Dynamics of concentrated polymer systems. Part 4.- Rheological properties," Journal of the Chemical Society, Faraday Transactions 2: Molecular and Chemical Physics, 75 (1979) 38-54.

G. H. Pollack, in *Cytoskeletal Mechanics - Models and Measurements in Cell Dynamics*, M. R. K. Mofrad, and R. D. Kamm Eds., Cambridge University Press (2006).

Ianniruberto, G., and Marrucci, G. "On compatibility of the Cox-Merz rule with the model of Doi and Edwards," Journal of Non-Newtonian fluid mechanics, 65, 2 (1996) 241-246.

Ianniruberto, G., Brasiello A., and Marrucci, G. “Simulations of fast shear flows of PS oligomers confirm monomeric friction reduction in fast elongational flows of monodisperse PS melts as indicated by rheooptical data,” Macromolecules, 45, 19 (2012) 8058-8066.

Kremer, K., and Grest, G. S. “Dynamics of entangled linear polymer melts: A molecular-dynamics simulation,” The Journal of Chemical Physics, 92, 8 (1990) 5057-5086.

Kuhn, W. “über die gestalt fadenförmiger moleküle in lösungen,” Kolloid-Zeitschrift, 68, 1 (1934) 2-15.

Larson, R. G. The Structure and Rheology of Complex Fluids. Oxford University Press, New York, 1999.

Lodge, T. P., Rotstein, N. A., and Prager, S. “Dynamics of entangled polymer liquids: Do linear chains reptate?,” Advances in Chemical Physics, 79 (1992) 1-132.

Marrucci, G. “Dynamics of entanglements: A nonlinear model consistent with the Cox-Merz rule,” Journal of non-Newtonian fluid mechanics, 62, 2 (1996) 279-289.

Marrucci, G. and Ianniruberto, G. “Effect of flow on topological interactions in polymers,” In Macromolecular symposia, Hüthig & Wepf Verlag, 117, 1 (1997) 233-240.

Marrucci, G., and Grizzuti, N. “Fast flows of concentrated polymers-predictions of the tube model on chain stretching,” Gazzetta Chimica Italiana, 118, 3 (1988) 179-185.

Maurin, B., P. Canadas, H. Baudriller, P. Montcourrier, and N. Bettache. “Mechanical model of cytoskeleton structuration during cell adhesion and spreading,” Journal of biomechanics, 41, 9 (2008) 2036-2041.

McLeish, T. C. B. “Tube theory of entangled polymer dynamics,” Advances in Physics, 51, 6 (2002) 1379-1527.

Mead, D. W. “Determination of molecular weight distributions of linear flexible polymers from linear viscoelastic material functions,” Journal of Rheology, 38, 6 (1994) 1797-1827.

Mead, D. W. “Development of the “binary interaction” theory for entangled polydisperse linear polymers,” Rheologica acta, 46, 3 (2007) 369-395.

Mead, D. W., Banerjee, N. and Park, J. "Constitutive model for entangled polymers incorporating binary entanglement pair dynamics and a configuration dependent friction coefficient," Journal of Rheology, 59, 2 (2015) 335-363.

Mead, D. W., Larson R. G., and Doi M., "A Molecular Theory for Fast Flows of Entangled Polymers," Macromolecules, 31 (1998) 7895-7914.

Mishler, S.D. and D.W. Mead, "Application of the MLD "Toy" Model to Extensional Flows of Broadly Polydisperse Linear Polymers: Comparison to Experimental data Sets," J. Non-Newtonian Fluid Mechanics, 197 (2013b) 80-90.

Mishler, S.D. and Mead, D. W. "Application of the MLD "Toy" Model to Extensional Flows of Broadly Polydisperse Linear Polymers: Model Development," Journal of Non-Newtonian Fluid Mechanics, 197 (2013a) 61-79.

Na, S., G. A. Meininger, and J. D. Humphrey. "A theoretical model for F-actin remodeling in vascular smooth muscle cells subjected to cyclic stretch," Journal of theoretical biology, 246, 1 (2007) 87-99.

Nava, M. M., M. T. Raimondi, and R. Pietrabissa. "Bio-chemo-mechanical models for nuclear deformation in adherent eukaryotic cells," Biomechanics and modeling in mechanobiology, 13, 5 (2014) 929-943.

Park, J., Mead, D. W. and Morton, M. D. "Stochastic simulation of entangled polymeric liquids in fast flows: Microstructure modification," Journal of Rheology, 56, 5 (2012) 1-25.

Pattamaprom, C. and R. G. Larson, "Constraint Release Effects in Monodisperse and Bidisperse Polystyrenes in Fast Transient Shearing Flows," Macromolecules 34, (2001) 5229-5237.

Pearson, D. S. "Recent advances in the molecular aspects of polymer viscoelasticity," Rubber chemistry and technology, 60, 3 (1987) 439-496.

Pearson, D., Herbolzheimer, E., Grizzuti, N., and Marrucci, G. "Transient behavior of entangled polymers at high shear rates," Journal of Polymer Science Part B: Polymer Physics, 29, 13 (1991) 1589-1597.

Read, D. J., K. Jagannathan, S. K. Sukumaran and D. Auhl, “A full-chain constitutive model for bidisperse blends of linear polymers,” J. Rheol. 56, (4), (2012) 823-873.

Rouse Jr, P. E. “A theory of the linear viscoelastic properties of dilute solutions of coiling polymers,” The Journal of Chemical Physics, 21, 7 (1953) 1272-1280.

Rubinstein, M. “Discretized model of entangled-polymer dynamics,” Physical Review Letters, 59, 17 (1987) 1946–1949.

Rubinstein, M. and Colby, R. H. Polymer Physics. 1st ed. Oxford University Press, UK, (2003).

Rubinstein, M., and Colby, R. H. “Self-consistent theory of polydisperse entangled polymers: Linear viscoelasticity of binary blends,” The Journal of chemical physics, 89, 8 (1988) 5291-5306.

Tsenoglou, C. "Viscoelasticity of binary homopolymer blends." In abstracts of Papers of the American Chemical Society, 1155 16th St, NW, Washington, DC 20036: Amer. Chemical Soc., 194 (1987) 219-POLY.

Tsenoglou, C. “Molecular weight polydispersity effects on the viscoelasticity of entangled linear polymers,” Macromolecules, 24, 8 (1991) 1762-1767.

Unterberger, M. J., and G. A. Holzapfel. “Advances in the mechanical modeling of filamentous actin and its cross-linked networks on multiple scales,” Biomechanics and modeling in mechanobiology, 13, 6 (2014) 1155-1174.

Vivoy, J. L., Rubinstein, M., and Colby, R. H. “Constraint release in polymer melts: tube reorganization versus tube dilation,” Macromolecules, 24, 12 (1991) 3587-3596.

Wasserman, S. H., and Graessley, W. W. “Effects of polydispersity on linear viscoelasticity in entangled polymer melts,” Journal of Rheology, 36, 4 (1992) 543-572.

Wingstrand, S. L., Alvarez, N. J., Huang, Q., and Hassager, O. “Linear and nonlinear universality in the rheology of polymer melts and solutions,” Physical review letters, 115, 7 (2015) 078302(5).

Xu, F., Morton, M. D. and Schieber J. D. “A full chain stochastic tube model for entangled melts and solutions of linear polymers,” Journal of Rheology, 50, 4 (2006) 477-494.

Yaoita, T., Isaki, T., Masubuchi, Y., Watanabe, H., Ianniruberto, G. and Marrucci, G. ‘Primitive chain network simulation of elongational flows of entangled linear chains: stretch/orientation-induced reduction of monomeric friction,” Macromolecules, 45, 6 (2012) 2773-2782.

Yaoita, T., Masubuchi, Y., and Watanabe, H. "Concept of stretch/orientation-induced friction reduction tested with a simple molecular constitutive equation." Journal of the Society of Rheology, Japan, 42, 3 (2014) 207-213.

Ylitalo, C. M., Fuller, G. G., Abetz, V., Stadler, R., and Pearson, D. S. “Relaxation dynamics of selected polymer chain segments and comparison with theoretical models,” Rheologica Acta, 29, 6 (1990) 543-555.

Zimm, B. H. “Dynamics of polymer molecules in dilute solution: viscoelasticity, flow birefringence and dielectric loss,” The journal of chemical physics, 24, 2 (1956) 269-278.

VITA

Nilanjana Banerjee was born in Kolkata, West Bengal, India, on February 20, 1986. In May 2008 she received her Bachelor of Technology (B.Tech) with Honors in Chemical Engineering from the Nirma Institute of Technology, Nirma University, Ahmedabad, Gujarat, India. She was also awarded the best student award during the Bachelor degree commencement ceremony. She did her summer training at Larson and Toubro – Chiyoda, Vadodara, India during the summer of 2007.

She received her Master's in Chemical Engineering (M.Chem.Engg.) with Honors from Institute of Chemical Technology, Mumbai University (formerly UDCT), Mumbai, India, in June 2010. Her Master's thesis was nominated for the ISTE/IPCL best Master's thesis award in 2010.

In December 2010, she joined the Chemical Engineering Department of Maharaja Sayajirao University, Vadodara, Gujarat, India, as a lecturer and taught till April, 2012. In May 2016, she received her Ph.D. in Chemical Engineering from the Missouri University of Science and Technology, Rolla, Missouri, USA. She has published conference and journal papers, some of which are listed with the references of this research.

Nilanjana Banerjee has been a member of the American Institute of Chemical Engineering (AIChE) since 2013. She has been a member of the Institute of Engineering and Technology (IET) since 2015.